INTRANASAL DELIVERY OF SELF-ASSEMBLY INSULIN NANOCOMPLEXES BASED ON SURFACE MODIFIED TRIMETHYL CHITOSAN

ANCHALEE JINTAPATTANAKIT

A THESIS SUBMITTED IN PARTIAL FULFILLMENT
OF THE REQUIREMENTS FOR
THE DEGREE OF DOCTOR OF PHILOSOPHY
(PHARMACEUTICS)
FACULTY OF GRADUATE STUDIES
MAHIDOL UNIVERSITY
2008

Thesis
Entitled

INTRANASAL DELIVERY OF SELF-ASSEMBLY INSULIN NANOCOMPLEXES BASED ON SURFACE MODIFIED TRIMETHYL CHITOSAN

……..
Ms. Anchalee Jintapattanakit
Candidate

……..
Assoc. Prof. Varaporn Junyaprasert, Ph.D.
Major-Advisor

……..
Prof. Thomas Kissel, Ph.D.
Co-Advisor

……..
Assoc. Prof. Penchom Peungvicha, Ph.D.
Co-Advisor

…….
Asst. Prof. Auemphorn Mutchimwong
Ph.D.
Acting Dean
Faculty of Graduate Studies

…….
Prof. Ampol Mitrevej, Ph.D.
Chair
Doctor of Philosophy Programme
in Pharmaceutics
Faculty of Pharmacy

Thesis
Entitled

INTRANASAL DELIVERY OF SELF-ASSEMBLY INSULIN NANOCOMPLEXES BASED ON SURFACE MODIFIED TRIMETHYL CHITOSAN

was submitted to the Faculty of Graduate Studies, Mahidol University
for the degree of Doctor of Philosophy (Pharmaceutics)
on
22 October, 2008

……..
Ms. Anchalee Jintapattanakit
Candidate

……..
Assoc. Prof. Achariya Sailasuta,
D.V.M., Ph.D.
Chair

……..
Assoc. Prof. Varaporn Junyaprasert, Ph.D.
Member

…….
Assist. Prof. Doungdaw Chantasart,
Ph.D.
Member

……..…
Assoc. Prof. Penchom Peungvicha, Ph.D.
Member

…….
Asst. Prof. Auemphorn Mutchimwong
Ph.D.
Acting Dean
Faculty of Graduate Studies
Mahidol University

…….
Assoc. Prof. Chuthamanee Suthisisang,
Ph.D.
Dean
Faculty of Pharmacy
Mahidol University

ACKNOWLEDGEMENTS

First of all, I would like to express my deepest gratitude and appreciation to Associate Professor Dr. Varaporn Junyaprasert, my major advisor, for giving me the opportunity to study the Ph.D., her invaluable advice, expert guidance, kindly support and friendliness. Most importantly, her graciousness will always be unforgettable.

I wish to express my grateful thank to Professor Dr. Thomas Kissel, my co-advisor, for his professional guidance, helpful criticism, superb supervision, kindly support and encouragement in this dissertation. I am impressed by his enthusiasm and creativity so much.

My special thanks are extended to Associate Professor Dr. Penchom Peungvicha, my co-advisor, for her helpful criticism and constructive suggestions for *in vivo* studies.

My greatest esteem goes to Associate Professor Dr. Achariya Sailasuta for her professional guidance, helpful criticism and kindly support, especially in histopathological studies.

I would like to express my grateful thank to Associate Professor Dr. Shirui Mao for her excellent guidance, kindness and abundant encouragement throughout my thesis as well as her friendship for me.

The Thailand Research Fund (TRF) through the Royal Golden Jubilee (RGJ) Ph.D. program (Grant No. PHD/0226/2545), the TRF Master Research Grants: TRF-MAG (Grant No. MRG-OSMEP505S175) and the German Academic Exchange Service (DAAD) are gratefully acknowledged for providing scholarships and research grant during my study in Thailand and at the Department of Pharmaceutics and Biopharmacy, Philipps-Universität, Marburg, Germany.

My great appreciation is extended to the National Metal and Materials Technology Center (MTEC, Pathumthani, Thailand) for GPC experiment.

I am very grateful to Professor Dr. Udo Bakowsky for the discussion of the AFM experiments. Thanks to Mr. Johannes Sitterber for AFM images. Thanks to Dr. Oliver Germershaus for CLSM images. Thanks to Mr. Klaus Keim for the excellent pictures and I wish to thank Ms. Eva Mohr for cell culture experiments.

My acknowledgements are extended to the administrative staff and technicians of the Faculty of Pharmacy, Mahidol University and of the Department of Pathology, Faculty of Veterinary Science, Chulalongkorn University for their supportive assistance during I was studying and doing the research in Thailand.

I would like to thank all my friends and my colleagues both in Thailand and in Germany, in particular at the Faculty of Pharmacy, Mahidol University, and at the Department of Pharmaceutics and Biopharmacy, Philipps-Universität, Marburg for their friendship, kindly support and cheerfulness. It is a pity that I cannot list their names in this limited page; however, all of them will be in my mind forever.

Last, but not least, I would like to express my infinite gratitude to my mom, dad, brothers and sister for their love, inspiration, encouragement and understanding throughout my life.

Anchalee Jintapattanakit

INTRANASAL DELIVERY OF SELF-ASSEMBLY INSULIN NANOCOMPLEXES BASED ON SURFACE MODIFIED TRIMETHYL CHITOSAN

ANCHALEE JINTAPATTANAKIT 4536902 PYPT/D

Ph.D. (PHARMACEUTICS)

THESIS ADVISORS: VARAPORN JUNYAPRASERT, Ph.D., THOMAS KISSEL, Ph.D., PENCHOM PEUNGVICHA, Ph.D.

ABSTRACT

This study aimed to investigate the potential use of nanocomplexes (NC) based on *N*-trimethyl chitosan (TMC) and its corresponding poly(ethylene glycol)-*graft*-TMC copolymers (PEGylated TMC) for intranasal insulin delivery. The results indicated that a suitable degree of quaternization (DQ) of TMC was 40%, which provided the highest water solubility; its physicochemical properties and cytotoxicity were independent of degree of dimethylation (DD). Regarding mucoadhesive properties, PEGylated TMC showed significantly higher levels of adhesion to mucus than unmodified TMC, due to the synergistic effects of interpenetration of PEG chains into the mucus and electrostatic interaction between positively charged TMC and anionic glycoproteins present in the mucus layer. The self-assembly insulin nanocomplexes (NC) prepared via the electrostatic interaction between the polymers and insulin showed that polymer/insulin (+/–) charge ratio played an important role in NC formation. Stable NC with high insulin association efficiency were obtained at or close to optimized polymer/insulin (+/–) charge ratio, depending on the polymer structure. Compared to insulin loaded nanoparticles (NP) prepared by ionotropic gelation with tripolyphosphate (TPP) counterions, NC were more stable in pH 6.8 phosphate buffer and could protect against the degradation of insulin at higher temperature and with proteolytic enzyme more efficiently than NP. Moreover, the presence of TPP accelerated the degradation of free insulin and insulin loaded NP by trypsin and the insulin degradation increased with increasing TPP concentration. From *in vivo* studies, the insulin NC showed about a 34 – 47% decrease in blood glucose concentration. The hypoglycemic response of the insulin NC increased with increasing polymer ratio and decreased with increasing PEG substitution degree which consistently correlated with the acute alteration in nasal morphology. The NC of TMC acted as a nasal absorption enhancer causing severe damage to nasal mucosa. In contrast, the NC of PEGylated TMC, especially PEG$(5k)_{680}$-g-TMC400-40 could enhance nasal absorption of insulin with mild irritation. However, the irritating effects of the NC on the rat nasal epithelium were reversible and the epithelium could be recovered after 24 h post nasal administration. After one-week daily administration of each insulin NC, it was shown that the nasal epithelium adapted to resist the acute effect. Finally, the results from *in vivo* studies indicated that NC based on PEG$(5k)_{680}$-g-TMC400-40 would be a potential carrier for safe and effective nasal delivery of insulin.

KEY WORDS : INTRANASAL DELIVERY / INSULIN / NANOCOMPLEXES / TRIMETHYL CHITOSAN / PEGYLATION

252 pp.

ระบบนำส่งยาทางจมูกของอินซูลินนาโนคอมเพลกซ์ที่เตรียมจากอนุพันธ์ไตรเมทธิล ไคโตแซน

(INTRANASAL DELIVERY OF SELF-ASSEMBLY INSULIN NANOCOMPLEXES BASED ON SURFACE MODIFIED TRIMETHYL CHITOSAN)

อัญชลี จินตพัฒนากิจ 4536902 PYPT/D

ปร.ด. (เภสัชการ)

คณะกรรมการควบคุมวิทยานิพนธ์: วราภรณ์ จรรยาประเสริฐ, Ph.D., THOMAS KISSEL, Ph.D., เพ็ญโฉม พึ่งวิชา, Ph.D.

บทคัดย่อ

วัตถุประสงค์ของการศึกษานี้เพื่อศึกษาศักยภาพของการใช้นาโนคอมเพลกซ์ที่เตรียมจากไตรเมทธิล ไคโตแซน (TMC) และ อนุพันธ์ PEGylated TMC ในการนำส่งอินซูลินทางจมูก ผลการศึกษาชี้ให้เห็นว่าดีกรีควอเทอร์ไนเซชันที่เหมาะสมของ TMC คือ 40% ซึ่ง TMC ละลายน้ำได้ดีที่สุดและดีกรีไดเมทธิเลชันไม่ส่งผลกระทบต่อคุณสมบัติทางกายภาพและความเป็นพิษของ TMC สำหรับคุณสมบัติในการยึดเกาะเยื่อเมือกพบว่า PEGylated TMC มีคุณสมบัติในการยึดเกาะเยื่อเมือกสูงกว่า TMC ซึ่งเป็นผลมาจากการแทรกซึมผ่านของสายโซ่ PEG ในเยื่อเมือก และการเกิดพันธะไอโอนิกระหว่างประจุบวกของ TMC และประจุลบของไกลโคโปรตีนในเยื่อเมือก อินซูลินนาโนคอมเพลกซ์ที่เตรียมจากอันตรกิริยาไฟฟ้าสถิตระหว่างพอลิเมอร์และอินซูลิน แสดงให้เห็นว่าอัตราส่วนระหว่างประจุบวกของพอลิเมอร์และประจุลบของอินซูลินมีบทบาทสำคัญในการเตรียมนาโนคอมเพลกซ์ นาโนคอมเพลกซ์ที่มีความคงตัวและมีประสิทธิภาพในการบรรจุอินซูลินสูงเตรียมได้ที่หรือใกล้กับอัตราส่วนระหว่างประจุบวกของพอลิเมอร์และประจุลบของอินซูลินที่เหมาะสมซึ่งขึ้นอยู่กับชนิดของพอลิเมอร์ เปรียบเทียบกับอินซูลินนาโนพาร์ติเคิลที่เตรียมจากเจลไอโอนิกของพอลิเมอร์กับไตรโพลีฟอสเฟต (TPP) อินซูลินนาโนคอมเพลกซ์มีความคงตัวในฟอสเฟตบัฟเฟอร์สูงกว่าอินซูลินนาโนพาร์ติเคิล และสามารถป้องกันการทำลายของอินซูลินจากความร้อนและเอนไซม์ได้สูงกว่านาโนพาร์ติเคิล นอกจากนี้พบว่าการมี TPP ในระบบจะเร่งการทำลายของอินซูลินโดยทริปซิน และการทำลายอินซูลินเพิ่มขึ้นเมื่อเพิ่มปริมาณ TPP จากการศึกษาการนำส่งอินซูลินนาโนคอมเพลกซ์ทางจมูกในสัตว์ทดลอง พบว่าอินซูลินนาโนคอมเพลกซ์ลดระดับน้ำตาลในเลือดได้ 34 – 47% จากระดับปกติ ประสิทธิภาพในการการลดระดับน้ำตาลในเลือดของอินซูลินนาโนคอมเพลกซ์เพิ่มขึ้นเมื่อเพิ่มปริมาณของพอลิเมอร์ และลดลงเมื่อเพิ่มดีกรีการแทนที่ของสายโซ่ PEG ประสิทธิภาพในการลดน้ำตาลในเลือดของอินซูลินนาโนคอมเพลกซ์มีความสัมพันธ์กับการเปลี่ยนแปลงเฉียบพลันของเนื้อเยื่อบุโพรงจมูก อินซูลินนาโนคอมเพลกซ์ที่เตรียมจาก TMC มีฤทธิ์เป็นสารเพิ่มการดูดซึมของอินซูลินทางจมูกที่มีผลระคายเคืองต่อเนื้อเยื่อบุโพรงจมูกในระดับสูง ในขณะที่อินซูลินนาโนคอมเพลกซ์ที่เตรียมจาก PEGylated TMC โดยเฉพาะ $PEG(5k)_{68\rho}$-g-TMC400-40 เพิ่มการดูดซึมของอินซูลินทางจมูกและมีผลระคายเคืองต่อเนื้อเยื่อบุโพรงจมูกในระดับต่ำ อย่างไรก็ตามการระคายเคืองของนาโนคอมเพลกซ์เป็นแบบชั่วคราว เนื้อเยื่อบุโพรงจมูกสามารถกลับคืนสู่สภาพเดิมได้หลังจากการให้ทางจมูก 24 ชั่วโมง จากการให้อินซูลินนาโนคอมเพลกซ์ทางจมูกติดต่อกันทุกวันเป็นเวลาหนึ่งสัปดาห์ พบว่าเนื้อเยื่อบุโพรงจมูกมีการปรับตัวตามการระคายเคืองเฉียบพลันของอินซูลินนาโนคอมเพลกซ์แต่ละชนิด โดยสรุปผลการศึกษาในสัตว์ทดลองบ่งชี้ว่านาโนคอมเพลกซ์ที่ตรียมจาก $PEG(5k)_{680}$-g-TMC400-40 มีศักยภาพในการเป็นตัวนำส่งอินซูลินทางจมูกที่มีความปลอดภัยและประสิทธิภาพ

252 หน้า

CONTENTS

		Page
ACKNOWLEDGEMENTS		**iii**
ABSTRACT (ENGLISH)		**iv**
ABSTRACT (THAI)		**v**
LIST OF TABLES		**viii**
LIST OF FIGURES		**x**
LIST OF ABBREVIATION		**xxiii**
CHAPTER		
I	**INTRODUCTION**	**1**
II	**LITERATURE REVIEW**	**7**
	1. Insulin	7
	2. The nasal cavity	12
	3. Protein-polyelectrolyte complexes	22
	4. Polymers	25
	5. Mucoadhesion	32
	6. Histological study	36
III	**MATERIAL AND METHOD**	**44**
IV	**RESULTS AND DISCUSSION**	**70**
	1. Synthesis and characterization of TMC polymers	70
	2. Characterization of PEGylated TMC copolymers	91
	3. Preparation and characterization of insulin NC	95
	4. Preparation and characterization of insulin NP	101
	5. Colloidal stability	110
	6. Effect of temperature on the stability of insulin	115
	7. Insulin protection from enzymatic degradation	117
	8. Adhesion of TMC and PEGylated TMC copolymers to mucus layer	131
	9. Binding and uptake of insulin NC	135

CONTENTS (continued)

10. Transport studies 141
11. CLSM visualization of localization of insulin NC on E12 cells 141
12. Hypoglycemic activity of nasal insulin NC in vivo 144
13. Histopathological effect of insulin NC on the nasal epithelium 152

V CONCLUSION 186

REFERENCES 190

APPENDIX 216

PUBLICATION AND PRESENTATIONS 249

BIOGRAPHY 252

LIST OF TABLES

Table		Page
1	Non-invasive insulin delivery options	11
2	Examples of absorption enhancers used in intranasal insulin delivery	13
3	Effect of substitution degree on the properties of TMC	29
4	Properties and IC_{50} values of PEGylated TMC copolymers (45)	31
5	Comparison between rat and human nasal cavity (201)	38
6	The reaction conditions in the synthesis of TMC polymers	49
7	A random sampling of rats for investigation of acute histopathological effects	64
8	Morphological signs of the rat nasal mucosa utilized as criteria for grading the membrane-damaging effects	69
9	Substitution degrees of different TMC polymers	71
10	Intrinsic viscosity values and relative molecular weight of different TMC polymers	74
11	Characteristics of the interaction between ss-mucin particle and TMC polymers	87
12	Cytotoxicity of TMC polymers on L929 fibroblast cells following 3 h incubation as determined by MTT assay (n = 4)	90
13	Properties and molecular weights of PEGylated TMC copolymers	92
14	Formulation and characteristics of the polyelectrolyte complexes and nanoparticles with insulin. The initial concentration of insulin was 1 mg/ml in all the formulations	99
15	Effect of polymer/insulin (+/–) charge ratio on the physicochemical properties of insulin NC. The initial concentration of insulin was 1 mg/ml in all the formulations	100
16	Formulation and characteristics of the NC and NP with insulin. The initial concentration of insulin was 1 mg/ml in all the formulations	106

LIST OF TABLES (continued)

Table		Page
17	Influence of TPP/polymer mass ratio on the properties of insulin NP[a]. The concentration of insulin and TMC are 1 mg/ml in all formulations	107
18	Effect of order of mixing on the properties of insulin NP. The concentration of insulin and TMC are 1 mg/ml in all formulations	109
19	Characterization of administered insulin solutions and NC	146
20	Pharmacodynamics after nasal administration of insulin in various formulations to rats	150
21	Summary of the effects of insulin NC on morphological changes of the rat nasal epithelium in region (ii) after 4 h single intranasal administration (n = 3)	156
22	Summary of the effects of insulin NC on morphological changes of the rat nasal epithelium in region (iii) after 4 h single intranasal administration (n = 3)	157
23	Summary of the effects of insulin NC on morphological changes of the rat nasal epithelium in region (ii) after one-week daily intranasal administration (n = 3)	174
24	Summary of the effects of insulin NC on morphological changes of the rat nasal epithelium in region (iii) after one-week daily intranasal administration (n = 3)	175
25	Published Mark-Houwink constants for chitosans with varying of DA and solvents of different pH and ionic strength, μ (264)	225

LIST OF FIGURES

Figure		Page
1	The primary structure of human insulin. Adapted from ref. (81).	8
2	Anatomy of the human nasal cavity (138).	15
3	Schematic diagrams of (A) respiratory epithelium (136) and (B) olfactory epithelium (140).	17
4	Micrograph showing a cell junction (arrow) of the epithelial cells with the tight junction area enlarged in the insert (139).	19
5	(a) Synthetic route of TMC (157) and (b) ^{1}H-NMR spectrum of TMC.	27
6	Synthetic route of PEGylated TMC copolymer (45).	30
7	(a) the two stages in mucoadhesion and (b) the interpenetration theory (167).	33
8	Light photomicrographs of the different types of surface epithelia that line the rat nasal airways. (A) olfactory epithelium (oe); (B) transitional epithelium (te); (C) and (D) respiratory epithelium (re); (E) stratified squamous epithelium (se). b, basal cells; bg, Bowman's glands; bo, bone; bv, blood vessels; c, ciliated cells; m, mucus (goblet) cells; n, nerve bundles; osn, olfactory sensory neurons; s, sustentacular cells; sg, subepithelial glands (135).	39
9	Illustration of the lateral wall and turbinates in the nasal passage of mouse. Vertical lines indicate the location of the anterior faces of 4 tissue blocks routinely sampled for light microscopic examination (T1 – T4). N, nasoturbinate; MT, maxilloturbinate; 1E-6E, 6 ethmoid turbinates; Na, naris; NP, nasopharynx; HP, hard palate; OB, olfactory bulb of the brain; S, septum; V, ventral meatus; MM, middle meatus; L, lateral meatus; DM, dorsomedial meatus; MS, maxillary sinus; NPM, nasopharygeal meatus; arrow in T2, nasopalatine duct (135).	42

LIST OF FIGURES (continued)

Figure		Page
10	Diagram of the surgical procedure and schematic diagram of the fixative perfusion of the rat nasal cavity.	66
11	Diagram illustration of (A) the nasal lateral wall and (B) the surface features of the oral cavity in rat. Those landmarks used to define cutting positions for the division of the nasal cavity into regions (i) – (v) are indicated: naris (Na); nasoturbinate (N); maxilloturbinate (MT); ethmoturbinates (E); nasopharynx (NP); olfactory bulb of the braine (OB); upper incisor root (I); incisive papilla (P); first palatal ridge (R1); second palatal ridge (R2); first upper molar (M) (72, 135).	67
12	^{1}H-NMR Spectra of TMC400-20-60 and TMC400-20-20, prepared in one reaction step and one reaction step with one addition step, respectively.	72
13	Intrinsic viscosity of TMC in 2%HAc/0.2 M NaAc at 25°C as a function of M_w determined by GPC.	76
14	Potentiometric titration and 1st derivative curves of different TMC polymers.	78
15	The pH dependence of water solubility of (a) TMC400-10-40 (DD/DQ = 3), (b) TMC400-40-40 (DD/DQ = 1) and (c) TMC400-80-10 (DD/DQ = 0.1).	80
16	Effect of dimethylation degree on the solubility of TMC. Polymer concentration was 5 mg/ml.	82
17	Effect of ionic strength on the water solubility of (a) TMC400-10-40 (DD/DQ = 3), (b) TMC400-40-40 (DD/DQ = 1) and (c) TMC400-80-10 (DD/DQ = 0.1). Polymer concentration was 5 mg/ml.	83
18	Change in observed particle size and zeta potential of ss-mucin particles when mixed with the various volumes of 1 mg/ml TMC400-40-40 solution. Concentration of ss-mucin suspension was 1 % w/v at pH 6.8.	85

LIST OF FIGURES (continued)

Figure		Page
19	Correlation between the ratio of DD/DQ of TMC and mucoadhesive bond strength measured by the mucin particle method. Each point represents the mean ± SD of three experiments.	88
20	Change in observed zeta potential of mucin particles when mixed with the various volumes of 1 mg/ml polymer solutions. Concentration of mucin suspension: 1% w/v, pH 6.8. The reported data are the mean ± SD of three experiments.	94
21	Schematic representation of insulin NC formation.	96
22	Evolution of particle size and Kcps value of TMC400-10/insulin complexes versus [Pol]/[Ins] mass ratio. (■) size; (□) Kcps. TMC400-10 solution (1 mg/ml) was titrated with insulin solution (1 mg/ml). Particle size and Kcps values of the NC were monitored by dynamic laser light scattering.	97
23	Atomic force microscopy images of (a) TMC400-40/insulin NC at optimized polymer/insulin mass ratio of 0.3:1 (5 × 5 μm), (b) TMC400-40/insulin NC at polymer/insulin mass ratio of 1:1 (5 × 5 μm), (c) three-dimensional image of 0.3:1 TMC400-40/insulin NC and (d) three-dimensional image of 1:1 TMC400-40/insulin NC. The inserts are height mode of each image.	102
24	Schematic representation of insulin NP formation.	103
25	Correlation between insulin/polymer (–/+) charge ratio and TPP/polymer mass ratio for NP formation of (a) TMC400-40, (b) $PEG(5k)_{40}$-g-TMC100-40.	105
26	Atomic force microscopy image of (a) insulin loaded TMC400-40 NP at optimal TPP:polymer:insulin mass ratio of 0.4:1:1 (5 × 5 μm) and (b) its three-dimensional image. The insert is height mode of image.	111

LIST OF FIGURES (continued)

Figure		Page
27	Colloidal stability of (a) TMC400-40 and (b) PEG(5k)$_{40}$-g-TMC100-40 after diluting with pH 6.8 phosphate buffer. Each value represents the mean ± SD of three experiments.	112
28	Effect of ionic strength on the dissociation of insulin NP prepared at different TPP:TMC400-40 ratio. Each value represents the mean ± SD of three experiments.	114
29	Effect of pH on the dissociation of insulin NP prepared at TPP:TMC400-40:insulin of 1.2:2:1 as a function of ionic strength. Each value represents the mean ± SD of three experiments.	116
30	Effect of quaternization degree on the stability of insulin in NC at different temperatures. Each value represents the mean ± SD of three experiments. *Statistically significant differences from the values of free insulin ($p < 0.05$). **Statistically significant differences from the values of at 15 min ($p < 0.05$).	118
31	Effect of PEG substitution degree on the stability of insulin in NC at different temperatures. Each value represents the mean ± SD of three experiments. *Statistically significant differences from the values of free insulin ($p < 0.05$). **Statistically significant differences from the values of at 0 min ($p < 0.05$).	119
32	Stability of insulin in TMC400-40 NC, TMC400-40 NP and PEG(5k)$_{40}$-g-TMC100-40 NC at different temperatures. Each value represents the mean ± SD of three experiments. * Statistically significant differences from the values of at 0 min ($p < 0.05$). ** Statistically significant differences from the values of TMC400-40 NC ($p < 0.05$).	120
33	Effect of (a) quaternization degree and (b) PEG substitution degree on the activity of ApM. Each value represents the mean ± SD of three experiments.	121

LIST OF FIGURES (continued)

Figure		Page
34	Stability of insulin in a presence of ApM (opened square) and in an absence of ApM (closed square). The initial concentration of insulin and ApM were 450 μg/ml and 50 mU/ml, respectively. Data represent mean ± SD of three experiments.	123
35	Effect of (a) quaternization degree and (b) PEG substitution degree on the activity of trypsin. Each value represents the mean ± SD of three experiments.	124
36	Effect of (a) quaternization degree and (b) PEG substitution degree on the enzymatic degradation of insulin by trypsin. Each value represents the mean ± SD of three experiments. The initial concentrations of insulin and trypsin were 450 μg/ml and 300 BAEE IU/ml, respectively. All NC prepared at optimal [P]:[Ins] mass ratio. * Statistically significant differences from the values of free insulin ($p < 0.05$). ** Statistically significant differences from the values of TMC400-40 ($p < 0.05$).	125
37	Effect of TPP on the enzymatic degradation of insulin by trypsin. Each value represents the mean ± SD of three experiments. The initial concentrations of insulin and trypsin were 450 μg/ml and 300 BAEE IU/ml, respectively. –✳– free insulin (w/ trypsin); –□– free insulin + TPP (w/o trypsin); –■– free insulin + TPP (w/ trypsin); –△– insulin NP with TPP:TMC400-40:insulin mass ratio of 0.2:1:1 (w/ trypsin); –▲– insulin NC with TMC400-40:insulin mass ratio of 1:1 (w/ trypsin).	127
38	(a) Effect of TPP:TMC400-40 mass ratio on the stability of insulin in NP and (b) Relationship between TPP:TMC400-40 mass ratio and degradation rate of insulin. Each value represents the mean ± SD of three experiments. The initial concentrations of insulin and trypsin	129

LIST OF FIGURES (continued)

Figure		Page
	were 450 μg/ml and 300 BAEE IU/ml, respectively.	
39	Enzymatic degradation of insulin by trypsin. Each value represents the mean ± SD of three experiments. The initial concentrations of insulin and trypsin were 450 μg/ml and 300 BAEE IU/ml, respectively. TMC400-40 NC = [P]:[Ins] of 0.3:1, TMC400-40 NP = [P]:[Ins]:[TPP] of 1:1:0.2, PEG(5k)$_{40}$-g-TMC100-40 NC = [P]:[Ins] of 1:1, PEG(5k)$_{40}$-g-TMC100-40 NP = [P]:[Ins]:[TPP] of 2:1:0.2. * Statistically significant differences from the values of free insulin (p < 0.05). ** Statistically significant differences from the values of NC (p < 0.05).	130
40	Binding of polymers as a function of (a) quaternization degree and (b) PEG substitution degree at 37°C with the E12 cell line. Polymer (250 μg/ml) solutions were incubated with the cells for 2 h. Error bars represent mean ± SD (n = 4). * p < 0.05, compared with that of Ch400 in (a) and that of TMC400-40 in (b).	132
41	Effect of NAC on polymer adherence to monolayers. Each point represents the mean ± SD of four experiments. * p < 0.05, compared with that of TMC400-40.	134
42	Effect of polymer:insulin mass ratio on the amount of insulin binding and uptake to E12 monolayer and percentage of amount of insulin released from TMC400-40/insulin NC. The concentration of insulin and mucin was of 125 μg/ml and 2 mg/ml, respectively. Each point represents mean ± SD (n = 4 for insulin binding and uptake and n = 3 for insulin release). * p < 0.05, compared with that of free insulin.	136
43	Schematic representation of behavior of insulin NC prepared (a) at optimal polymer:insulin mass ratio and (b) at higher polymer:insulin mass ratio after adhering to mucus layer.	138

LIST OF FIGURES (continued)

Figure		Page
44	Amount of insulin binding and uptake to E12 monolayer and percentage of amount of insulin released from NC as a function of (a) quaternization degree and (b) PEG substitution degree. NC were prepared at polymer:insulin mass ratio of 2:1. The concentration of mucin was of 2 mg/ml. Each point represents mean ± SD (n = 4 for insulin binding and uptake and n = 3 for insulin release). * $p < 0.05$, compared with that of free insulin. ** $p < 0.05$, compared with that of TMC400-40.	139
45	Percentage of amount of insulin internalized / attached in E12 cell monolayers after 2 h incubation. Each point represents the mean ± SD of three experiments. ** $p < 0.05$.	142
46	Confocal micrograph images of E12 cell monolayers incubated with TMC400-40-insulin NC for 2 h at 37°C (a) green filter, (b) red filter, (c) blue filter, (d) overlay of a,b,c. TMC400-40 was labeled with Oregon Green 488, insulin was labeled with TRITC and nuclei were labeled with DAPI.	143
47	Three-dimensional xz- and yz-projections of confocal images of E12 cell monolayers incubated with (a) TRITC-labeled insulin, (b) Oregon Green 488-labeled TMC400-40 and (c) double-labeled NC for 2 h at 37°C.	145
48	Effect of insulin:polymer mass ratio on the mean plasma glucose levels following nasal administration of 4 IU/kg insulin NC to rat. Data represent mean ± SEM of six experiments.	148
49	Effect of PEG substitution degree on the mean plasma glucose levels following nasal administration of 4 IU/kg insulin NC to rat. The NC were prepared at insulin:polymer mass ratio of 1:5. Data represent mean ± SEM of six experiments.	149

LIST OF FIGURES (continued)

Figure		Page
50	Diagrammatic representation of the lateral wall and turbinates in the nasal airway of the rat and anterior faces of region (ii) and region (iii) of the rat nasal cavity. N, nasoturbinate; MT, maxilloturbinate; E, ethmoid turbinates; HP, hard palate; S, septum; V, ventral meatus; MM, middle meatus; L, lateral meatus; DM, dorsomedial meatus.	154
51	Photomicrographs of untreated rat nasal epithelium. (a) respiratory epithelium; (b) olfactory epithelium; b, basal cell; c, ciliated cell; g, goblet cell; lp, lamina propria with Bowman's glands; n, bundles of nerve fibers; NS, nasal septum; osn, olfactory sensory neuron; s, supporting (sustentacular) cell. HE staining.	155
52	Diagram of location of lesions in region (ii) after 4 h exposed to (a) insulin solution, (b) Ins/TMC400-40 NC (1:0.3), (c) Ins/TMC400-40 NC (1:1), (d) Ins/TMC400-40 NC (1:5), (e) Ins/PEG(5k)$_{298}$-g-TMC400-40 NC (1:5) and (f) Ins/PEG(5k)$_{680}$-g-TMC400-40 NC (1:5). N, nasoturbinate; MT, maxilloturbinate; HP, hard palate; S, septum; V, ventral meatus; MM, middle meatus; L, lateral meatus; DM, dorsomedial meatus. Dose of insulin was 4 IU/kg.	158
53	Diagram of location of lesions in region (iii) after 4 h exposed to (a) insulin solution, (b) Ins/TMC400-40 NC (1:0.3), (c) Ins/TMC400-40 NC (1:1), (d) Ins/TMC400-40 NC (1:5), (e) Ins/PEG(5k)298-g-TMC400-40 NC (1:5) and (f) Ins/PEG(5k)680-g-TMC400-40 NC (1:5). E, ethmoid turbinates; HP, hard palate; S, septum; V, ventral meatus; MM, middle meatus; L, lateral meatus; DM, dorsomedial meatus. Dose of insulin was 4 IU/kg.	159
54	Photomicrographs of a vertical section from (a) region (ii) and (b) region (iii) of the rat nasal cavity 4 h after dosing 20 μl of 4 IU/kg insulin solution. L, undosed side; R, dosed side; S, nasal septum. HE staining.	161

LIST OF FIGURES (continued)

Figure		Page
55	Photomicrographs of a vertical section from (a) region (ii) and (b) region (iii) of the rat nasal cavity after 4 h nasal administration of Ins/TMC400-40 NC (4 IU/kg insulin, Ins:Pol = 1:0.3). The dosed side (R) of region (ii) shows moderate goblet cell distension (GD) and that of region (iii) shows slight vascular congestion (VC) and moderate subepithelial edema (SE). L, undosed side; S, nasal septum. HE staining.	162
56	Photomicrographs of a vertical section from (a) region (ii) and (c) region (iii) of the rat nasal cavity after 4 h nasal administration of Ins/TMC400-40 NC (4 IU/kg insulin, Ins:Pol = 1:1). Figure 56b is higher magnification for dosed side (R) of Figure 56a showing discharged mucus (m), pyknotic nuclei (PN) and epithelial disruption (d). The dosed side (R) of region (iii) shows mucus hypersecretion (m) and vascular congestion. L, undosed side; S, nasal septum. HE staining.	163
57	Photomicrographs of a vertical section from region (ii) of the rat nasal cavity after 4 h nasal administration of Ins/TMC400-40 NC (4 IU/kg insulin, Ins:Pol = 1:5). Figure 57b is higher magnification for dosed side (R) of Figure 57a showing a denuded basement membrane with discharged mucus (m) containing cells shed from the epithelium in the lumen. L, undosed side; S, nasal septum; d, epithelial disruption. HE staining.	164
58	Photomicrographs of a vertical section from region (iii) of the rat nasal cavity after 4 h nasal administration of Ins/TMC400-40 NC (4 IU/kg insulin, Ins:Pol = 1:5). Figure 58b is higher magnification for dosed side (R) of Figure 58a showing a discharged mucus (m) containing cells shed from the epithelium in the lumen., subepithelial	165

LIST OF FIGURES (continued)

Figure		Page
	edema (SE) and epithelial disruption (d). L, undosed side; S, nasal septum. HE staining.	
59	Photomicrographs of a vertical section of dosed side from (a) region (ii) and (b) region (iii) of the rat nasal cavity after 4 h nasal administration of Ins /PEG(5k)298-g-TMC400-40 NC (4 IU/kg insulin, Ins:Pol = 1:5). E, ethmoid turbinate; d, epithelial disruption; N, nasoturbinate; S, nasal septum; SE, subepithelial edema. HE staining.	168
60	Photomicrographs of a vertical section from (a) region (ii) and (b) region (iii) of the rat nasal cavity after 4 h nasal administration of Ins /PEG(5k)$_{680}$-g-TMC400-40 NC (4 IU/kg insulin, Ins:Pol = 1:5). The dosed side (R) of region (ii) goblet cell distension (GD) and that of region (iii) shows vascular congestion (VC). L, undosed side; S, nasal septum. HE staining.	169
61	Photomicrographs of respiratory epithelium from region (ii) after 24 h nasal administration of insulin/TMC400-40 NC (4 IU/kg insulin, Ins:Pol = 1:5). (a) undosed side showing normal respiratory epithelium; (b) dosed side showing epithelial regeneration with mucus secretion; bv, blood vessel; c, ciliated cell; g, goblet cell; MS, mucus secretion; S, nasal septum. HE staining.	171
62	Photomicrographs of olfactory epithelium from region (iii) after 24 h nasal administration of insulin/TMC400-40 NC (4 IU/kg insulin, Ins:Pol = 1:5). (a) undosed side showing normal olfactory epithelium; (b) dosed side showing olfactory epithelium regeneration with respiratory metaplasia (white arrow head); S, nasal septum. HE staining.	172

LIST OF FIGURES (continued)

Figure		Page
63	Diagram of location of lesions in region (ii) after one-week daily exposed to (a) insulin solution, (b) Ins/TMC400-40 NC (1:0.3), (c) Ins/TMC400-40 NC (1:1), (d) Ins/TMC400-40 NC (1:5), (e) Ins/PEG(5k)$_{298}$-g-TMC400-40 NC (1:5) and (f) Ins/PEG(5k)$_{680}$-g-TMC400-40 NC (1:5). N, nasoturbinate; MT, maxilloturbinate; HP, hard palate; S, septum; V, ventral meatus; MM, middle meatus; L, lateral meatus; DM, dorsomedial meatus. Dose of insulin was 4 IU/kg.	176
64	Diagram of location of lesions in region (iii) after one-week daily exposed to (a) insulin solution, (b) Ins/TMC400-40 NC (1:0.3), (c) Ins/TMC400-40 NC (1:1), (d) Ins/TMC400-40 NC (1:5), (e) Ins/PEG(5k)$_{298}$-g-TMC400-40 NC (1:5) and (f) Ins/PEG(5k)$_{680}$-g-TMC400-40 NC (1:5). E, ethmoid turbinates; HP, hard palate; S, septum; V, ventral meatus; MM, middle meatus; L, lateral meatus; DM, dorsomedial meatus. Dose of insulin was 4 IU/kg.	177
65	Photomicrographs of rat nasal epithelium after one-week daily nasal administration. (a) respiratory epithelium from region (ii) treated with insulin solution (4 IU/kg) showing moderate goblet cell distension and subsequent extension in epithelium height; (b) respiratory epithelium from region (ii) treated with Ins/TMC400-40 NC (4 IU/kg insulin, Ins:Pol = 1:0.3) showing slight goblet cell hyperplasia; (c) respiratory epithelium from region (ii) treated with Ins/TMC400-40 NC (4 IU/kg insulin, Ins:Pol = 1:1) showing epithelial hyperplasia; (d) olfactory epithelium lining ethmoid turbinate from region (iii) treated with Ins/TMC400-40 NC (4 IU/kg insulin, Ins:Pol = 1:1) showing respiratory metaplasia with goblet cell hyperplasia; g, goblet cell; GD, goblet cell distension; L, undosed side; R, dosed side; oe, olfactory epithelium; S, nasal septum. HE staining.	179

LIST OF FIGURES (continued)

Figure		Page
66	Photomicrographs of respiratory epithelium from region (ii) after one-week daily nasal administration of insulin/TMC400-40 NC (4 IU/kg insulin, Ins:Pol = 1:1) showing (a) goblet cell distension and mucus secretion (PAS staining), (b) goblet cell hyperplasia (HE staining) (c) cystic formation (HE staining) and (d) regeneration with thickening of epithelial layer (HE staining). C, cyst; g, goblet cell; GD, goblet cell distension; MS, mucus hypersecretion.	181
67	Photomicrographs of olfactory epithelium from region (iii) after one-week daily nasal administration of insulin/TMC400-40 NC (4 IU/kg insulin, Ins:Pol = 1:1) showing (a) cystic formation and respiratory metaplasia (arrow head), (b) respiratory metaplasia, (c) epithelial hyperplasia with respiratory metaplasia (arrow head) and (d) pressure atrophy of olfactory epithelium (double-headed arrows) with subepithelial gland hyperplasia. C, cyst; G, subepithelial gland. HE staining.	182
68	Photomicrographs of a vertical section of dosed side from (a) region (ii) and (b) region (iii) of the rat nasal cavity after one-week daily nasal administration of Ins/PEG(5k)298-g-TMC400-40 NC (4 IU/kg insulin, Ins:Pol = 1:5). Figure 68a shows respiratory epithelium with goblet cell hyperplasia and cystic formation. Figure 68b shows olfactory epithelium with pressure atrophy of the olfactory epithelium (double-headed arrows), epithelial discontinuation and subepithelial gland hyperplasia. C, cyst; DE, discontinuation of epithelium; G, subepithelial gland; PN, pyknotic nuclei; R, dosed side; S, nasal septum. HE staining.	183
69	HPLC chromatogram of insulin.	218
70	Standard curve of insulin.	219

LIST OF FIGURES (continued)

Figure		Page
71	The ubbelohde capillary viscometer (262).	221
72	A representative plot for intrinsic viscosity calculation (TMC400-40). Both η_{red} and η_{inh} are plotted on the same graph and the common intercept of the plots on the ordinate at c = 0 is the intrinsic viscosity.	223
73	The representative calculation of viscosity-average molecular weight of the chitosan.	226

LIST OF ABBREVIATIONS

%	percent
~	approximately
°C	degree Celsius
Å	angstrom
η	viscosity
η_{sp}	specific viscosity
η_{red}	reduced viscosity
η_{rel}	relative viscosity
η_{inh}	inherent viscosity
$[\eta]$	intrinsic viscosity
τ	turbidity
AB	alcian blue
ACN	average count number
AE	association efficiency
ANOVA	analysis of variance
AFM	atomic force microscopy
AOC	area over the curve
ApM	aminopeptidase-M
BAEE	N-benzoyl-L-arginine ethylester
BCA	Bicinochoninic acid
CLSM	confocal laser scanning microscope
C_{min}	minimum concentration
cm^2	square centrimeter (s)
CNS	central nervous system
Da	Dalton (s)
DAPI	4,6-diamidino-2-phenylindole

LIST OF ABBREVIATIONS (continued)

DMEM	dulbecco's modified Eagle's medium
DMSO	dimethylsulfoxide
dl	deciliter (s)
DLS	dynamic light scattering
DD	degree of dimethylation
DO_3	degree of *O*-methylation at 3-hydroxy group
DO_6	degree of *O*-methylation at 6-hydroxy group
DQ	degree of quaternization
EDTA	ethylenediaminetetraacetic acid
ELS	electrophoretic light scattering
Eq.	equation
et al.	et alli, and others
etc.	et celera, and other things
F_{dyn}	relative pharmacodynamic availability
FCS	fetal calf serum
GPC	gel permeation chromatography
h	hour (s)
HE	haematoxylin and eosin
^{1}H-NMR	proton nuclear magnetic resonance
HPLC	high pressure liquid chromatography
Hz	hertz
i.e.	id est, that is
i.n.	intranasal administration
i.p.	intraperitoneal injection
IC_{50}	concentration that inhibits cell growth by 50% as compared with control cell growth
IDDM	insulin-dependent diabetes mellitus
IU	immunizing unit, international unit
Kcps	kilo counts per second

LIST OF ABBREVIATIONS (continued)

kDa	kilo Dalton (s)
kg	kilogram (s)
L	liter (s)
NAC	N-acetyl-L-cysteine
NC	nanocomplexes
NIDDM	non-insulin-dependent diabetes mellitus
NP	nanoparticles
mg	milligram (s)
min	minute (s)
ml	milliliter (s)
mM	millimolar (s)
mm	millimeter (s)
mm^2	square millimeter (s)
mPas	millipascal second
MTT	3-(4,5-dimethylthiazol-2-yl)-2,5-diphenyltetrazoliumbromide
MW	molecular weight
M_n	number-average molecular weight
M_v	viscosity-average molecular weight
M_w	weight-average molecular weight
M_w/M_n	polydispersity (the ratio of weight-average to number-average molecular weight)
nm	nanometer (s)
PAS	periodic acid Schiff
PBS	phosphate buffered saline
PCS	photon correlation spectroscopy
PEG	poly(ethylene glycol)
pH	the negative logarithm of the hydrogen ion concentration
pI	isoelectric point
PID	polydispersity index

LIST OF ABBREVIATIONS (continued)

PPC	protein-polyelectrolyte complexes
PY	process yield
QELS	quasi-electric light scattering
r^2	coefficient of determination
rpm	revolutions per minute
s	second (s)
s.c.	subcutaneous injection
SD	standard deviation
SEM	standard error of mean
SLS	static light scattering
SPR	surface plasmon resonance
T_{min}	time to minimum concentration
TEER	transepithelial electrical resistance
TFA	trifluoroacetic acid
TMC	N-trimethyl chitosan
TRITC	tetra-methyl-rhodamine isothiocyanate
µl	microliter (s)
µg	microgram (s)
µm	micrometer (s)
v/v	volume by volume
w/v	weight by volume
w/w	weight by weight

CHAPTER I
INTRODUCTION

Human insulin is a 5808 Da protein consisting of 51 amino acids. The protein itself is composed of 2 chains, denoted as A and B, and linked by disulfide bridges between cysteine residues. It has been introduced into clinical practice since 1922 as a therapeutic drug for the treatment of Type 1 diabetes (also called insulin-dependent diabetes mellitus, IDDM) (1). Up to date, it has been indicated in the treatment of Type 2 diabetes or non-insulin-dependent diabetes mellitus (NIDDM) (2, 3). The administration of insulin in the form of a bolus subcutaneous injection is the basis of insulin therapy which is disturbing and poorly accepted by patient, particularly when multiple daily injections are required. In addition, the subcutaneous injection causes a problem to glycaemic control since the pharmacokinetics of conventional insulin preparations given by this route make it difficult in simulating the fast release of endogenous insulin at mealtimes (4).

Although oral route offers a number of inherent advantages over injection; namely it is inexpensive, easy and convenient to administer and relatively free from side effects, it is well known that the bioavailability of insulin after oral application is limited due to its instability in the gastrointestinal tract (enzymatic barrier) and low permeability through the intestinal mucosa (absorption barrier) (5). These problems enforce up to now non-oral routes of insulin have been developed consisting of buccal, sublingual, rectal, ocular, intravaginal, transdermal, intranasal and pulmonary (6-8). Amongst these, intranasal is the most promising due to several unique advantages (9), such as rapid absorption, comparatively high bioavailability, bypass of first-pass hepatic metabolism, ease of convenience and self-medication, and patient compliance. Moreover, the pharmacokinetic profile of intranasal insulin is similar to that obtained by intravenous injection and bears close resemblance to the ‘pulsatile’ pattern of endogenous insulin secretion during mealtimes. It was suggested that

intranasal therapy has considerable potential for controlling post-prandial hyperglycemia in the treatment of both Type 1 and Type 2 diabetes (10).

However, effective insulin absorption via the nasal route is low due to its high molecular weight and hydrophilicity (11). Several strategies have been explored so far to enhance the absorption efficacy of insulin by the nasal route, including the uses of surfactants, permeation enhancers, protease inhibitors, carrier systems and chemical modifications of insulin (10, 12). Amongst these, the use of colloidal polymeric particulate delivery systems, particularly mucoadhesive nanoparticles (NP) represents a promising concept (13-17).

Among the mucoadhesive polymers used for preparing insulin-loaded NP, most experience has been gained with chitosan because of its excellent biocompatibility, biodegradability and mucoadhesive property (13-16, 18). However, chitosan is a polymer that lacks the advantage of good solubility at physiological pH values. This fact implies that chitosan is effective as an absorption enhancer only in a limited area where the pH values are closed to its pKa. From this reason, it may not be a suitable carrier for targeted peptide and protein drugs to nasal cavity. To further enhance the solubility of chitosan and to improve its mucoadhesive and/or permeation enhancing properties, various derivatives such as trimethyl chitosan (TMC) (19), *N*-carboxymethyl chitosan, *N*-sulfo-chitosan (20), thiolated chitosan (21, 22) and PEGylated chitosan (23) have been developed. Currently, TMC has received considerable attention as a novel excipient in drug delivery systems.

TMC is a partially quaternized derivative of chitosan firstly synthesized by Muzzarelli and Tanfani (24) in an attempt to increase solubility of chitosan in water at neutral and basic pH values. The increase in solubility is achieved by replacing the primary amino group on the C-2 position of chitosan with quaternary amino groups (25). It has been shown that TMC can decrease the transepithelial electrical resistance (TEER) of Caco-2 cell monolayers and increase the transport of several hydrophilic compounds, peptide and protein drugs both *in vitro* (Caco-2 cells) (26-29) and *in vivo* (rats and pigs) (30-32). Recently, TMC has been used in drug and gene delivery not only in peroral route (33) but also in ocular (34), intranasal (17, 35, 36), buccal (37, 38), pulmonary (39, 40) and rectal (41) routes.

It is well known that polymer structure is a main factor influencing its physicochemical properties. Several research groups have studied the structure-physicochemical property relationship of TMC and reported that the properties of TMC depend on degree of quaternization (DQ) at 2-amino groups and degree of *O*-methylation at 3- and 6-hydroxy groups (DO_3 and DO_6, respectively) (19, 29, 42). The best permeation enhancement of peptide and protein drugs is achieved when using TMC with DQ ca. 48% (29). Moreover, high DO_3 and DO_6 found in TMC with high DQ decrease the solubility of the polymer (19). Although mucoadhesive properties and cytotoxicity of TMC with different DQ have been explored, the results are controversial. Synman et al. (42, 43) found that the mucoadhesive properties of TMC decreased with an increase in DQ, whereas Sandri et al. (37) reported the opposite results. Regarding the cytotoxicity, Thanou et al. (44), Amidi et al. (17) and Florea et al. (39) indicated that TMC was nontoxic even at high DQ. However, Mao et al. (45) found that TMC with DQ of 40% exhibited time- and dose-dependent cytotoxic responses which increased with increasing molecular weight. Similar results had been found by Kean et al. (46) who showed that the cytotoxicity of TMC increased with increasing DQ. These discrepancies may be attributed to different degrees of dimethylation (DD) of TMC. TMC with the same DQ but different in DD may show different properties in the mucoadhesion and cytotoxicity. In general, the mucoadhesion and cytotoxicity of TMC can probably be attributed to the interaction between positively charged groups of TMC and anionic components (sialic acid) of the glycoproteins in mucus layer and on the surface of epithelial cells (45). We hypothesized that an increase in DD aside from DQ may affect the interaction of polymer and mucus layer/epithelial cells, resulting in the reduction in mucoadhesion and cytotoxicity. However, to the best of our knowledge, no experimental data are available to support this hypothesis. Therefore, the influence of the DQ together with the DD on the mucoadhesive properties and cytotoxicity was simultaneously elucidated.

Recently, novel polymer, PEGylated TMC copolymer has been developed by grafting activated poly(ethylene glycol) (PEG) onto TMC via amino groups (45). Polymers are water soluble over the entire pH range of 1-14 and exhibit biocompatibility improvement. It was found that PEGylation with PEG 5 kDa is

sufficient to increase the biocompatibility of TMC and appears to be beneficial for drug carrier containing insulin (45, 47) and plasmid DNA (48). Since the copolymers are positively charged and consist of PEG chain, they would increase the mucoadhesive properties via (i) interpenetration of PEG chains into the mucus and (ii) ionic interactions between cationic groups of modified TMC and the anionic moieties within the mucus layer. PEGylated TMC copolymer is therefore an appropriate polymer to use for preparing insulin-loaded NP. However, to our knowledge no studies to date have been reported about their mucoadhesive properties.

In studies of mucoadhesive polymers, many techniques have been used to measure mucoadhesion of polymers under *in vitro* conditions. However, in several studies, the mucoadhesive properties of polymer were only evaluated in either the contact stage (49, 50) or consolidation stage (51, 52). Currently, many methods have been developed and utilized to investigate the interaction between mucoadhesive polymer/particles and mucus substrates, including a mucin particle method (53), an in *vitro* HT29-MTX-E12 (E12) cell culture experiment (54) and a confocol laser scanning microscope (CLSM) (53-55). Each technique provides different information which can be used to complement each other to accomplish the fully information on the mucoadhesive mechanism of mucoadhesive polymers.

In recent years, nanoparticulate systems have been identified as suitable peptide/protein carriers. In particular, NP are able to protect drug from degradation, to improve permeation/penetration of the drugs across mucosal surface and also to control the release of the encapsulated or adsorbed drug (56, 57). The NP possess marked mucoadhesive properties that can prolong the residence time of drug carrier in the nasal cavity and also increase the intimacy of contact between drug and mucus membrane at the absorption sites. With regard to chitosan based formulations, nearly all insulin-loaded NP have been prepared by ionotropic gelation with tripolyphosphate (TPP) counterions (16, 58-61). However, no report has been published about insulin-loaded TMC and PEGlyated TMC NP. Therefore, insulin NP based on TMC and PEGylated TMC copolymers were prepared in this study and influence of process parameters on the properties of NP was investigated.

Due to amphoteric nature of proteins, they can interact with polyanionic and polycationic polymers below and above their isoelectric points (pI) to form

nanocomplexes (NC) or protein-polyelectrolyte complexes (PPC). All of the states of protein NC may be achieved by the selection of the polyelectrolyte, choice of ionic strength and pH, and control of the concentration of the macromolecular components (62) and in some cases, order of mixing (47, 63). From this concept, insulin can be formed NC with positively charged chitosans/chitosan derivatives at pH above its pI (apparent pI 6.4). Insulin/chitosan NC was first mentioned by Dyer et al. (16) and investigated in details by Mao et al.(47). Therefore, polyelectrolyte complexation can be used as an alternative method for preparing insulin loaded TMC and PEGylated TMC NP. Since insulin NC are prepared in the absence of TPP compared to insulin NP, the influence of TPP on the physiochemical properties of particles and stability of insulin should be elucidated. The information obtained from this study will be useful for the preparation of the carriers to avoid unforeseen adverse effects from the third component.

Although *in vitro* cell culture models, such as Caco-2 cells and Calu-3 cell are frequently used to characterize drug transport and metabolism of nasal drug delivery (17, 64-67), the experimental conditions are far from the actual environment of the nasal cavity. The results could vary among different experimental models and the *in vitro* results might not correlate with the *in vivo* results. To avoid such problems, an in vivo rat model was used in this study to investigate the efficacy of TMC and PEGylated TMC NC as nasal absorption enhancers of insulin.

In general, in clinical use of nasal peptide/protein drug formulations, apart from efficiency of drug absorption improvement, the interaction of nasal peptide/protein drug formulations with the nasal epithelium have to be considered and their safety should be verified. The effects of nasal drug formulations on the nasal epithelium have been studied by using several models, including *in vitro* cytotoxicity assays with mucus-producing, submucosal gland carcinoma cell line Calu-3 (17, 39, 67), *in vitro* measurements of chicken embryo trachea (17, 44, 68), determination of the release of marker compounds from the rat nasal cavity (69) and histopathological evaluation of the nasal cavity (69-71). Since the anatomical division of the rat nasal cavity by the midline septum enables the assessment of histopathological effects by direct comparison of the treated and untreated side (72), the evaluation of nasal histology have gained to study toxicity of several nasal absorption enhancers (69, 73-

75). Furthermore, it can be used to study chronic inhalation toxicity of materials used in industry (76-79). Importantly, the toxicological studies of a longer exposure period should further characterize for their safety profiles.

Therefore, this study was designed to develop insulin-loaded NP based on TMC and PEGylated TMC copolymers and to fabricate a new alternative nano-carrier for nasal insulin delivery called NC in the absence of TPP. Their physiochemical properties were compared. The physiological properties of polymers such as water solubility, mucoadhesive property and cytotoxicity were investigated. Insulin NC and NP were prepared and the influences of various parameters on their physicochemical properties were investigated. These properties were determined in terms of particle size, average count number (Kcps), particle size distribution (PID), zeta potential, process yield, % drug association efficiency and particle morphology. The colloidal and chemical stabilities were evaluated by dynamic laser light scattering and HPLC methods, respectively. Mucoadhesion of polymers and corresponding insulin NC were studied with free mucin using a mucin particle method and with mucus-secreting E12 monolayer using a cellular association assay. Their adhesion to mucus layers was visualized by CLSM. Furthermore, to evaluate the advantages of insulin NC as an intranasal delivery, the *in vivo* absorption of insulin across nasal mucosa was investigated in Wistar rats. Concomitantly, the histological effects of NC on the rat nasal epithelium were studies using a perfusion fixation technique.

The ultimate goals of this study were:

- to investigate the influence of polymer structure of TMC and PEGylated TMC copolymer on water solubility, cytotoxicity and mucoadhesive property;

- to develop and compare the physicochemical properties of insulin nano-carrier systems from TMC and PEGylated TMC copolymer using two techniques: polyelectrolyte complexation and ionotropic gelation with TPP counter ion;

- to study *in vivo* nasal absorption of insulin NC and histopathology of nasal epithelium following single and one-week daily nasal administration of insulin NC.

CHAPTER II
LITERATURE REVIEW

1. Insulin

Insulin is a polypeptide hormone synthesized in and secreted from the β cells within the islets of Langerhans in the pancreas. Major function of insulin is to counter the concerted action of a number of hyperglycemia-generating hormones and to maintain low blood glucose levels. Besides, insulin has a substantial effect on small vessel muscle tone, controls storage and release of triglycerides and cellular uptake of both amino acids and some electrolytes (80). Insulin has been introduced into clinical practice since 1922 as a therapeutic drug for the treatment of Type 1 diabetes (insulin-dependent diabetes mellitus, IDDM), ad disease characterized by β cell failure and insulin deficiency (1). To this day, insulin supplementation is often required to attain good glycemic control in Type 2 diabetes (non-insulin-dependent diabetes mellitus, NIDDM) which characterized by defects in both insulin secretion and insulin action (2, 3).

1.1 Insulin structure

The insulin molecule consists of two polypeptide chains. The A-Chain contains 21 amino acids and B-Chain 30 amino acids which are linked by disulphide brides between cysteine (Cys) residues. A third disulfide bond occurs within the A-Chain. The primary structure (amino acid sequence) of human insulin is shown in Figure 1. In dilute solution and in the circulation, insulin exists as a monomer which the A-Chain forms two antiparallel α-helices and the B-Chain forms an α-helix, turn β-strand conformation. However, in most pharmaceutical formulations it forms a dimer. In the presence of zinc ions and at higher insulin concentrations, three insulin dimers form a stable hexamer (6:2, insulin/zinc) (80, 81). Insulin structure and molecular weight varies slightly between species. Human insulin has a molecular

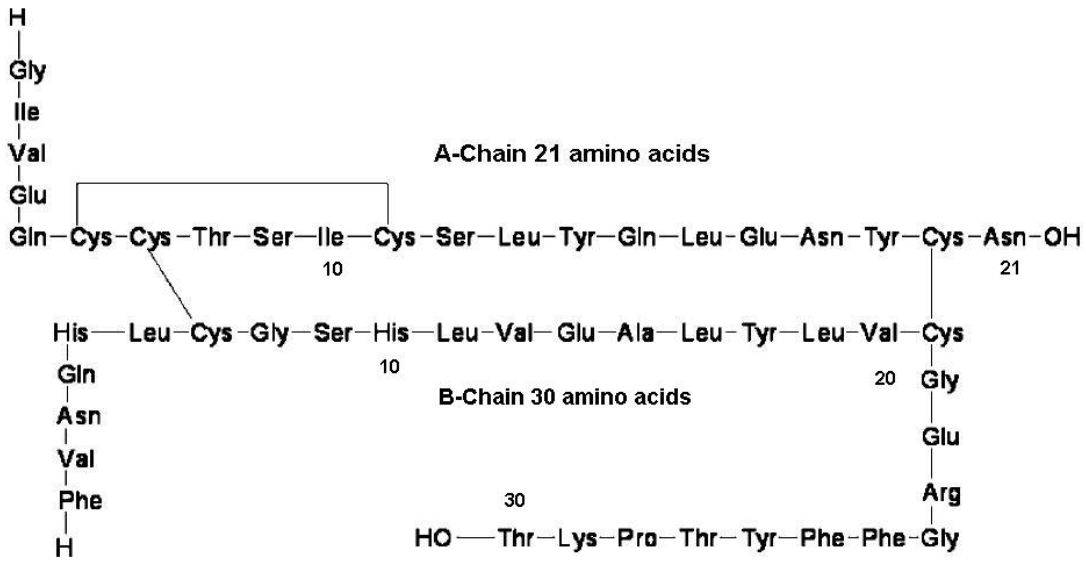

Figure 1. The primary structure of human insulin. Adapted from ref. (81).

weight of 5808 Da and an isoelectronic point (pI) of approximately 5.4. Below its pI, insulin has a net positive charge and is soluble at pH < 4.5. Above the pI, insulin has a net negative charge and is soluble at pH > 6.3. The human insulin is identical to pig insulin, an animal insulin which has been used extensively for diabetes treatment, except that the last amino acid of the B-Chain (B30) for the pig is alanine (Ala) instead of threonine (Thr). Bovine insulin (also used therapeutically) differs from human insulin at three positions. The Thr at position B30 and A8 of human insulin is replaced by Ala and Isoleucine (Ile) at position A10 is replaced by Valine (Val) (80).

1.2 Insulin administration: current status

Since insulin was first used successfully in humans to treat the symptoms of diabetes mellitus, subcutaneous injection has been the only route of delivery of insulin therapy to diabetic patients. The appropriate insulin dosage is dependent upon the glycemic response of the individual to food intake and exercise regimens. For virtually all Type 1 and many Type 2 patients, the time course of insulin action requires three or more injections per day to meet glycemic goals. This represents a major cause of reduced compliance to treatment. In addition, the subcutaneous therapeutic regimen is central to the problem of glycemic control since insulin absorption via the subcutaneous route is generally slow and sustained and, thus, dose not mimic the normal pulsatile pattern of endogenous insulin secretion on the non-diabetic (4, 82). To improve the control of post-prandial hyperglycemia in diabetics, many insulin analogues have been developed (81, 83, 84). Molecular engineering or the substitution of amino acids into the native primary sequence produces novel analogues such as insulin Lispro (Humalog®), insulin Aspart (Novolog®), insulin Glargine (Lantus®) and insulin Glulisine (Apidra®). They have been effective in modifying pharmacokinetics to produce rapid-acting or slow-release biopharmaceuticals (81, 83). Besides, conjugating fatty acid or polyethylene glycol (PEG) to the side chains of the amino acids of insulin, such as insulin Detemir (Levemir®) and InsuLar™, also act to modified pharmacokinetics (81, 84). However, they still require injection regimen in the treatment.

Due to the disadvantages of injectable therapy, other alternative, non-parenteral routes for the delivery of insulin in an attempt to improve glycemic control

have been explored including oral, sublinglual, buccal, pulmonary, nasal, transdermal, rectal, ocular, intravaginal as listed in Table 1. Amongst these, the oral delivery is the most convenient and acceptable route. Unfortunately, insulin's oral bioavailability is limited because insulin is too large and hydrophilic to readily cross the intestinal mucosa and insulin undergoes extensive enzymatic and chemical degradation, in particular by α-chymotrypsin and trypsin (5, 85). At present time, the nasal and pulmonary routes have received great attention due to their several advantages: large surface for drug absorption, low thickness epithelial barrier, extensive vascularization and relatively low proteolytic activity compared to other administration routes, together with the absence of the first-pass effect. Moreover, the ready accessibility of intranasal and pulmonary administrations makes them possible for patients on long term therapy to self-medication (86, 87). In case of pulmonary delivery of insulin, the studies are mainly focused on the development of pulmonary insulin delivery devices such as Exubera™ (Nektar Therapeutics, Pfizer; Aventis SA) and AERx® iDMS (Aradigm Corporation; Novo Nordisk A/S). Both of them are in phase III testing and the results thus far demonstrate comparable efficacy to that of subcutaneous insulin (6, 8, 88).

1.3 Intranasal insulin delivery

Actually, intranasal delivery of insulin was first proposed in 1935, but did not generate enthusiasm until the 1980s. The plasma pharmacokinetic profile following intranasal insulin is similar to that obtained by intravenous injection and, incontrast to subcutaneous insulin delivery, bears close resemblance to the 'pulsatile' pattern of endogenous insulin secretion during meal-times. The literature suggests that intranasal insulin therapy has considerable potential for controlling post-prandial hyperglycemia in the treatment of both Type 1 and Type 2 diabetes (10). Gizurarson and Bechgaard (125) studied the nasal enzyme activity towards human insulin and reported that the enzymatical degradation is not found to be limiting for and intranasal application of insulin. However, effective insulin absorption via the nasal route is low. Hilsted et al. (111) studied the effective of intranasal insulin in 31 patients with type 1 diabetics and found that the doses of intranasal insulin needed to achieve specified levels of glycemic control were about 20 times higher than the doses needed with

Table 1. Non-invasive insulin delivery options

Non-invasive routes	References
Oral	(58, 89-95)
Buccal	(96-99)
Sublingual	(100, 101)
Intranasal	(10, 16, 71, 74, 102-111)
Pulmonary	(60, 88, 112-115)
Transdermal	(116-118)
Ocular	(119, 120)
Rectal	(121-123)
Intravaginal	(123, 124)

subcutaneous injection. The main barriers to insulin absorption include the very active mucociliary clearance (126), and low permeability of the nasal epithelium (11). Indeed, the nasal epithelium has been shown to effectively exclude many drugs with molecular sizes larger than 1 kDa (11). Several strategies have been explored so far to enhance the absorption efficacy of insulin by the nasal route, including the use of surfactants, phospholipids, bioadhesive polymers and carrier systems (Table 2). They are able to modulate nasal epithelial permeability to insulin and/or prolong the residence time of the drug formulation in the nasal cavity. However, many studies reported that most achievements of increased plasma insulin levels by surfactant and phospholipids have been related to the potential membrane irritation or damage as evidenced by protein release, epithelial disruption, excessive mucus discharge and cilliary toxicity (73, 74, 127). Clinically, the use of lecithin, bile salts or laureth-9 as absorption enhancers for nasal absorption enhancement caused nasal irritation in patients (8). Drejer et al. (128) reported that intranasal insulin administration with a medium-chain phospholipids (didecanoyl-L-α-phosphatidylcholine) as an absorption enhancer caused rapid increase in the serum insulin concentration in healthy individuals, reaching glucose reducing peak in 20 – 45 min. Therefore, the design of insulin carrier systems avoiding harmful effects has become a topic of intensive research. The use of colloidal particulate delivery systems, particularly bioadhesive nanoparticles represents a promising concept (15, 16, 18, 71).

2. The nasal cavity

The nose is a structurally and functionally complex organ in the upper respiratory tract. It is the primary site of entry for inhaled air in the respiratory system of mammals and therefore has many important and diverse functions. The nose not only serves as the principal organ for the sense of smell, but is also functions to efficiently filter, warm and humidify the inhaled air before it reaches the lower airways (10, 135).

2.1 Anatomy of the nose

The nasal cavity is divided into two halves by the nasal septum and extends posterior to the nasopharynx, while the most anterior part of the nasal cavity, the nasal

Table 2. Examples of absorption enhancers used in intranasal insulin delivery

Absorption enhancers	References
Surfactants and bile salts	
- Tetradecylmaltoside	(129)
- Polyoxyethylene-9-lauryl ether	(73)
- Glycodeoxycholate	(73)
- Sodium glycocholate	(130)
- Dodecylmaltoside	(131)
Phospholipids	
- Didecanoyl-L-α-phosphatidylcholine	(127, 128)
- Lysophosphatidylcholines	(73, 74)
Mucoadhesive polymers	
- Chitosan	(102)
- Thiolated Chitosan	(107)
- *N*-[(2-hydroxy-3-trimethylammonium) propyl] chitosan	(132)
- Cabopol	(104)
- Hydroxypropyl methylcellulose	(104)
Collodial particulate systems	
- Microparticles	(133, 134)
- Nanoparticles	(15, 16, 106)
- Nanocomplexes	(65, 71)

vestibute, opens to the face through the nostril. Each of the two nasal cavities is limited by the septal wall and the lateral wall. The atrium is an intermediate region between the vestibule and the respiratory region, the respiratory region is dominated by inferior, middle and superior turbinates (Figure 2). These folds provide the nasal cavity with a very high surface area compared to its small volume (10, 136, 137). The nasal cavity has a total volume of 15 – 20 ml and a total surface area of about 150 cm^2 which can be divided into three functional regions: the vestibular region (the anterior 10 – 20 cm^2); the respiratory region (about 130 cm^2), occupying the majority of the main part of the nasal cavity and important for the absorption of drugs into the systemic circulation; and the olfactory region (10 – 20 cm^2 in the roof of the nasal cavity) (10, 136).

2.2 Advantages of the nose for drug delivery

Compared to other non-parenteral routes such as buccal, peroral, rectal, transdermal and vaginal, intranasal administration has many advantages. Recently, Ugwoke et al. (137) has summarized the advantages of nose for drug delivery. These include

1. A large surface area available for drug deposition and absorption. The effective absorption surface area of the nasal epithelium is even higher as a result of the presence of microvilli.
2. The nasal epithelium is thin, porous (especially when compared to other epithelial surfaces) and highly vascularized. This ensures high degree of absorption and rapid transport of absorbed substances into the systemic circulation for initiation of therapeutic action.
3. A porous endothelial basement membrane that poses no restriction to transporting the drug into general circulation.
4. Absorbed substances are transported directly into the sustemic circulation thereby avoiding the first pass metabolic effect generally experienced following oral drug administration.
5. In some cases, drugs can be absorbed directly into the CNS after nasal administration bypassing the tight blood-brain barrier.

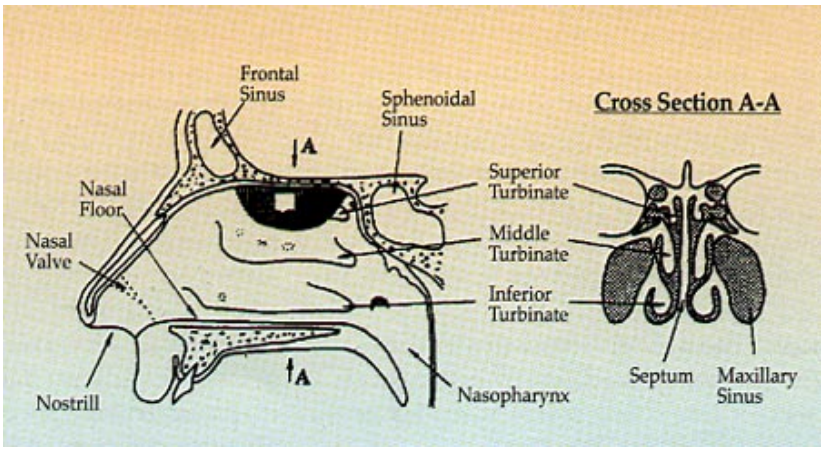

Figure 2. Anatomy of the human nasal cavity (138).

6. Generally speaking, the enzymatic activity of the nasal epithelium is lower than that of the gastrointestinal tract or liver and higher bioavailability of drugs especially proteins and peptides can be achieved. In addition, enzyme inhibitors are more effective following nasal than oral application because of a higher degree of dilution in the latter than in the former.
7. Realization of pulsatile delivery of some drug like human growth hormone, insulin, etc., is higher with nasal drug delivery.
8. The nose is amenable to self-medication that not only lowers the cost of therapy but improves patient compliance as well. The risk of over-dosage is low and nasal lavage can be used to remove unabsorbed excess drug.
9. Reformulation of existing drugs as nasal drug delivery products offers companies the possibility to extend the life cycle of their products.

2.3 Barriers to nasal absorption

In spite of the above advantages and potentials of the nasal drug delivery, there are some major limitations to application of drugs via the nose.

2.3.1 Nasal mucosa

The mucus membranes or mucosa lining the human nasal cavity consist of two layers: the luminal surface epithelium and the underlying connective tissue or laminar propria. The epithelial cells in the nasal vestibule are stratified, squamous and keratinized with sebaceous glands. Due to its nature, the nasal vestibule is very resistant to dehydration and can withstand noxious environmental substances and limits permeation of substances.

The respiratory epithelium is the major lining of the human nasal cavity which consists of four major types of cells, the ciliated and non-ciliated columnar cells, the goblet cells and the basal cells (Figure 3a). Each ciliated cell contains about 100 cilia, while both ciliated and non-ciliated cells possess about 300 microvilli each. Mucus is mainly secreted by the goblet cells.

The olfactory epithelium is found in the posterior part of the nasal cavity. Although it constitutes only about 5% of the total area of the human nasal

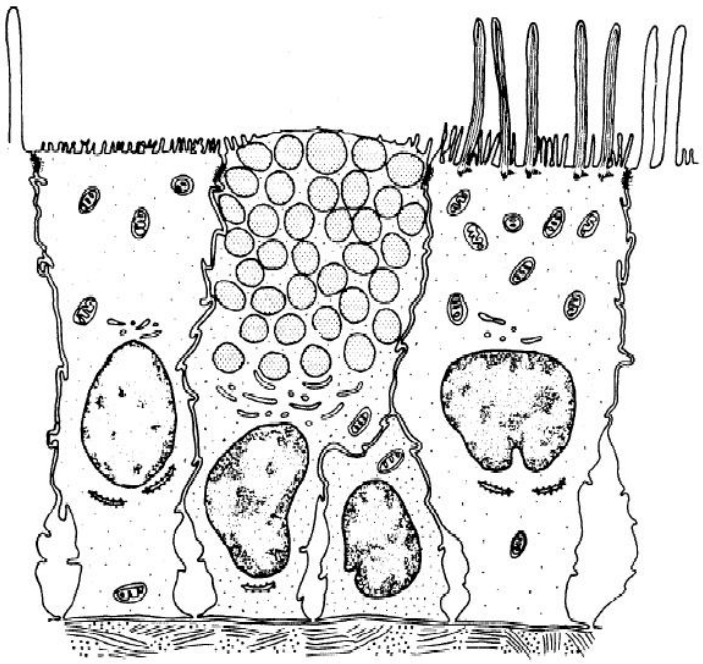

(A)

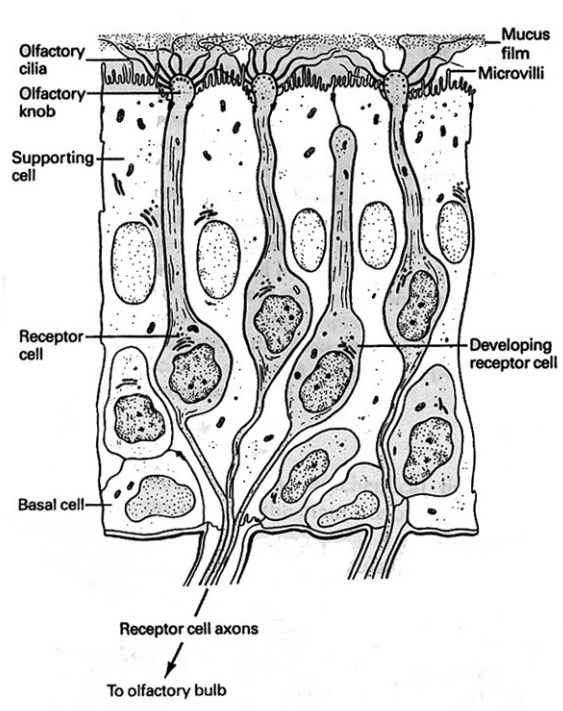

(B)

Figure 3. Schematic diagrams of (A) respiratory epithelium (136) and (B) olfactory epithelium (140).

cavity, it is of considerable interest in drug delivery because it provides a direct pathway from this region of the nasal cavity to brain. The olfactory epithelium comprises sustentacular cells that provide mechanical support by ensheathing neuronal receptor cells and basal cells that are able to differentiate into neuronal receptor cells as needed (10, 68, 136, 137, 139).

Both respiratory and olfactory epithelial cells are interconnected on the apical side of the membrane by narrow belt-like structures that totally surround the cells, the junctional complexes. These complexes comprise in series the zona occludens (tight junction), the zona adherens and the macula adherens which form a dynamic regulatable semi-permeable diffusion barrier between the epithelial cells. Figure 4 shows a cell junction in epithelial cells. The normal diameter of the tight junctions in the nasal cavity is considered to be of the order of 3.9 – 8.4 Å. Although absorption enhancers are able to open tight junctions, it is unlikely these would be able to increase the diameter to more than 10 – 15 times the normal diameter, that is, up to 15 nm (139). This expects that the smallest nanosized particles will only be able to penetrate the nucosal membrane by the paracellular route in a limited quantity. McMartin et al. (11) reported the nasal route is suitable for the efficient, rapid input of variety of drugs of molecular weight below 1000 Da. Therefore, larger particles would have to cross the membrane using a transmudosal route, for example, by endocytosis or a carrier- or receptor-mediated transport processes.

2.3.2 Mucus and mucociliary clearance

Most of the luminal surfaces of the nasal mucosa are covered by a watery, sticky material called mucus. The mucus is produced by goblet cells in the surface epithelium and subepithelial glands in the lamina propria. Mucus secretion is a complex mixture of many substances and consists of about 95% water, 2% mucus glycoproteins (mucins), 1% salts, 1% of other proteins such as albumin, immunoglobulin, lysozyme and lactoferrin, and < 1% lipids. The glycoproteins give mucus its characteristic rheological (visco-elastic) properties which are related to its function of providing a protection coating to the nasal epithelium and mucociliary clearance. About 1.5 – 2 L of nasal mucus is produced daily. This mucus blanket consists of two fluid layers: a viscous gel layer (mucus or epiphase) floats on a less

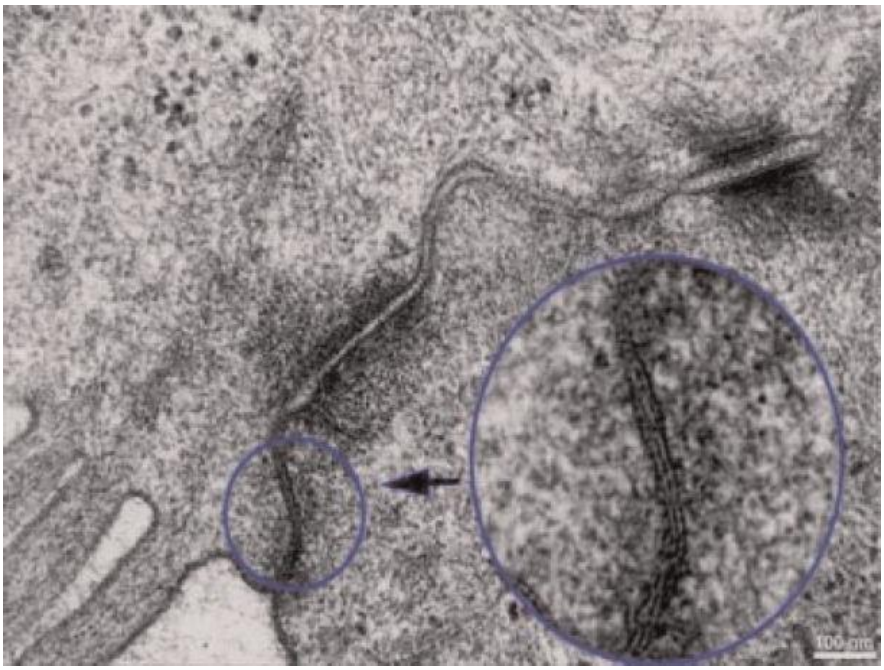

Figure 4. Micrograph showing a cell junction (arrow) of the epithelial cells with the tight junction area enlarged in the insert (139).

viscous sol layer (periciliary fluid layer or hypophase) (10, 68, 136, 137, 141). Both layers are about 5 μm thick. (136, 137). The thickness and viscosity of an overlying mucus layer can significantly influence the rate of drug entry into the underlying tissue. Mastuyama et al. (110, 142, 143) found that the use of *N*-acetyl-L-cystheine (NAC), a potent mucolytic agent in powder formulation or combined use of NAC and a nonionic surfactant in liquid formulation could remarkably increase the nasal absorption of drug. In the NAC reduces the mucus viscosity, which enables drug or surfactant molecules to diffuse more efficiently onto the epithelial membrane to increase nasal mucosal permeability of drug.

Another factor importance for low membrane transport is the general rapid clearance of the administered formulation from the nasal cavity due to the mucociliary clearance mechanism. It is one of the functions of the upper respiratory tract is to prevent noxious substances (allergens, bacteria, viruses, toxins etc.) from reaching the lung. When such materials adhere to, or dissolve in the mucus lining of the nasal cavity, they are transported towards the nasopharynx for eventual discharge into the gastrointestinal tract. Mucus is transported by the symmetric beating action of cilia which beat at a frequency about 10 Hz. Normal mucociliary transit time in humans has been reported to be 12 – 15 min. Transit times of more than 30 min are considered to be abnormal and are indicative of impaired mucociliary clearance. The average rate of nasal clearance is about 8 mm/min, ranging from less than 1 to more than 20 mm/min (10, 68, 137). The rate of mucus turnover has a significant effect on the performance of mucoadhesive delivery systems, since the dosage from will only remain attached to the mucosal tissue for the time period that the mucus remains in contact with the nasal surface. The mucociliary clearance can be influenced by environmental, pathological conditions and nasal drug delivery which can affect ciliary beat frequency and mucus production, or mucus viscosity will all lead to increase or decrease in the mucociliary clearance. It has been suggested that the thickness and composition of the double layer are important for mucocialiary transport. If the sol layer is too thin, ciliary beating will be inhibited by the viscous surface layer. On the other hands, if the sol layer is too thick, the gel layer looses its contact with cilia and thus mucociliary clearance is impaired (136). Mayer and Illum (126) studied the effect of anesthetics on the nasal absorption of insulin in rats. They

found that the differences in absorption of insulin are proposed to be due to an effect of the anesthetic agents to a variable degree in the muciliary clearance. Moreover, it is found that the deposition of a formulation in the anterior part of the nasal cavity can decrease clearance and promote absorption as compared to deposition further back in the nasal cavity (144). Nasal spray devices generally deposit the dose in the atrium and on the anterior regions of the inferior and middle turbinates which are largely covered by squamous epithelium; therefore clearance rate is slow. Drops tend to be deposited more posteriorly over a larger area in the respiratory epithelium and/or olfactory region where the administered formulations are cleared more rapidly by the mucociliary clearance systems. As compared between respiratory and olfactory nucosae, turnover time of mucus covering the olfactory mucosa is much slower than that of mucus covering the respiratory mucosa with a turnover time of probably several days (135).

2.3.3 Nasal enzyme

Although the intranasal route avoids the hepatic first-pass metabolism associated with low oral bioavailability, the enzymatic barrier of the nasal mucosa creates a pseudo-first-pass effect which may constitute a significant barrier to peptide absorption. The metabolic enzymes present in nasal cavity include cytochrome P-450 enzymes (oxidative Phase I enzymes), conjugative Phase II enzymes, non-oxidative enzymes and proteolytic enzymes (145). The cytochrome P-450 activity has been found in the olfactory region of the nasal epithelium. Among the exopeptidases and endopeptidases which are active in the nasal mucosa, aminopeptidases, especially aminopeptidase M (ApM) appear to play an important role (145, 146). Activity of ApM was found mostly in the fibrocytes which adhered to basal membrane of the epithelium and glands (147). Gizurarson and Bechgaard (125) studied the degradation of insulin in human nasal washings and reported that less than 0.5% of the intranasally applied insulin dose may be destroyed by local enzymes during the time of absorption. Among the endopeptidases involves, it has been reported that chymotrypsin- and trypsin- like activity is found to be responsible for the initial cleavage of human calcitonin in excised bovine nasal mucosa and the primary metabolites obtained are then cleaved by aminopeptidase activity (148). Sarkar (145)

suggested that the absorption of peptide drugs can be improved by using aminoboronic acid derivatives, amastatin and other enzyme inhibitors.

3. Protein-polyelectrolyte complexes

In the past decade, nanoparticles (NP) have interestingly been investigated as potential carriers for hydrophilic macromolecules such as proteins and vaccines. Although a wide variety of techniques are available for preparing NP such as solvent evaporation, interfacial polymerization and emulsion polymerization methods, most of these approaches involve the use of organic solvents, heat or vigorous agitation which may inactivate the proteins or cause the burst release effect. In recent years, self-assembly of proteins with natural or synthesis polyelectrolytes to form protein-polyelectrolyte complexes (PPC) has drawn increasing attention (47, 149, 150). PPC formation leads to particles with dimensions on a colloidal level, generating optically homogeneous and stable nano-dispersions. Indeed, PPC are not new and have been used extensively in biology and industrial applications over many years for protein purification, immobilization and stabilization of enzymes (151). However, only recently has it been used as drug carriers, especially for DNA condensation and complexation (48, 152, 153).

3.1 The formation of PPC

Due to amphoteric nature of proteins, they can interact with polyanionic and polycationic polymers below and above their isoelectric points (pI) to form PPC (62). All of the states of PPC may be achieved in form of soluble complexes, precipitates or coacervates. The factors influencing the PPC formation are the selection of the polyelectrolyte, choice of ionic strength and pH, and control of the concentration of the macromolecular components and sometimes order of mixing (47, 62). Tsuboi et al. (154) had summarized the main conclusions derived from the number of studies of PPC formation as follows:

1. PPC are formed mainly through electrostatic forces;
2. In salt-free systems, at least, protein molecules are complexed with flexible polyelectrolytes through the stoichiometric formation of ion pairs (or salt linkages) between oppositely charged groups;

3. The ion pairs between the polyelectrolyte and protein molecules are very labile and may be severed by changes in pH as well as by the addition of small ions and polyions;
4. There is an appreciable retention of biochemical function in the resultant complexes; therefore, changes in the three-dimensional conformations of the protein molecules caused by complexation are not so large as to cause a loss of original functions.

From this concept, insulin can be formed PPC with positively charged chitosans / chitosan derivatives such as *N*-trimethyl chitosan (TMC) at pH above its pI of 5.4 (apparent pI 6.4):

$$\text{insulin-COO}^{-+}\text{Na} + \text{Cl}^{-+}\text{N(CH}_3)_3\text{-TMC} \rightarrow \text{insulin-COO}^{-+}\text{N(CH}_3)_3\text{-TMC} + \text{NaCl}$$

Insulin-chitosan PPC is first mentioned by Dyer et al. (16) and investigated in detail by Mao et al. (47) which can be used as an alternative method for preparing protein loaded NP.

3.2 Characterization of PPC formation by turbidimetric titration

There are numerous techniques have been applied to the characterization of PPC, comprising of turbidimetric titration, quasi-elastic light scattering (QELS), static light scattering (SLS), electrophoretic light scattering (ELS) and sedimentation (151, 154). Amongst these, the turbidimetric titration is a simple and sensitivity technique used to investigate the interaction between protein and polyelectrolyte (47, 62, 149, 155).

Since turbidity (τ) is known to be proportional to both the molecular weight and the concentration of particles in a system, the process of PPC formation could be studied by monitoring changes in τ during the titration of protein solutions with a polyelectrolyte. The titration of V_i ml of protein solution with V_t ml of polyelctrolyte titrant with a fixed concentrations of C_{PE} (in g/ml) gives rise to m_x molecules of PPC with a weight-average molecular weigh (M_x). τ may then be expressed as:

$$\tau = HM_xC_x \quad \text{(Eq. 1)}$$

where H is the proportionality constant which depends on the wavelength of light and the refractive index of the medium. C_x is the weight concentration of the PPC (g/ml) with can be given by Eq. 2:

$$C_x = m_x \frac{M_x/N_A}{(V_t + V_i)} \quad \text{(Eq. 2)}$$

where N_A is Avogadro's number.

If only intrapolymer PPC is formed during the titration, then its M_x may be expressed as

$$M_x = M_{PE} + nM_{pro} \quad \text{(Eq. 3)}$$

where n denotes the average number of bound protein molecules per one polyion chain, M_{PE} is the average molecular weight of polyelectrolytes and M_{pro} is the absolute molecular weight of the proteins. Under this assumption of intrapolymer PPC formation, m_x in Eq. 2 is equal to the number (m_{PE}) of polyions added into the system. Thus, C_x can be written as

$$C_x = \left(1 + n\frac{M_{pro}}{M_{PE}}\right)\left(\frac{C_{PE}}{V_i + V_t}\right)V_t \quad \text{(Eq. 4)}$$

Substitution of Eqs. 3 and 4 into Eq. 1 gives

$$\tau = H\left(M_{PE} + nM_{pro}\right)\left(1 + n\frac{M_{pro}}{M_{PE}}\right)\left(\frac{C_{PE}}{V_i + V_t}\right)V_t \quad \text{(Eq. 5)}$$

In practice, the absorbance ($A = (\tau I)/2.3$, where I is cell length) is measured under condition of $V_i \gg V_t$, so Eq. 5 is more conveniently written as

$$A = H\left(\frac{1}{2.3}\right)\left(\frac{C_{PE}}{V_t}\right)\left\{M_{PE} + \left(2n + \frac{n^2 M_{pro}}{M_{PE}}\right)M_{pro}\right\}V_t \qquad \text{(Eq. 6)}$$

If n is constant with V_t, then

$$A = (\text{constant})V_t \qquad \text{(Eq. 7)}$$

As noted above, complexes formed in a salt-free solution are stoichiometric, corresponding to constant n. Therefore, n may be obtained from the slope of A vs V_t (154).

4. Polymers

Among the mucoadhesive polymers used for preparing insulin-loaded NP, most experience has been gained with chitosan (poly[β-(1-4)-2-amino-2-deoxy-D-glucopyranose]) because of its excellent biocompatibility, biodegradability and mucoadhesive property (13-16, 18). However, chitosan is a polymer that lacks the advantage of good solubility at physiological pH values. This fact implies that chitosan would be effective as an absorption enhancer only in a limited area where the pH values are closed to its pKa. For this reason, it may not be a suitable carrier for targeted peptide and protein drugs to nasal cavity. To further enhance the solubility of chitosan and to improve its mucoadhesive and/or permeation enhancing properties, various derivatives such as trimethyl chitosan (TMC) (19), *N*-carboxymethyl chitosan, *N*-sulfo-chitosan (20), thiolated chitosan (21, 22), PEGylated chitosan (23) and PEGylated TMC (45) have been developed. In this study, two chitosan derivatives (TMC and PEGylated TMC) are selected to use as the polymers for preparing insulin loaded NP.

4.1 *N,N,N*-trimethyl chitosan

TMC is a partially quaternized derivative of chitosan which is well-soluble in a wide pH range (pH 1-14) up to 10% (w/v) concentration and shows mucoadhesive propertiy (37, 42, 156). Up to date, TMC has received considerable attention in drug

and gene delivery not only in peroral route (156) but also in ocular (34), intranasal (17, 35, 36), buccal (37, 38), pulmonary (39, 40) and rectal (41) routes.

4.1.1 TMC synthesis

TMC iodide was firstly synthesized by Muzzarelli and Tanfani using formaldehyde and sodium borohydride (24). The increase in solubility is achieved by replacing the primary amino group on the C-2 position of chitosan with quaternary amino groups (25). In 1998, Sieval et al. prepared TMC chloride by reductive methylation of chitosan with methyl iodide as a reagent and *N*-methylpyrrolidone as a solvent in the present of a strong base at elevated temperature as presented in Figure 5a (19). Since that time, almost TMC have been prepared in this manner. The degree of substitution of TMC can be controlled by means of the number of reaction steps, the duration of each reaction step, the type of base and the amount of methyl iodide (19, 157, 158). However, this procedure is not *N*-selective and significant *O*-methylation is observed in TMC with high degree of quaternization (DQ) (19).

4.1.2 Degree of substitution

In general, structure of TMC is characterized by ^{1}H-NMR using D_2O at high temperature of 80°C in order to shift the signal of HOD to a higher field, which allows quantifying the H signals of glucosamine residues. The degree of substitutions in term of DQ, degree of dimethylation (DD) and degree of *O*-methylation at 3- and 6-hydroxy groups (DO_3 and DO_6, respectively) are calculated using data obtained from the ^{1}H-NMR spectra (Figure 5b) according to the previously described method (19, 157, 158) using Eqs. 8 – 11:

$$\%DQ = \left[\frac{[(CH_3)_3]}{[H]} \times \frac{1}{9}\right] \times 100 \quad \text{(Eq. 8)}$$

$$\%DD = \left[\frac{[(CH_3)_2]}{[H]} \times \frac{1}{3}\right] \times 100 \quad \text{(Eq. 9)}$$

$$\%DO_3 = \left[\frac{[(3\text{-}OCH_3)]}{[H]} \times \frac{1}{3}\right] \times 100 \quad \text{(Eq. 10)}$$

(a)

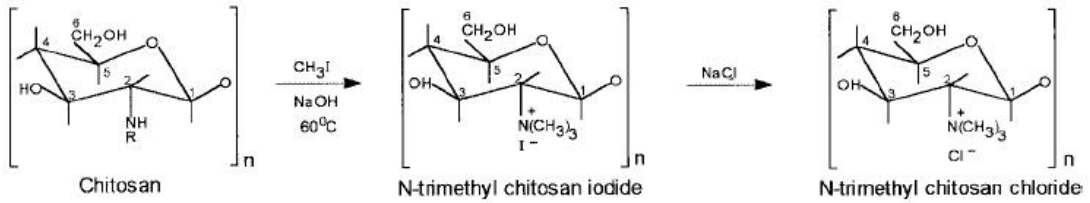

(b)

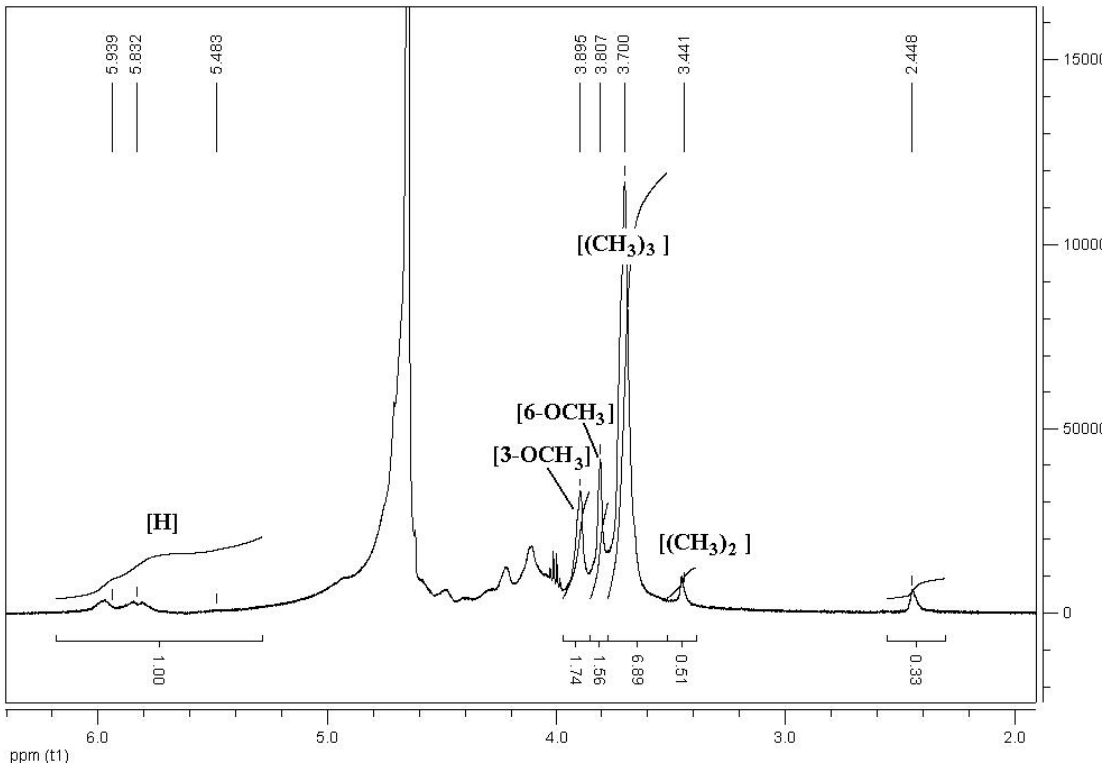

Figure 5. (a) Synthetic route of TMC (157) and (b) ^{1}H-NMR spectrum of TMC.

$$\%DO_6 = \left[\frac{\left[(6\text{-}OCH_3)\right]}{\left[H\right]} \times \frac{1}{3} \right] \times 100 \qquad \text{(Eq. 11)}$$

where $[(CH_3)_3]$ is the integral of trimethyl amino group at 3.3 ppm, $[(CH_3)_2]$ is the integral of dimethyl amino group at 3.0 ppm, $[(3\text{-}OCH_3)]$ is the integral of methyl group for 3-hydroxyl group at 3.5 ppm, $[(6\text{-}OCH_3)]$ is the integral of methyl group for 6-hydroxyl group at 3.4 ppm and [H] is the integral of the ^1H peaks between 4.7 and 5.7 ppm.

It is well known that polymer structure is a main factor influencing its physicochemical properties. Several research groups have studied the structure-physicochemical property relationship of TMC and reported that the properties of TMC depend on DQ, DO_3 and DO_6 as summarized in Table 3.

4.2 Poly(ethylene glycol)-graft-trimethyl chitosan copolymer

PEGylated TMC copolymers were developed by Mao at al. (45) in an attempt to both increase the solubility of chitosan and improve the biocompatibility of TMC, which were prepared via reacting TMC with methoxy-PEG-hydroxysuccinimide (NHS-mPEG) as shown in Figure 6. Based on ^1H-NMR spectra, PEGylated TMC copolymer shows resonance signal at ~3.6 (CH_2), ~6.0 (C=C), ~3.0 ($N(CH_3)_2$) and ~3.3 ($N^+(CH_3)_3$).

It was found that PEGylation with PEG 5 kDa was sufficient to increase the biocompatibility of TMC and appeared to be beneficial for drug carrier containing insulin (45, 47) and plasmid DNA (48). Since the copolymers are positively charged and consist of PEG chain, they would increase the mucoadhesive properties via (i) interpenetration of PEG chains into the mucus (163, 164) and (ii) ionic interactions between cationic groups of modified TMC and the anionic moieties within the mucus layer. PEGylated TMC copolymer is therefore an appropriate model polymer to use in adhesion studies.

The properties and IC_{50} values of PEGylated TMC copolymers used in the present work are summarized in Table 4.

Table 3. Effect of substitution degree on the properties of TMC

Degree of substitution	Properties	Reference
1. DQ	- solubility	(19, 159)
	- mucoadhesion	(37, 42, 43)
	- cytotoxicity	(17, 39, 44-46, 160)
	- permeation enhancer	(26, 28, 29, 34, 37, 39, 159, 161, 162)
2. DO_3, DO_6	- solubility	(19)

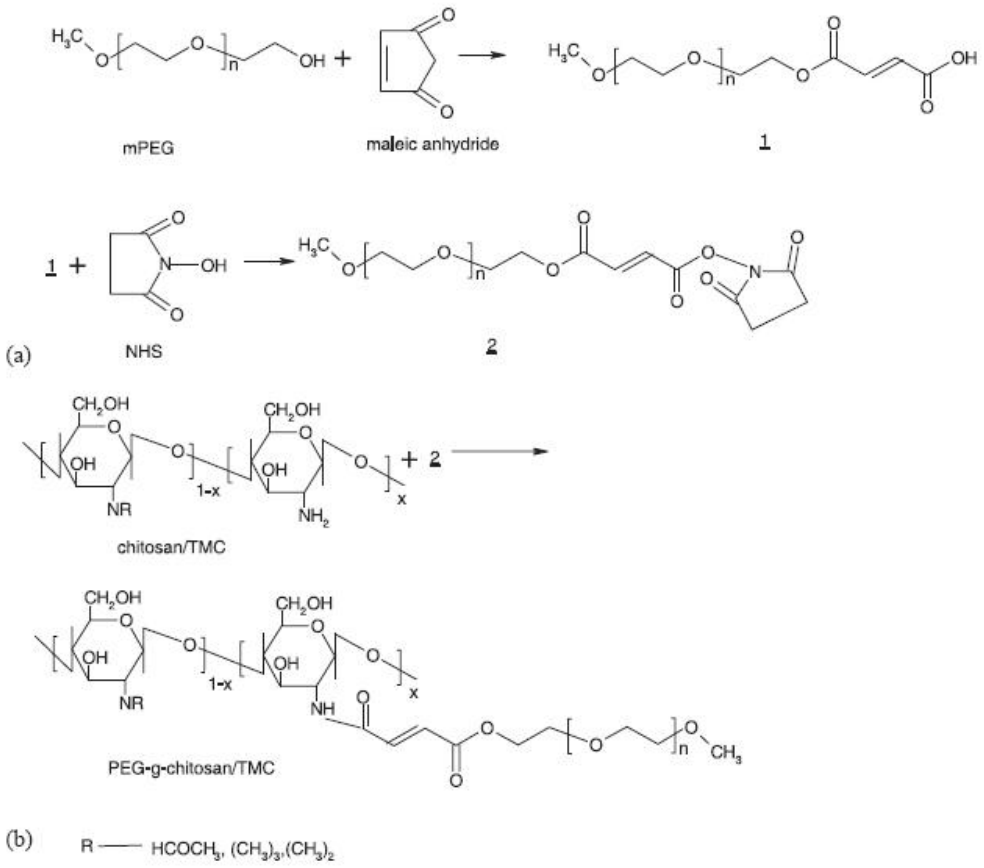

Figure 6. Synthetic route of PEGylated TMC copolymer (45).

Table 4. Properties and IC_{50} values of PEGylated TMC copolymers (45)

Polymer	Degree of substitution (%)[a]	TMC content [%(w/w)]	Theoretical MW (g/mol)	Dalton/ charge[b]	IC_{50} of pure polymers (μg/ml)	
					3 h	24 h
$PEG(5k)_{40}$-g-TMC100	6.4	32.8	300000	640	> 500	40
$PEG(5k)_{298}$-g-TMC400	12.0	22.7	1890000	1042	220	> 500
$PEG(5k)_{640}$-g-TMC400	25.7	11.1	3600000	2446	370	> 500
$PEG(5k)_{680}$-g-TMC400	27.4	10.6	3800000	2655	380	> 500

Cell viability was quantified by MTT assay with a L929 cell line.

[a]Calculated by ^{1}H NMR measurement.

[b]Denoted as Dalton per charge.

5. Mucoadhesion

Bioadhesion is defined as the attachment of synthetic or biological macromolecules to a biological tissue. In the pharmaceutical sciences, when the adhesive attachment is to mucus or a mucous membrane, the phenomenon is referred to as mucoadhesion. In the early 1980s, academic research groups pioneered the concept of mucoadhesion as a new strategy to improve the therapeutic effect of various drugs. The bioadhesion and mucoadhesion may offer certain advantages (165, 166), inducing:

1. Increased absorption rates by minimizing diffusion barriers.
2. Increased residence time leading to enhanced adsorption.
3. Improved localization of drug delivery systems on a certain surface area for purpose of local therapy or for drug liberation at the 'absorption window'.
4. Improved intimacy of contact with the absorption membrane providing the basis for a high concentration gradient as driving force of drug absorption.
5. Improved bioavailability through the protection of bioactive molecules from physical and chemical degradation.

5.1 Mechanism of mucoadhesive

The mucoadhesive phenomenon is a complex process. Several theories have been put forward to explain the mechanisms of polymer-mucin interaction that leads to mucoadhesion, including the electronic theory, the wetting theory, the absorption theory, the diffusion theory and the fracture theory. Taking into account all these theories, the mucoadhesion may be summarized into a two-step process. Initially, an intimate surface contact between the bioadhesive polymers and mucous tissue has to be established (contact stage), and in a consecutive step, both phases may interdiffuse or interpenetrate to a certain extent and formation of secondary chemical bonds, such as electrostatic and hydrophobic interactions, hydrogen bonding, and Van der Waals interactions, occur to consolidate and strengthen the adhesive joint, leading to prolonged adhesion (consolidation stage) (167) as seen in Figure 7a.

(a)

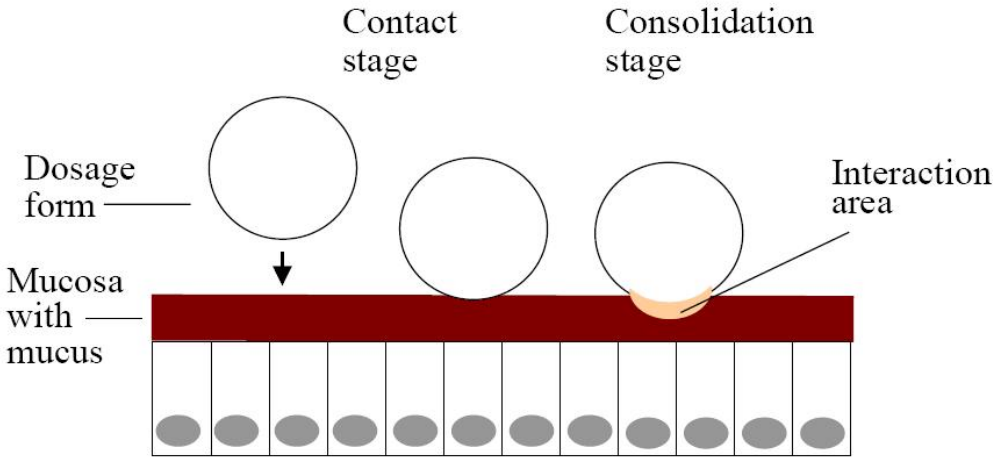

(b)

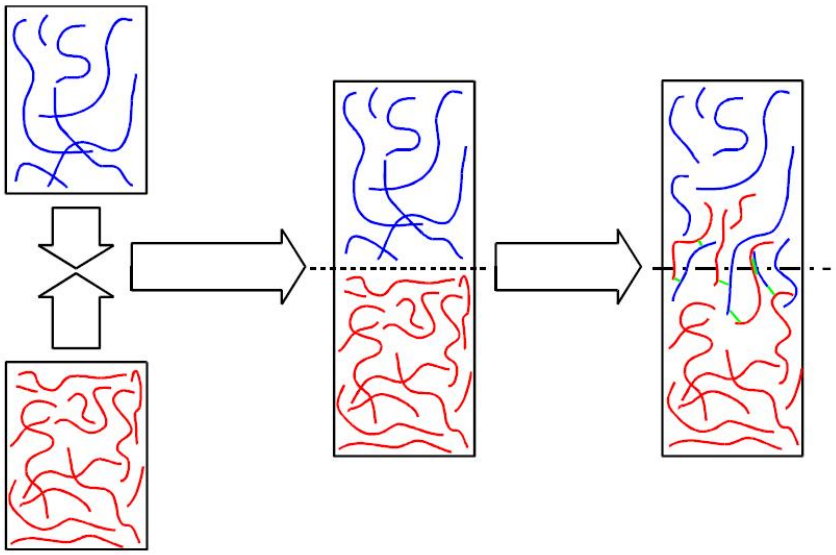

Figure 7. (a) the two stages in mucoadhesion and (b) the interpenetration theory (167).

5.2 Mucoadhesion test

A variety of techniques have been used to measure bioadhesion and mucoadhesion in vitro in each stage. Unfortunately, there is no standard test method established for mucoadhesion, and consequently the data obtained are often subjective and difficult to compare due not only to the different parameters used but also to the fact that the results obtained depend on the experimental conditions (52).

According to contact stage, the major technique used to study mucoadhesion is tensiometric methods (37, 42, 168-172) which measure the force necessary to separate the two surfaces after the mucoadhesive bond. The mucoadhesive strength of polymers can be determined by using the intrinsic mucoadhesivity, maximum force of detachment and work of adhesion. Other methods used to explain mucoadhesive mechanism in the contact stage are the measurement of contact angle or surface tension which examines the surface energy thermodynamics of mucus and the mucoadhesive polymer (173, 174) and the rotating cylinder method which uses time of adhesion as a measure of the strength of the mucoadhesion (169, 170).

A rheological examination (175-182) is widely used to evaluate the consolidation stage of mucoadhesive interaction, on the concept that the viscosity of polymer/mucin mixture is the net result of the resistance to flow exerted by individual chain segments, physical chain entanglements and (non) covalent intermolecular interactions, which are the same as the interaction involved in the process of mucoadhesion. Several values have been used as an in vitro parameter to determine the mucoadhesive properties of polymers. Those are viscosity (η), storage modulus (G'), loss modulus (G'') and loss tangent ($\tan \delta$). Apart from the rheological method, turbidimetric measurements (51, 183, 184), analytical ultracentrifugation (185, 186), fluorescence polarization method (187), spectroscopic investigation (179, 188) are also used to study the mucoadhesive interaction between polymers and mucin.

In case of particulate systems, most studies of their mucoadhesiveness have been performed in animals (*in vivo*) (189-191) and/or excised gut tissues (*ex vivo*) (51, 54, 171, 183, 189-193). The concept of these studies is the measurement of the remained or adsorbed fluorescent- / radioactive-labeled particles after applying to animals or to isolated gut tissues. Moreover, the mucoadhesiveness of particles can

be examined by measuring mucin adsorbed on particles, allowing to measure adsorption kinetics and adsorption isotherms (51, 183).

At the present time, many methods have been developed and utilized to investigate the interaction between mucoadhesive polymers/particles and mucous substrates, including mucin particle method (53), a surface plasmon resonance (SPR) (49, 53, 194), an atomic force microscopy (AFM) (195, 196), A confocal laser scanning microscope (CLSM) (53-55, 197, 198), an *in vitro* cell culture model (54) and a flow cytometry (198).

In this study, the mucin particle method, *in vitro* cell culture model and CLSM had been used as experimental techniques for investigation of mucoadhesion of polymers and PPC. The details of them are described as the following.

5.2.1 The mucin particle method

The mucin particle method is a simple mucoadhesion test for polymer developed by Takeuchi et al. (53). The adhesive properties between polymer and mucin are determined by using the change in particle size and zeta potential of the original mucin particles after mixing with polymer solutions. Moreover, it had been reported that using the precisely size-controlled mucin, the occupying area of one chitosan molecule on the surface of a mucin particle could be calculated and this could be successfully applied to evaluate the coating phenomenon of the particulate systems with chitosan in developing the systems.

5.2.2 In vitro cell culture model

Generally, studies on the adhesion of polymers to mucosal surfaces have mainly used tensiometry as a method of choice. However, it dose not allow quantitative assessment of the adherence of soluble polymers to fresh viable tissue under physiologic conditions. Recently, Keely et al. (54) had developed *in vitro* mucus-secreting HT29-MTX-E12 (E12) cell culture model to study the adhesion of soluble polymers under physiologic conditions in which epithelial barrier function could be examined in parallel. It was found that E12 monolayers gave similar data to isolated rat intestine sacs.

The E12 cell is the sub-clone of the human colon carcinoma HT29 cell line treated with metrotrexate (MTX) (199). It forms tight junctions, confluents monolayers and elaborates a 150 μm continuous mucus gel layer that corresponds to in vivo measurement of human small intestine. Moreover, it expresses the mucins MUC1 and MUC2 which are found in the small intestine and are implicated in host-pathogen relationships. The adherence of polymers to E12 monolayers is determined by measuring the fluorescence intensity of the polymer solution and/or the cell-associated polymer (54, 200).

5.2.3 CLSM

The CLSM had become a well-established technique to visualize the three-dimensional (3D) surface structure of samples. The 3D distribution of emitted fluorescence inside (transparent) samples has been used to characterize the mucoadhesive properties of the polymers and particulate systems both *in vivo* (53, 55, 197) and *in vitro* (54, 198). For *in vivo* study, at the appropriate time after administration of fluorescent-labeled polymers or particles, the intestinal tissues are removed, washed with physiological medium and fixed in fixation medium. The specimens are sliced to generate sections for confocal laser scanning microscopic observation. In case of *in vitro* experiments, mucosal cells or monolayer are incubated with fluorescent-labeled bioadhesive polymers/particles. After washing unbound polymers/particles, the cells are then examined under confocal laser scanning microscope. The extent of adhering on the mucosa or absorbing in submucosa level is observed by fluorescence intensity. Furthermore, confocal laser scanning images can be applied to explain their mechanism and effectiveness after administration of drugs.

6. Histological study

In general, in clinical use of nasal peptide/protein drug formulations, apart from efficiency of drug absorption improvement, the interaction of nasal peptide/protein drug formulations with the nasal epithelium should be considered and their safety can be verified. Histopathological evaluation of the nasal cavity is one of several methods which determine the effects of nasal drug formulations on the nasal epithelium (69-71).

The estimation on human risk from nasal drug formulations is a complex process that may include direct observation of exposed people, but more often relies on extrapolations from toxicology studies using laboratory animal species such as rat, dog and monkey (135, 201). The noses of humans and laboratory animals have major structural differences. A comparison of nasal cavity surface area as a function of body weight shows the relationship rat > dog > monkey > human. Calculations of dose multiples in laboratory animals, relative to humans, are affected by these relationships (201).

In this study, the interaction of nasal insulin formulation with the nasal epithelium was studied using the rat model. A comparison of the nasal anatomy of human and rat is summarized in Table 5. Since the anatomical division of the rat nasal cavity by the midline septum enables the assessment of histopathological effects by direct comparison of the treated and untreated side (72), the evaluation of nasal histology has gained to study toxicity of several nasal absorption enhancers (69, 73-75). Furthermore, it was used to study chronic inhalation toxicity of materials used in industry (76-79).

6.1 Cellular composition of nasal surface epithelium

Besides the differences in the gross architecture of the nose among different laboratory animals, there are also specie differences in the surface epithelial cell populations lining the nasal passages. However, pathological evaluation of all laboratory animal species used generally considers the possible changes seen in the four basic epithelial types. These include squamous epithelium, transitional epithelium, respiratory epithelium and olfactory epithelium as shown in Figure 8 (135, 202, 203).

6.1.1 Stratified squamous epithelium

It is composed of a basal layer covered with several layers of squamous epithelial cells that become successively flatter towards the mucosal surface (Figure 8E). It lines the vestibule and ventral meatus.

Table 5. Comparison between rat and human nasal cavity (201)

	Rat	Human
Weight (kg)	0.25	70.0
Nares cross section (mm^2)	0.7	140.0
Length (cm)	2.3	8.0
Surface area (cm^2)	10.4	181.0
Surface area/weight[a] (cm^2/kg)	41.6	2.6
Volume[a] (ml)	0.4	19.0
Turbinate complexity	Double scroll	Simple scroll

[a]Both sides

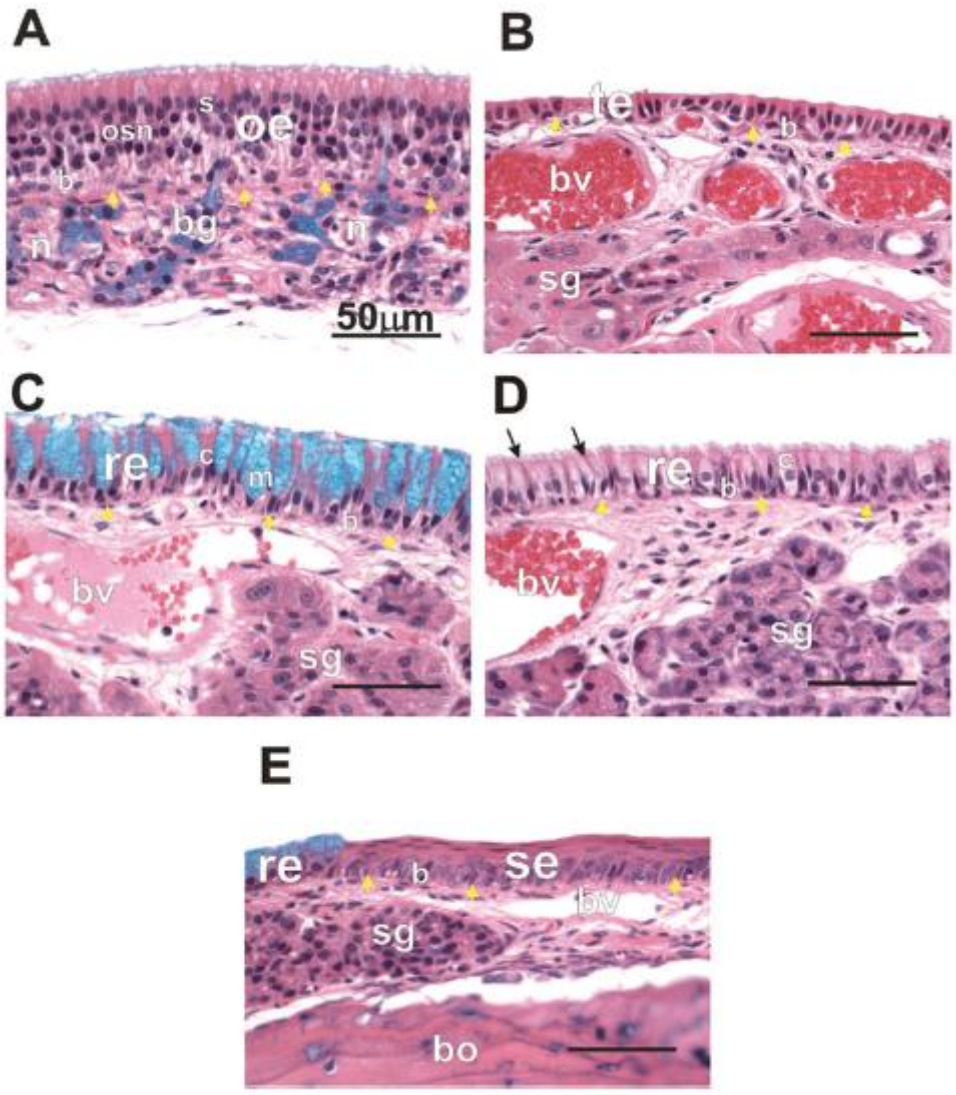

Figure 8. Light photomicrographs of the different types of surface epithelia that line the rat nasal airways. (A) olfactory epithelium (oe); (B) transitional epithelium (te); (C) and (D) respiratory epithelium (re); (E) stratified squamous epithelium (se). b, basal cells; bg, Bowman's glands; bo, bone; bv, blood vessels; c, ciliated cells; m, mucus (goblet) cells; n, nerve bundles; osn, olfactory sensory neurons; s, sustentacular cells; sg, subepithelial glands (135).

6.1.2 Transitional epithelium

It lines the tips and lateral aspects of parts of the naso and maxilloturbinates and the lateral wall of the anterior nasal cavity. This epithelium is one to two cells thick and is primarily made up of non-ciliated cuboidal and short columnar cell resting on basal cells (Figure 8B).

6.1.3 Respiratory epithelium

The majority of the nonolfactory nasal epithelium of laboratory animals and humans is ciliated respiratory epithelium. Nasal respiratory epithelium in the rat is composed of six morphologically distinct cell types: mucus, ciliated, nonciliated columnar, cuboidal, brush, and basal (Figure 8C, D). It covers most of the naso and maxilloturbinates medially, the nasal septum and ventral ethmoid turbinates.

6.1.4 Olfactory epithelium

The major difference in nasal epithelium among animal species is the percentage of the nasal airway that is covered by olfactory epithelium. The olfactory in humans is limited to an area of about 500 mm^2, which is only 3% of the total surface area of the nasal cavity. On the contrary, approximately 50% of the nasal cavity surface area in F344 rats is lined by this epithelium. It is composed of tall sustentacular cells, olfactory neurons and basal cells (Figure 8A). The sustentacular cells are tall, secretory cells and support the olfactory neurons. The olfactory neurons are lined up between the sustentacular cells and their nuclei form a prominent layer, which is five to six nuclei thick. In rat, it lines the ethmoid turbinates and some of the anterior dorsal meatus. Bowman's glands produce abundant enzymes important in metabolism of xenobiotics and secrete the mucus that protects the surface epithelium in this area.

6.2 Standard sections of the nasal cavity

Cutting of standardized upper respiratory tract sections and learning the normal histologic anatomy of cell populations of those sections is very important as it enables more accurate interpretation of the effects on cell types that will vary with location of the level of the section. In general, four sections of the rat nasal turbinates

are always cut in the same locations of the upper palate as illustrated in Figure 9 (202, 203).

6.2.1 Section 1

The first section is cut at the level of the upper incisor teeth (T1 in Figure 9). The nasal cavity is divided into two halves by the nasal septum, which contain a central core of hyaline cartilage. The cavities contain a dorsal meatus, a middle meatus and a ventral meatus. The nasal lumen is lined by stratified squamous epithelium in the ventral meatus, transitional epithelium on the lateral aspect of the nasal and maxillary turbinates and lateral walls, and respiratory epithelium on the medial septum and medial aspect of the turbinates. Olfactory epithelium can line the dorsal meatus.

6.2.2 Section 2

The second section is taken at the level of the incisive papilla (T2 in Figure 9). At this level, bilateral communication with the oral cavity via the incisive ducts can be observed. The incisor teeth are still present in this section and the nasolachrymal duct may still be observed. The dorsal meatus is lined by olfactory epithelium. Squamous epithelium lines the nasopalatine duct ventrally. The respiratory epithelium lines the nasal septum, the turbinates and lateral walls (the transitional epithelium has disappeared).

6.2.3 Section 3

The third section is taken at the level of the second palatal ridge (T3 in Figure 9). This section includes the maxillary sinuses and Steno's glands. The epithelium lining the nasal cavity in this level is predominantly olfactory epithelium covering the ethmoid turbinates, with respiratory epithelium lining the ventral portion of the median septum, maxillary sinuses and nasopharyngeal duct.

6.2.4 Section 4

The fourth section is taken at the level of the first upper molar tooth (T4 in Figure 9). The nasopharyngeal duct is visible and is lined by respiratory

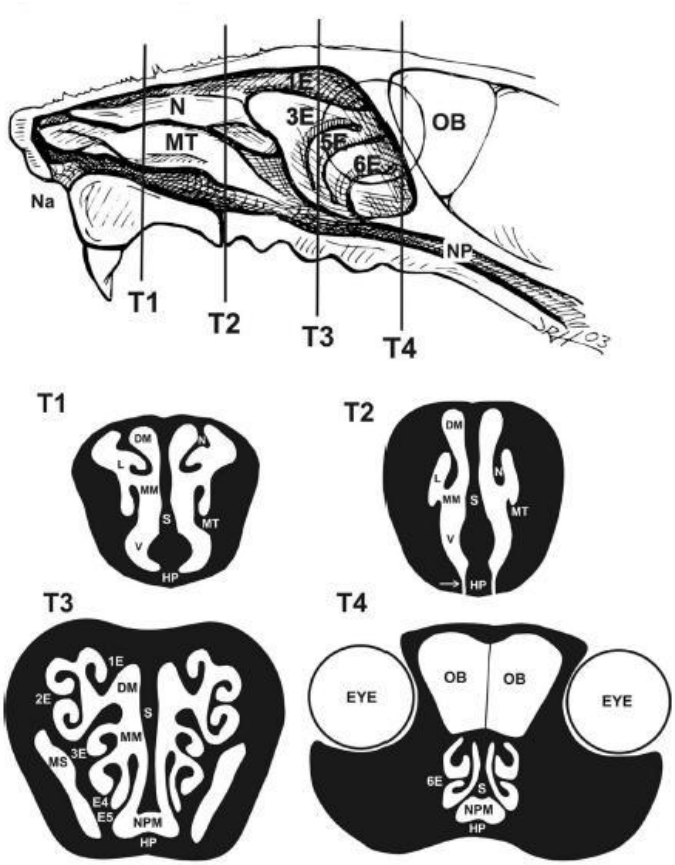

Figure 9. Illustration of the lateral wall and turbinates in the nasal passage of mouse. Vertical lines indicate the location of the anterior faces of 4 tissue blocks routinely sampled for light microscopic examination (T1 – T4). N, nasoturbinate; MT, maxilloturbinate; 1E-6E, 6 ethmoid turbinates; Na, naris; NP, nasopharynx; HP, hard palate; OB, olfactory bulb of the brain; S, septum; V, ventral meatus; MM, middle meatus; L, lateral meatus; DM, dorsomedial meatus; MS, maxillary sinus; NPM, nasopharygeal meatus; arrow in T2, nasopalatine duct (135).

epithelium. Nasal associated lymphoid tissue (NALT) is visible in either side of the nasopharyngeal duct. The epithelium in this region covering the ethmoid turbinates is almost entirely olfactory.

CHAPTER III
MATERIALS AND METHODS

MATERIALS

The reagents and substances used in the current study are listed as the following:

1. Polymers

PEGylated TMC copolymers used in the present study are listed below. The following nomenclature was adopted for the copolymers: PEG(x)$_n$-g-TMCy, where x denoted the molecular weight (MW) of PEG in Da, y denotes the MW of 40% DQ TMC in kDa, and the subscript n represents the average number of PEG chains per TMC macromolecule.

1.1 PEG(5k)$_{40}$-g-TMC100

1.2 PEG(5k)$_{298}$-g-TMC400

1.3 PEG(5k)$_{640}$-g-TMC400

1.4 PEG(5k)$_{680}$-g-TMC400

2. Cell lines

2.1 Mucus-secreting HT29-MTX-E12 cell line (E12, Passage 43-50, Philipps Universität Marburg, Germany)

2.2 A mouse connective tissue fibroblast cell line (L929, Passage 10-12, DSMZ, Braunschweig, Germany)

3. Animal

3.1 Wistar male rats (National Laboratory Animal Centre, Mahidol University)

4. Other chemicals

4.1 Recombinant human insulin (Lot number 125K1270, 28.5 IU/mg, Sigma-Aldrich, USA)

4.2 Chitosan with MW ~ 400 kDa and degree of deacetylation 84.7% (Lot number 414556, Fluka Biochemika, Germany)

4.3 Sodium iodide (NaI, Lot number 27822872, Carl Roth GmbH, Karlsruhe, Germany)

4.4 *N*-methylpyrrolidinone (Lot number 442487, Fluka Biochemika, Germany)

4.5 Methyl iodide (Lot number 12620, Riedel-de Haen, Germany)

4.6 95% Ethyl alcohol (Carl Roth GmbH, Karlsruhe, Germany)

4.7 Diethyl ether (Carl Roth GmbH, Karlsruhe, Germany)

4.8 Mucin from porcine stomach, Type III (Lot number 064K7005, Sigma-Aldrich, Deisenhofen, Germany)

4.9 Tripolyphosphate (TPP, Lot number 46H1055, Sigma-Aldrich, Deisenhofen, Germany)

4.10 Tris (hydroxymethyl) aminomethane (Tris, Lot number 450412, Fluka Biochemika, Germany)

4.11 Oregon Green carboxylic acid succinimidyl ester (Oregon Green 488, Molecular Probes,Eugene, OR, USA)

4.12 Tetramethylrhodamine isothiocyanate (TRITC, Lot number 1244157, Fluka Biochemika, Germany)

4.13 Bicinochoninic acid (BCA) assay kit (Pierce Chemical Company, Rockford, IL, USA)

4.14 Sterile water for injection (Thai nakorn patana Co.,LTD, Nonthaburi, Thailand)

4.15 Trifluoroacetic acid (TFA, Lot number 125K0121, Sigma-Aldrich, Deisenhofen, Germany)

4.16 Acetonitrile HPLC grade (Lot number 07070224, Lab-Scan Analytical Science, Bangkok, Thailand)

4.17 N-benzoyl-L-arginine ethylester hydrochloride (BAEE, Lot number 1222932, Fluka Biochemika, Germany)

4.18 Trypsin 1:250 from porcine pancrease (Lot 016K7681, 1060 BAEE unit/mg, Sigma-Aldrich, Deisenhofen, Germany)

4.19 Aminopeptidase M (APM, Lot number 110K7680, 141.60 IU/ml, Sigma-Aldrich, USA)

4.20 L-Leucine-p-nitroanilide (Lot number 024K5114, Sigma-Aldrich, USA)

4.21 Dulbecco's modified Eagle's medium, DMEM (Gibco, Eggenstein, Germany)

4.22 10% fetal calf serum, FCS (Gibco, Eggenstein, Germany)

4.23 3-(4,5-dimethyl-thiazol-2-yl)-2, 5-diphenyl tetrazolium bromide, MTT (Sigma-Aldrich, Deisenhofen, Germany)

4.24 Bicinochoninic acid (BCA) assay kit (Pierce Chemical Company, Rockford, IL, USA)

4.25 Dimethylsulfoxide (DMSO, Merck, Darmstadt, Germany)

4.26 3-(4, 5-dimethyl-thiazol-2-yl)-2, 5-diphenyl tetrazolium bromide (MTT, Sigma-Aldrich, Deisenhofen, Germany)

4.27 FluorSave™ Reagent (Calbiochem, Darmstadt, Germany)

4.28 Sodium deoxycholate (Lot number 034K0144, Sigma-Aldrich, USA)

4.29 Tiletamine HCl / Zolazepam HCl mixture (Zolitil®100, Lot number 819008, VIRBAC Laboratories, Carros, France)

4.30 Xylazine (X-Zine, 20 mg/ml, Lot number 179019, L.B.S. Laboratory Ltd., Part, Bangkok, Thailand)

4.31 PGO Enzyme (Lot number 105K6027, Sigma-Aldrich, USA)

4.32 O-Dianisidine dihydrochloride (Lot number 78F5037, Sigma-Aldrich, USA)

4.33 D-Glucose anhydrous (Lot number AF310197, UNILAB, Ajax Finechem, Australia)

4.34 Formaldehyde solution 35-40% (Lot number 06030187, Lab-Scan Analytical Science, Bangkok, Thailand)

4.35 Formic acid 98-100% (Lot number 0608289, Fisher Scientific, UK)

4.36 Sodium phosphate monobasic ($NaH_2PO_4.H_20$, Lot number A978421, BDH Chemicals, Poole, UK)

4.37 Sodium phosphate dibasic ($Na_2HPO_4.2H_20$, Lot number 711479, UNILAB, Ajax Finechem, Australia)

4.38 Sodium citrate ($Na_3C_6H_5O_7.2H_20$, Lot number AF604098, UNILAB, Ajax Finechem, Australia)

EQUIPMENT

1. Three necks round bottle flask equipped with reflux condenser
2. Lyophilizator Beta 1 (Crist, Osterode, Germany)
3. Ubbelohde capillary viscometer (Schott AVS-360, Schott AG, Mainz, Germany)
4. FT-NMR spectroscopy (AMX500,500 MHz, Bruker)
5. UV/Vis spectrophotometer (UV-160, Shimadzu, Kyoto, Japan)
6. Lambda 35 UV/Vis spectrophotometry (Perkin Elmer™, CA, USA)
7. Autosizer Lo-C (Malvern Instruments, Herrenberg, Germany)
8. Zetasizer Nano ZS (Malvern Instruments, Herrenberg, Germany)
9. High performance liquid chromatography (Shimadzu Corporation, Kyoto, Japan):
   - LC-10AT VP pump
   - SCL-10 A VP controller
   - SPD-10A VP UV detector
   - Computer integrator (Class-VP version 6.14 SP2 software program)
10. Vydac™ 300A, C4, 5μm, 250 x 4.6 mm ID HPLC column (Hesperia, CA, USA)
11. Gel Permeation Chromatography (Waters Corporation, MA, USA)
    - Waters 600E pump
    - Waters 2410 RI detector
    - Computer integration (Waters Empower™ 2 software program)
12. Ultrahydrogel™ linear column (MW resolving range 1,000 – 20,000,000, Waters Corporation, MA, USA)
13. Atomic force microscopy (NanoWizard™, JPK Instruments, Berlin, Germany)
14. Volt ohmmeter equipped with Endohm electrodes (EVOM, World Precision Instruments, Berlin, Germany)
15. Confocal laser scanning microscopy (Zeiss Axiovert 100 M, Jena, Germany)
16. Titertek Plus MS 212 ELISA reader (ICN, Eschwege, Germany)

17. Automate Microplate Reader (ELISA) (Wallac Victor 1420, Perkin Elmer™, CA, USA)
18. Fluorescence spectroscopy LS 50B (Perkin Elmer, Überlingen, Germany)
19. Rotating thermostat (Rotatherm, Liebisch, Germany)
20. Thermostat 5320 (Eppendorf AG, Hamburg, Germany)
21. pH meter equipped with microelectrode (Accument® AB15, Fisher Scientific, Rockwood, TN, USA)
22. PD-10 column Sephadex G-25 (Amersham Bioscience, Germany)
23. Ultracentrifuge (Hettich universal 30F, Hettich, Tuttlingen, Germany)
24. Magnetic 6-station stirrer (PermeGear V6A Stirrer, PermeGear, Inc., Bethlehem, PA, USA)
25. Ultrasonic bath (Branson 1200, Connecticut, USA)
26. Shaker Incubator (Model FSIE-SP, LABCON, Labotec, South Africa)
27. Vortex mixer (Julabo®, Paramix III, Julabo Labortech GmbH, Seelbach, Germany)
28. Peristaltic pump (Watson Marlow 505S, Watson – Marlow Limited , UK)
29. Nikon ECLIPSE E400 microscope (Nikon Corporation, Japan)
30. Nikon digital camera COOLPIX 995 (Nikon Corporation, Japan)
31. Olympus CX31 microscope (Olympus Corporation, Tokyo, Japan)
32. 7.1 mega pixel C7070 wide zoom Camedia camera (Olympus Corporation, Tokyo, Japan)

METHODS

1. Synthesis of TMC polymers

TMC differing in DQ and DD were prepared by reductive methylation of the parent chitosan with methyl iodide in the presence of NaOH using the procedure described by Polnok et al. (158) with some modifications. The reaction conditions of each step in the synthesis of the TMC polymers are described below and summarized in Table 6.

Table 6. The reaction conditions in the synthesis of TMC polymers

Polymer no.	Reaction step 1[a]	Addition step 1[b]	Addition step 2[b]
1	1 h	-	-
2	1 h	0.5 h	-
3	1.5 h	-	-
4	1 h	1 h	
5	1.5 h	1.5 h	-
6	1 h	1 h	1 h

[a]Twelve milliliters of 15% NaOH added with 12 ml CH_3I in *N*- methylpyrrolidinone containing 2 g chitosan and 4.8 g NaI.

[b]Added with 12 ml of 15% NaOH with 6 ml CH_3I.

1.1 Reaction step 1

A mixture of 2 g chitosan, 4.8 g of sodium iodide, 12 ml of 15% sodium hydroxide (NaOH) solution was mixed in 80 ml of *N*-methylpyrrolidinone on an oil bath at 60°C for 60 min. Subsequently, 12 ml of methyl iodide was added to the mixture and the reaction was carried for the desired time in the present of a reflux condenser.

1.2 Addition step

Prior to precipitation of the product from the solution mixture at the end of the previous reaction step, an additional 12 ml of 15% NaOH solution and 6 ml of methyl iodide were added . The reaction was further continued at 60°C for the desired time.

The product (*N*-trimethyl chitosan iodide) was precipitated with a mixture of 95% ethanol and diethyl ether, washed twice with diethyl ether on a glass filter and finally dried in a vacuum chamber.

1.3 Ion-exchange step

In order to exchange the iodide counter-ions of the TMC for chloride counter-ions, the products prepared as described above were dissolved in 30 ml of 10% (w/v) sodium chloride (NaCl) solution for 2 h and subsequently precipitated by using the mixture of 95% ethanol and diethyl ether. The products were then dissolved in 30 ml of water and precipitated with the mixture of 95% ethanol and diethyl ether to remove the remaining sodium chloride. The final products were dried in the vacuum chamber for 24 h before further characterization.

2. Characterization of TMC polymers

2.1 Determination of degree of substitution

^{1}H-NMR spectra of TMC polymers were recorded on JEOL GX 400D (Tokyo, Japan) by dissolving samples in D_2O at 80°C with suppression of the water peak. The degrees of substitution corresponding to %DQ, %DD, $\%DO_3$ and $\%DO_6$ were calculated using data obtained from ^{1}H-NMR spectra according to the Eqs. 8 – 11.

$$\%DQ = \left[\frac{[(CH_3)_3]}{[H]} \times \frac{1}{9}\right] \times 100 \quad \text{(Eq. 8)}$$

$$\%DD = \left[\frac{[(CH_3)_2]}{[H]} \times \frac{1}{3}\right] \times 100 \quad \text{(Eq. 9)}$$

$$\%DO_3 = \left[\frac{[(3\text{-}OCH_3)]}{[H]} \times \frac{1}{3}\right] \times 100 \quad \text{(Eq. 10)}$$

$$\%DO_6 = \left[\frac{[(6\text{-}OCH_3)]}{[H]} \times \frac{1}{3}\right] \times 100 \quad \text{(Eq. 11)}$$

where $[(CH_3)_3]$ is the integral of trimethyl amino group at 3.3 ppm, $[(CH_3)_2]$ is the integral of dimethyl amino group at 3.0 ppm, $[(3\text{-}OCH_3)]$ is the integral of methyl group for 3-hydroxyl group at 3.5 ppm, $[(6\text{-}OCH_3)]$ is the integral of methyl group for 6-hydroxyl group at 3.4 ppm and [H] is the integral of the ^1H peaks between 4.7 and 5.7 ppm.

2.2 Determination of molecular weight

Weight-average molecular weight (M_w), number-average molecular weight (M_n) and molecular weight dispersion (M_w/M_n) of TMC and copolymers were determined by a gel permeation chromatography (GPC) (Waters Co., Ltd., Washington, USA) at 30°C. The GPC equipment consisted of ultrahydrogel linear column (M_w resolving range of 1,000 – 20,000,000), Waters 600E pump and Waters 2410 refractive index detector. The eluent was 0.5 M acetate buffer. A flow rate was maintained at 0.6 ml/min. The amount of injected sample volume per run was 20 μl. The standard used to calibrate the column was pullulans (M_w 5,900 – 788,000). All data provided by The GPC system were collected and analyzed using Empower GPC software (Waters Co., Ltd., Washington, USA).

2.3 Intrinsic viscosity measurement

Intrinsic viscosities [η] of TMC were determined in 2% acetic acid/0.2 M sodium acetate (2% HAc/0.2 M NaAc) using an automated Ubbelohde capillary

viscometer (Schott AVS-360, Schott AG, Mainz, Germany) with a 0.63 mm capillary diameter at 25 ± 0.1°C in triplicate. Solution concentrations were adjusted in order to obtain relative viscosity value in the range of 1.1 – 1.5 which was suitable for the calculation of [η] (184). Six different concentrations were tested for each sample and each concentration was measured 5 times. The running times of solution and solvent were used to calculate the specific viscosity (η_{sp}), reduced viscosity (η_{red}) and inherent viscosity (η_{inh}). In order to obtain the most accurate values, [η] was determined as an average of extrapolating both Huggins ($\eta_{sp}/c \sim c$) and Kraemer ($\eta_{inh} \sim c$) plots on the ordinate at c = 0 (204) as shown in Appendix B.

2.4 Determination of potentiometric titration curve

Potentiometric titration curve of TMC was constructed by dissolving 20 mg of polymer in 2 ml of 0.1 N hydrochloric acid (HCl) solution. A titrant was a solution of 0.1 N NaOH. Under continuous stirring, titrant was added stepwise and the volume of added NaOH and pH values of solution were recorded thoroughly (34).

2.5 Estimation of water solubility

The pH dependence of the water solubility of TMC was estimated using turbidity measurements. The test sample was dissolved in 0.1 N HCl solution. With the stepwise addition of 0.1 N or 1.0 N NaOH solution, the transmittance of the solution was recorded on a Shimadzu UV-160 Spectrophotometer using a quartz cell with an optical path length of 10 mm at 600 nm. The test was performed at room temperature (205).

In order to investigate effect of ionic strength, the ionic strength of 0.1 N HCL and 1.0 N NaOH solutions were adjusted by NaCl to achieve the desired ionic strength of 0.05, 0.15 and 0.5 M.

2.6 *In vitro* mucoadhesion measurement

An investigation of the mucoadhesive bond strength between polymers and mucin, main component of mucus was carried out using a mucin particle method developed by Takeuchi et al. (53). Submicron-sized mucin (ss-mucin) suspension

(1% w/v) was prepared by suspending and continuously stirring mucin type III powder in 10 mM Tris buffer pH 6.8 for 10 h. Mucin suspension was then incubated at 37°C overnight. The size of mucin was reduced by ultrasonication (Branson 1200, Connecticut, USA) until particle size was around 300 - 400 nm. It was then centrifuged at 4000 rpm for 20 min to extract ss-mucin particles in the supernatant portion.

One ml of 1% w/v ss-mucin suspension was mixed with different volumes of 1 mg/ml polymer solutions under mild magnetic stirring. Then the particle size and zeta potential values were measured. All experiments were performed in triplicate.

2.7 Cytotoxicity testing

In vitro cytotoxicity of TMC was evaluated using a MTT assay according to the method described by Fischer et al. (206). A mouse connective tissue fibroblast cell line, L929 (DSMZ, Braunschweig, Germany) was plated into 96-well microtiter plates at a density of 8000 cells/well. After 24 h incubation, culture medium was replaced by 100 μl of serial dilutions of the polymers in serum supplemented tissue culture medium and the cells were incubated for 3 h. Subsequently, polymer solutions were aspirated and replaced by 200 μl DMEM without serum. Twenty microliters sterile filtered MTT stock solution in phosphate buffered saline (PBS) pH 7.4 (5 mg/ml) were added in each well reaching a final concentration of 500 μg MTT/ml. After 4 h incubation, unreacted dye was aspirated and the formazin crystals were dissolved in 200 μl/well DMSO. Absorption was measured at 570 nm with a background correction of 690 nm using a Titertek Plus MS 212 ELISA reader (ICN, Eschwege, Germany). The relative cell viability (%) compared to control wells containing cell culture medium without polymer was calculated by $[A]_{test}/[A]_{control} \times 100$ (n = 4). The IC_{50} was calculated as a polymer concentration which inhibited growth of 50% of cells relative to non-treated control cells.

3. Characterization of PEGylated TMC copolymers

3.1 Determination of molecular weight

See methods 2.2.

3.2 *In vitro* mucoadhesion measurement

See methods 2.6.

4. Insulin nanocomplex formation

4.1 Preparation of insulin nanocomplexes

Insulin solution was prepared in two steps (71): (1) insulin powder was dissolved insulin in 87% (v/v) 1.15×10^{-2} N HCl and (2) 13% (v/v) 0.1 N Tris solution was added, resulting in a clear insulin solution in Tris buffer with low ionic strength (I = 0.01) and pH 7.4. Polymer solutions of appropriate concentrations were prepared by dissolving the dry polymer powder in 10 mM Tris buffer and adjusted to pH 7.4. Insulin nanocomplexes (NC) were prepared by self-aggregation, utilizing the electrostatic interactions between the positively charged polymers and negatively charged insulin as a driving force (47). The NC were prepared by mixing equal volumes of insulin and polymer solution at the desired ratio under gentle magnetic stirring. The mixture was then incubated for 20 min at room temperature.

4.2 Determination of stoichimetric ratio of insulin and polymer

The stoichiometry between insulin and each polymer was investigated by type III turbidimetric titration (62) in which insulin solution was added to polymer solutions at constant pH of 7.4. The resulting particle size and Kilo counts per second (Kcps) values were measured by dynamic laser light scattering using an Autosizer Lo-C (Malvern Instruments, Herrenberg, Germany). The point at which particle size began increasing dramatically and the Kcps value reached a plateau were denoted as the endpoint of the titration. The optimal [polymer]/[insulin] mass and charge ratios were calculated.

5. Insulin nanoparticle formation

5.1 Preparation of insulin nanoparticles

Insulin nanoparticles (NP) were prepared, based on the ionotropic gelation with TPP (207). Polymer and insulin solutions were prepared as described in section 4.1. TPP was dissolved in purified water at various concentrations. The NP were spontaneously formed upon incorporation of equal volume of TPP solution in the

polymer solution under gentle magnetic stirring at room temperature. Insulin solution was premixed with equal volume of either polymer solution or TPP solution before the addition of TPP solution. The final pH values were in the range of 7.4 – 7.7.

5.2 Determination of optimal ratio of TPP and polymer

The optimal condition at which NP were formed was established using titration method and dynamic laser light scattering as previously described in section 4.2. Mixtures of polymer and insulin with different polymer / insulin (+/–) charge ratio were titrated against TPP solutions and resulting particle size and Kcps values were measured.

6. Physicochemical characterization of insulin NC and NP

6.1 Particle size analysis

Measurements of particle size and average count number in term of Kcps value were performed on freshly prepared samples by photon correlation spectroscopy (PCS) using an Autosizer Lo-C (Malvern Instruments, Herrenberg, Germany) equipped with a 10 mW HeNe laser (633 nm) at 90° angle at the temperature of 25°C. For data analysis, the viscosity (0.88 mPas) and the refractive index (1.33) of distilled water at 25°C were used for calculation. Arithmetic mean and SD were calculated from 3 consecutive runs, and samples were analyzed using Malvern PCS software.

6.2 Zeta potential analysis

The zeta potentials of NC and NP were obtained by laser Doppler velocimetry (LDV) using a Zetasizer Nano ZS (Malvern Instruments, Herrenberg, Germany) equipped with a 4 mW HeNe laser at a wavelength of 633 nm at a 173° backward scattering angle. The viscosity (0.88 mPas) and the refractive index (1.33) of distilled water at 25°C were used for data analysis The measurements were performed in a folded capillary cell (Malvern Instruments, Herrenberg, Germany) at least three replication. Dispersion Technology Software 5.00 (Malvern Instruments, Herrenberg, Germany) was used for data acquisition and analysis.

6.3 Morphology measurement

Atomic force microscopy (AFM) was used to characterize the morphology of particles using a NanoWizard™. The samples were diluted with ultrapure water and 10 μl of the diluted sample was applied to a freshly cleaved mica surface and allowed to adhere to the surface for a few minutes. The supernatant was removed and the samples were allowed to air-dry ca. 10 min. Commercially available silicon tips attached to I-type silicon cantilevers with a length of 230 μm, a resonance frequency of about 170 kHz and a scan frequency of 0.8 – 1.1 Hz used. All measurements were performed in tapping mode.

6.4 Determination of insulin association efficiency and process yield

The amount of insulin entrapped in the NC and NP was calculated from the difference between the total amount added to the solution and the amount of non-associated insulin remaining in the supernatant. Triplicate batches of NC or NP were centrifuged at 14,000 rpm for 30 min at room temperature. A pellet was then lyophilized and weighed. The insulin content in the supernatant was determined using a Shimadzu HPLC (Shimadzu, Japan) system equipped with a pump (LC-10AT VP), a controller (SCL-10A VP) and a UV detector (SPD-10A VP) at 230 nm. A Vydac™ C4 column (5 μm, 4.6 × 250 nm) (Hesperia, CA, USA) was employed with a flow rate of 1 ml/min using 30:70 acetonitrile:H_2O containing 0.1% trifluoroacetic acid (TFA) as mobile phase. Insulin association efficiency (AE) and process yield (PY) were calculated by the following equations.

$$\mathrm{AE} = \frac{\text{Total insulin amount} - \text{Free insulin amount}}{\text{Total insulin amount}} \times 100\% \qquad \text{(Eq. 12)}$$

$$\mathrm{PY} = \frac{\text{Particle weight}}{\text{Total solids (polymer} + \text{insulin} + \text{TPP) weight}} \times 100\% \qquad \text{(Eq. 13)}$$

7. Colloidal stability studies

In order to investigate the stability of NC and NP in physiological fluid, NC and NP were mixed with pH 6.8 phosphate buffer (PBS) in different ratios. To study

effect of salt on the colloidal stability, an ionic strength of the solutions was adjusted by adding NaCl. This was achieved by mixing various NC and NP with a series of concentrated sodium chloride solutions. The integrity was immediately monitored after mixing by dynamic laser light scattering.

8. Insulin stability study

8.1 Temperature stability study

Two milliliters of NC or NP suspensions, containing 500 μg/ml insulin, were incubated at room temperature, 37°C, and 50°C. At predetermined time interval (0, 15, 60, 145, 360 min), an aliquot (100 μl) was withdrawn. To all withdrawn samples, small amount of 0.25% acetic acid solution was added to dissolve particles and then diluted with 10 mM Tris buffer to 1 ml volume. Insulin content was determined by HPLC. In addition, the stability of pure insulin upon different temperatures (room temperature, 37°C, and 50°C) was measured under the same conditions. The stability of samples was determined in triplicate.

8.2 Enzymatic stability study with trypsin

8.2.1 Trypsin activity

In vitro evaluation of trypsin activity in the presence of polymers was investigated using the method described previously (57). Briefly, 900 μl of polymer solution and TPP solution were mixed with 100 μl of trypsin solution (3000 N-Benzoyl-L-arginine ethylester (BAEE) IU/ml in 10 mM Tris buffer pH 7.4). Subsequently the mixtures were incubated at 37°C for 30 min. The enzymatic activity in the mixture was determined from the change of the absorbance at 253 nm/min, using BAEE as the substrate. 200 μl of supernatant was pipetted into a 1-cm cell. After adding 257.1 μg of BAEE dissolved in 3 ml of 10 mM Tris buffer (pH 7.4), the increase in absorbance (ΔA 253 nm) caused by the hydrolysis of this substrate to *N*-α-benzoylarginine (BA) was recorded at 30 sec intervals for 5 min using Lambda 35 UV/Vis spectrophotometry (Perkin Elmer™, CA, USA). In addition, the enzymatic activity in the absence of polymer and TPP was measured under the same condition.

8.2.2 Insulin degradation by trypsin

First, trypsin was dissolved in 10 mM Tris buffer pH 7.4, and the concentration was adjusted to 3000 BAEE IU/ml. 100 μl of the solution was then added to 900 μl of insulin solution, NC and NP suspensions containing 500 μg/ml of insulin. The initial concentrations of insulin and trypsin in the sample solution (1 ml) were 450 μg/ml and 300 BAEE IU/ml, respectively. Three vials of mixture were taken out at predetermined time points and an ice-cold 0.1% TFA solution was added in order to stop enzymatic degradation and to dissolve the remaining complexes. The insulin concentration was then quantified by HPLC.

8.3 Enzymatic stability study with aminopeptidase M

8.3.1 Aminopeptidase M activity

In vitro evaluation of aminopeptidase M (ApM) activity in the presence of polymer was investigated using the method described previously (208). Briefly, 100 μl polymer solution was mixed with 50 μl of ApM solution (200 mU/ml in 10 mM Tris buffer pH 7.4) and the mixture was incubated for 30 min at 37°C. Thereafter, 50 μl of L-leucine-*p*-nitroanilide in a final concentration of 1 mM was added, the increase in absorbance (ΔA 405 nm) caused by the hydrolysis of this substrate was recorded at 10 min intervals for 60 min at 37°C with an automate Microplate Reader (ELISA) (Wallac Victor 1420, Perkin Elmer™, CA, USA). The concentration of the *p*-nitroanilide was calculated by interpolation of an according standard curve. For positive control, polymer was omitted. In order to examine whether polymer can hydrolyze L-leucine-*p*-nitroanilide, the hydrolysis activity of polymer in the absence of enzyme was compared.

8.3.2 Insulin degradation by aminopeptidase M

The stability of insulin against ApM, major enzyme in nasal mucosa, was examined as follows. A stock solution of ApM (500 mU/ml) was prepared in 10 mM Tris buffer pH 7.4. 100 μl of the solution was then added to 900 μl of insulin solution, NC and NP suspensions containing 500 μg/ml of insulin. The initial concentrations of insulin and ApM in the sample solution (1 ml) were 450 μg/ml and

50 mU/ml, respectively. At predetermined time points, three vials of mixture were taken out and the ice-cold 0.1% TFA solution was added in order to stop enzymatic degradation and to dissolve the remaining complexes. The insulin concentration was then quantified by HPLC.

9. Insulin release study in the presence of mucin

Effect of mucin on the release of insulin from NC was determined by adding 100 μl of mucin solution in 900 μl NC and the mixtures were incubated at 37°C. At appropriate time intervals, individual samples were centrifuged at 14,000 rpm for 30 min and the amount of insulin in supernatant was measured using HPLC. All experiments were performed in triplicate.

10. Cell culture experiment

10.1 Fluorescent labeled insulin

Insulin was labeled with tetra-methyl-rhodamine isothiocyanate (TRITC) following the previously described method (65). Insulin was dissolved at a concentration of 4.50 mg/ml in a sodium carbonate/-hydrogen carbonate buffer pH 9.3. A solution of TRITC (1 mg/ml) in dimethyl sulfoxide (DMSO) was quickly added (molar ratio of insulin / TRITC 1:2.9) and the mixture was stirred for 18 h at 4°C under light exclusion. The reaction was quenched with an excess of ammonium chloride and stirred for another 4 h. TRITC-labeled insulin was separated with a PD-10 column Sephadex G-25 (Amersham Pharmacia Biotech, Freibure, Germany) with pH 7.4 PBS. After collecting the appropriate fraction, crude TRITC labeled insulin was obtained by lyophilization.

10.2 Fluorescent labeled polymers

Polymers were labeled with Oregon Green carboxylic acid succinimidyl ester (Oregon Green 448) following the previously described method (209). Polymer (100 mg) was dissolved in 2 ml purified water. One hundred microliter of 5 mg/ml Oregon Green 448 in DMSO was added dropwise in polymer solution under stirring in the dark for 24 h at room temperature. Labeled polymer was then purified by PD-10 column Sephadex G-25 (Amersham Pharmacia Biotech, Freibure, Germany) with pH

7.4 PBS. After collecting the appropriate fraction, crude Oregon green 488 labeled polymer was obtained by lyophilization.

10.3 Cell culture

HT29-MTX-E12 (E12) cells (199) at passage numbers 43-50 were grown and subcultured as previously described (210). E12 cells were routinely maintained in Dulbecco's modified Eagle's medium (DMEM) supplemented with 10% fetal calf serum (FCS), 1% nonessential amino acids and 1% L-glutamine at 10% CO_2, 95% R.H. and 37°C. Cells were seeded at a density of 6×10^4 cell/cm^2 on 24-well cell culture plates or 6-well uncoated polycarbonate Transwell^{TM} filter inserts (0.4 μm pore size, area: 4.71 cm^2) and cultivated over 21 days. The medium was changed every second day.

10.4 Binding and uptake experiment

Cell binding and uptake studies were performed using E12 cell monolayers according to the method as described previously (197). The uptake medium was 10 mM Tris buffer, supplemented with 100 mM glucose, 1.17 mM $CaCl_2$ and 1.03 mM $MgCl_2$ pH 7.4. After 2 h incubating with polymer solutions (250 μg/ml) or insulin NC containing 125 μg/ml insulin, the cells were lysed by solubilizing the cells with a mixture of 2% sodium dodecyl sulfate (SDS) and 50 mM EDTA pH 8.0 (1:1), and determined by fluorescence spectroscopy using 96-well plate reader, LS 50B (Perkin Elmer, Überlingen, Germany) at excitation/emission wavelengths of 493/515 nm for polymer and 534/567 nm for insulin NC. Uptake was expressed as the amount (micrograms) of polymer associated with a unit weight (1 mg) of cellular protein (mean ± SD, n = 4). The protein content of the cell lysate was determined via bicinchoninic acid (BCA) assay kit (Pierce Chemical Company, Rockford, IL, USA) according to the manufacture's protocol. To further evaluate the barrier properties of mucus, E12 monolayers were preincubated with the uptake medium consisting of 10 mM mucolytic agent, N-acetyl-L-cysteine (NAC) for 60 min at 37°C. Subsequently, monolayers were washed twice with the uptake medium before experiment.

10.5 Transport across E12 monolayers

Transport studies were performed at 21 days post-seeding. The integrity of the monolayers was checked by measuring the transepithelial electrical resistance (TEER) values before and after the experiment using a volt ohmmeter (EVOM, World Precision Instruments, Berlin, Germany) equipped with Endohm electrodes, as described previously (197). Monolayers with TEER value below 50 $\Omega \cdot cm^2$ were excluded from experiments (199). The permeability of insulin NC across monolayers was examined according to the previous report (65). In brief, filter inserts were rinsed with transport buffer pH 7.4 and allowed to equilibrate at 37°C for 15 min. The apical buffer was replaced with 1.5 ml of NC (insulin 250 μg/ml). Every 20 min up to 2 h, samples (1 ml) were collected from the basolateral side and subsequently replaced with fresh the transport medium. Insulin was assayed by fluorescence spectroscopy. Each experiment was performed in triplicate.

10.6 Confocal laser scanning microscopy (CLSM)

E12 cells grown on glass cover slides for 2 days were treated with insulin, polymer and the complexes (insulin concentration 250 μg/ml). After 2 h incubation at 37°C, the cells were washes three time with ice-cold transport buffer, fixed with 3.7% paraformaldehyde in PBS pH 7.4 at room temperature for 30 min and counterstained with DAPI (4,6-diamidino-2-phenylindole, 0.2 μg/ml) for 20 min, both under light exclusion. Samples were embedded in FluorSave™ Reagent (Calbiochem, Darmstadt, Germany) and imaged by CLSM (Zeiss Axiovert 100 M Microscope coupled to a Zeiss LSM 510 scanning device, Jena, Germany) which was equipped with Zeiss Neofluor 40*/1.3 objective. Excitation wavelength was 364 nm (long pass filter (LP) 385 nm) for DAPI, 488 nm (LP 505 nm) for Oregon Green 488 and FITC, and 543 nm (LP 567 nm) for TRITC (197, 209). All images were recorded by using the multitracking mode in which each fluorescence channel was scanned individually.

11. Animal experiment

Nasal absorption studies were performed in Wistar male rats obtained from National Laboratory Animal Centre (Mahidol University, Nakhon Pathom, Thailand).

Animal experiments were approved by the local ethical committee as shown in Appendix D and were conducted according to the prescribed requirements.

11.1 Hypoglycemic activity in healthy rats

11.1.2 Animal preparation and dosing

Rats were acclimatized for one week before the study. Rats weighting 250 – 300 g were fasted for 18 h, but water is supplied ad libitum. Six rats were assigned for each experiment. Rats were anesthetized by intraperitoneal injection (i.p.) of a mixture of zoletil (tiletamin HCL/zolazepam HCl mixture, 50 mg/kg) and xylazine (10 mg/kg) and anesthesia was maintained with 1/3 additional zoletil/ xylazine as needed throughout the experiment (211, 212). The rats were placed in a supine position. The nasal formulations (20 μl, insulin dose 4 IU/kg) were administered using a 50 μl Hamilton microsyringe with a blunt needle inserted approximately 0.5 cm into the right nostril (marked on the tip) after the initial dose of anesthetic agent 30-45 min. For a control, the buffer without insulin was intranasally administered to the rats. Insulin solution was also subcutaneously (s.c.) administered to the rats (0.5 IU/kg) to calculate the relative pharmacodynamic availability (F_{dyn}).

11.1.2 Blood glucose measurement

Blood samples were collected from the tip of the tails of anesthetized animals in heparinized haematocrit tubes (Modulohm A/S, Herlev, Denmark) at -20, -10 before formulation application and at 5, 15, 30, 45, 60, 90, 120, 180, 240 min after postadministration. The samples were then centrifuged at 3,000 rpm for 5 min to obtain serums and stored at -20 °C until analysis. Blood glucose levels were determined with blood glucose assay kit using the glucose oxidase method. Glucose content was calculated as a percentage of the mean value of the first three measurements of each animal. The values of blood glucose baselines ranged from 150 to 200 mg/dl and were normalized for each experiment at 100%. The blood glucose content at various times thereafter was calculated as a percentage of this initial value in each animal.

11.1.3 Analysis of data

Minimum blood glucose concentration (C_{min}) and time to minimum concentration (T_{min}) were determined directly from the pharmacodynamic time profile. Areas over the curves were calculated for the various groups for the times 0 – 240 min ($AOC_{0\text{-}240}$) using the linear trapezoidal method. Pharmacodynamic availability relative to s.c. (F_{dyn}) was calculated with Eq. 14.

$$F_{dyn} = \frac{AOC_{i.n.} \times Dose_{s.c.}}{AOC_{s.c.} \times Dose_{i.n.}} \times 100\% \qquad \text{(Eq. 14)}$$

where “i.n.” and “s.c.” represent “intranasal” and “subcutaneous”, respectively.

Results are shown as the mean values (± SEM) of 6 animals. Statistical analysis was performed by one-way analysis of variance (ANOVA), followed Scheffe *post hoc* for individual group comparisons with SPSS software version 11.5. The level of significance was set at $p < 0.05$.

11.2 Histological study

A nasal irritation study was conducted to determine the response of rat nasal mucosa to nasal insulin formulations. Animals were prepared and treated as described in section 11.1.1.

11.2.1 Dosing experiments

A total of twelve groups of three rats each were used in this study: the first group received no treatment (intact control); two groups received only the buffer (buffer control); two groups received insulin solution; three groups received insulin/TMC400-40 NC; two groups received insulin/PEG$(5k)_{298}$-g-TMC400-40 NC; and the last two groups received insulin/PEG$(5k)_{680}$-g-TMC400-40 NC.

To investigate acute histopathological effects, the rats were sampled and killed after finishing *in vivo* absorption experiments (Table 7). To investigate the reversibility of the nasal membrane integrity, the rats were returned to their cages 24 h before killing. To investigate subacute histopathological effects, the rats were daily nasal administered for one week with the same procedure and were led to death on the

Table 7. A random sampling of rats for investigation of acute histopathological effects

Treatments	No. of *in vivo* absorption experiments					
	1	2	3	4	5	6
Buffer	X	X		X		
Ins sol	X		X		X	
Ins/TMC400-40 NC (1:0.3)	X		X		X	
Ins/TMC400-40 NC (1:1)	X		X		X	
Ins/TMC400-40 NC (1:5)		X	X			X
Ins/PEG$(5k)_{298}$-g-TMC400-40 NC (1:5)		X		X		X
Ins/PEG$(5k)_{680}$-g-TMC400-40 NC (1:5)		X		X		X

eighth day. The rats were allowed to recover and resume their normal conscious state after each daily administration. The rats were recorded for their weight and sleeping time everyday in order to adjust the dose of a mixture of zoletil and xylazine for optimum sedation in each rat.

11.2.2 Tissue preparation

The rats were euthanized by exsanguinations under zoletil/xylazine anesthesia. An incision was made in the esophagus to insert a silicone cannula into the posterior end of the nasal cavity as shown in Figure 10. The nasal cavity of rats was flushed with 10% neutral-buffered formalin using a peristaltic pump for approximately 20 min. After perfusion fixation the animals were then decapitated and the mandibles, skin, brain and excess soft tissue were removed from the skull. The specimens were subsequently immersed in fresh fixative for 48 h. Specimens were decalcified in formic acid – sodium citrate solution for 2 weeks. The decalcifation solution was changed every second day. The nose was cut at 2 transverse regions using a razor blade as described by Chandler et al. (72). Region (ii) was taken from the upper incisor teeth to the incisive papilla and region (iii) was taken from the incisive papilla to the second palatal ridge (Figure 11). All regions were processed through to paraffin wax blocks using routine histological methods. Sections were cut serially at 5 μm thickness, mounted and strained with haematoxylin and eosin (HE). Besides, some slides were stained with alcian blue (AB) to identify acidic mucopolysaccharides and with periodic acid Schiff (PAS) to identify neutral mucopolysaccharides.

11.2.3 Light microscopic examination and scoring of effects

Cross-sections of the nasal cavity were examined using on Olympus CX31 microscope equipped with a 7.1 mega pixel C7070 wide zoom Camedia camera (Olympus Corporation, Tokyo, Japan). The appearance and distribution of normal rat nasal epithelium were identified in sections from intact control animals. In each section from region (ii) and (iii) of test animals, the state of the nasal epithelium on the dosed (right) side of the septum was qualitatively compared with the tissue on the undosed (left) side. Comparison was made between tissues treated with insulin

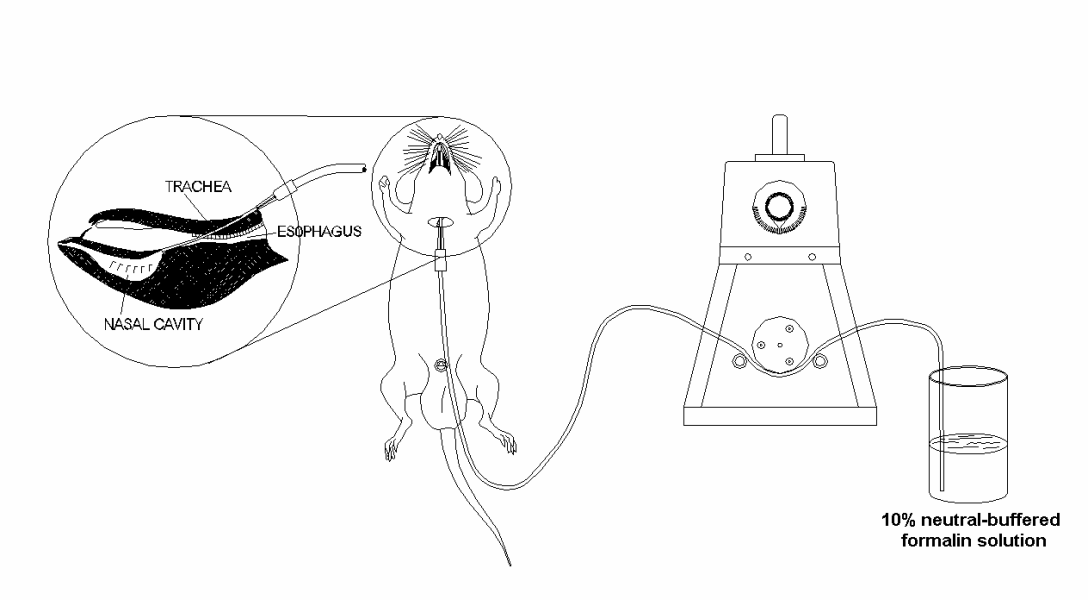

Figure 10. Diagram of the surgical procedure and schematic diagram of the fixative perfusion of the rat nasal cavity.

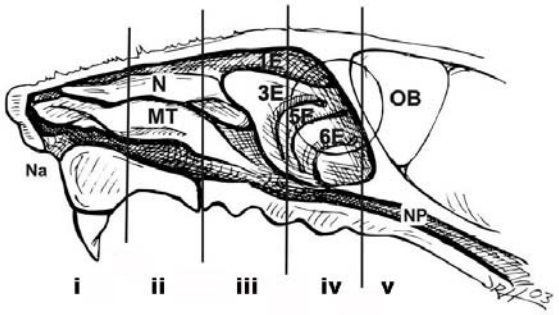

(A)

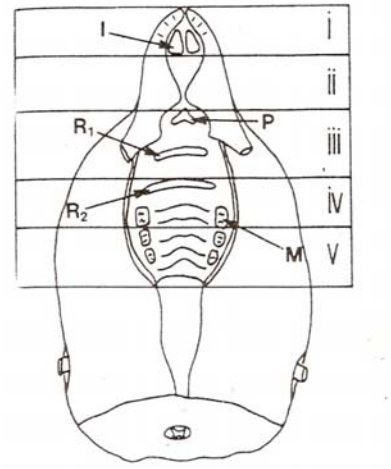

(B)

Figure 11. Diagram illustration of (A) the nasal lateral wall and (B) the surface features of the oral cavity in rat. Those landmarks used to define cutting positions for the division of the nasal cavity into regions (i) – (v) are indicated: naris (Na); nasoturbinate (N); maxilloturbinate (MT); ethmoturbinates (E); nasopharynx (NP); olfactory bulb of the brain (OB); upper incisor root (I); incisive papilla (P); first palatal ridge (R1); second palatal ridge (R2); first upper molar (M) (72, 135).

solution and with polymer/insulin NC. The tissue treated with various nasal formulations was also compared with that exposed to buffer only.

The morphology changes of the epithelium of the nasal cavity was evaluated and scored into three levels of irritation based on the criteria described by Tengamnuay et al. (69). Since responses of nasal epithelium to severe injury after long-term exposure are not similar to those after single exposure, the morphological signs of severe irritation for the nasal epithelium after long-term intranasal administration were modified. The morphological signs of the rat epithelium utilized as criteria for grading the membrane-damaging effects after single and one-week daily intranasal administration are summarized in Table 8.

12. Calculation and statistics

Results are depicted as mean ± SD at least three measurements. The *t*-test or one way ANOVA with the Scheffe test applied *post hoc* for paired comparisons were performed to compare two or multiple groups, respectively. All analyses were determined using the SPSS program (SPSS 11.5.0 for windows) and differences were considered to be significant at a level of $p < 0.05$.

Table 8. Morphological signs of the rat nasal mucosa utilized as criteria for grading the membrane-damaging effects

Degree	Histological lesions	
	After 4 h administration[a]	After one-week daily administration
i. Mild	- Mucus hypersecretion (MS) - Goblet cell distention (GD)	- Mucus hypersecretion (MS) - Goblet cell distention (GD)
ii. Moderate	- Vascular congestion (VC) - Subepithelial edema (SE) - Discontinuation of epithelial cells (DE)	- Vascular congestion (VC) - Subepithelial edema (SE) - Discontinuation of epithelial cells (DE)
iii. Severe	- Pyknotic nuclei of epithelial cells (PN) - Sloughing of epithelial cells (SL) - Hemorrhage (H)	- Epithelial hyperplasia (HP) - Epithelial metaplasia (MP) - Atrophy (A)

[a]Based on the criteria described by Tengamnuay et al. (69).

CHAPTER IV
RESULTS AND DISCUSSION

1. Synthesis and characterization of TMC polymers

1.1 The degrees of substitution

In the present study, TMC was synthesized based on one methylation reaction step followed by subsequent addition steps because it had been demonstrated that the high DQ of TMC with a low degree of *O*-methylation could be achieved as compared to the use of multiple reaction steps (158). Moreover, it was time-saving owing to the reduction of certain in-process procedures – precipitation, centrifugation and drying of the intermediate product. The degrees of substitution of various TMC polymers are listed in Table 9. For ease of discussion, the abbreviation TMC*x*-*y*-*z* was used to describe the polymers where *x* denotes the molecular weight of starting chitosan, *y* represents the DQ in percent and *z*, the DD in percent.

As seen in Table 9, using a one-step reaction, TMC400-10-40 was obtained with 13.9% DQ and the high substitution degree of DD at 39.1%. When extending the reaction duration from 1 to 1.5 h, DQ increased to 23.4% and DD significantly increased to 65.2% (TMC400-20-60). However, when increasing additional step for 0.5 h, DQ increased to 23.0% similar to TMC400-20-60 whereas DD decreased to 20.8% (TMC400-20-20). Similarly, it was observed that by extending duration of additional step of TMC400-20-20 from 0.5 to 1 h, DQ of TMC increased from 23.0% to 32.1% and DD from 20.8% to 33.0% (TMC400-30-30), therefore an increase in reaction duration increased both DQ and DD. Comparing between TMC400-20-60 and TMC400-40-40 as well as between TMC400-30-30 and TMC400-80-10, it was obviously seen that an increase of number of reaction step increased DQ but decreased DD.

Figure 12 shows the ^{1}H-NMR spectra of TMC400-20-20 and TMC400-20-60. The ^{1}H signal intensity of dimethylamino group (-N(CH_3)$_2$) of TMC400-20-60 was stronger than that of TMC400-20-20. The ratio between the integral of the *N*-

Table 9. Substitution degrees of different TMC polymers

Polymers	Reaction time (h / h / h)[a]	DQ (%)[b]	DD (%)[b]	3O-CH_3 (%)[b]	6O-CH_3 (%)[b]
TMC400-10-40	1.0 / - / -	13.9	39.1	2.4	7.0
TMC400-20-20	1.0 / 0.5 / -	23.0	20.8	11.3	16.7
TMC400-20-60	1.5 / - / -	23.4	65.2	3.9	9.0
TMC400-30-30	1.0 / 1.0 / -	32.1	33.0	5.1	9.5
TMC400-40-40	1.5 / 1.5 / -	39.0	39.3	4.9	9.3
TMC400-80-10	1.0 / 1.0 / 1.0	76.6	8.5	58.0	52.0

[a]Reaction times of reaction step 1 / addition step 1 / addition step 2

[b]Calculated by ^{1}H NMR analysis

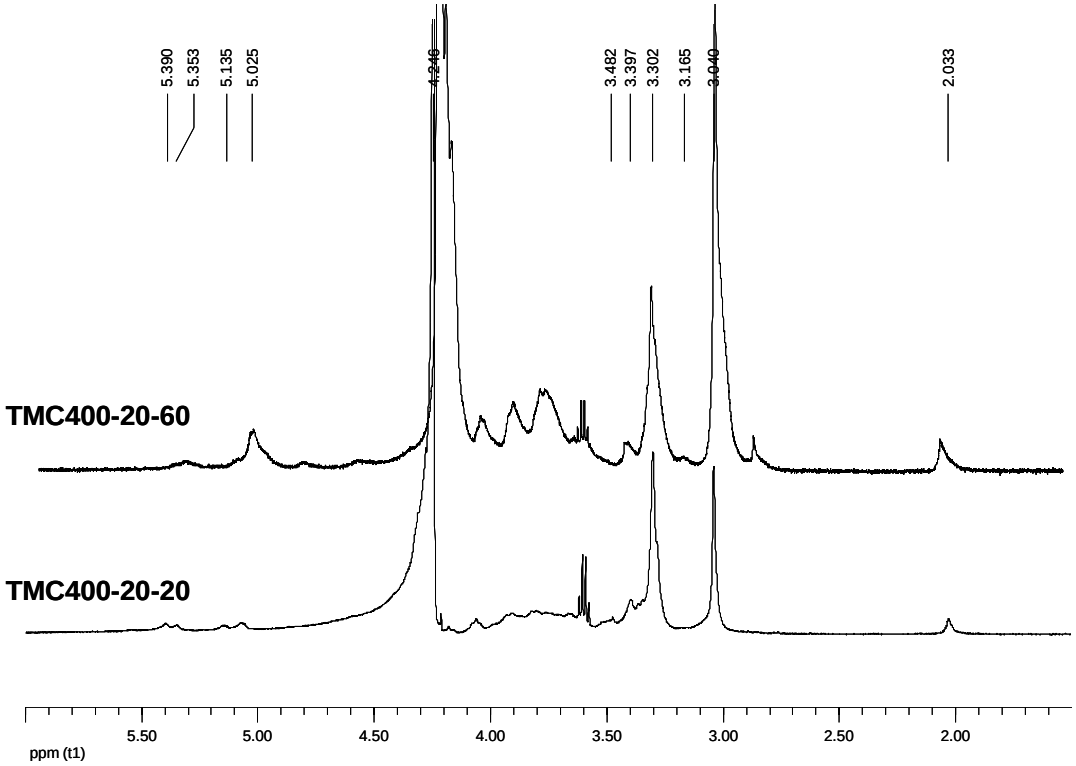

Figure 12. ^{1}H-NMR Spectra of TMC400-20-60 and TMC400-20-20, prepared in one reaction step and one reaction step with one addition step, respectively.

trimethylamino group ($N^+(CH_3)_3$) and that of the *N*-dimethylamino group ($N(CH_3)_2$) was approximately 1:3 for TMC400-20-60 and 1:1 for TMC400-20-20. The results obtained may be explained by the less basic environment and reduction of methylating agent, CH_3I in the extended reaction step of TMC400-20-60 which would slow down conversion of an intermediate $N(CH_3)_2$ to a $N^+(CH_3)_3$. Similarly, Curti et al. (213) reported that the *N*-methylation of chitosan or the average DQ was strongly affected by the reaction conditions, i.e. the alkalinity of the medium and the availability of CH_3I.

From the results obtained, it could be suggested that high DQ of TMC with low DD could be obtained by increasing the number of reaction steps, whereas high DQ of TMC with high DD was resulted by extending the duration of reaction.

1.2 Molecular weight

A summary of the M_w and M_w/M_n determined by GPC of TMC polymers is presented in Table 10. All TMC had a relatively wide molecular weight distribution with a polydispersity index in the range of 2.9 – 4.9.

In comparison with starting chitosan, the M_w values of all TMC were markedly decreased. The results agreed well with the discovery made by Mao at al. (214) who observed that the resulting molecular weight of TMC depended on the initial molecular weight of chitosan. Significant molecular weight decrease was observed when chitosan molecular weight was larger that 100 kDa. Although a decrease in M_w of TMC with increasing DQ was not distinctly observed as reported by Snyman et al. (215), it was found that the M_w depended on the synthesis procedure. It increased with the extension of reaction duration correlated to an increase in DQ and DD as seen in TMC400-10-40/TMC400-20-60 and TMC400-20-20/TMC400-40-40. Therefore, an addition of methyl groups to the amino groups of chitosan resulted in TMC with high M_w.

On the contrary, the M_w decreased with increasing number of reaction steps or additional steps as seen in TMC400-10-40/TMC400-20-20 and TMC400-20-60/TMC400-40-40. This was due to the degradation of the polymer in the strong basic environment. The results obtained are consistent with those previously reported by Hamman and Kotźe (157) who observed that intrinsic viscosity, an indication of

Table 10. Intrinsic viscosity values and relative molecular weight of different TMC polymers

Polymers	Reaction time (h / h / h)[a]	[η] (dl/g)[b]	M_w (× 10^4 g/mole)[c]	M_w/M_n[c]
TMC400-10-40	1.0 / - / -	2.18	37.8	4.86
TMC400-20-20	1.0 / 0.5 / -	2.09	28.6	3.91
TMC400-20-60	1.5 / - / -	2.48	54.2	4.74
TMC400-30-30	1.0 / 1.0 / -	2.48	n.d.	n.d.
TMC400-40-40	1.5 / 1.5 / -	2.15	36.5	2.89
TMC400-80-10	1.0 / 1.0 / 1.0	2.01	26.6	3.50

n.d. = Not determined

[a]Reaction times of reaction step 1 / addition step 1 / addition step 2

[b][η] for the starting chitosan was 10.70 dl/g.

[c]M_w and M_w/M_n for the starting chitosan were 87.2 × 10^4 g/mole and 3.50, respectively.

the molecular weight, of TMC increased with increasing reaction duration and decreased with increasing number of reaction steps. Therefore, it can be concluded that the molecular weight of TMC is affected by addition of methyl groups to the amino groups of chitosan and the polymer degradation by the strong basic environment.

1.3 Intrinsic viscosity

Based on the fact that [η] is closely related to polymer-chain conformation, the dependence of [η] upon the molecular weight gives information concerning the conformation and the extension of the polymer according to the Mark-Houwink equation:

$$[\eta] = KM_v^{a} \qquad \text{(Eq. 15)}$$

where K and a are empirical constants for given solute-solvent system and temperature, [η] is the intrinsic viscosity and M_v is the so-called viscosity-average molecular weight which can be substituted with the weight-average molecular weight, M_w. The Mark-Houwink exponent a is used as a parameter to determine the conformation of a polymer. Polymers in the shape of a sphere, random coil or rod have exponent a values of 0, 0.5 ~ 0.8 and 1.8, respectively (216, 217).

The intrinsic viscosities of TMC in 2%HAc/0.2 M NaAc at 25°C are given in Table 10. Regardless of the substitution degrees, it was found that the [η] of polymer solution increased with an increase in the M_w of the polymer. This is consistent with the previous report by Snyman et al. (215) who observed that the decrease in absolute molecular weight was correlated well with the decreased [η] of TMC polymers.

Figure 13 shows the plot of log [η] versus log M_w. The values of 0.39 and 2.14×10^{-4} were obtained for a and K, respectively. The value of Mark-Houwink exponent a suggested that TMC behaved like a spherical structure, approximating a random coil. The result is inconsistent with the observation of Synman et al. (43) who reported that TMC possessed a rod-shaped conformation. This discrepancy could be due to the difference in experimental conditions such as ionic strength, solvent, temperature, and pH value of solution (218, 219).

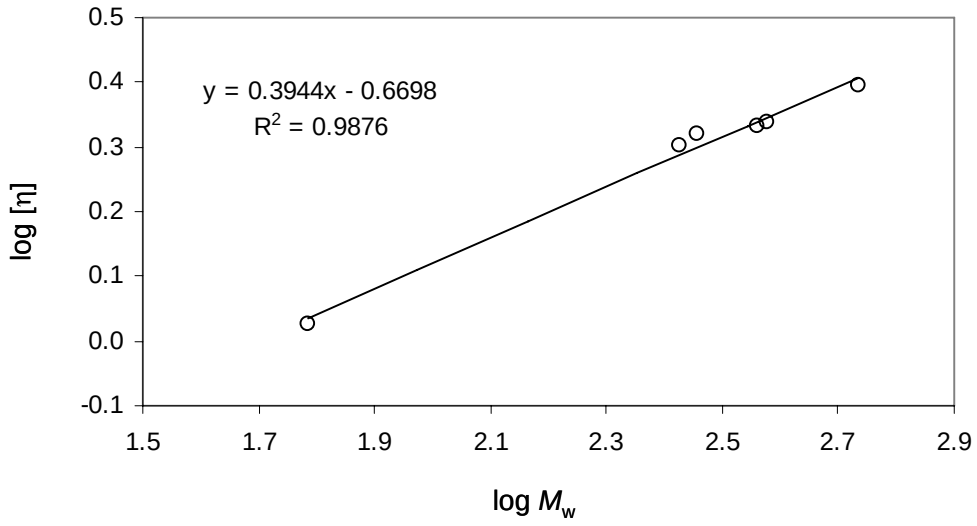

Figure 13. Intrinsic viscosity of TMC in 2%HAc/0.2 M NaAc at 25°C as a function of M_w determined by GPC.

In general, the polymer conformation and the polymer-solvent interactions depend on the number of positive charges (NH_3^+) of chitosan which are related to the degree of deacetylation. Low value of deacetylation degree results in a rigid conformation, leading to a higher degree of expansion of chitosan (204). In the buffer of 2%HAc/0.2 M NaAc (pH 4.5), chitosan with deacetylation degree of 85% exhibits random coil structure (220). Since TMC were a cationic polyelectrolyte with pK_a value of about 6.5 (data shown in section 1.4), all non-quaternized amino groups were protonated at low pH of the solvent. In this case, electrostatic repulsion forces of the protonated amino groups were hindered due to pendent methyl groups of TMC, leading to the condensed conformation.

1.4 Potentiometric titration curves

A potentiometric titration is one of the simplest methods used to determine the degree of deacetylation of chitosan (221, 222). Recently, it has been used with data from elemental analysis to determine DQ of TMC polymers (34).

In this study, a titration curve was generated by dissolving TMC in HCl solution and then titrating potentiometrically with NaOH solution. Figure 14 shows potentiometric titration and 1st derivative curves of different TMC polymers. The potentiometric titration curves of all TMC exhibit two inflection points. The first of which corresponds to the neutralization of the free acidity, while the second indicates the complete deprotonation of the protonated non-quaternized amine groups. The difference between the two inflection points along the abscissa (shown in 1st derivative curve in Figure 14) yields the moles of OH^- required to deprotonate the protonated non-quaternized amino groups of TMC and reflects to the amount of $–NH_2$, $-NH(CH_3)$, and $–N(CH_3)_2$ in the titrant solution. Assuming that the rest of the sample is $–N^+(CH_3)_3$ and $-NHCOCH_3$, the DQ value of the specimen can readily be obtained (34).

Since TMC was composed of not only quaternized amines but also mono- and di-methylated amines, it was found that the difference between the two inflection points was affected by DQ and DD. Number of OH^- required to deprotonate the protonated non-quaternized amino groups increased with increasing DD (2.47 mmol OH^-/g polymer for TMC400-20-20 compared to 2.63 mmol OH^-/g polymer for

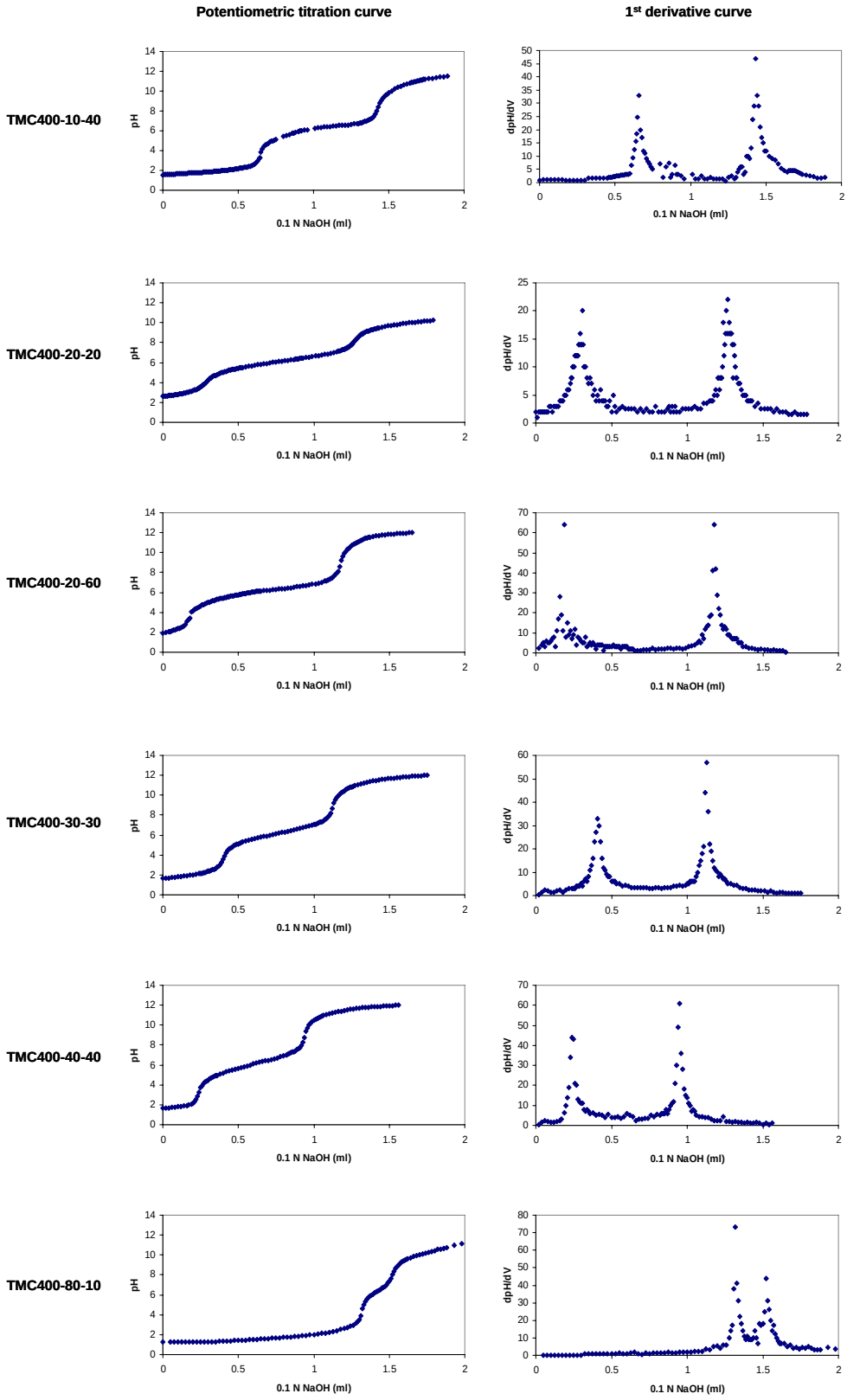

Figure 14. Potentiometric titration and 1st derivative curves of different TMC polymers.

TMC400-20-60). When considering DD in range 30-40%, number of OH^- required decreased linearly with the increase of DQ with regression coefficients of 0.98. Moreover, it was observed that at DD/DQ ratio ≤ 1, number of OH^- required decreased with increasing DQ with a linear correlation of 0.99. Therefore, DD would affect the number of OH^-, leading to an error for calculation of DQ. For an accurate result by this method, DQ should be determined and compared within almost the same value of DD or at DQ much higher than DD. In addition to the use of this method to determine DQ, the pK_a of all TMC polymers could be evaluated to be in the range of 6.1 – 6.4. During titration, the solution of TMC with DQ < 24% became cloudy when the pH > 6, which was not found in higher DQ of TMC (discussed in detail in section 1.5)

It is well documented in the literature that results obtained from pH-potentiometric titration are influenced by several factors. Balázs and Sipos (223) reported that the moisture content of the air-dry chitosan samples and the ash content caused variations in the values of degree of deacetylation. The precipitation of chitosan during titration also resulted in an error in the determination of deacetylation degree (221). The precipitated chitosan reduced the concentration and could cover the surface of electrode, and thus the electrode would lose its accuracy. From the limitation of pH-potentiometric titration and results obtained in this study, it was found that this method would not be suitable for characterization of TMC polymer.

1.5 Solubility of TMC polymers

1.5.1 Effect of quaternization and dimethylation degrees

Figure 15 shows the pH dependence of the transmittance of the TMC with different DD/DQ. As seen in Figure 15a, the water solubility of TMC with DD/DQ of 3 (TMC400-10-40) was high at acidic pH but decreased at pH a little over neutrality. The solubility of TMC400-10-40 in basic pH was abruptly decreased when increasing concentration. In contrast, the solubility of TMC with DD/DQ of 1 (TMC400-40-40) was high and retained over a wide pH range (Figure 15b). The water solubility of TMC was substantially decreased with DD/DQ of 0.1 (TMC400-80-10), as seen by the low % transmittance (Figure 15c). However, the solubility of TMC having DD/DQ ≤ 1 was not pH dependent (Figures 15b and 15c). Comparison

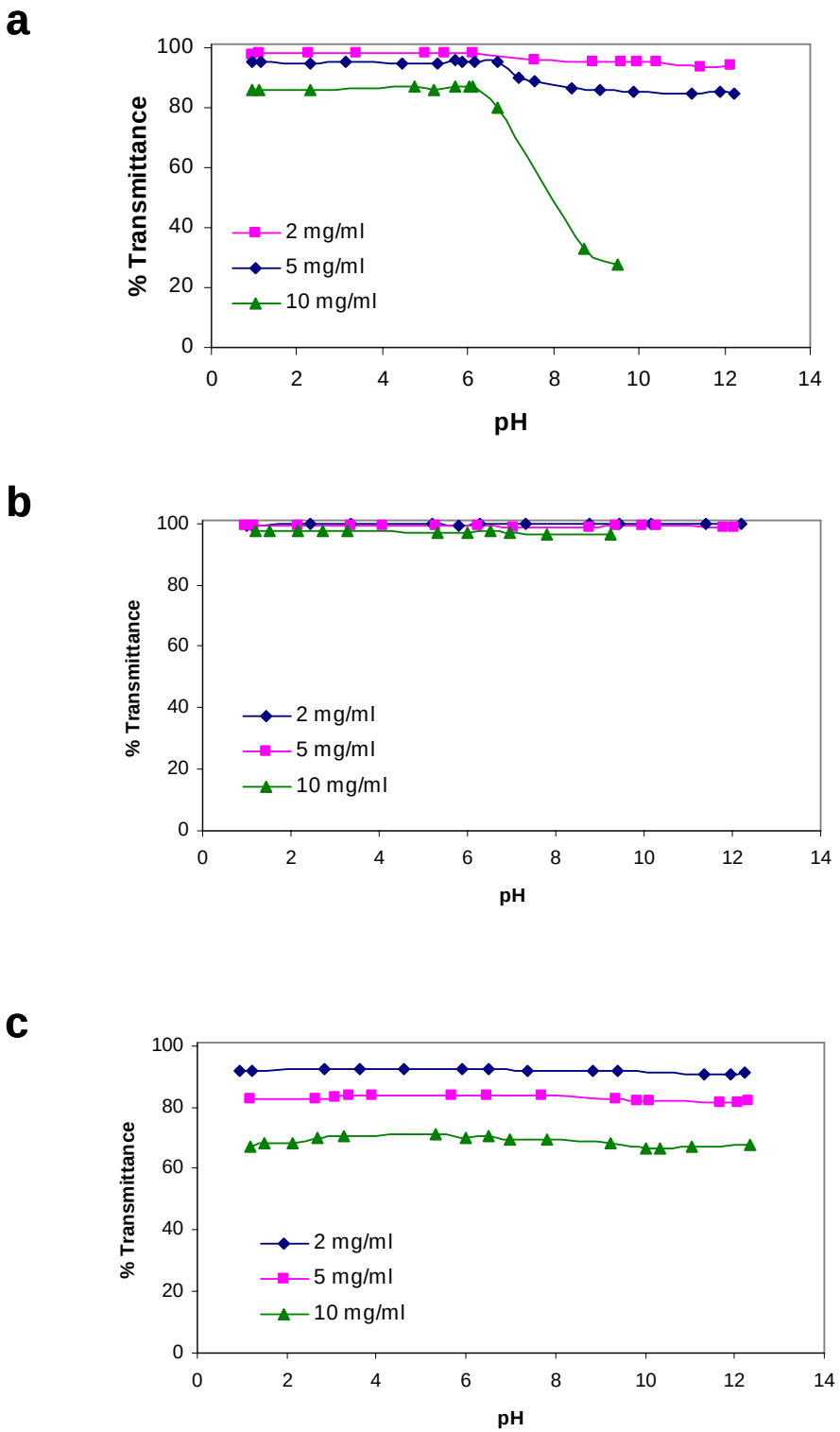

Figure 15. The pH dependence of water solubility of (a) TMC400-10-40 (DD/DQ = 3), (b) TMC400-40-40 (DD/DQ = 1) and (c) TMC400-80-10 (DD/DQ = 0.1).

between the pH dependence of water solubility of TMC400-20-20 and that of TMC400-20-60 (Figure 16), it would obviously clarify that the water solubility of TMC was DD/DQ dependent.

The results were comparable to the finding obtained from potentiometric titration mentioned previously. The lower solubility of the high DQ of TMC (TMC80-10) was expected due to high degree of *O*-methylation at the 3- and 6-hydroxyl groups (19). However, the opposite result was found in the low DQ of TMC as reported by Kotze et al. (159) who indicated that TMC with low DQ of 12.6% was highly soluble over a wide pH range even at high concentration of 10% w/v. This discrepancy may be from different DD of TMC. It is possible that the water solubility of TMC polymers with low DQ and relatively high DD decreased in an basic solution because they included about 65-75% of non-quaternized residues, mainly in forms of $–N(CH_3)_2$, $–NH(CH_3)$ and $–NH_2$. The high pendent methyl groups hindered intra- and/or intermolecular interactions resulting in the decreased solubility of the TMC with low DQ.

1.5.2 Effect of ionic strength

The effect of ionic strength on the water solubility of TMC was also investigated. Figure 17 shows pH dependence of water solubility of TMC with different DD/DQ as a function of ionic strength. For TMC with DD/DQ = 3, ionic strength did not affect the solubility of polymers at pH lower than their pK_a 6.5, after that the solubility decreased with increasing pH and ionic strength of the medium and the decrease was more pronounced in the higher ionic strength solution (Figure 17a). On the other hand, the ionic strength did not affect the solubility of TMC with DD/DQ = 1, as shown in Figure 17b. In case of TMC400-80-10 (DD/DQ = 0.1), although slight decrease in water solubility was observed at higher ionic strength, the solubility was retained over a wide pH range (Figure 17c).

It is known that ionic strength affects the hydrodynamic behavior of chitosan and its derivatives. Yang et al. (224) reported that viscosities of *N*-alkylated mono-/disaccharide chitosans with low substitution degree decreased with an increase in ionic strength, while change in solubility of high substitution degree of chitosan with ionic strength was not marked. Holme and Perlin (225) also observed that ionic

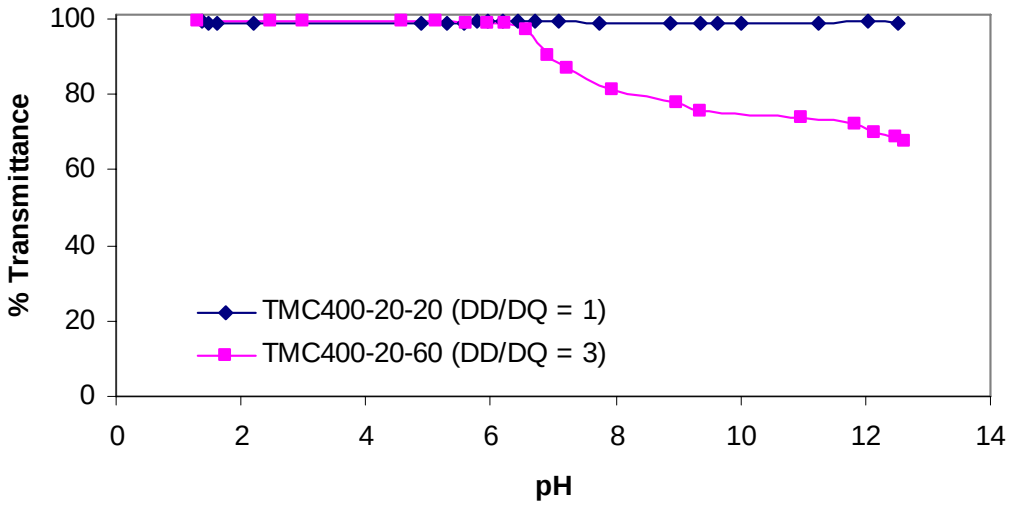

Figure 16. Effect of DD on the solubility of TMC. Polymer concentration was 5 mg/ml.

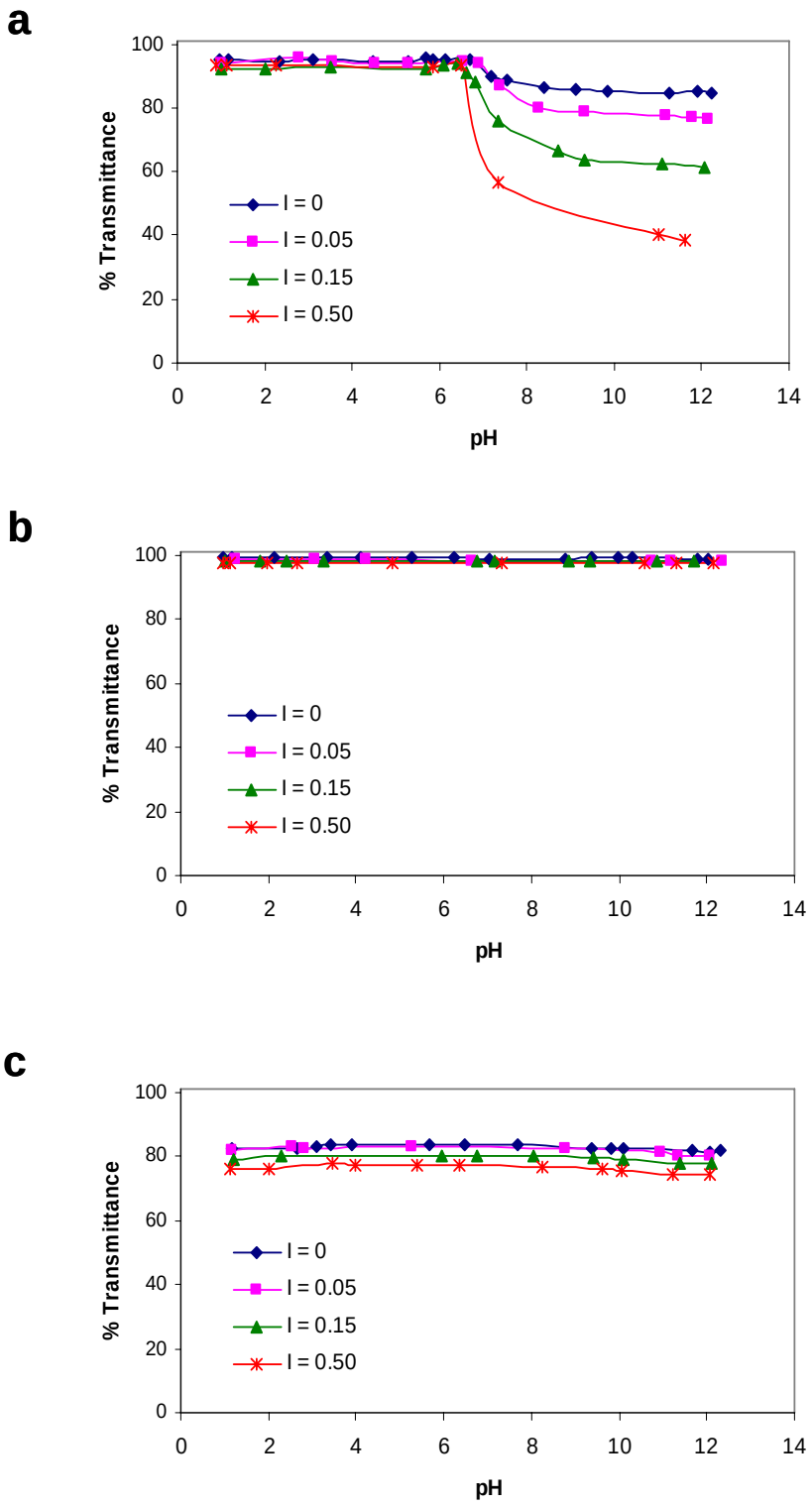

Figure 17. Effect of ionic strength on the water solubility of (a) TMC400-10-40 (DD/DQ = 3), (b) TMC400-40-40 (DD/DQ = 1) and (c) TMC400-80-10 (DD/DQ = 0.1). Polymer concentration was 5 mg/ml.

strength had an effect on the solubility of *N*-sulfated chitosan. Generally, in high ionic strength solutions, the concentration of the counter-ions is raised which screens the protonated amino group of chitosan and in turn the solubility becomes reduced (226). This may provide some evidence to support the findings in our experiment.

Taken together, the data from Figures 15 – 17 imply that the charge density of TMC, represented by DQ, would be an important factor determining its water solubility and the optimum value was an intermediate DQ of 30 – 40% at which DD did not affect the water solubility. The influence of DD on the solubility properties of TMC was obviously observed when DQ was lower than 24%.

1.6 Polymer-mucin interactions

In this work, mucoadhesive properties of TMC were evaluated by using the mucin particle method based on the change in surface properties of mucin particle, particle size and zeta potential, by the adhesion of the polymer. It was expected that suspension of ss-mucin particles when mixed with a polymer solutions, would induce the ss-mucin particles to aggregate if the polymer had a strong affinity to them. Procine gastric mucin type III, a commercially available mucin, was chosen in this study. Leitner et al. (182) stated that there is no significant difference in the results obtained with native mucus and hydrated commercial mucin.

The interaction was determined at pH 6.8 in Tris buffer where chitosan was insoluble and lost mucoadhesive properties. Figure 18 shows evolution of particle size and zeta potential of ss-mucin particles versus added volume of 1 mg/ml TMC400-40-40 solution. Two regions could be defined. In region I, polymer did not affect the size and zeta potential of ss-mucin. Increases in size and zeta potential were observed in region II where the aggregation occurred after the zeta potential of ss-mucin exceed the critical zeta potential of ss-mucin (ca. -7 mV). This finding can be explained by DLVO theory (227). It is well known that the mucoadhesion can be attributed to a two-step process (167). Initially, an intimate surface contact between the bioadhesive polymers and mucus tissue has to be established (contact stage). In a consecutive step, both phases may interdiffuse or interpenetrate to a certain extent and formation of secondary chemical bonds, such as electrostatic and hydrophobic interactions, hydrogen bonding and van der Waals interactions, which occur to

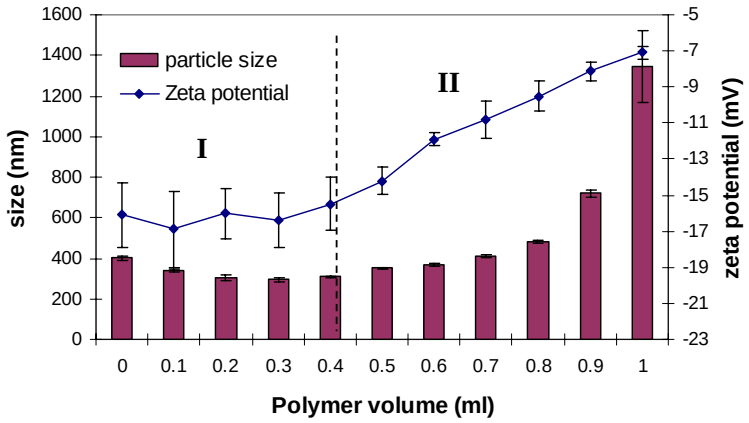

Figure 18. Change in observed particle size and zeta potential of ss-mucin particles when mixed with the various volumes of 1 mg/ml TMC400-40-40 solution. Concentration of ss-mucin suspension was 1 % w/v at pH 6.8.

consolidate and strengthen the adhesive joint, leading to prolonged adhesion (consolidation stage). In comparison, region I can be assumed as the contact stage whereas region II refers to the consolidation stage.

With regard to region I, it was also found that all TMC with different DQ and DD exhibited equal volume of 0.4 ml, indicating that this region was polymer structure independent. The results suggest that the DQ and DD did not affect the intimate contact between TMC and mucin. This could be explained from the same conformation of TMC polymers.

The slope of zeta potential profiles in region II and an extrapolated critical volume (V_c) of polymer used to neutralize negative charge of ss-mucin to zero could be used as indices of mucin-polymer adhesive bond strength of TMC polymers. The stronger the mucoadhesive bond strength, the higher the value of slope as well as the lower the V_c value was observed. By referring to the results of ss-mucin – polymer interaction studies (Table 11), it can be deduced that TMC exhibited mucoadhesive characteristic and the rank order of mucoadhesive bond strength of TMC was TMC400-80-10 > TMC400-20-20 > TMC400-40-40 > TMC400-10-40 > TMC400-20-60. In addition, the mucoadhesion of TMC depended on the proportion of DD to DQ. The mucoadhesive bond strength of TMC linearly decreased with increased the ratio of DD/DQ, as shown in Figure 19. At the same DQ of 20%, the mucoadhesive bond strength of TMC400-20-60 was threefold lower than that of TMC400-20-20. The results obtained could be explained by the electrostatic interaction between positively charged amino groups of TMC and the negatively charged sialic acid residue of mucus glycoproteins or mucins. When increasing DD, the high number of methyl pendent groups acted to shield the positive charges of TMC which reduced the interaction between polymer and mucin and hence the decreased mucoadhesive properties.

Taken together, the data obtained suggest that mucoadhesive properties of TMC were influenced by the combination of positive charge density and steric hindrance of pendent groups on polymer.

Table 11. Characteristics of the interaction between ss-mucin particle and TMC polymers

Polymer	Slope (mV/ml)	V_c[a] (ml)
TMC400-10-40	5.8 ± 0.4	3.0 ± 0.2
TMC400-20-20	13.1 ± 1.4	1.4 ± 0.1
TMC400-20-60	4.6 ± 0.4	3.7 ± 0.5
TMC400-30-30	n.d.	n.d.
TMC400-40-40	11.3 ± 0.3	1.7 ± 0.0
TMC400-80-10	15.3 ± 2.0	1.3 ± 0.1

n.d. = Not determined

The data are expressed as the means ± SD of three experiments.

[a]The extrapolated volume of 1 mg/ml polymer solution used to neutralize negative charge of 1% w/v ss-mucin to zero

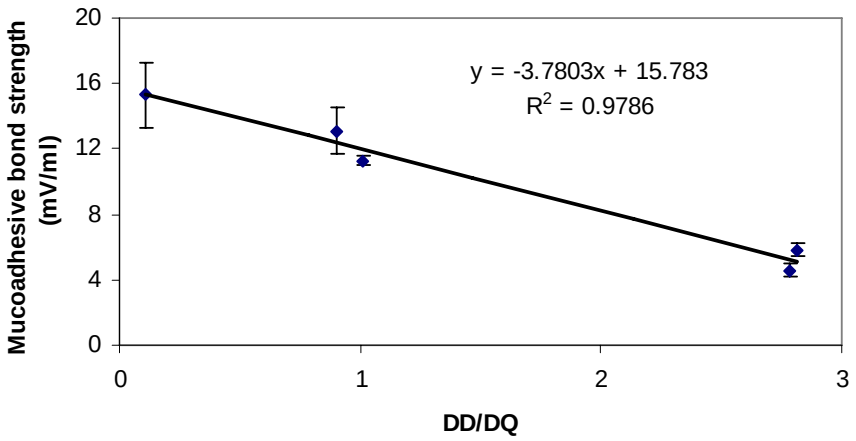

Figure 19. Correlation between the ratio of DD/DQ of TMC and mucoadhesive bond strength measured by the mucin particle method. Each point represents the mean ± SD of three experiments.

1.7 Cytotoxicity

The effects of polymer structure on L929 cells were investigated by testing cell viability via MTT assay. The concentration of TMC resulting in 50% inhibition of cell growth, IC_{50} value was evaluated. The results are summarized in Table 12. TMC400-80-10 was particularly toxic with an IC_{50} of 10 μg/ml. At the same DD/DQ of 1 (TMC400-20-20, TMC400-30-30 and TMC400-40-40), the cytotoxicity of TMC increased with increasing DQ. However, TMC400-10-40 and TMC400-20-60 were shown to be completely non-toxic with IC_{50} > 1 mg/ml. These appear consistent with the conclusion earlier drawn by Kean et al. (46) who reported that cytotoxicity of TMC increased with increasing DQ of the TMC. Haas et al. (160) reported that the cytotoxicity on COS-1 cells of TMC with a low DQ (4%) and intermediate DQ (10% and 18%) was less than that of chitosan, meanwhile TMC with high DQ of 66% appeared to be more toxic.

Considering the effect of DQ and DD, it was found that cytotoxicity of TMC was influenced by the proportion ratio of DD to DQ. The cytotoxicity of TMC began to decrease when DD/DQ ratio was higher than 1 and TMC showed non-toxic property when ratio of DD to DQ was about 3:1. Since the cytotoxicity of TMC would probably be a consequence of its relatively positive charge (206, 228), this phenomenon could be explained by the steric effect of methyl pendent groups of dimethylamino groups which shielded a proportion of the positive charges present on TMC decreasing the interaction of the positively charged amino groups of TMC with the anionic compartments of glycoproteins on the cell membrane. For TMC having DD ≤ DQ, the amount of methyl pendent groups from dimethylamino groups was insufficient to shield its positive charges, leading low cell viability. Similarly, Mao et al. (45) reported that grafting PEG on TMC polymer chain can improve the biocompatibility of TMC and the extent of which is substitution degree and PEG molecular weight dependent.

Taking data from cytotoxicity and mucoadhesion in consideration, it was observed that cytotoxicity data fairly correlated with mucoadhesive bond strength. These confirmed that the electrostatic interaction between the positively charged amino groups of TMC and the negatively charged residues in mucus layer and on cell

Table 12. Cytotoxicity of TMC polymers on L929 fibroblast cells following 3 h incubation as determined by MTT assay (n = 4)

Polymer	IC_{50} (μg/ml)
TMC400-10-40	>1000
TMC400-20-20	24
TMC400-20-60	>1000
TMC400-30-30	21
TMC400-40-40	12
TMC400-80-10	10

membrane was the predominant mechanism for mucoadhesion and cytotoxicity of TMC.

2. Characterization of PEGylated TMC copolymers

The M_w and mucoadhesive properties of PEGylated TMC copolymers used in this study were characterized. The physicochemical properties in terms of thermal properties, water solubility and cytotoxicity of PEGylated TMC copolymers had been previously reported (45). The copolymers used were designated as PEG(5k)$_n$-g-TMCx-*y*, where subscript *n* represents the average number of 5 kDa PEG chains per TMC *x* kDa macromolecule of *y* % DQ.

2.1 Molecular weight

As shown in Table 13, the M_w of PEGylated TMC copolymers was much smaller than that of the parent TMC400-40, even though theoretical molecular weight of copolymers should be greater. This may be caused from instrumental analysis and molecular size of copolymers. When using GPC for determining molecular weight, it mostly requires calibration with known molecular mass standards such as pullulen. An eluation time of polymers from a column depends on their molecular size. The large molecular size which is eluated earlier from the column is considered a higher M_w. In this study, the acidic eluent may cause a maximum expansion of the cationic polymers, leading to fast separate from the column. However, in case of copolymers, PEG partly shielded the positive charges of TMC, resulting in decrease in electrostatic repulsion of the polymer. Consequently, the polymer chain became more condensed and was retarded when eluted from the gel column, indicating relatively low M_w. Likewise, Petersen et al. (229) observed the same phenomenon occurred with polyethylenimine (PEI)-*graft*-PEG block copolymers. Glodde et al. (230) determined the hydrodynamic diameter of PEG-*graft*-PEI copolymers with dynamic light scattering (DLS) and found that PEGylated PEI 2 kDa and PEGylated PEI 25 kDa copolymers with PEG 5 kDa exhibited very small hydrodynamic diameters.

Table 13. Properties and molecular weights of PEGylated TMC copolymers

Polymer	Substitution[a] (%)	Theoretical MW[b] ($\times 10^3$ g/mole)	M_w[c] ($\times 10^3$ g/mole)	M_w/M_n[c]
TMC400-40	-	400	364.7	2.89
$PEG(5k)_{298}$-g-TMC400-40	12.0	1890	8.2	1.35
$PEG(5k)_{640}$-g-TMC400-40	25.7	3600	7.4	1.30
$PEG(5k)_{680}$-g-TMC400-40	27.4	3800	8.1	1.34

n.d. = Not determined

[a]Reported by Mao et al. (45)

[b]Calculation based on the composition of the copolymer

[c]Determined by GPC with pullulan standard

2.2 Polymer-mucin interactions

The effects of PEG chain on the interaction between mucin and polymer in pH 6.8 Tris buffer were determined by the mucin particle method based on the change in surface zeta potential of mucin due to the adhesion of the mucin and polymer. Figure 20 shows the zeta potential of mucin versus polymer volume which two regions can be defined. In region I, the amount of polymer solution added does not affect the zeta potential of mucin. In contrast, an increase in zeta potential with increasing the amount of polymer solution can be observed in region II.

With regard to region I, compared to unmodified TMC400-40, the polymer volume independent region extended with an increase in the average number of PEG chains per TMC molecule as shown in Figure 20. These results suggest the initial adhesion between polymer and mucin decreased with increasing PEG substitution degree. In general, the conformation of polymer plays an important role in an initimate contact between mucoadhesive and mucus membrane. The polymer with random coil conformation shows higher mucoadhesive than that with spherical and rigid rod shape conformations (231). For mucin, it was reported that the hydrodynamic model of mucin conforms to a random coil within a spherical solvent domain (141). Based on GPC results, it was assumed that the PEGylated TMC copolymers had more condensed structure as compared to nearly random coil structure of TMC as previously discussed in section 1.3. This would cause a reduction in intimate adhesion of the PEGylated copolymers to mucin, leading to large polymer volume in region I.

As shown in Figure 20, when compared to unmodified TMC400-40, the slope of profiles ($R^2 > 0.96$) in region II, representing mucoadhesive bond strength of polymer, decreased with increasing level of PEG grafting which were 5.217, 2.162, 1.506 and 1.543 for TMC400-40, PEG$(5k)_{298}$-g-TMC400-40, PEG$(5k)_{640}$-g-TMC400-40 and PEG$(5k)_{680}$-g-TMC400-40, respectively. Based on the fact that the mucoadhesion of cationic polymer such as chitosan is mainly influenced by the positive charge of polymer in the consolidation stage (51, 53, 185), the decrease in mucoadhesion of copolymer could probably be from the steric effect of PEG chains which hinder the electrostatic interaction between the positively charged groups of copolymer and the negatively charged groups of mucin.

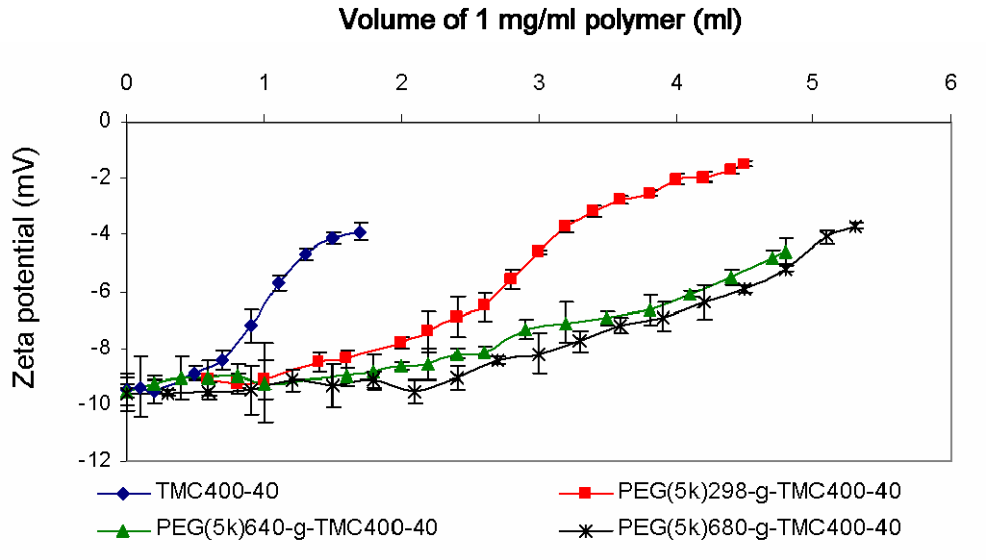

Figure 20. Change in observed zeta potential of mucin particles when mixed with the various volumes of 1 mg/ml polymer solutions. Concentration of mucin suspension: 1% w/v, pH 6.8. The reported data are the mean ± SD of three experiments.

3. Preparation and characterization of insulin NC

From a range of TMC polymers, TMC400-10-40, TMC400-40-40 and TMC400-80-10 were selected to evaluate the influences of DQ and DD/DQ on the insulin NC formation. Self-assembled insulin NC were prepared by electrostatic interactions between positively charged polymer and negatively charged insulin as a driving force (Figure 21).

3.1 Stoichiometric ratio of polymer and insulin in NC

Although turbidimetric titration is a simple and sensitivity technique used to investigate the interaction between protein and polyelectrolyte (47, 62, 149, 155), such technique still have a drawback due to the fact that turbidity (100-T(%)) is influenced not only increased number of particle formed but also increased size, causing inaccurate results. This problem can be solved by dynamic light scattering which gave the results of particle size and particle concentration, measuring in term Kcps, in the same time. Additional, from preliminary study, Kcps values obtained correlated with turbidity results, simultaneously measured.

As reported previously (47), the NC formation process is influenced by a variety of parameters including the system pH, sequence of mixing, polymer/protein ratio and concentration, polymer molecular weight and structure, ionic strength, etc. Amongst all of these parameters, the most important factor appears to be the system pH. From preliminary experiments, the suitable pH for preparing insulin NC with TMC and PEGylated TMC copolymers was 7.4. Therefore, the stoichiometric ratio of polymer and insulin was investigates in 10 mM Tris buffer, pH 7.4. At such pH, human insulin carries two negative charges per molecule (232) while all primary and quaternized amino groups of TMC and copolymer are protonated. The polymer/insulin (+/–) charge ratio was calculated according to the mass of the two components.

As depicted in Figure 22, during titration of polymer solution with insulin solution, uniform and nano-sized NC can be formed only at ≥ optimal polymer/insulin mass ratio. The amount of complexes formed, in term of Kcps value, increased with decreasing polymer/insulin mass ratio until reach an optimal ratio. At lower this critical point, larger complexes were obtained and flocculation occurred in a short

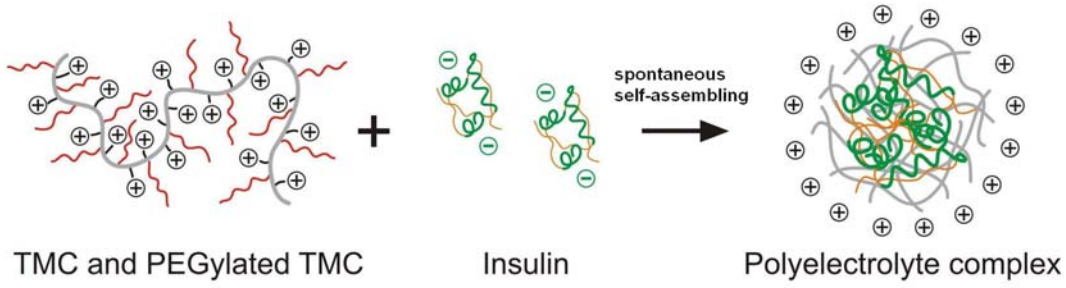

Figure 21. Schematic representation of insulin NC formation.

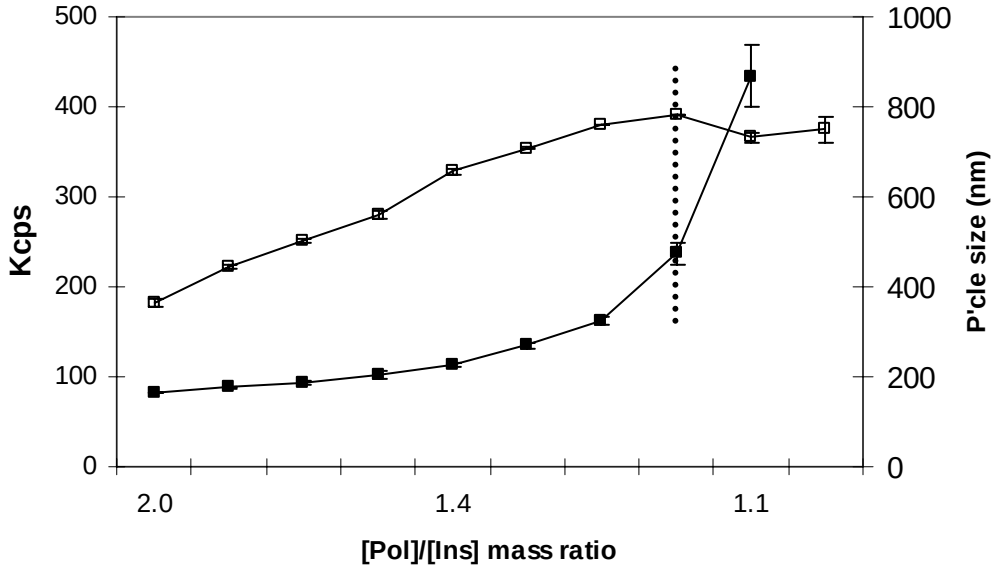

Figure 22. Evolution of particle size and Kcps value of TMC400-10/insulin complexes versus [Pol]/[Ins] mass ratio. (■) size; (□) Kcps. TMC400-10 solution (1 mg/ml) was titrated with insulin solution (1 mg/ml). Particle size and Kcps values of the NC were monitored by dynamic laser light scattering.

period of time. The optimal (+/–) charge ratio between polymer and insulin was calculated from the polymer/insulin mass ratio at the critical point which was found to be polymer structure dependent. The optimal polymer/insulin (+/–) charge ratios of TMC and copolymers were summarized in Table 14. These finding suggest that the stoichiometry of the NC are primarily determined by the charge density of the polymers.

The properties of the self-assembled insulin NC prepared at optimal polymer/insulin (+/–) charge ratio are described in Table 14. All complexes had a size in the range of 154 – 298 nm, a positive surface charge and high insulin AE (> 90%). In general, the zeta potential of NC depended on positive surface charge density of polymers. In term of TMC, the zeta potential of TMC/insulin NC was mainly influenced by DQ of TMC which increased with increasing DQ. In case of PEGylated TMC400-40 copolymer, the presence of the PEG macromolecule acted to shield a proportion of the positive charges present on TMC resulting in a reduction of the colloidal zeta potential (2.3 – 13.6 mV) as compared to that of unmodified TMC400-40 NC (24.7 mV).

3.2 Effect of polymer/insulin (+/–) charge ratio

As shown in Table 15, soluble insulin NC prepared at optimized polymer/insulin (+/–) charge ratio displayed high insulin AE and PY with low polydispersity index (PDI), consistent with the observation as an opalescent solution. On the contrary, the particle size, AE and PY of NC decreased while the zeta potential and PDI increased with the increasing (+/–) charge ratio of polymer to insulin ($p < 0.05$). These results agree well with the results reported by Fredheim and Christensen (233) who found that the maximum yield of lignosulfonate-chitosan complexes was performed at optimal ligonosulfonate/chitosan (w/w) mixing ratio. The precipitated yield declined when increasing ratio of chitosan. These finding can probably be explained by the conformation of polymer (43). When polymer concentration increased, the charge density and sterical hindrances between the pendant groups (methyl groups and PEG segments) increased, resulting in low flexibility of polymer chains. These hinder insulin to interact with polymer chains, causing low AE and PY.

Table 14. Formulation and characteristics of insulin NC. The initial concentration of insulin was 1 mg/ml in all the formulations

Polymer	Mass ratio[a] (Pol : Ins)	Charge ratio[b] (Pol : Ins)	Particle size (nm)	Polydispersity Index	Zeta potential (mV)	Association Efficiency (%)	Process yield (%)
TMC400-10	1.2 : 1	3 : 1	298 ± 9	0.36 ± 0.04	14.2 ± 0.7	97 ± 1	87 ± 2
TMC400-40	0.3 : 1	2 : 1	181 ± 7	0.13 ± 0.03	24.7 ± 1.5	97 ± 1	78 ± 1
TMC400-80	0.3 : 1	4 : 1	198 ± 5	0.37 ± 0.02	39.6 ± 3.5	94 ± 0	61 ± 5
$PEG(5k)_{40}$-g-TMC100-40	1.0 : 1	5 : 1	232 ± 6	0.28 ± 0.06	24.3 ± 2.2	93 ± 0	45 ± 1
$PEG(5k)_{298}$-g-TMC400-40	1.0 : 1	3 : 1	154 ± 13	0.19 ± 0.03	13.6 ± 0.8	95 ± 1	58 ± 4
$PEG(5k)_{640}$-g-TMC400-40	1.0 : 1	2 : 1	190 ± 6	0.18 ± 0.03	2.3 ± 0.3	93 ± 0	65 ± 2
$PEG(5k)_{680}$-g-TMC400-40	1.5 : 1	2 : 1	225 ± 11	0.15 ± 0.06	6.4 ± 0.3	95 ± 0	47 ± 8

The data are expressed as the means ± SD of three batches.

[a] Optimized polymer/insulin mass ratio for preparation of insulin NC

[b] Calculation based on the polymer / insulin mass ratio at pH 7.4

Table 15. Effect of polymer/insulin (+/–) charge ratio on the physicochemical properties of insulin NC. The initial concentration of insulin was 1 mg/ml in all the formulations

Formulation	Mass ratio Pol/Ins	Charge ratio (Pol/Ins)[b]	Particle size (nm)	Polydispersity index	Zeta potential (mV)	Association Efficiency (%)	Process yield (%)
TMC400-10 NC-1	1.2 : 1[a]	3 : 1	298 ± 9	0.36 ± 0.04	14.2 ± 0.7	97 ± 1	87 ± 2
TMC400-10 NC-2	2 : 1	4 : 1	116 ± 5*	0.26 ± 0.10	20.7 ± 1.5*	58 ± 6	n.d.
TMC400-40 NC-1	0.3 : 1[a]	2 : 1	181 ± 7	0.13 ± 0.03	24.7 ± 1.5	97 ± 1	78 ± 1
TMC400-40 NC-2	1 : 1	6 : 1	142 ± 3*	0.33 ± 0.02*	29.2 ± 1.7*	31 ± 2*	34 ± 1*
TMC400-40 NC-3	2 : 1	12 : 1	104 ± 4*	0.37 ± 0.03*	33.4 ± 2.0*	27 ± 1*	10 ± 1*
TMC400-80 NC-1	0.3 : 1[a]	4 : 1	198 ± 5	0.37 ± 0.02	39.6 ± 3.5	94 ± 0	61 ± 5
TMC400-80 NC-1	2 : 1	25 : 1	132 ± 10*	0.47 ± 0.08*	46.9 ± 1.0*	3 ± 1	n.d.
PEG(5k)$_{40}$-g-TMC100-40 NC-1	1 : 1[a]	5 : 1	232 ± 6	0.28 ± 0.06	24.3 ± 2.2	93 ± 0	45 ± 1
PEG(5k)$_{40}$-g-TMC100-40 NC-2	2 : 1	10 : 1	159 ± 5*	0.29 ± 0.03	27.5 ± 1.5*	36 ± 3*	24 ± 2*
PEG(5k)$_{298}$-g-TMC400-40 NC-1	1 : 1[a]	3 : 1	154 ± 13	0.19 ± 0.03	13.6 ± 0.8	95 ± 1	58 ± 4
PEG(5k)$_{298}$-g-TMC400-40 NC-2	2 : 1	6 : 1	128 ± 5*	0.25 ± 0.07	22.7 ± 0.9*	39 ± 3*	n.d.
PEG(5k)$_{640}$-g-TMC400-40 NC-1	1 : 1[a]	2 : 1	190 ± 6	0.18 ± 0.03	2.3 ± 0.3	93 ± 0	65 ± 2
PEG(5k)$_{640}$-g-TMC400-40 NC-2	2 : 1	3 : 1	104 ± 1*	0.20 ± 0.01	8.0 ± 0.9*	42 ± 2*	n.d.
PEG(5k)$_{680}$-g-TMC400-40 NC-1	1.5 : 1[a]	2 : 1	225 ± 11	0.15 ± 0.06	6.4 ± 0.3	95 ± 0	47 ± 8
PEG(5k)$_{680}$-g-TMC400-40 NC-2	2 : 1	3 : 1	147 ± 4*	0.18 ± 0.04	13.0 ± 0.8	71 ± 3	n.d.

The data are expressed as the means ± SD of three batches. n.d., not determined.

[a] Optimized polymer/insulin mass ratio for preparation of NC

[b] Calculation based on the polymer / insulin mass ratio at pH 7.4

* Statistically significant differences ($p < 0.05$) compared with that of NC at optimal polymer/insulin mass ratio

Additionally, a decrease of associated insulin amount in NC and an increase of positively charged polymer chains towards the external aqueous medium could promote complex condensation, consequently a decreased particle size and high zeta potential NC were obtained.

3.3 Morphology of the insulin NC

In this study, morphology of the NC was visualized by AFM in tapping mode in order to avoid damage of sample surface. It is demonstrated to be a valuable tool in visualization and quantification of particle. Moreover, AFM readily provides shape and structural information of analyzed particles, which cannot be obtained by light scattering (234). Figures 23a and 23b display an overview at a scan size (5 × 5 μm) of representative fresh insulin NC prepared at the optimized polymer/insulin mass ratio of 0.3:1 and at the polymer/insulin mass ratio of 1:1, respectively. The inserts are height mode of each image. The particle size obtained from AFM images were smaller than those obtained from dynamic laser light scattering data. An average diameter of the NC was approximately 95 nm. Additionally, excessive TMC400-40 chains were observed in the NC prepared at polymer/insulin mass of 1:1 as seen in Figure 12b, confirming the low yield of NC formation. From three-dimensional images of the NC (Figures 23c and 23d), the NC were spherical or almost spherical and had a relatively smooth surface. Similar finding was previously reported by Mao et al. (47).

4. Preparation and characterization of insulin NP

To evaluate the feasibility of insulin NP formation by ionotropic gelation with TPP crosslinker, TMC400-40 and PEG(5k)$_{40}$-g-TMC100-40 were used as representative of TMC and PEGylated TMC copolymers, respectively. Insulin NP were prepared by ionotropic gelation in a two-step procedure; (a) the complex formation between the two oppositely charged polyelectrolytes, polymer and insulin, and (b) cross-linking with TPP anions as depicted in Figure 24.

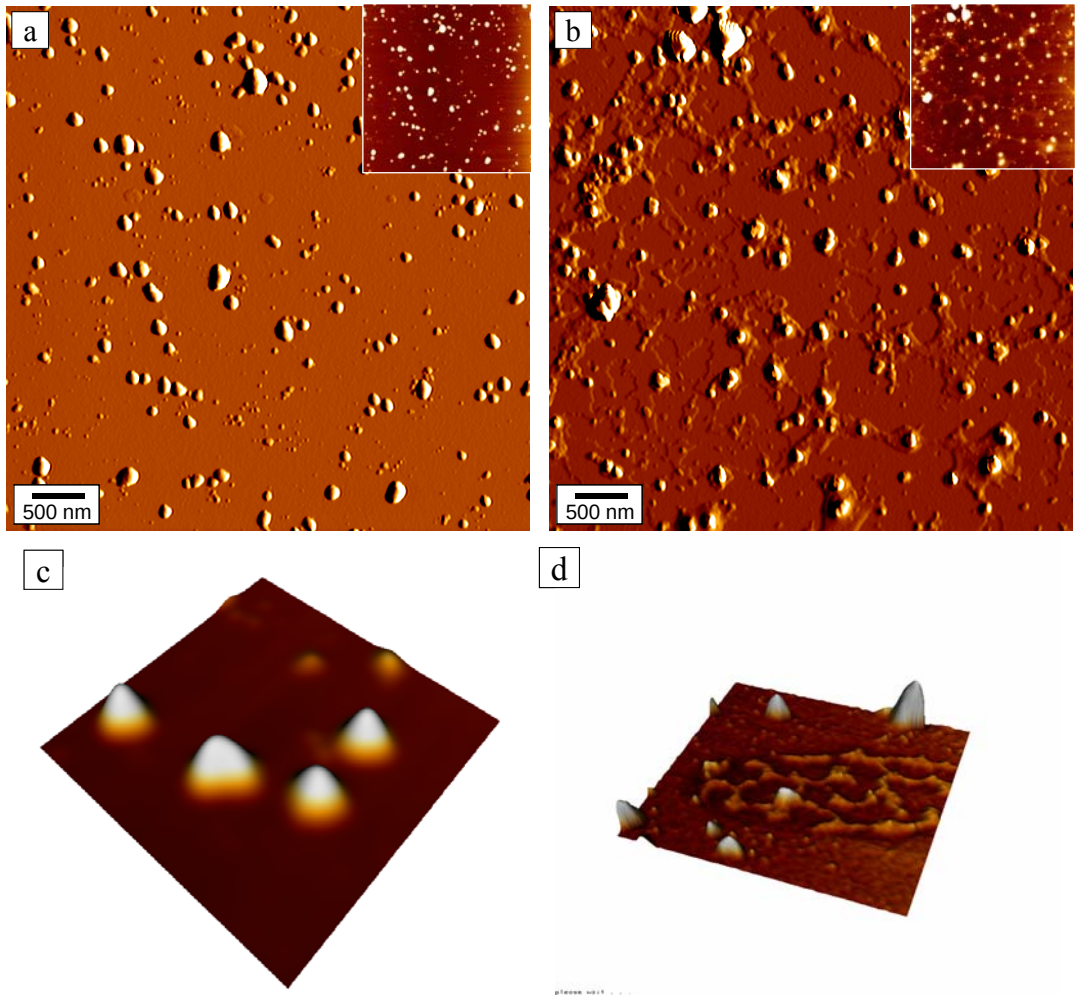

Figure 23. Atomic force microscopy images of (a) TMC400-40/insulin NC at optimized polymer/insulin mass ratio of 0.3:1 (5 × 5 μm), (b) TMC400-40/insulin NC at polymer/insulin mass ratio of 1:1 (5 × 5 μm), (c) three-dimensional image of 0.3:1 TMC400-40/insulin NC and (d) three-dimensional image of 1:1 TMC400-40/insulin NC. The inserts are height mode of each image.

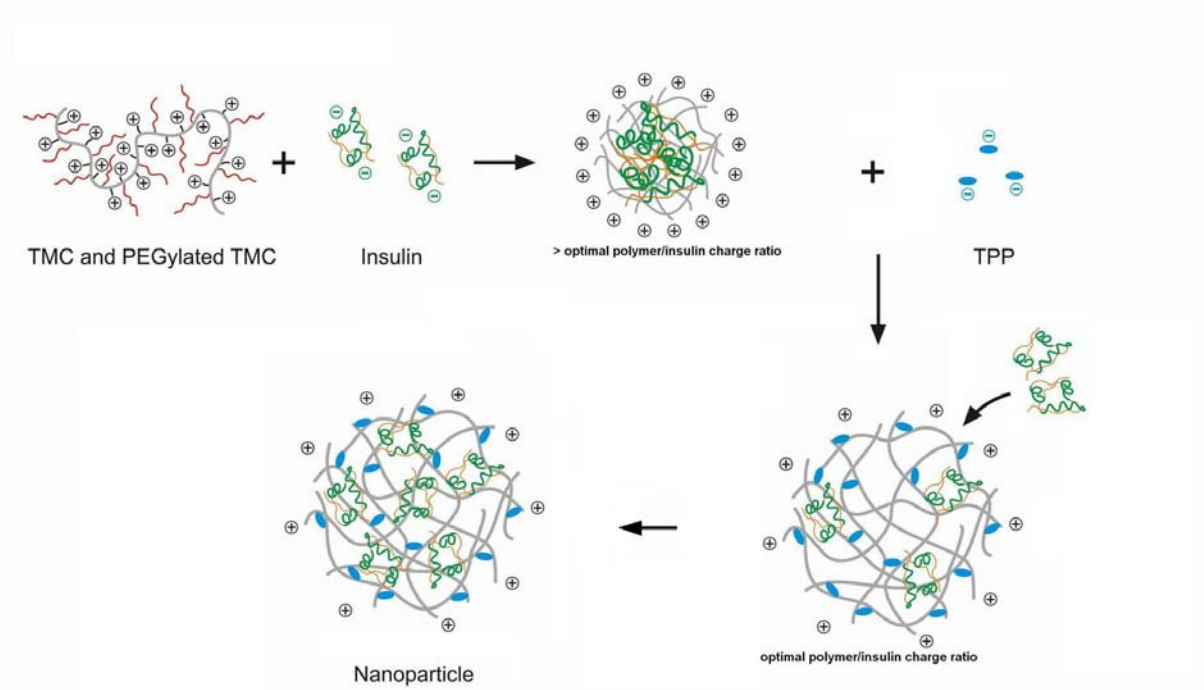

Figure 24. Schematic representation of insulin NP formation.

4.1 Optimal ratio of TPP and polymer in NP

Many studies have reported that the quantity of TPP in a given formulation has a significant effect on the protein encapsulation and characteristic of NP (58-60, 235). Therefore, the optimal amount of TPP in formulation was investigated in detail.

The optimal condition at which NP were formed was established using dynamic light laser scattering as previously described (47). Mixtures of polymer and insulin with different polymer / insulin (+/–) charge ratio were titrated against TPP solution, and particle size and Kcps values were measured. The points at which the Kcps values reached a maximum or plateau were denoted as the end point of titration. When adding the TPP solution into polymer-insulin mixtures, Kcps values of mixture increased until a plateau, referred to a TPP amount independent region which was reached at a specific TPP volume. After this point, the addition of an excess amount of TPP led to a drop in the Kcps values together with considerable increase of particle size. A linear relationship was observed between the logarithm of optimal TPP/polymer mass ratio and insulin/polymer (–/+) charge ratio with correlation coefficient of 0.9968 for TMC400 and 0.9916 for PEG(5k)$_{40}$-g-TMC100-40 as shown in Figure 25.

The properties of insulin NC prepared at optimal TPP/Polymer mass ratio are described in Table 16. In case of NP prepared at optimal polymer/insulin ratio (TMC400-40 NP-1), no difference in AE and PY between TMC400-40 NC-1 and TMC400-40 NP-1 was observed, but particle size of NP was significant larger than that of the NC and flocculation occurred in a short period of time. In case of NP prepared at higher optimal polymer/insulin ratio, compared to NC at the same polymer/insulin ratio, the particle size, AE and PY increased while the zeta potential and PDI decreased ($p < 0.05$).

4.2 Effect of TPP concentration

Taking TMC400-40 as an example, the effect of TPP amount on the NP formation was investigated. As shown in Table 17, compared to NC at the same polymer/insulin mass ratio of 1:1 (+/– charge ratio of 6:1), incorporation of TPP with respect to TMC400-40 led to a significant increase in the size, AE and PY ($p < 0.05$) and led to a significant decreased ($p < 0.05$) zeta potential and PDI. The AE and PY

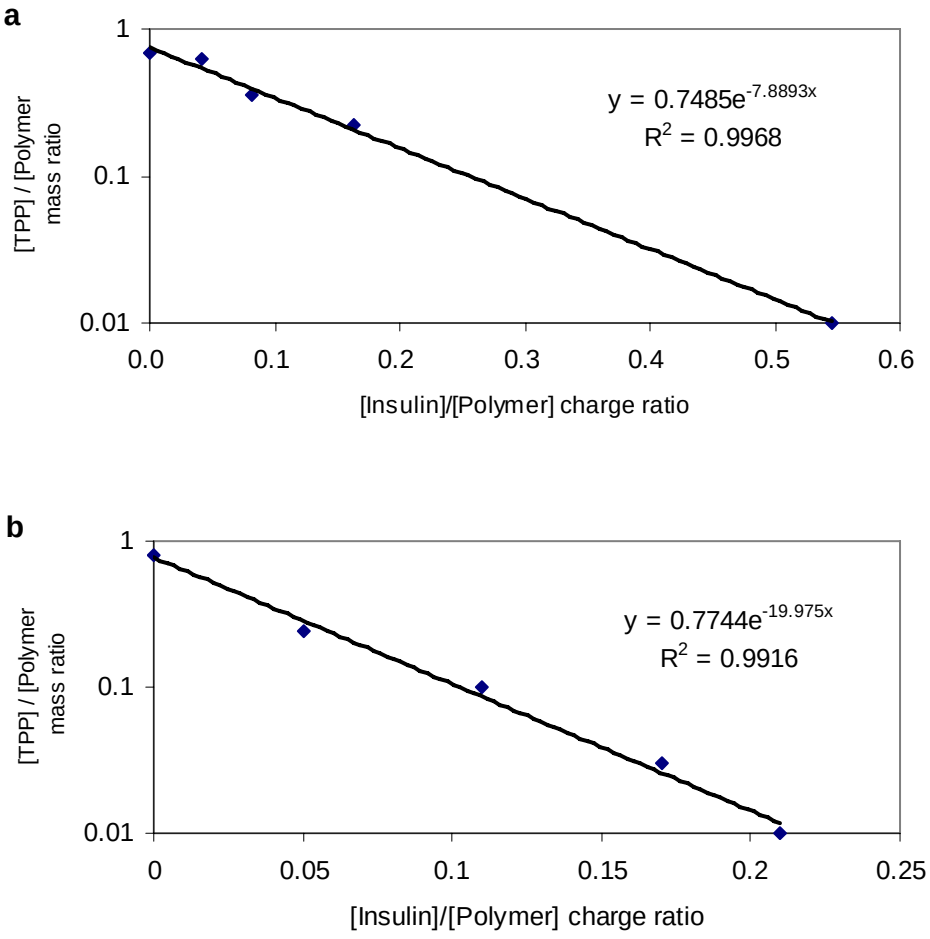

Figure 25. Correlation between insulin/polymer (–/+) charge ratio and TPP/polymer mass ratio for NP formation of (a) TMC400-40, (b) $PEG(5k)_{40}$-g-TMC100-40.

Table 16. Formulation and characteristics of the NC and NP with insulin. The initial concentration of insulin was 1 mg/ml in all the formulations

Formulation	Mass ratio		Charge ratio (Pol/Ins)[b]	Particle size (nm)	Polydispersity index	Zeta potential (mV)	Association Efficiency (%)	Process yield (%)
	Pol : Ins	TPP : Pol						
TMC400-40 NC-1	0.3 : 1[a]		2 : 1	181 ± 7	0.13 ± 0.03	24.7 ± 1.5	97 ± 1	78 ± 1
TMC400-40 NP-1	0.3 : 1[a]	0.6 : 1	2 : 1	443 ± 28*	0.27 ± 0.07*	12.3 ± 0.3*	86 ± 2	73 ± 4
TMC400-40 NC-2	1 : 1		6 : 1	142 ± 3	0.33 ± 0.02	29.2 ± 1.7	31 ± 2	34 ± 1
TMC400-40 NP-2	1 : 1	0.4 : 1	6 : 1	227 ± 6*	0.14 ± 0.04*	17.1 ± 0.9*	87 ± 2*	67 ± 1*
TMC400-40 NC-3	2 : 1		12 : 1	104 ± 4	0.37 ± 0.03	33.4 ± 2.0	27 ± 1	10 ± 1
TMC400-40 NP-3	2 : 1	0.6 : 1	12 : 1	228 ± 4*	0.11 ± 0.02*	8.6 ± 0.7*	87 ± 0*	33 ± 0*
$PEG(5k)_{40}$-g-TMC100-40 NC	2 : 1		10 : 1	159 ± 5	0.29 ± 0.03	27.5 ± 1.5	36 ± 3	24 ± 2
$PEG(5k)_{40}$-g-TMC100-40 NP	2 : 1	0.1 : 1	10 : 1	317 ± 11*	0.18 ± 0.05*	21.0 ± 1.4*	92 ± 0*	58 ± 6*

The data are expressed as the means ± SD of three batches.

[a] Optimized polymer/insulin mass ratio for preparation of NC

[b] Calculation based on the polymer / insulin mass ratio at pH 7.4

* Statistically significant differences ($p < 0.05$) compared with that of NC at the same polymer/insulin mass ratio

Table 17. Influence of TPP/polymer mass ratio on the properties of insulin NP[a]. The concentration of insulin and TMC are 1 mg/ml in all formulations

Mass ratio TPP : Pol	Average count number (Kcps) [b]	Particle size (nm)	Polydispersity index	Zeta potential (mV)	Association efficiency (%)	Process yield (%)
0.0 : 1	283 ± 18	142 ± 3	0.33 ± 0.02	29.2 ± 1.7	31 ± 2	34 ± 1
0.1 : 1	886 ± 95	217 ± 13	0.38 ± 0.05	26.3 ± 1.8	46 ± 2	50 ± 6
0.2 : 1	1257 ± 113	205 ± 10	0.22 ± 0.03	22.5 ± 1.1	76 ± 2	57 ± 6
0.4 : 1	2078 ± 147	227 ± 6	0.14 ± 0.04	17.1 ± 0.9	87 ± 0	67 ± 1
0.6 : 1	2641 ± 152	257 ± 9	0.14 ± 0.04	12.6 ± 1.0	88 ± 0	50 ± 6

The data are expressed as the means ± SD of three batches.

[a] NP were obtained by premixing insulin with polymer solution, prior to NP formation.

[b] Measured at 90° angle through a 100-μm pin hole

* Statistically significant differences ($p < 0.05$) compared with that of TMC400-insulin premixed NP

increased with an increase in the TPP:TMC400-40 mass ratio until a maximum AE and PY was reached with TPP:TMC400-40 mass ratio of 0.4:1 at which the lowest PDI was obtained. After this ratio, the AE did not increase further but the PY started to decrease. The results obtained indicate that at the TMC400-40/insulin mass ratio of 1:1, the 0.4:1 TPP/TMC400-40 mass ratio is the optimal ratio for preparing insulin NP. Additionally, the results showed linear relationship as a function of the TPP amount with correlation coefficients of 0.9845, 0.9926, 0.9153 and 0.8770 for ACN, zeta potential, PY and AE, respectively.

Compared with insulin, TPP has a much smaller molecular with a higher negative charge density. It can dominate interaction of insulin with positively charged polymers causing a reduction in the positive charge density of polymers, and also in (+/–) charge ratio between polymer and insulin which can be seen from a reduction of zeta potential of particles when increasing TPP amount. The structure of particle is then loose, leading to a larger size and it is very likely that this structure allows them to capture more insulin (Figure 24). Similar result was found by Grenha et al. (60) who observed that insulin AE of chitosan NP increased with increasing TPP concentration. Recently, Boonsongrit et al. (61) reported that adding TPP did not affect the entrapment efficiency of insulin-chitosan microparticles when they were formed at optimal chitosan / insulin mass of 1.25:1. Therefore, it is reasonable to assume that polymer/insulin (+/–) charge ratio plays an important role in NC and NP formation. The highest insulin AE of NP with a narrow size distribution could be achieved when polymer/insulin (+/–) charge ratio was close to optimal ratio by using specific TPP amount.

4.3 Effect of order of mixing

In some cases, the mixing order influenced NC or NP formation (47, 63). In order to investigate the effect of the order of mixing on physicochemical properties of NP, insulin was premixed with either the TPP solution or the polymer solution prior to NP formation. For ease of discussion, polymer-insulin premixed NP and TPP-insulin premixed NP are designated as p-NP and t-NP, respectively. As shown in Table 18, no differences in zeta potential, PY were found between p-NP and t-NP ($p > 0.05$), while bigger size with higher ACN were observed with p-NP ($p < 0.05$). For

Table 18. Effect of order of mixing on the properties of insulin NP. The concentration of insulin and TMC are 1 mg/ml in all formulations

Formulation	Mass ratio		Average count Number (Kcps)[d]	Particle size (nm)	Polydispersity index	Zeta potential (mV)	Association Efficiency (%)	Process yield (%)
	Pol : Ins	TPP : Pol						
p-TMC400-40 NP[a]	1 : 1	0.2 : 1	1257 ± 113	205 ± 10	0.22 ± 0.03	22.5 ± 1.1	76 ± 2	57 ± 6
t-TMC400-40 NP[b]	1 : 1	0.2 : 1	1081 ± 86*	184 ± 6*	0.21 ± 0.02	22.6 ± 0.9	70 ± 1*	58 ± 4
p-PEG(5k)$_{40}$-g-TMC100-40 NP[a]	2 : 1	0.1 : 1[c]	210 ± 23	317 ± 11	0.18 ± 0.05	21.0 ± 1.4	92 ± 0	58 ± 6
t-PEG(5k)$_{40}$-g-TMC100-40 NP[b]	2 : 1	0.1 : 1[c]	176 ± 5*	259 ± 10*	0.26 ± 0.03*	21.8 ± 1.3	93 ± 1	50 ± 4

The data are expressed as the means ± SD of three batches.

[a] NP were obtained by premixing insulin with polymer solution, prior to NP formation.

[b] NP were obtained by premixing insulin with TPP solution, prior to NP formation.

[c] Optimal TPP : polymer mass ratio for NP formation

[d] Measured at 90° angle through a 100-μm pin hole for TMC400-40 NP and a 50-μl pin hole for PEG(5k)$_{40}$-g-TMC100-40 NP

* Statistically significant differences ($p < 0.05$) compared with that of polymer-insulin premixed NP

insulin AE, it was observed that AE of p-TMC400-40 NP was significant higher than t-TMC400-40 NP ($p < 0.05$) which can probably be explained by competition between insulin and TPP to interact with TMC400-40. In contrast, the mixing order did not affect AE of PEG(5k)$_{40}$-g-TMC100-40 NP. This could be from NP of PEG(5k)$_{40}$-g-TMC100-40 was prepared at optimal TPP:polymer mass ratio. However, the results obtained are inconsistent with previous reports by Ma et al. (236) who found that the mixing order did not affect the size and average count number of insulin loaded chitosan NP while The AE of TPP-insulin premixed NP was slightly higher than that of chitosan-insulin premixed NP. This discrepancy can probably be from the pH of system. In general, insulin loaded chitosan NP was prepared at pH 5.5 in which insulin was positively charged like chitosan. When insulin was premixed with chitosan, they would compete to interact with TPP resulting in the low insulin AE. On the other hand, when insulin was premixed with TPP, TPP would bind with the positively charged chitosan and insulin to form an electrostatically stabilized chitosan-TPP-insulin complexes, causing the high insulin AE (236).

4.4 Morphology of the insulin NP

Figure 26a displays the AFM image of representative fresh insulin NP at optimal TPP:TMC:insulin mass ratio of 0.4:1:1. The NP had a narrow size distribution and their size was approximately 117 nm which was lower than the size of 205 nm obtained from dynamic laser light scattering data. Morphologically, the nanoparticles were spherical or almost spherical or oval and had a relatively smooth surface (Figure 26b).

5. Colloidal stability

5.1 Collodial stability in physiological fluid

In order to evaluate the stability of the NC and NP in the physiological fluids, various ratios of NC and NP were diluted in pH 6.8 phosphate buffer and the integrity of particles was measured. No apparent change in particle size was observed; therefore, only the evolution of number of particles formed in term of Kcps values are presented in Figure 27 which clearly showed that the % Kcps of NP was much less than that of NC at the same dilution ratio. The NC appeared to be stable when

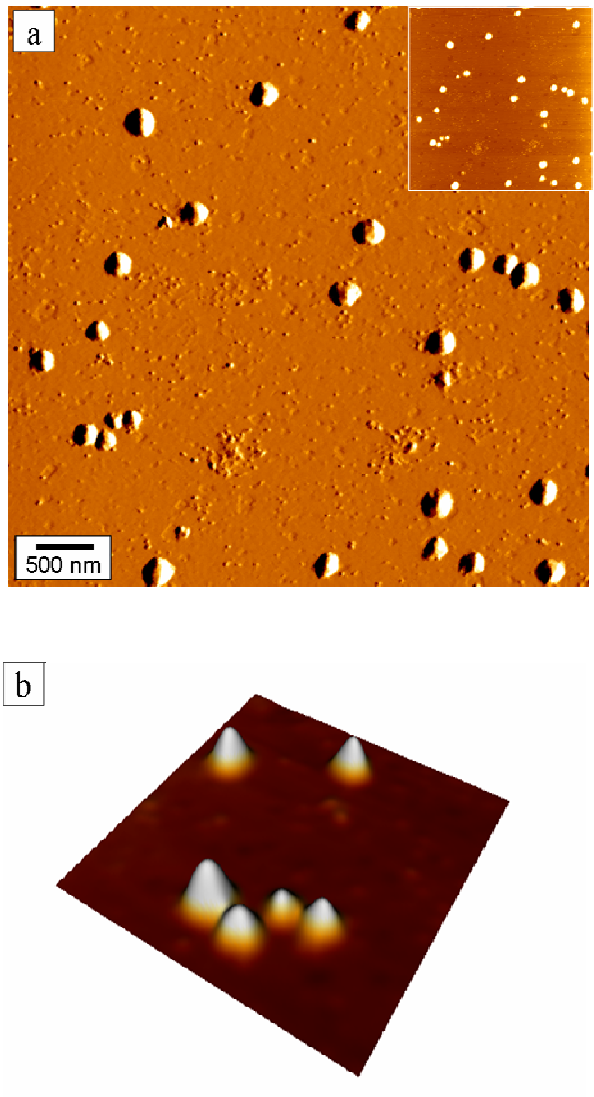

Figure 26. Atomic force microscopy image of (a) insulin loaded TMC400-40 NP at optimal TPP:polymer:insulin mass ratio of 0.4:1:1 (5 × 5 μm) and (b) its three-dimensional image. The insert is height mode of image.

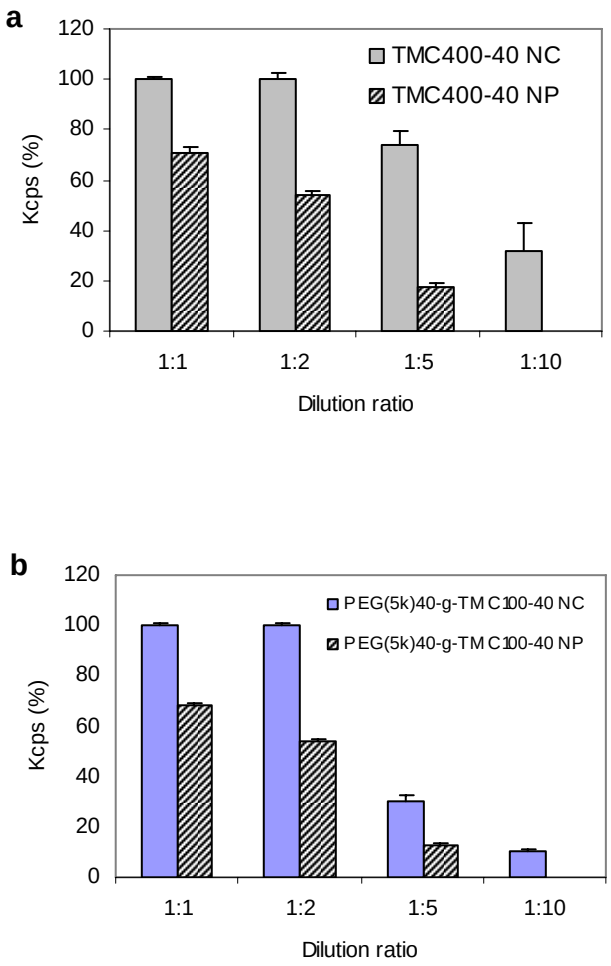

Figure 27. Colloidal stability of (a) TMC400-40 and (b) $PEG(5k)_{40}$-g-TMC100-40 after diluting with pH 6.8 phosphate buffer. Each value represents the mean ± SD of three experiments.

volume ratio of NC:buffer was < 1:2 with no apparent change in Kcps values and particle size. Twenty six percent of TMC400-40 NC and 87% of PEG(5k)$_{40}$-g-TMC100-40 NC were dissociated when buffer was increased to the 1:5 NC:buffer volume ratio. In contrast to NP, 30% dissociation NP immediately occurred at NP:buffer volume ratio of 1:1, irrespective to the NP structures and dissociation clearly increased with increasing volume of phosphate buffer. A linear correlation between the percent of Kcps remained and the added volume of phosphate buffer was observed with regression coefficient of 0.996 for TMC400-40 and 1.000 for PEG(5k)$_{40}$-g-TMC100-40.

The results obtained were comparable to the results report previously by Boonsongrit et al. (61) who found that most of insulin was released within 10 min from the chitosan- insulin microspheres in the pH 7.4 phosphate buffer and in the pH 3 HCl solution indicating the dissociation of microspheres. We hypothesized that the stability of NC and NP depended on the electrostatic interaction intensity between polymer and insulin. The attraction between polymer and insulin could be reduced by TPP leading to a decrease in physical stability of NP compared to NC prepared at the same conditions. Another possible explanation for the NC and NP dissociation in pH 6.8 phosphate buffer is that the pH of the NC and NP dilutions was close to pH 6.8 of phosphate buffer when increasing ratio of buffer. The effect of pH on the colloidal stability of insulin NC and NP was discussed in detail in section 5.3.

5.2 Effect of ionic strength of the medium

In order to investigate the effect of salt on the colloidal stability of insulin NP, the ionic strength of the solution was adjusted by adding NaCl. Figure 28 presents the change of Kcps value of TMC400-40/insulin NP at different ionic strength solution. In case of NC prepared in an absence of TPP, no apparent change in Kcps values was observed even at ionic strength of 75 mM. On the other hand, dissociation of NP increased with increasing ionic strength. Influence of TPP on the dissociation of particles was obviously observed when the ionic strength was higher than 50 mM. This phenomenon is probably the results of reduced attraction between the oppositely charged polyelectrolytes contributed by the presence of TPP in formulation and the counter-ion environment (237).

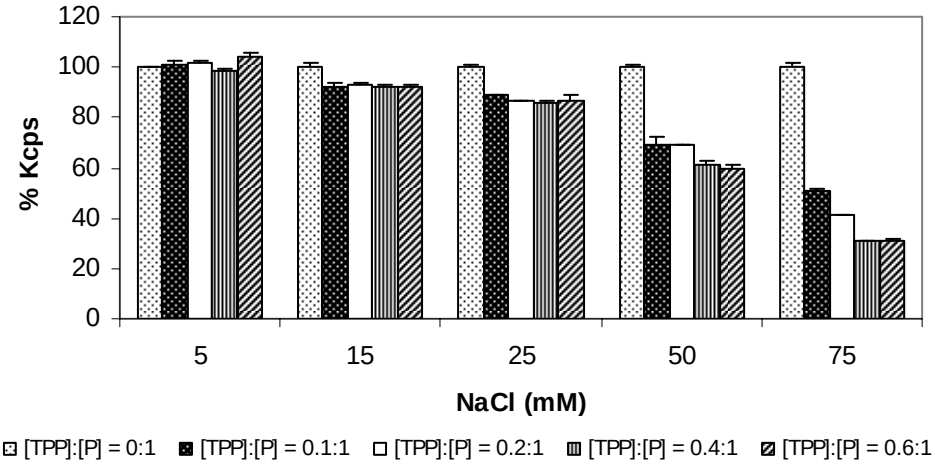

Figure 28. Effect of ionic strength on the dissociation of insulin NP prepared at different TPP:TMC400-40 ratio. Each value represents the mean ± SD of three experiments.

5.3 Effect of pH

From the preliminary experiment, the equivalent pH value for insulin NC and NP formation was also approximately 7.4. In order to confirm whether the electrostatic interaction between polymer and insulin influenced the stability of NC and NP, TMC400-40 NP were prepared at different pH of 5.0, 6.8 and 7.4 and their stabilities in a series of concentrated NaCl solutions were evaluated. As shown in Figure 29, the colloidal stability of insulin NP decreased with decreasing the system pH. These could be explained from the electrostatic interaction intensity between polymer and insulin at different pH. It is well known that the charge density of insulin was pH dependent (apparent Ip of insulin is 6.4). At the pH of 5.0 where insulin exhibits weakly negatively charged, NP with particle size of 860 nm were obtained indicating a weak interaction between polymer and insulin. Thirty percent of NP dissociation was observed when ionic strength of the solution was 5 mM and 60% NP dissociation at ionic strength of the solution of 15 mM with no apparent change in particle size. On the other hand, NP with particles of 511 nm and 306 nm were obtained when preparing at pH 6.8 and 7.4, respectively. Only 20% dissociation of NP was found at the ionic strength of 25 mM.

6. Effect of temperature on the stability of insulin

Some studies indicated that elevated temperature facilitates NC and NP formation with the low aggregation tendency (238). Proteins are very labile molecules sensitive to thermal stress (239-241). Therefore, stability of insulin in the NC and NP at different temperatures was investigated and compared with that of free insulin solution.

The results of insulin stability at three different temperatures are shown in Figures 30 – 32. It was demonstrated that the NC and NP could protect insulin from degradation even at higher temperature. At temperature < 50°C, insulin itself was quite stable for at least 2.5 h and degradation was observed at 6 h even at room temperature.

In the case of NC, they could protect insulin from degradation for at least 6 h even at temperature of 50°C while approximately 50% of free insulin was degraded. Furthermore, no difference in results was observed among TMC NC with different

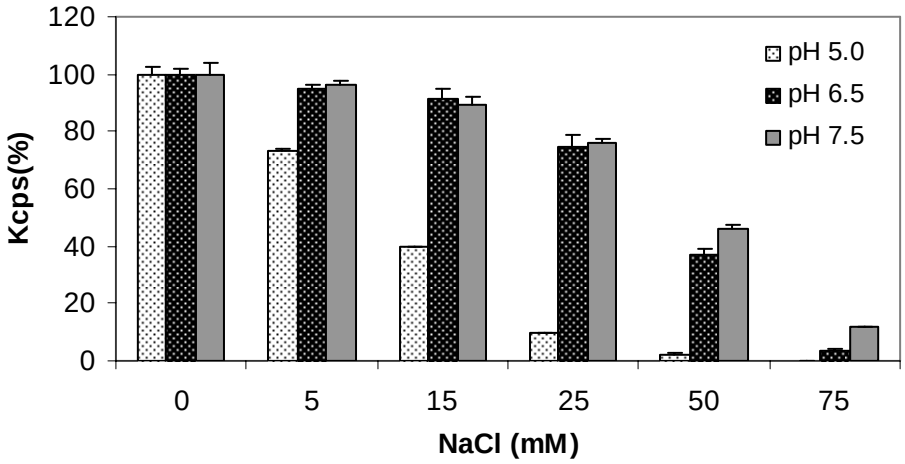

Figure 29. Effect of pH on the dissociation of insulin NP prepared at TPP:TMC400-40:insulin of 1.2:2:1 as a function of ionic strength. Each value represents the mean ± SD of three experiments.

DQ (Figure 30) and between unmodified TMC400-40 and PEGylated TMC400-40 NC (Figure 31) ($p > 0.05$). As seen in Figure 32, the NP also could protect insulin at least 6 h even at 50°C and their protecting effect at 50°C was higher than that at 20°C ($p < 0.05$). Akiyoshi et al. (242) also observed this phenomenon. This is probably due to the facilitation of NP formation and compaction at elevated temperature which can be seen from the increased Kcps values (ca. 10-20%) with a slight decrease in particle size (ca. 10%), compared to the value at 20°C. Generally, an increase in temperature increases entropy of system which is associated with the release of small counterions initially bond to the polymers, resulting in compaction of particles (233, 243).

With regard to TMC400-40, the protecting effect of NC was higher than that of NP, especially at 6 h ($p < 0.05$). These results could be explained from insulin association mechanism. The NC were formed by only columbic interactions between negatively charged insulin and positively charged polymer, which increased with increasing temperature resulting in more NC (47). On contrary, the ionic gelation method, cross-linked polymer chains by TPP to form reticular structure in which insulin could be captured and that the interaction between polymer and insulin could be impaired by TPP molecules. Therefore, the polyelectrolyte complexation is an efficient way to improve the stability of insulin.

7. Insulin protection from enzymatic degradation

7.1 Stability of insulin in the present of aminopeptidase M

Although nasal delivery avoids the hepatic first pass effects, the enzymatic barrier of the nasal mucosa might cause a presystemic first pass effect. Among the exopeptidases and endopeptidases which are active in the nasal mucosa, aminopeptidases, especially aminopeptidase M (ApM), appear to play an important role (145, 146). Activity of ApM was found mostly in the fibrocytes which adhered to basal membrane of the epithelium and glands (147). Therefore, the stability of insulin against AMP and a potential role of NC in protecting insulin from ApM digestion should be verified.

Firstly, the possible inhibitory effect of polymers on the ApM was examined. As seen in Figure 33, it was found that all polymers did not affect the ApM activity.

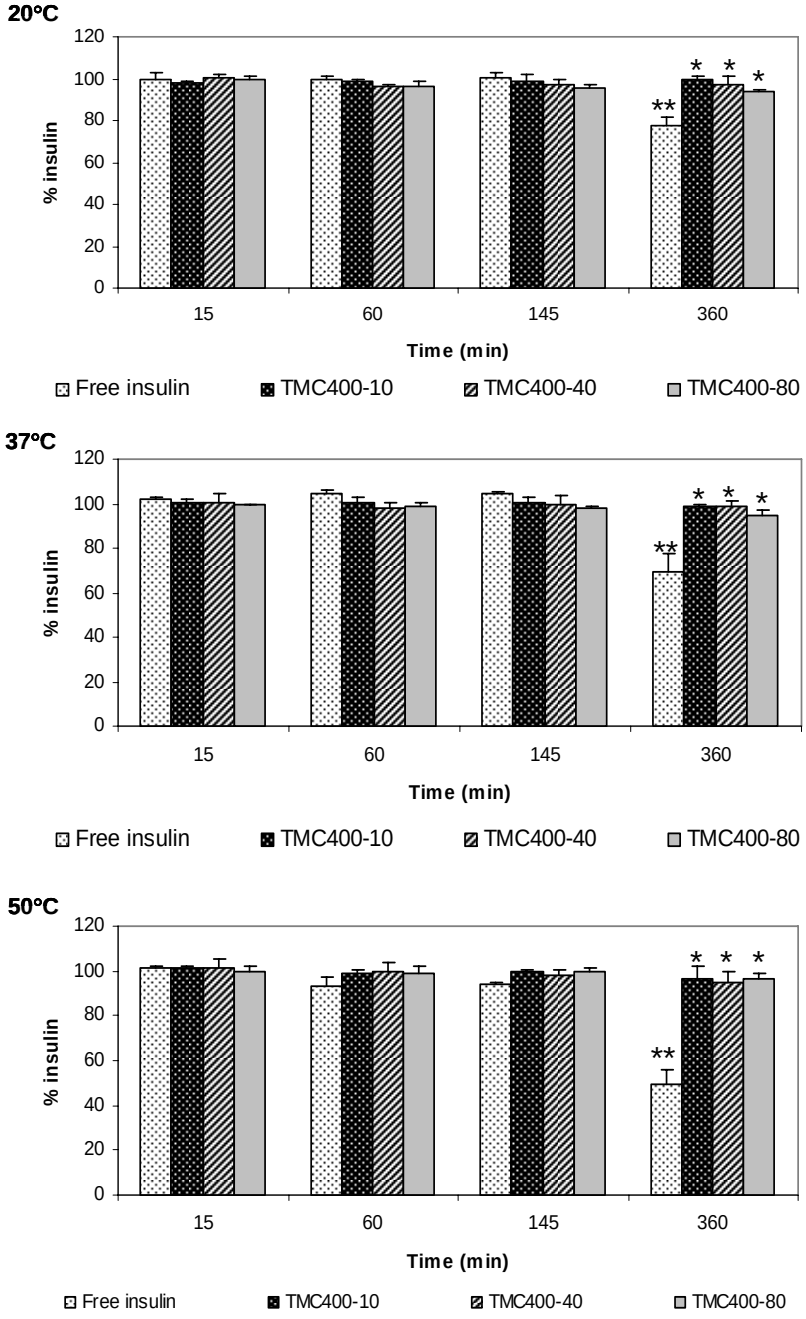

Figure 30. Effect of quaternization degree on the stability of insulin in NC at different temperatures. Each value represents the mean ± SD of three experiments. *Statistically significant differences from the values of free insulin ($p < 0.05$). **Statistically significant differences from the values of at 15 min ($p < 0.05$).

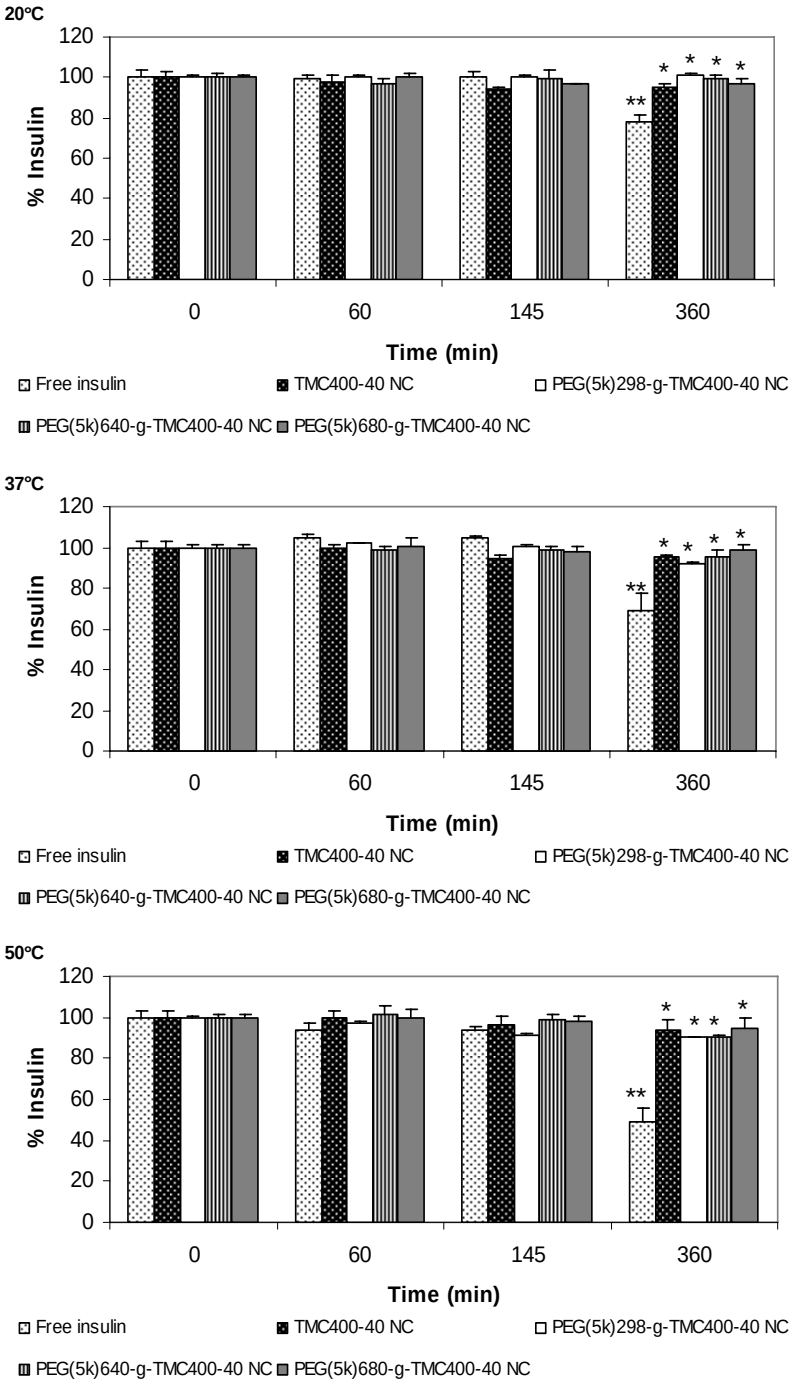

Figure 31. Effect of PEG substitution degree on the stability of insulin in NC at different temperatures. Each value represents the mean ± SD of three experiments. *Statistically significant differences from the values of free insulin ($p < 0.05$). **Statistically significant differences from the values of at 0 min ($p < 0.05$).

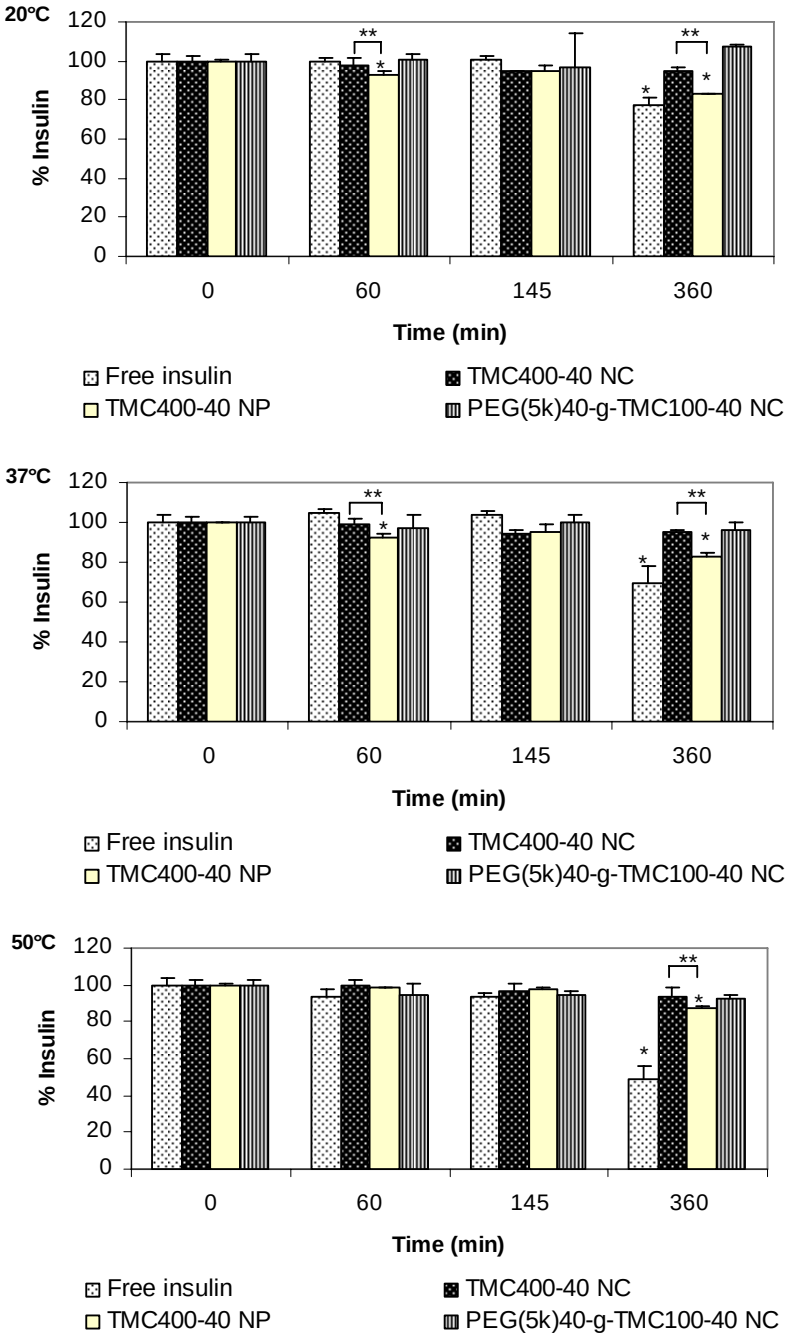

Figure 32. Stability of insulin in TMC400-40 NC, TMC400-40 NP and PEG(5k)$_{40}$-g-TMC100-40 NC at different temperatures. Each value represents the mean ± SD of three experiments. * Statistically significant differences from the values of at 0 min ($p < 0.05$). ** Statistically significant differences from the values of TMC400-40 NC ($p < 0.05$).

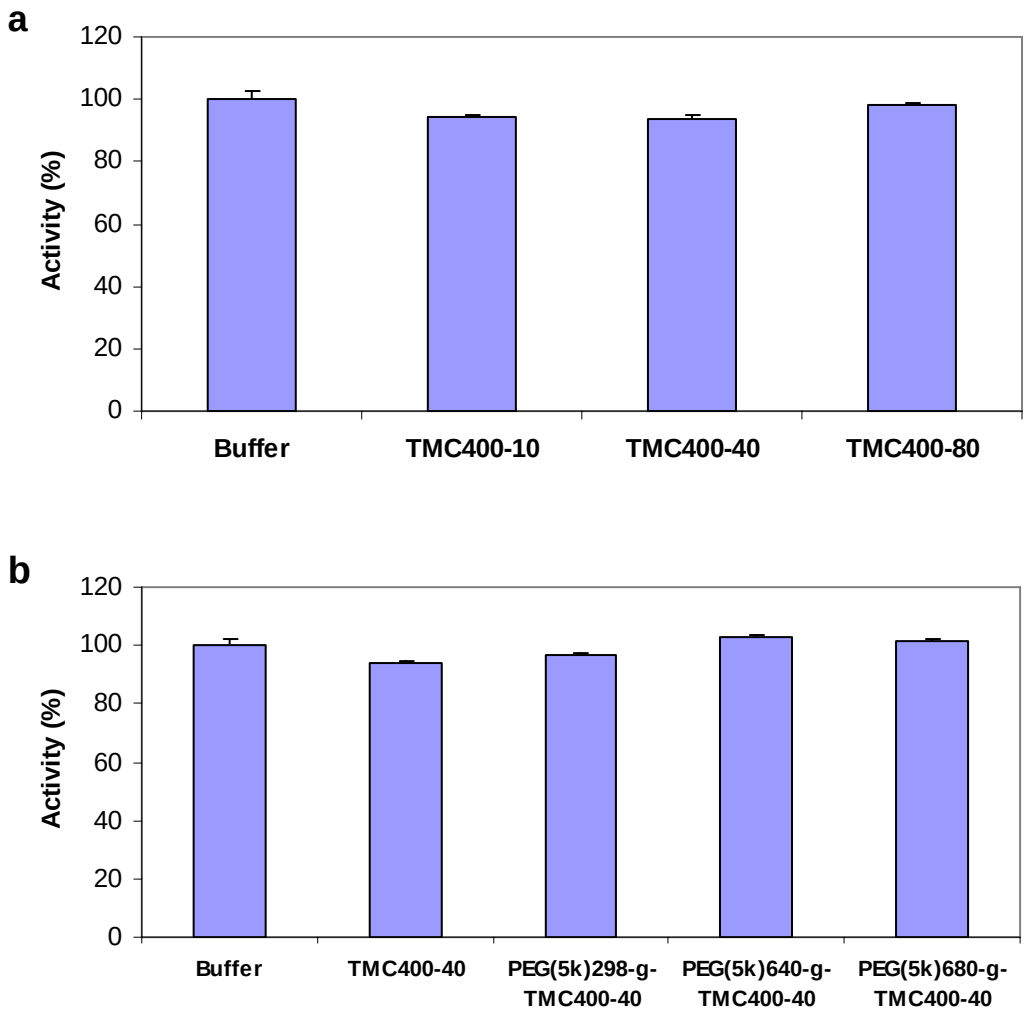

Figure 33. Effect of (a) quaternization degree and (b) PEG substitution degree on the activity of ApM. Each value represents the mean ± SD of three experiments.

Figure 34 presents the enzymatic degradation of free insulin by ApM. No significant difference of insulin contents after incubation with and without ApM was observed ($p > 0.05$). This implies that free insulin, insulin NC and NP were not degraded by ApM. The results are fully consistent with the observation of Gizurarson and Bechgaard (125) who reported that insulin is not degraded by nasal enzymes.

7.2 Stability of insulin in the present of trypsin

Although ApM is the predominant enzyme appeared in the nasal membrane, Lang et al. (148) reported that chymotrypsin- and trypsin-like endopeptidases were found to be responsible for the initial cleavage of human calcitonin in excised bovine nasal mucosa. The subsequent metabolic degradation of the primary metabolites followed the trypical sequential pattern of ApM activity. Indeed, trypsin and chymotrypsin are the major poteolytic enzymes cleaving various bonds within the insulin molecule. Therefore the potential role of NC and NP in protecting insulin from trypsin should not be neglected.

7.2.1 Effect of polymer on the activity of trypsin

The possible inhibitory effects of polymers on trypsin were examined. As presented in Figure 35, although the activity of trypsin in the present of polymers was slightly higher than buffer control, the difference was insignificantly different. Similar results were reported by Kotźe et al. (244) and Lueβen et al. (245) who reported that TMC did not affect the trypsin activity.

7.2.2 Effect of DQ on the stability of insulin

In order to examine the ability of TMC NC in insulin protection from trypsin, the free insulin and insulin associated NC were treated with trypsin. After the incubation with trypsin, the amount of insulin remaining was determined. The results are shown in Figure 36a for NC prepared from TMC with different DQ.

The unprotected insulin in the control experiment was significantly degraded in the present of trypsin and only 30% of the insulin remained after 1 h. In contrast, partial protection of insulin from trypsin digestion was observed with TMC NC ($p < 0.05$) and no significant difference in the protective effect of NC prepared

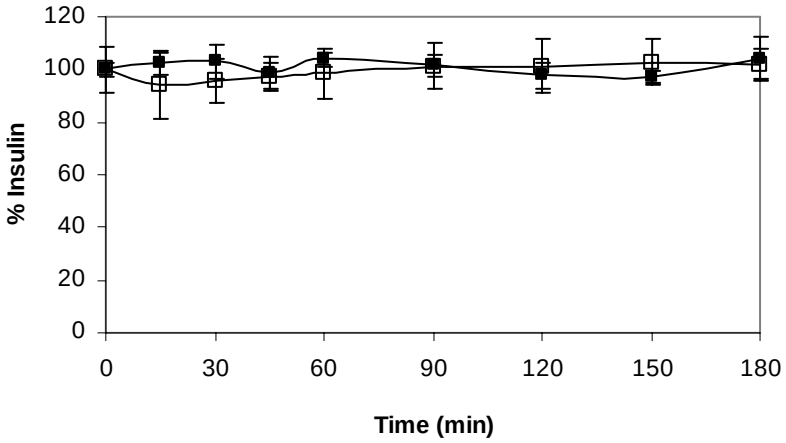

Figure 34. Stability of insulin in a presence of ApM (opened square) and in an absence of ApM (closed square). The initial concentration of insulin and ApM were 450 µg/ml and 50 mU/ml, respectively. Data represent mean ± SD of three experiments.

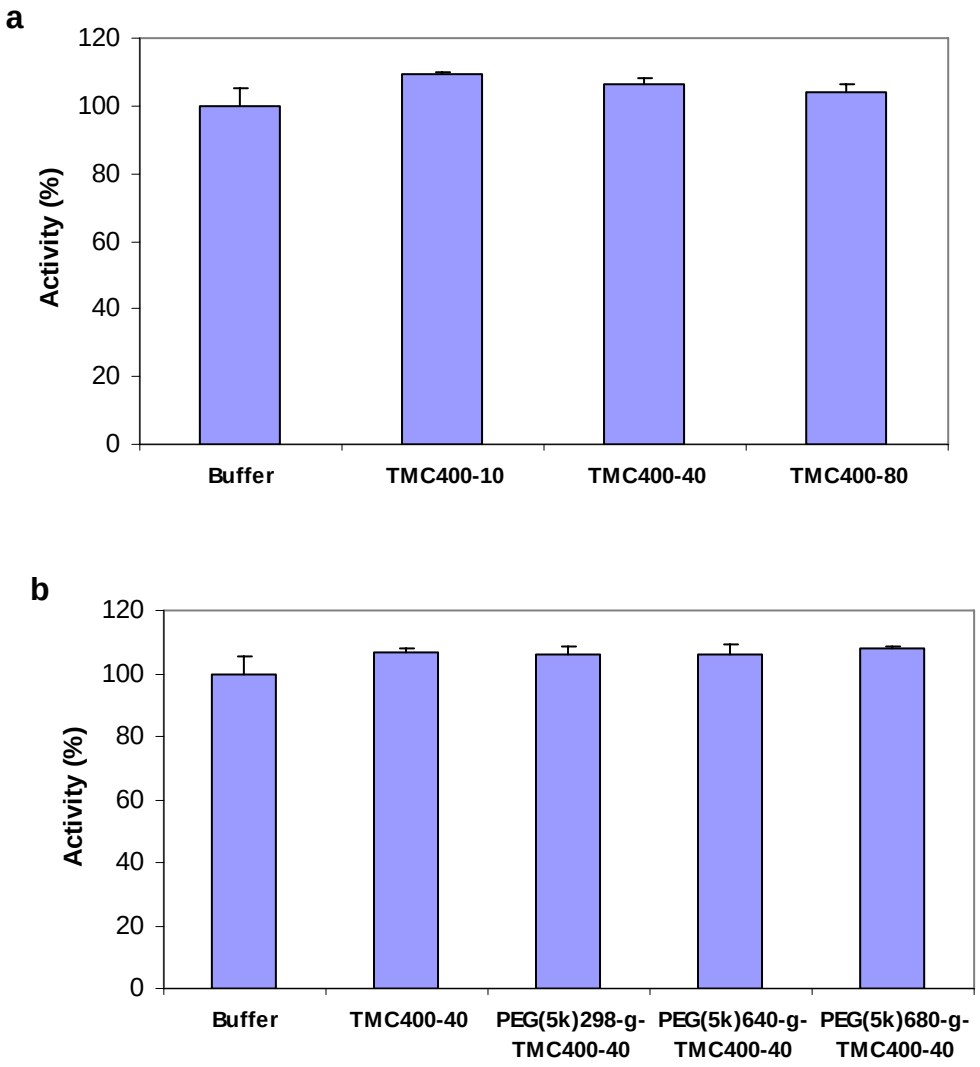

Figure 35. Effect of (a) quaternization degree and (b) PEG substitution degree on the activity of trypsin. Each value represents the mean ± SD of three experiments.

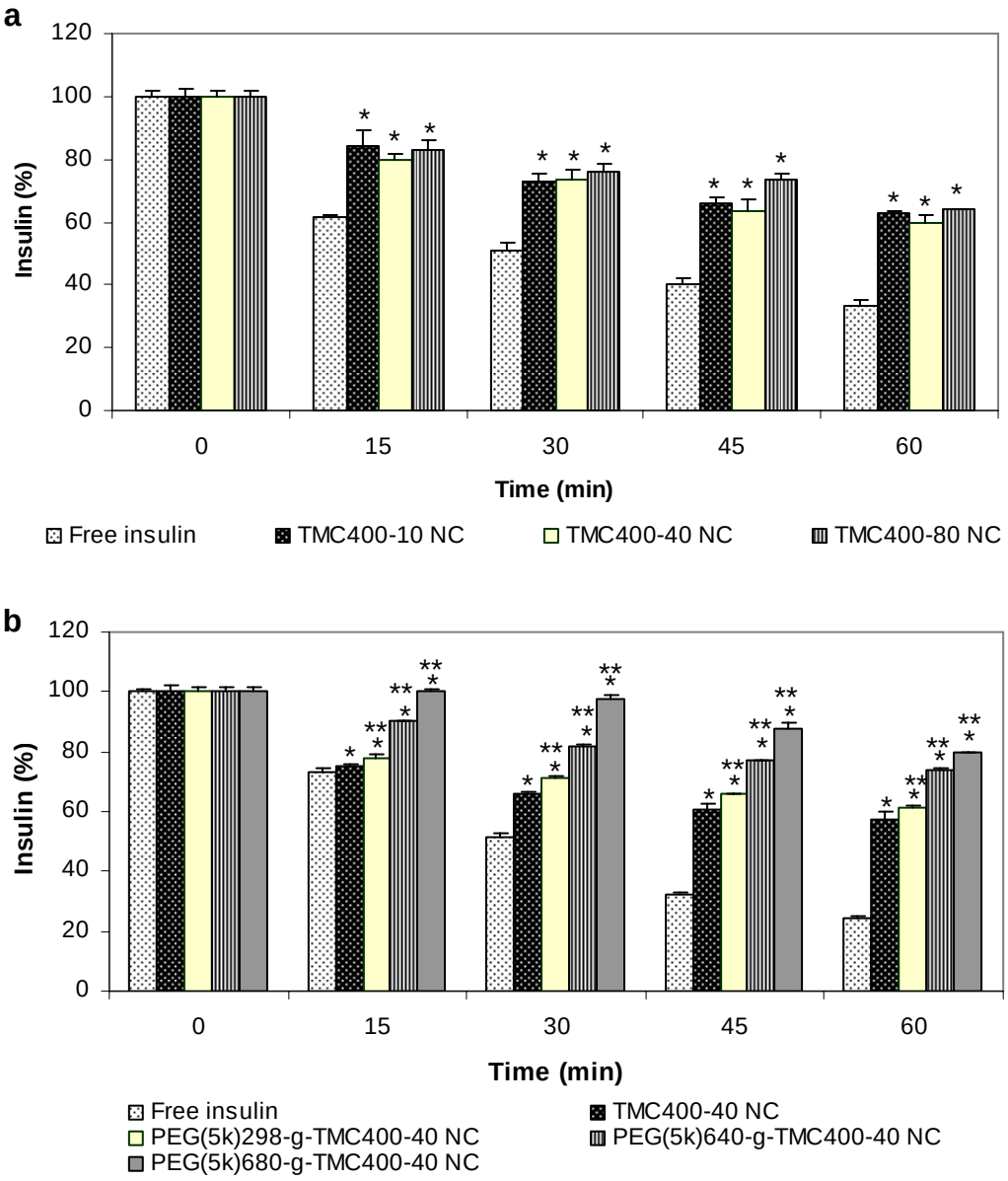

Figure 36. Effect of (a) quaternization degree and (b) PEG substitution degree on the enzymatic degradation of insulin by trypsin. Each value represents the mean ± SD of three experiments. The initial concentrations of insulin and trypsin were 450 μg/ml and 300 BAEE IU/ml, respectively. All NC prepared at optimal [P]:[Ins] mass ratio. * Statistically significant differences from the values of free insulin ($p < 0.05$). ** Statistically significant differences from the values of TMC400-40 ($p < 0.05$).

from TMC with different DQ was observed ($p > 0.05$). Moreover, it was observed that the degradation of insulin associated NC increased with time. Previously, Bernkop-Schnürch and Dundalek (246) observed that trypsin can penetrate and digest proteins in NP which may provide some evidence in support of the facts in the experiment.

7.2.3 Effect of PEG substitution degree on the stability of insulin

As shown in Figure 36b, the protective effect of all PEGylated TMC400-40 NC was higher than that of unmodified TMC400-40 NC ($p < 0.05$). This is probably due to a consequence of the steric effect of polyethylene glycol segments that hinders the enzyme access to the protein (92, 247). These results are in agreement with observation made by Mao et al. (47), suggesting that PEGylated TMC copolymers could improve the stability of insulin in NC due to hydrophilic PEG chains.

7.2.4 Effect of TPP on the stability of insulin

In order to evaluate the potential role of NP in protecting insulin from proteolytic enzyme, the enzymatic stability of insulin associated NP was investigated comparing to its insulin associated NC. The effect of TPP itself on the insulin degradation was also established.

As demonstrated in Figure 37, under the experimental conditions, about 86.7 ± 2.5% of free insulin control solution was degraded within 1 h. In an absence of trypsin, free insulin was not degraded by TPP. Surprisingly, TPP accelerated the degradation of free insulin by trypsin which can be seen from a dramatically decreasing in residue amount of insulin in the presence of TPP. In general, insulin molecule is composed of 2 chains: A-chain with 21 amino acids and B-chain with 30 amino acids, linked by disulfide bridges between cysteine residues. Trypsin cleaves insulin initially at only two sites, at the carboxyl side of residues B29-Lys and B22-Arg (248). Since the bonds susceptible to tryptic cleavage are located at the carboxyl terminus of the B-chain, hydrophobic domain of insulin, it is possible that TPP affects the conformation or secondary structure of insulin, resulting in such

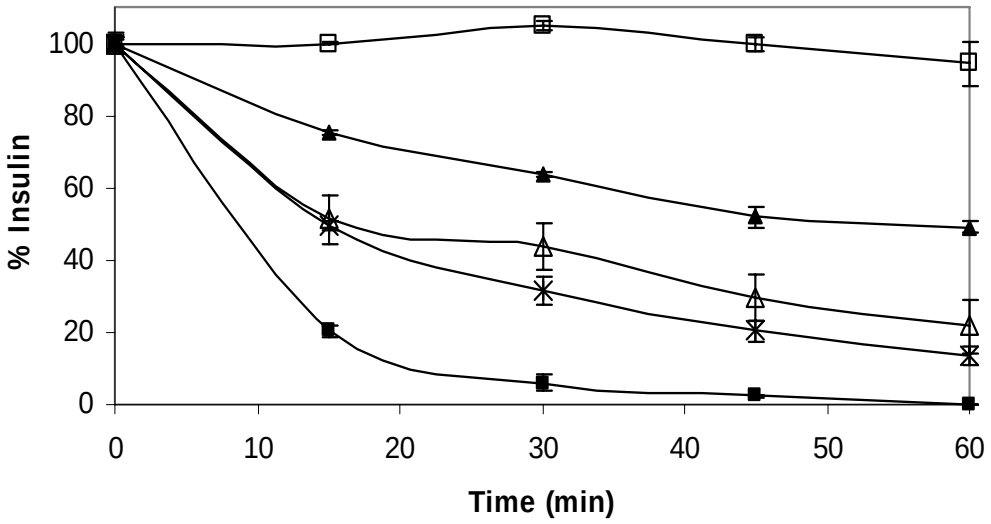

Figure 37. Effect of TPP on the enzymatic degradation of insulin by trypsin. Each value represents the mean ± SD of three experiments. The initial concentrations of insulin and trypsin were 450 μg/ml and 300 BAEE IU/ml, respectively. –✳– free insulin (w/ trypsin); –□– free insulin + TPP (w/o trypsin); –■– free insulin + TPP (w/ trypsin); –△– insulin NP with TPP:TMC400-40:insulin mass ratio of 0.2:1:1 (w/ trypsin); –▲– insulin NC with TMC400-40:insulin mass ratio of 1:1 (w/ trypsin).

segment is easily attacked by trypsin. However, this hypothesis needs to be further studied in more detail.

It was observed that preparing insulin in form of NP with TMC can protect insulin from trypsin digestion. However, the protective effect of NP was still lower than insulin NC prepared without the use of TPP. Furthermore, the degradation of insulin loaded NP increased with increasing TPP (Figure 38a). A linear relationship between amount of TPP and insulin degradation rate constant was established as presented in Figure 38b. Figure 39 depicts the residual amount of insulin after incubation of insulin alone and insulin associated NC and NP prepared from TMC400-40 and PEG(5k)$_{40}$-g-TMC100-40 with trypsin. The results confirmed that the NC could protect insulin from degradation with trypsin more efficiently than NP ($p < 0.05$) and the protective effect of PEGylated TMC was higher than that of TMC both in NC and NP ($p < 0.05$).

Since polymers did not affect the trypsin activity, this indicated that the protective effect is unlikely due to the inhibitory of trypsin's activity but probably due to a shielding effect of polymer on insulin. This shielding effect is achieved through polymer/insulin interaction. Similarly, Malkov et al. (90) reported insulin could be protected from trypsin digestion by binding of N-[8-(2-hydroxybenzoyl)amino] caprylate (SNAC) to insulin. Akiyoshi et al. (242) also found the complexed insulin with cholesterol-bearing pullulan (CHP) was significantly protected from enzymatic degradation by α-crymotrypsin. Attack of the enzyme was effectively prevented because insulin was tightly complexed to the CHP self-aggregate. Therefore, the less protective effect of NP could be explained by the loose interaction of TMC and insulin by TPP together with the accelerating effect of TPP on the degradation of insulin by trypsin.

Taking all the above results into consideration, complexation with PEGylated TMC copolymers are a promising strategy for insulin carriers. Therefore, the NC were used for further experiments

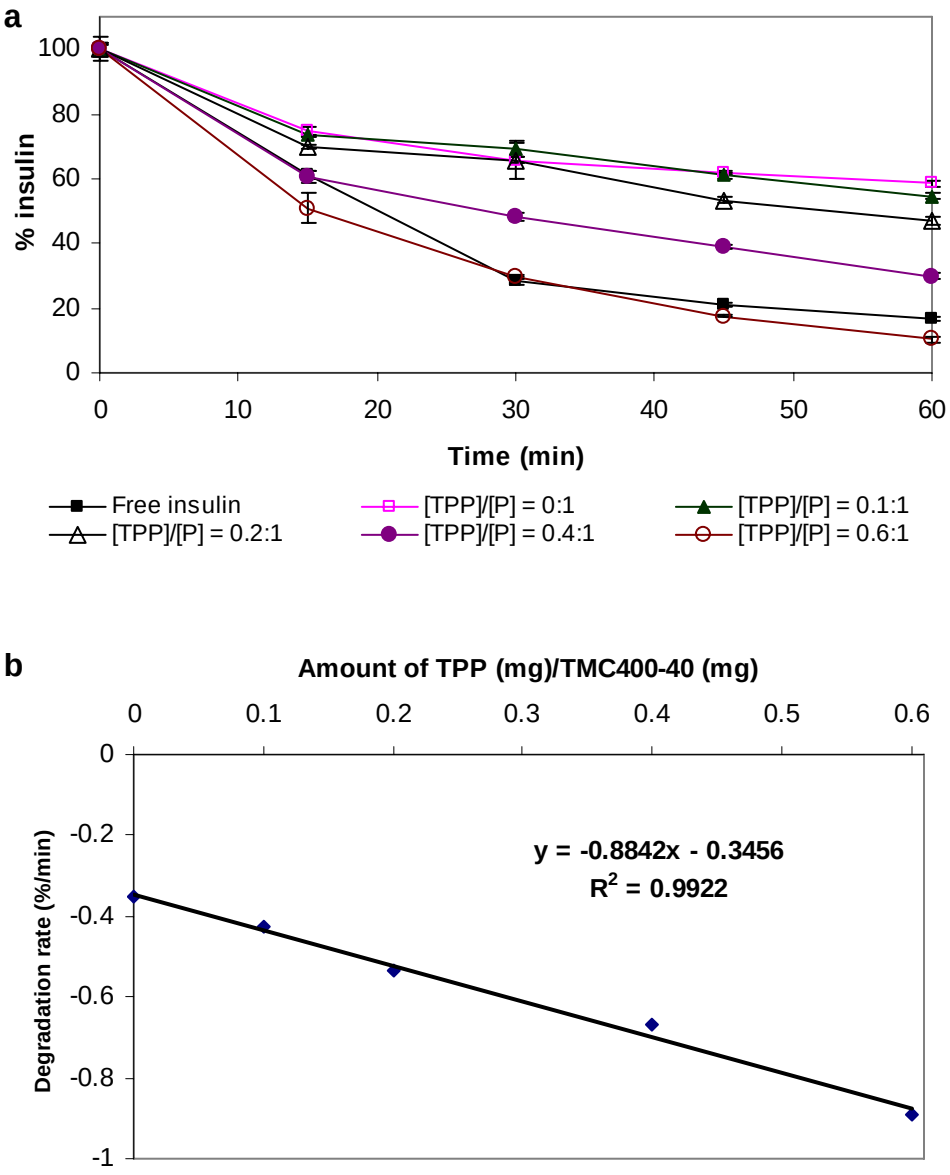

Figure 38. (a) Effect of TPP:TMC400-40 mass ratio on the stability of insulin in NP and (b) Relationship between TPP:TMC400-40 mass ratio and degradation rate of insulin. Each value represents the mean ± SD of three experiments. The initial concentrations of insulin and trypsin were 450 µg/ml and 300 BAEE IU/ml, respectively.

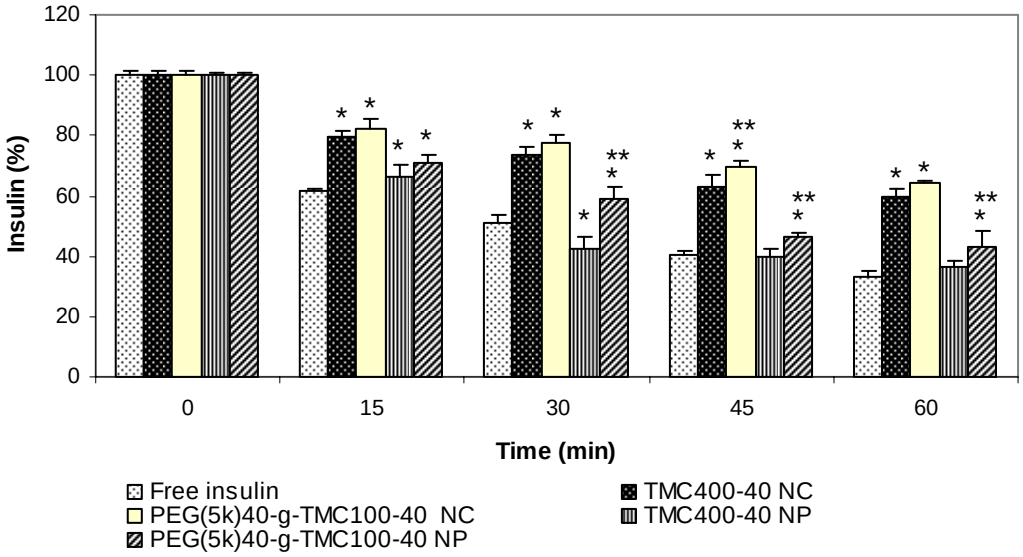

Figure 39. Enzymatic degradation of insulin by trypsin. Each value represents the mean ± SD of three experiments. The initial concentrations of insulin and trypsin were 450 μg/ml and 300 BAEE IU/ml, respectively. TMC400-40 NC = [P]:[Ins] of 0.3:1, TMC400-40 NP = [P]:[Ins]:[TPP] of 1:1:0.2, PEG(5k)$_{40}$-g-TMC100-40 NC = [P]:[Ins] of 1:1, PEG(5k)$_{40}$-g-TMC100-40 NP = [P]:[Ins]:[TPP] of 2:1:0.2. * Statistically significant differences from the values of free insulin ($p < 0.05$). ** Statistically significant differences from the values of NC ($p < 0.05$).

8. Adhesion of TMC and PEGylated TMC copolymers to mucus layer

In the present work, the mucoadhesion of fluorescent labeled polymers to the E12 monolayers was assessed using a cellular association assay under physiological condition.

8.1 Effect of quaternization degree

In comparison, chitosan 400 kDa (Ch400) was used as a control. Since chitosan was not dissolved at pH 7.4, the Ch400 solution was prepared in 10 mM Tris buffer pH 6.8. The binding results of the polymer solutions after 2 h incubation with the E12 cells are shown in Figure 40a. The amount of TMC binding to the cells was significantly higher than Ch400 ($p < 0.05$) and the adhesion increased with increasing DQ. The results were comparable to the results obtained from mucin particle method. Similarly, Sandri et al. (37) reported that mucoadhesion of TMC toward bovine submaxillary mucin dispersion and porcine buccal mucosa increased with increasing DQ.

8.2 Effect of degree of PEG substitution

The binding of PEGylated TMC copolymers to the E12 monolayers was investigated and compared to unmodified TMC400-40 (Figure 40b). The amount of polymer binding to the cells was considerably higher than unmodified TMC400-40 ($p < 0.05$). Of the three levels of PEG substitution, PEG$(5k)_{298}$-g-TMC400-40 showed the highest level of adhesion to the E12 monolayers at 3.4 times over that of TMC400-40 and the adhesion decreased with increasing degree of PEG substitution with linear correlation coefficients of 0.94. The improvement of mucoadhesion of three copolymers may be resulted from the interpenetration of PEG chains which reinforces the adhesion of the copolymer to the mucus layer.

Similarly, Serra et al. (164) reported that PEG grafted poly(acrylic acid) composed of 60% PEG exhibited the highest mucoadhesion while that composed of 20%, 40% and 80% PEG showed lower mucoadhesion. Therefore, it was noted that maximum mucoadhesion can be achieved by grafting appropriate amounts of PEG. Polymers containing too dense PEG chains on the backbone result in repulsive interaction between PEG chains among themselves and some of PEG chains are

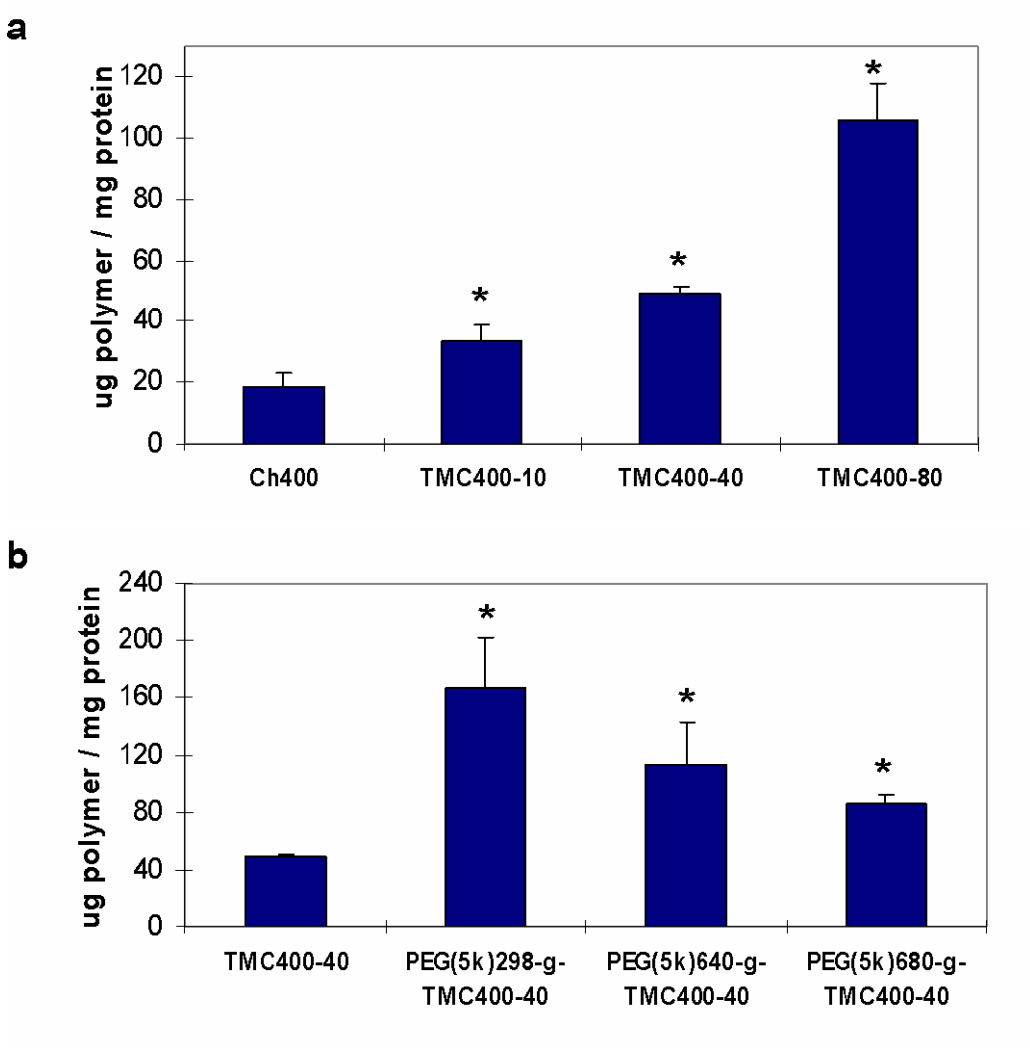

Figure 40. Binding of polymers as a function of (a) quaternization degree and (b) PEG substitution degree at 37°C with the E12 cell line. Polymer (250 μg/ml) solutions were incubated with the cells for 2 h. Error bars represent mean ± SD (n = 4). * $p < 0.05$, compared with that of Ch400 in (a) and that of TMC400-40 in (b).

displaced inside the backbone of the polymer leaving small amount of PEG chains available at the interface for interpenetration into the mucus (164).

However, when compared to unmodified TMC, the finding was contrary to the results obtained from mucin particle method which showed that mucoadhesion of all PEGylated TMC copolymers was significantly lower than unmodified TMC400-40 ($p < 0.05$) (Figure 20). This discrepancy can be probably explained by the different experimental conditions. In this experiment, adhesion of polymers was investigated with mucus gel layer which produced from glycoproteins (mucin), lipids, water, sloughed epithelial cells and electrolytes (141). In mucin particle method, adhesion of polymers was investigated with free mucin to which intensity of electrostatic interaction between polymer and mucin plays and important role while interpenetration of PEG chains of copolymer did not involved in the adhesion process. The result implies that the mucin particle method might be not suitable for investigating the interpenetration effect of mucoadhesive polymers.

8.3 Role of mucus

To investigate whether PEG chain interpenetration involved in the mucoadhesion enhancement, the adhesion of TMCs and PEGylated TMC copolymers to E12 monolayers was compared in the presence and absence of the mucolytic agent, NAC. It was reported that NAC at a concentration of 10 mM does not affect the integrity of the cell monolayers (197, 249). Since untreated E12 monolayers were covered with a mucus layer whereas NAC-treated E12 monolayers were not, “mucoadhesive” and “bioadhesive” were designated as adherence of polymers to untreated and NAC-treated E12 monolayers, respectively. The data showed that binding of the copolymers was higher than that of unmodified TMC400-40 both in untreated E12 and NAC-treated E12 (Figure 41). This might be due to the structure of E12 monolayers containing goblet cells with apical clustered mucin granules (199).

As seen in Figure 41, TMC displayed similar level of adherence between NAC-treated E12 and untreated E12 ($p > 0.05$). The findings obtained from TMC were comparable to the results reported by Keely et al. (54) who observed that TMC adhered equally to E12 monolayers and intestinal sac in the presence and absence of

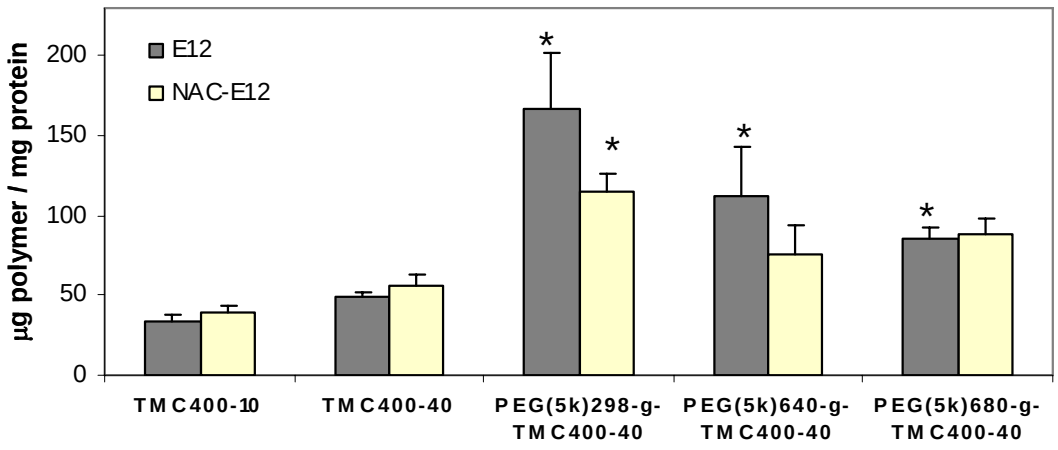

Figure 41. Effect of NAC on polymer adherence to monolayers. Each point represents the mean ± SD of four experiments. * $p < 0.05$, compared with that of TMC400-40.

NAC. Gernha et al. (67) also observed that chitosan nanoparticles strongly adhered at the cell surface membrane of Calu-3 even after mucus removal.

In term of PEGylated TMC copolymers, although the differences among groups were not statistically significant ($p > 0.05$), trends were observed that levels of adherence of copolymers reduced after removal of the mucus layer prior to incubation and the reduction of adhesion decreased with an increase in PEG substitution degree. This is probably due to grafting too dense PEG chains on TMC backbone, as previously discussed.

Taking all data in the consideration, the results imply that electrostatic interaction is a major factor in the adhesion of TMC, causing either mucoadhesion (mucus layer) or bioadhesion (epithelial membrane). On the other hand, the mucoadhesion of PEGylated TMC copolymers is influenced not only by electrostatic interaction but also the interpenetration of PEG chains at the interface of the mucus layer. Mucoadhesion of copolymers could be improved by grafting appropriate amounts of PEGs.

9. Binding and uptake of insulin NC

In the present work, the binding and uptake of fluorescent labeled insulin NC to the E12 monolayers was assessed using a cellular association assay under physiological condition. Since mucin is a major constituent in the mucus layer, the studies of insulin release from the NC in the presence of mucin were performed to investigate the behavior of the NC after adhesion on mucus layer.

9.1 Effect of polymer:insulin mass ratio

In the assay, the term “insulin uptake” included bound or internalized insulin in forms of NC and free insulin. To investigate the effect of polymer concentration on the insulin uptake, the NC of TMC400-40 were prepared at the different polymer:insulin mass ratio of 0.3:1 (optimal ratio), 1:1 and 2:1. Properties of the complexes were summarized in Table 15. Figure 42 presents the relationship of the insulin uptake (free insulin and insulin NC) in E12 cells and the insulin released from the NC. There was no evidence of insulin uptake by the NC of TMC400-40 prepared at optimal polymer:insulin mass ratio of 0.3:1 ($p > 0.05$) which correlated to the

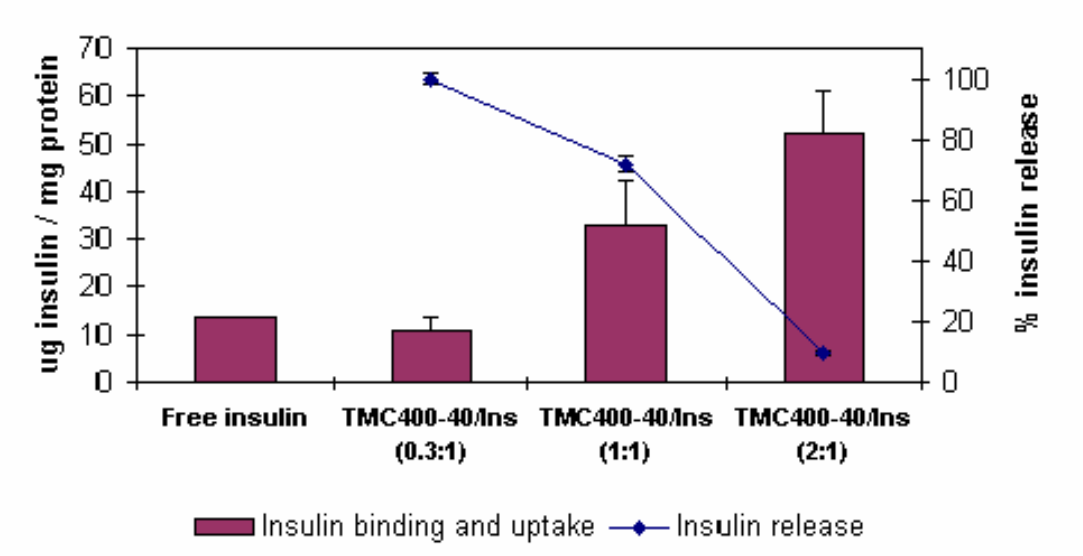

Figure 42. Effect of polymer:insulin mass ratio on the amount of insulin binding and uptake to E12 monolayer and percentage of amount of insulin released from TMC400-40/insulin NC. The concentration of insulin and mucin was of 125 μg/ml and 2 mg/ml, respectively. Each point represents mean ± SD (n = 4 for insulin binding and uptake and n = 3 for insulin release). * $p < 0.05$, compared with that of free insulin.

complete discharge of insulin from the NC. On the other hand, The NC prepared at TMC400-40:insulin mass ratio of 1:1 and 2:1 improved insulin uptake significantly ($p < 0.05$). The uptake of insulin NC increased with increasing ratio of polymer which correlated to a decrease in release of insulin from the NC.

In the formation of insulin NC with TMC and PEGylated TMC copolymers, it was found that polymer/insulin (+/–) charge ratio is an essential factor in NC formation which depends on the polymer structure. The stable and uniform NC with high insulin AE can be formed at optimal polymer/insulin (+/–) charge ratio and aggregation of the complexes occurs when apparent polymer/insulin (+/–) charge ratio is below optimal ratio (47). In case of the NC prepared at the optimal charge ratio of the polymer and insulin (0.3:1), insulin formed strong interaction with the polymer, leading to the highest AE and insulin could not be released from the NC. After the NC adhered on the mucus layer of E12 monolayers, the polymer charges were neutralized by the negative charges of mucin leading to reduction in polymer and insulin interaction and thus increase in the release of insulin (Figure 43a). In case of the NC prepared at higher polymer:insulin mass ratio (1:1 and 2:1), the polymer/insulin (+/–) charge ratio increased and small amount of polymer/insulin NC could be formed with low AE resulting in the high amount of free insulin. After adhering on the mucus layer, the apparent polymer/insulin (+/–) charge ratio decreased and allowed the polymer to capture more unassociated insulin, resulting in the reduction in the insulin release (Figure 43b).

9.2 Effect of polymer structure

To facilitate the direct comparison, all insulin NC were investigated at polymer and insulin concentration of 250 and 125 μg/ml, respectively. Properties of the complexes were summarized in Table 15.

As seen in Figure 44a, compared to free insulin solution and Ch400 NC, all TMC NC improved insulin uptake significantly ($p < 0.05$). The uptake of insulin NC increased with increasing DQ of TMC which correlated to an increase in binding of polymers to the E12 cells and zeta potential of NC. Moreover, it was found that insulin uptake was inversely proportion to the insulin released data. The results

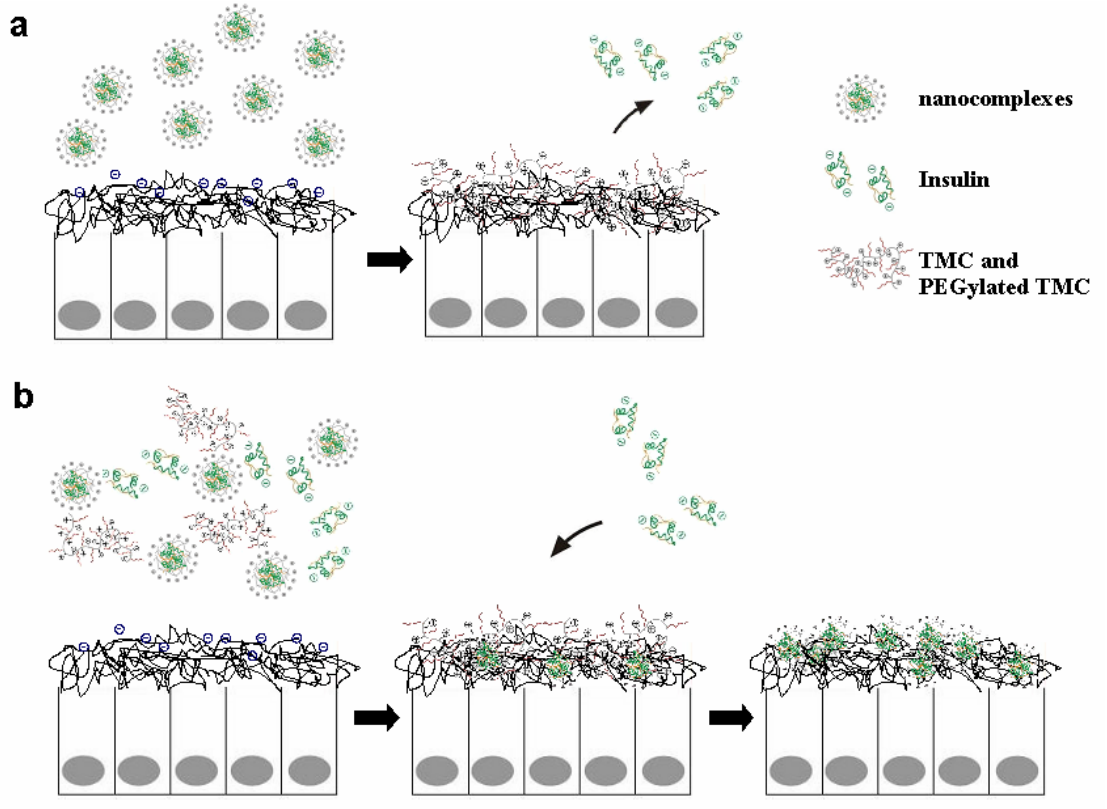

Figure 43. Schematic representation of behavior of insulin NC prepared (a) at optimal polymer:insulin mass ratio and (b) at higher polymer:insulin mass ratio after adhering to mucus layer.

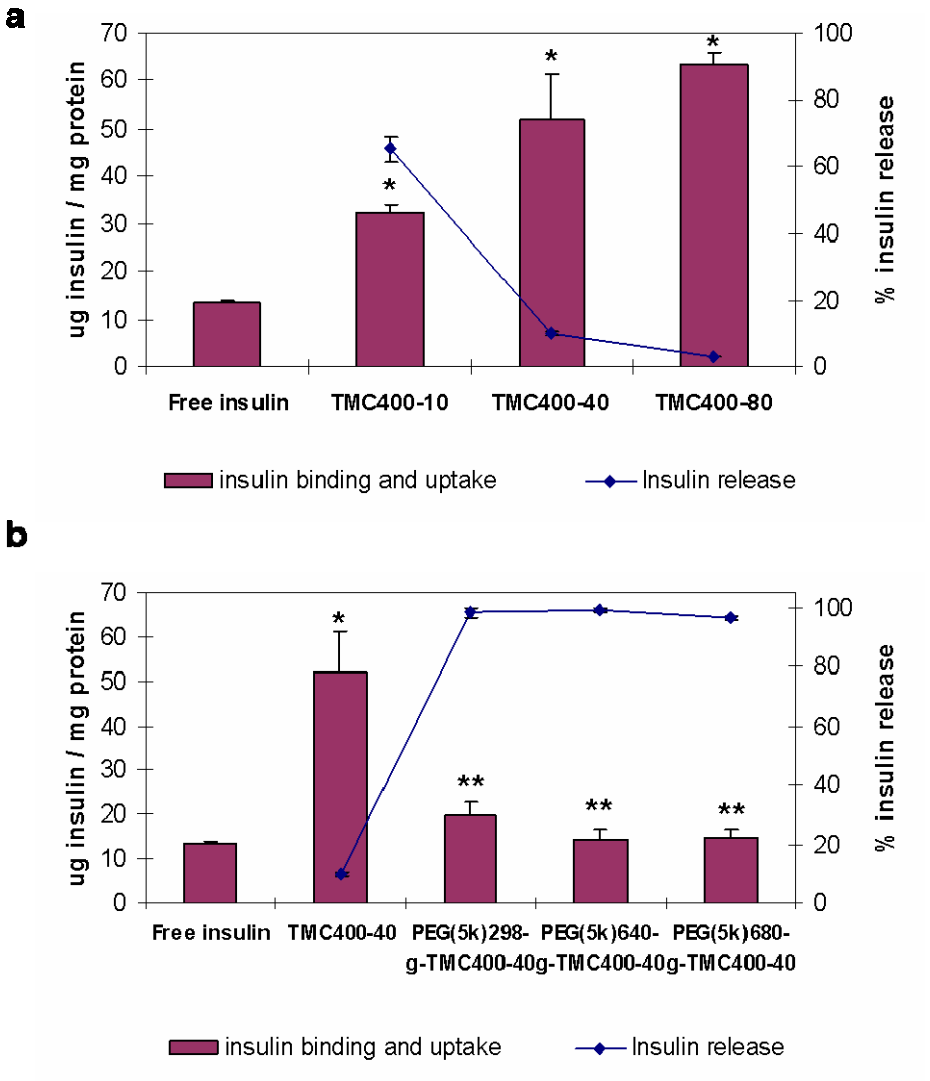

Figure 44. Amount of insulin binding and uptake to E12 monolayer and percentage of amount of insulin released from NC as a function of (a) quaternization degree and (b) PEG substitution degree. NC were prepared at polymer:insulin mass ratio of 2:1. The concentration of mucin was of 2 mg/ml. Each point represents mean ± SD (n = 4 for insulin binding and uptake and n = 3 for insulin release). * $p < 0.05$, compared with that of free insulin. ** $p < 0.05$, compared with that of TMC400-40.

obtained can be explained by optimal polymer:insulin mass ratio of each NC listed in Table 14. As demonstrated previously, insulin rapidly released from NC in the presence of mucin when NC prepared at the optimal polymer:insulin mass ratio. Since ratio between polymer and insulin (2:1) used for preparing NC was closer to the optimal polymer:insulin mass ratio of TMC400-10 NC (1.2:1) than those of TMC400-40 NC (0.3:1) and TMC400-80 (0.3:1), insulin was released from TMC400-10 NC higher than TMC400-40 NC and TMC400-80 NC. In addition, another factor affected the release of insulin in the presence of mucin is the interaction intensity between polymer and insulin. The stronger interaction of polymer and insulin results in lower insulin released. Therefore, at the polymer:insulin mass ratio of 0.3:1, TMC400-80 formed complexes with insulin stronger than TMC400-40, resulting in the low release of insulin from the NC and hence high insulin uptake.

Figure 44b presents the relationship of the insulin uptake in E12 cells and the insulin released from the NC of PEGylated TMC copolymers compared to the NC of unmodified TMC400-40. Interestingly, although copolymers showed high mucoadhesion than unmodified TMC400-40, the adhesion and uptake of their insulin NC was lower than the NC prepared from unmodified TMC400-40 ($p < 0.05$). Furthermore, there was no evidence that PEGylated TMC copolymer-insulin NC improved the uptake of insulin ($p > 0.05$) since the amount of insulin uptake of the PEGylated TMC/insulin NC was comparable to that of the free insulin solution. The finding may be due to the complete release of insulin from the NC into free insulin after adhering on mucus layer. As reported previously (47), the interaction intensity between PEGylated TMC and insulin was lower than that between TMC and insulin. In addition, it was reported that insulin had high affinity in PEG rich environment and PEG chain could form a complex and stabilize insulin (247, 250). Therefore, it seems reasonable to assume that except for the weak interaction between insulin and positive charge moieties of the copolymers, a certain proportion of insulin was retained with the PEG moieties conjugated in the TMC matrix, leading to the complete release of insulin after PEG chains penetrated into mucus layer during binding to the mucin.

10. Transport studies

The permeability of different structured NC across the E12 monolayers was investigated. The amount of insulin in basolateral compartment, the amount of insulin remained in the apical compartment and the amount of internalized or attached insulin in the E12 monolayers after 2 h incubation were measured. The E12 monolayers had a mean TEER of 98 ± 14 $\Omega \cdot cm^2$.

There was no evidence of insulin permeation across the E12 monolayers since fluorescent signal of TRITC labeled insulin could not be detected on the basolateral side of the monolayers exposed to free insulin and different structured NC. However, an inverse finding was reported by Keely et al. (54), indicating that TMC increased the permeability of FD-4 across E12. Florea et al. (39) also reported that TMC enhanced octreotide across Calu-3 monolayers. This discrepancy could be explained by the different drugs, transport pathway of drug, experiment time and polymer concentration employed.

Based on the results that only TMC-insulin NC enhanced the insulin uptake in the cells, the amounts of internalized or attached insulin in the E12 monolayers treated with different TMC/insulin NC were determined. The results are shown in Figure 45. Compared with free insulin, TMC enhanced the amount of insulin attached or internalized in the E12 cells which increased with increasing DQ. It can be explained by the mucoadhesive ability of TMC which increased with increasing DQ and hence provided more time for internalization of insulin in the cells. The results obtained were in accordance with the results from insulin release studies and binding and uptake studies.

11. CLSM visualization of localization of insulin NC on E12 cells

The CLSM was used to visualize the localization of polymer and NC, E12 cells treated with fluorescent labeled NC. Based on the binding and uptake data, the NC prepared from TMC400-40 was used to investigate the localization of polymer and NC on E12 cells. The NC were prepared at higher polymer:insulin mass ratio in order to distinguish polymer and complex localizations. Confocal micrograph images of TMC400-40-insulin NC prepared at polymer:insulin mass ratio of 1:1 are shown in Figure 46. The yellow color (NC), resulting from the co-localization of green

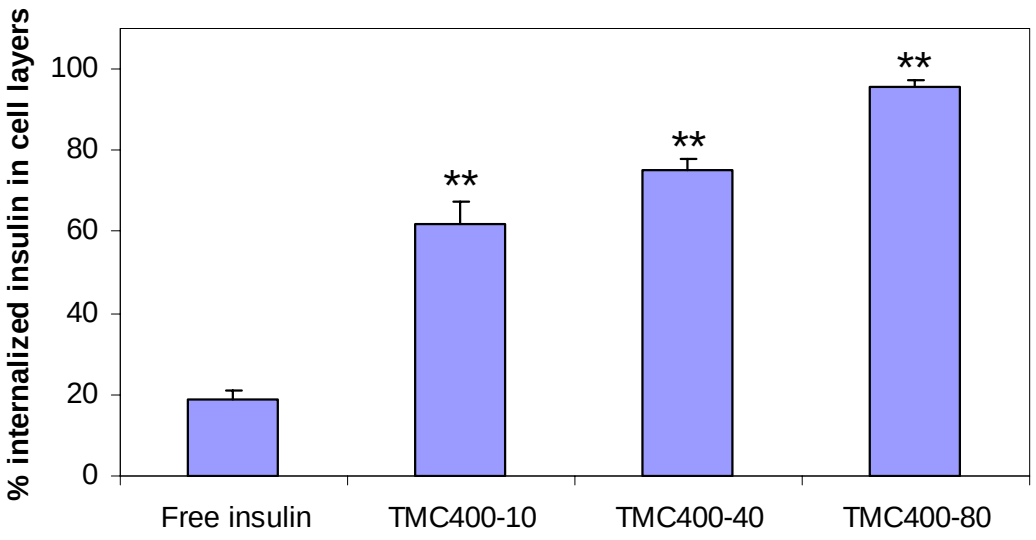

Figure 45. Percentage of amount of insulin internalized / attached in E12 cell monolayers after 2 h incubation. Each point represents the mean ± SD of three experiments. ** $p < 0.05$.

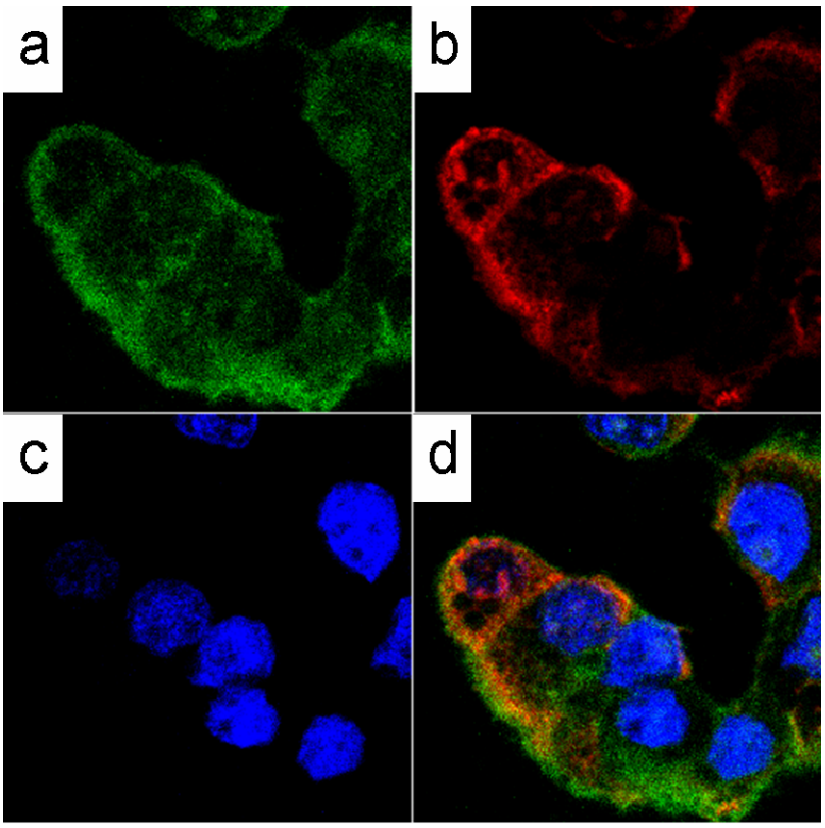

Figure 46. Confocal micrograph images of E12 cell monolayers incubated with TMC400-40-insulin NC for 2 h at 37°C (a) green filter, (b) red filter, (c) blue filter, (d) overlay of a,b,c. TMC400-40 was labeled with Oregon Green 488, insulin was labeled with TRITC and nuclei were labeled with DAPI.

(TMC400-40) and red (insulin), and green color mostly distributed on the apical cell membrane with small amounts in the cytoplasm and perinuclear areas, indicating that most of complexes and free TMC400-40 located on the cell membrane. The results were confirmed by the three-dimensional xz- and yz-projections of confocal images (Figure 47), demonstrating that TMC400-40 and the complexes were adhered mostly on the cell membrane due to the present of the green and yellow colors over the cell membrane.

In corroboration with the adherence and transport studies, it is reasonable to conclude that TMC polymer and its corresponding insulin NC adhered to the mucus layer covering E12 monolayers.

12. Hypoglycemic activity of nasal insulin NC in rats

Based on results obtained, TMC400-40 and two corresponding PEGylated TMC400-40 copolymers, PEG(5k)$_{298}$-g-TMC400-40 and PEG(5k)$_{680}$-g-TMC400-40 were selected to evaluate the influence of PEG grafting on the nasal insulin absorption. The doses of insulin for both i.n. and s.c. were selected based on the expected pharmacological effect and the respective route of administration (71). Recently, Yu et al. reported that osmolarity of nasal formulation affected nasal insulin absorption (102). Besides, it is possible that hypo- or hyperosmotic formulations might cause lesion on the nasal epithelium. In order to omit these effects, all nasal insulin formulations were prepared in isotonic Tris buffer. The properties of self-assembled insulin NC used in the present work are described in Table 19. All complexes had a size in the range of 150 – 237 nm with a positive surface charge of 10.0 – 13.9 mV.

Studies of nasal absorption were conducted in anesthetized, male Wistar rats, the absorption of insulin was evaluated by monitoring the hypoglycemic effect after intranasal administration of insulin NC. It is well documented in the literature that the values of the blood glucose baselines are in the range of 75 – 105 mg/dl for healthy rats and 350 – 500 mg/dl for diabetic rats (71). However in this experiment the blood glucose baselines of anesthesized rats were in the range of 110 – 290 mg/dl. This is probably a consequence of stress effect by anesthetic agents. Ahsan et al. also observed similar phenomenon with the use of ketamine/xylazine mixture (131).

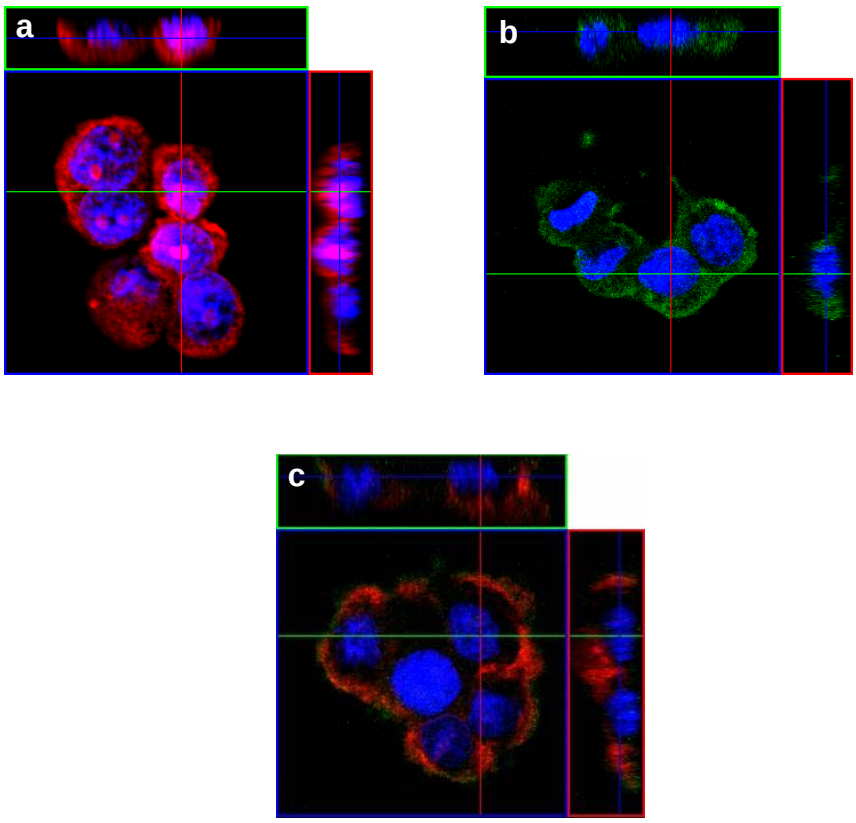

Figure 47. Three-dimensional xz- and yz-projections of confocal images of E12 cell monolayers incubated with (a) TRITC-labeled insulin, (b) Oregon Green 488-labeled TMC400-40 and (c) double-labeled NC for 2 h at 37°C.

Table 19. Characterization of administered insulin solutions and NC

Formulation[a]	Insulin conc. (IU/kg)	Polymer conc (mg/kg)	Mass ratio (Ins:Pol)	Particle size (nm)	Zeta potential (mV)
Ins sol, s.c.	0.5	-	-	-	-
Ins sol, i.n.	4.0	-	-	-	-
Ins/TMC400 NC (1:0.3)	4.0	0.04	1.0 : 0.3	181 ± 2	7.4 ± 1.4
Ins/TMC400 NC (1:1)	4.0	0.14	1.0 : 1.0	182 ± 5	14.9 ± 1.3
Ins/TMC400 NC (1:5)	4.0	0.70	1.0 : 5.0	223 ± 3	13.9 ± 1.0
Ins/PEG(5k)$_{298}$-g-TMC400 NC (1:5)	4.0	0.70	1.0 : 5.0	150 ± 1	10.3 ± 1.0
Ins/PEG(5k)$_{680}$-g-TMC400 NC (1:5)	4.0	0.70	1.0 : 5.0	237 ± 7	10.0 ± 1.7

The characteristic data of insulin NC are expressed as the mean ± SD of three batches.

[a]Prepared in isotonic 10 mM Tris buffer

The hypoglycemic effects of various insulin NC versus a reference (s.c. administration) are presented in Figures 48 and 49. The corresponding pharmacodynamic parameters including C_{min}, T_{min}, $AOC_{0\text{-}240\ min}$ and F_{dyn} are listed in Table 20. Blood glucose levels were not reduced initially after administration of the isotonic Tris buffer as control; however, slight reduction with fluctuation of the blood glucose with time (< 10% of the basal level) was observed after 30 min. This result could be attributed to hypoglycemic effect of insulin in rats. In the control group (4.0 IU/kg insulin, i.n. administration), a slight decrease in blood glucose concentration was observed. The partial decrease in blood glucose in this control group could be resulted from an effect of anesthetic agent on the mucociliary clearance as suggested by Mayor and Illum (126). The s.c. reference of 0.5 IU/kg insulin yielded a C_{min} equal to 36% of the basal glucose concentration after 113 min.

12.1 Effect of polymer concentration

Using TMC400-40 as an example to investigate insulin bioavailability related to the amount of instilled polymer, insulin NC were prepared at different insulin/TMC400-40 mass ratios of 1:0.3 (optimal ratio), 1:1 and 1:5. As seen in Figure 48, the decrease in blood glucose levels in rats treated with insulin/TMC400-40 NC was significantly different ($p < 0.05$) than that in the control groups. All insulin/TMC400-40 NC decreased blood glucose level up to in range 37 – 46% of the basal blood glucose level at about 91 – 103 min after nasal instillation. From Table 20, the F_{dyn} over 4 h of all insulin/TMC400-40 NC was in the range of 9.1 – 12.3%, which was higher than that of the control group (3.9%). In addition, $AOC_{0\text{-}240\ min}$ and F_{dyn} of rat groups induced with insulin/TMC400-40 NC increased with the increase in TMC400 ratio. Although the differences among groups were not statistically significant ($p > 0.05$), a trend was observed: T_{min} increased and C_{min} decreased with an increase in TMC400-40 ratios.

In general, a suitable ratio of both insulin and polymer is necessary for optimal NC formation (47). Increase in the ratio of polymer could reduce the specific advantages of nano-carriers. The increased bioavailability of NC prepared at higher polymer concentration could be likely related to the assessment of the unassociated free polymer to the epithelium and tight junction proteins, resulting in tissue damage

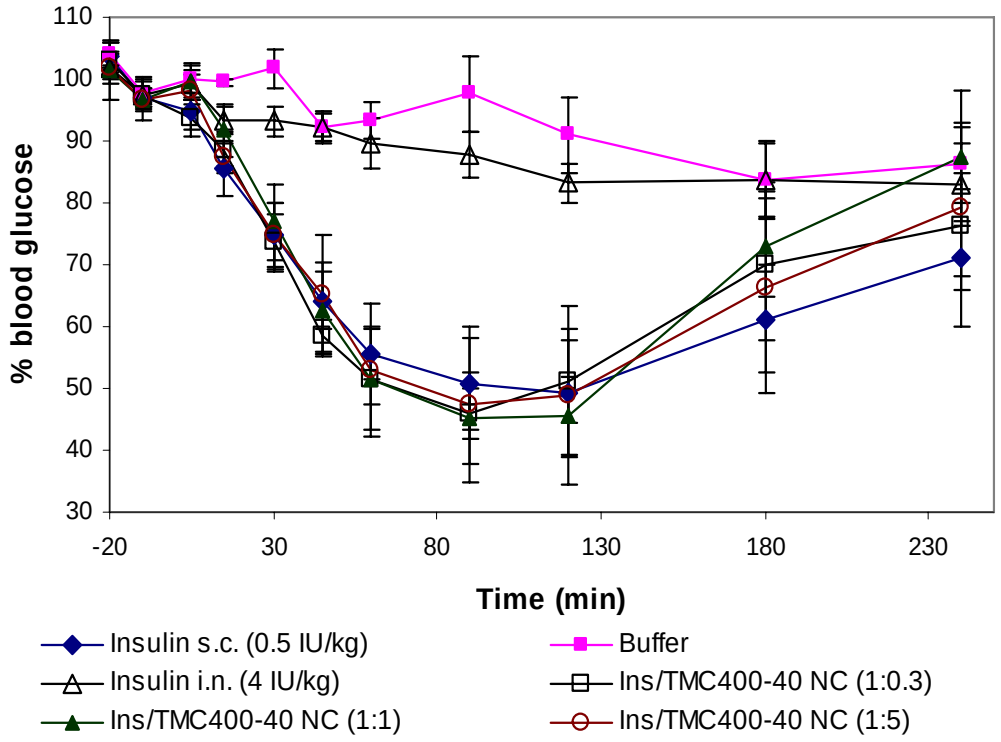

Figure 48. Effect of insulin:polymer mass ratio on the mean plasma glucose levels following nasal administration of 4 IU/kg insulin NC to rat. Data represent mean ± SEM of six experiments.

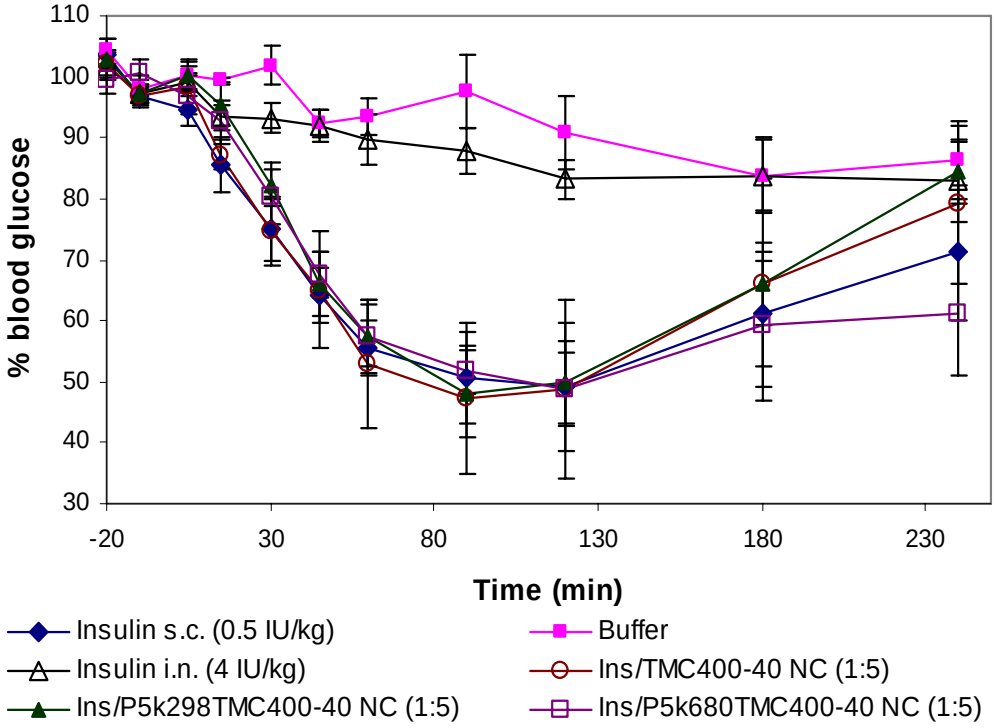

Figure 49. Effect of PEG substitution degree on the mean plasma glucose levels following nasal administration of 4 IU/kg insulin NC to rat. The NC were prepared at insulin:polymer mass ratio of 1:5. Data represent mean ± SEM of six experiments.

Table 20. Pharmacodynamics after nasal administration of insulin in various formulations to rats

Formulation	*n*	T_{min} (min)	C_{min} (%basal glucose)	$AOC_{0\text{-}240\ min}$ (%min)	F_{dyn} (%)
Ins sol[a], s.c.	6	112.9 ± 4.1	35.5 ± 3.4	10541 ± 598	100.0 ± 5.7
Ins sol[b], i.n.	6	-	-	3279 ± 600	3.9 ± 0.5
Ins/TMC400 NC[b] (1:0.3), i.n	6	91.5 ± 4.0	46.1 ± 2.6	7703 ± 775*	9.1 ± 0.9*
Ins/TMC400 NC[b] (1:1), i.n.	6	101.4 ± 4.0	37.0 ± 3.3	9302 ± 841*	11.0 ± 1.0*
Ins/TMC400 NC[b] (1:5), i.n.	6	103.3 ± 4.2	38.3 ± 2.0	10377 ± 444*	12.3 ± 0.5*
Ins/$PEG(5k)_{298}$-g-TMC400 NC[b] (1:5), i.n.	6	98.1 ± 2.5	33.8 ± 2.5	9889 ± 579*	11.7 ± 0.7*
Ins/$PEG(5k)_{680}$-g-TMC400 NC[b] (1:5), i.n.	6	119.8 ± 2.4	47.2 ± 3.3	8935 ± 631*	10.6 ± 0.7*

Data represent as Mean ± SEM

[a]Insulin concentration of 0.5 IU/kg

[b]Insulin concentration of 4.0 IU/kg

* Statistically significant difference ($p < 0.05$) compared with that of intranasal insulin solution

and/or enhanced insulin absorption. Similar observation was published by Simon et al. who reported that insulin/amine modified poly(vinyl alcohol)-*graft*-poly(L-lactide) NC containing a threefold higher polymer concentration increased insulin bioavailability more effective than NC containing optimal polymer concentration (71). Illum et al. (251) and Yu et al. (102) also observed an influence of chitosan concentration of insulin bioavailability.

12.2 Effect of PEG substitution degree

Based on the studies performed in vitro mucus-secreting E12 cell culture model, PEGylated TMC could not improve insulin uptake as compared to unmodified TMC. In order to investigate the effect of PEG substitution degree on *in vivo* nasal insulin absorption, the hypoglycemic effects of intranasal administration of insulin/PEG(5k)$_{298}$-g-TMC400-40 NC and insulin/PEG(5k)$_{680}$-g-TMC400-40 NC were compared to that of insulin/TMC400-40 NC. The results are shown in Figure 49 and Table 20. Nasal administration of the insulin/PEGylated TMC NC reduced blood glucose level significantly as compared to the control insulin solution ($p < 0.05$). However the inverse finding was reported by Mao et al. (65), indicating that insulin/PEG(5k)$_{40}$-g-TMC100 NC did not enhance nasal insulin absorption in diabetic rats. This discrepancy could be from the low molecular weight and concentration of polymer used. In addition, it should be noted that the pharmacodynamic was investigated with healthy rats in this studies. Indeed, in diabetic rat, deficiency of insulin results in severe changes in metabolism, decreased activity of the sympathetic nervous system, dehydration, glycosuria, and osmotic diuresis (252). Therefore, the responses of diabetic rats to insulin formulation might differ from that of healthy rats (253).

From Table 20, the F_{dyn} of nasal administration of insulin NC composed of PEGylated TMC was lower than that of insulin/unmodified TMC NC and the F_{dyn} decreased with increasing PEG substitution ratio. However, the differences among groups were not statistically significant ($p > 0.05$). The results are inconsistent with results from Zhang et al. who observed that in vivo efficacy of PEG-g-chitosan nanoparticles on nasal insulin absorption increased with increasing PEG content (106). This discrepancy could be from the toxicity of chitosan and TMC. With regard to

cytotoxicity of TMC and PEGylated TMC reported by Mao et al. (45), it was found that the F_{dyn} of nasal administration of the different structure NC correlated strongly with their cytotoxicity, implying that the improved nasal insulin absorption was probably dependent on tissue damaging effect of the NC. However, this hypothesis needs to be clarified by nasal histological study.

As stated above, the hypoglycemia of healthy rats could be influenced by rat insulin which can be seen from the slight decrease in blood glucose concentration in the rat groups treated with nasally applied isotonic Tris buffer. This finding implies that the changes in blood glucose concentration might be a synergism of administered insulin and rat insulin. Therefore, the efficacy of NC formulation on the hypoglycemia after nasal administration should be confirmed by insulin blood level and corresponding pharmacokinetic data. Since responses of healthy and diabetic rats to environmental stress factors are different (253), the efficacy of NC formulation should be investigated further in diabetic rats.

13. Histopathological effect of insulin NC on the nasal epithelium

It was often suggested that the use of intranasal penetration enhancers could be accompanied by histological damage to the nasal tissue, increasing membrane permeability. Therefore, from a practical point of view, morphological integrity of nasal epithelium after nasal administration of each NC needs to be examined.

A basic requirement for comparability of the histological results is that the administered dose is deposited on a restricted area. The dose volume of 20 µl used in this study was sufficiently small to allow for direct comparison of the nasal membranes between the dosed (right) side and the undosed (left) side of the nasal cavity. Moreover, the rats were anesthetized by i.p. injection of the zoletil®/xylazine mixture, instead of by ether (diethyl ether) inhalation since there is a report that induction of ether irritates the respiratory tract and may provoke excessive mucus secretions, pulmonary edema and airway obstruction (254). These might affect mistaken on scoring morphological charges of nasal epithelium.

Histological evaluation was made in the region (ii) and region (iii) cross-sections of the excised nasal where mainly lined with respiratory and olfactory epithelia, respectively (74, 202). A regional map of the epithelial lesions along nasal

cavity was also recorded to explore the irritating degree of the insulin NC and to identify the susceptibility of different epithelial cell types to the different insulin NC.

13.1 Morphology of untreated rat nasal epithelium

A diagrammatic representation of the anterior face of regions (ii) and (iii) is depicted in Figure 50. In the region (ii), the nasal cavity is divided into two halves by the nasal septum. The cavities contain a dorsal meatus, a middle meatus and a ventral meatus which the following morphology of cells was observed. Squamous epithelium lined the ventral meatus. The nasal septum was covered with typical respiratory epithelium consisting of ciliated pseudostratified columnar cells, goblet cells and basal cells. The epithelium on the anterior turbinate surfaces was ciliated pseudostratified columnar (Figure 51a). On the dorsal part of the septum and the dorsal meatus, the olfactory epithelium was located.

In the anterior section of region (iii), clear division of the nasal cavity into two sides was still observed. The ethmoid turbinates was seen at the level of the second palatal ridge of region (iii) where the nasal cavity is incompletely divided into two halves. The epithelium lining the nasal cavity in region (iii) was predominantly olfactory epithelium which consists of tall sustentacular cells, olfactory sensory neurons and basal cells (Figure 51b).

13.2 Acute histopathological effect of nasal insulin formulations

For acute histopathological studies, tissue preparation was carried out after 4 h once administration of insulin solution or insulin NC, so that toxicological effects of longer-lasting adhesion of polymer residues were could be observed. The septal area and all of the undosed (left) side of the nasal cavity was clear of epithelium. Therefore, the undosed side of the nasal cavity was consistently used as the control side of the same samples. Tables 21 and 22 summarize the extent of the morphological changes of the nasal epithelium in region (ii) and (iii) observed after 4 h exposure to the nasal insulin formulations. The distribution of epithelial lesions of regions (ii) and (iii) after 4 h exposed to each nasal formulation are summarized in Figures 52 and 53, respectively.

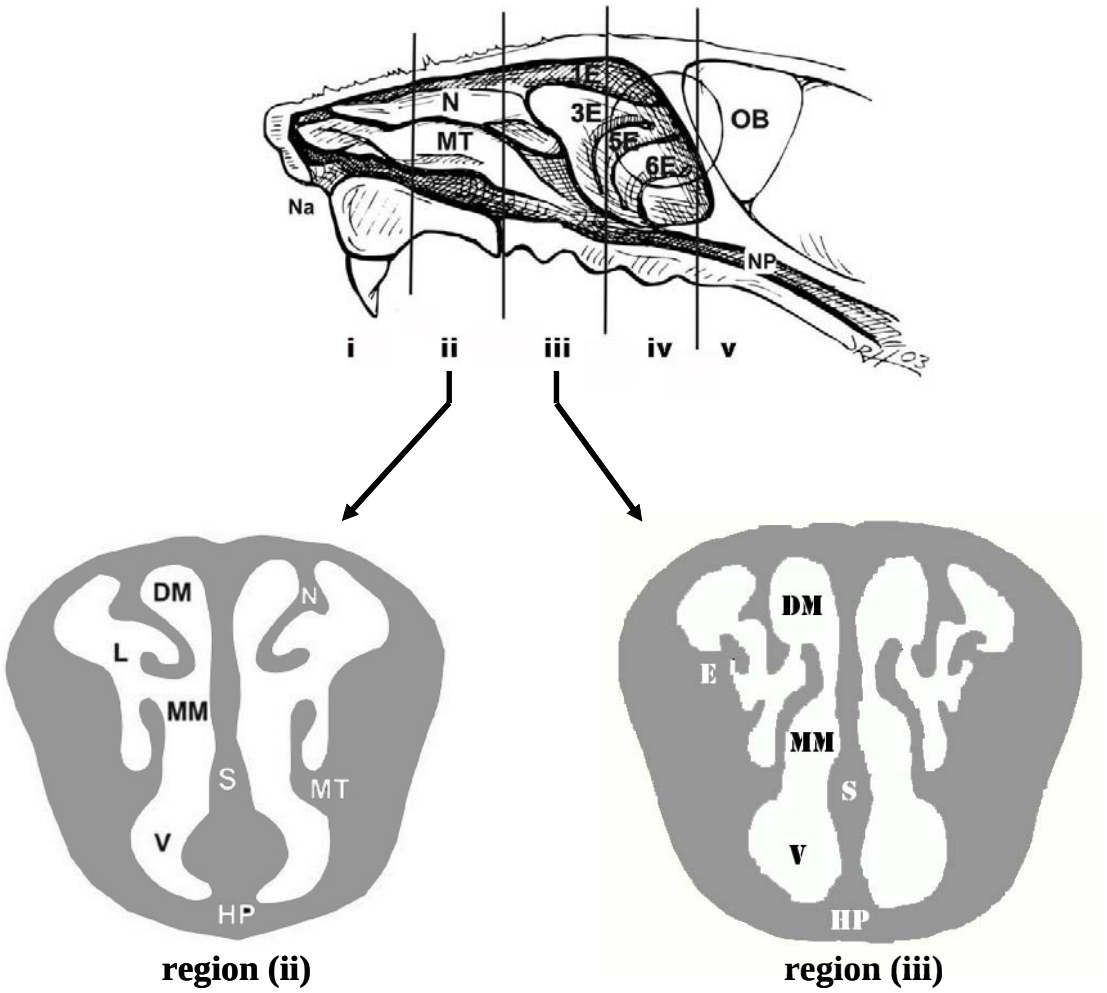

Figure 50. Diagrammatic representation of the lateral wall and turbinates in the nasal airway of the rat and anterior faces of region (ii) and region (iii) of the rat nasal cavity. N, nasoturbinate; MT, maxilloturbinate; E, ethmoid turbinates; HP, hard palate; S, septum; V, ventral meatus; MM, middle meatus; L, lateral meatus; DM, dorsomedial meatus.

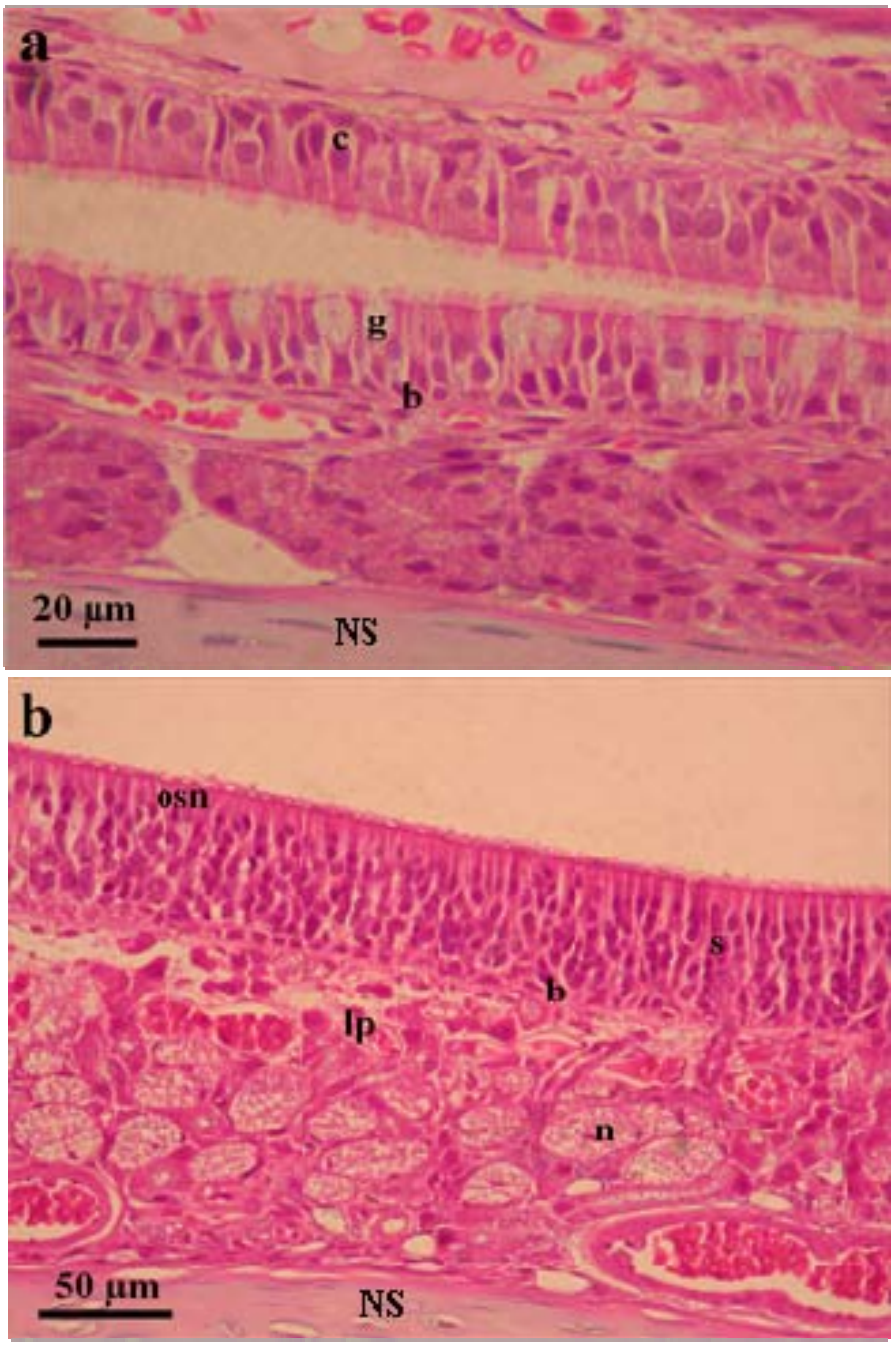

Figure 51. Photomicrographs of untreated rat nasal epithelium. (a) respiratory epithelium; (b) olfactory epithelium; b, basal cell; c, ciliated cell; g, goblet cell; lp, lamina propria with Bowman's glands; n, bundles of nerve fibers; NS, nasal septum; osn, olfactory sensory neuron; s, supporting (sustentacular) cell. HE staining.

Table 21. Summary of the effects of insulin NC on morphological changes of the rat nasal epithelium in region (ii) after 4 h single intranasal administration (n = 3)

Treatments	Rat	Mild		Moderate			Severe		
	No.	MS	GD	VC	SE	DE	PN	SL	H
Buffer	1	-	-	-	-	-	-	-	-
	2	-	-	-	-	-	-	-	-
	3	-	-	-	-	-	-	-	-
Ins sol	1	-	-	-	-	-	-	-	-
	2	-	-	-	-	-	-	-	-
	3	-	-	-	-	-	-	-	-
Ins/TMC400-40 NC (1:0.3)	1	-	++	-	+	-	-	-	-
	2	-	+	-	-	-	-	-	-
	3	-	+++	-	-	-	-	-	-
Ins/TMC400-40 NC (1:1)	1	++	-	-	+	-	+	+	+
	2	++	-	-	++	-	+	+	-
	3	+	-	-	+	-	+	+	+
Ins/TMC400-40 NC (1:5)	1	+++	-	+	+++	+++	+++	+++	+++
	2	++	-	++	+++	+++	+++	+++	+++
	3	+++	-	+	++	+++	+++	+++	+++
Ins/PEG(5k)$_{298}$-g-TMC400-40 NC (1:5)	1	-	++	-	++	-	+	+	+
	2	+	++	-	+	-	-	-	-
	3	-	++	-	++	-	-	-	-
Ins/PEG(5k)$_{680}$-g-TMC400-40 NC (1:5)	1	+	+	+	+	-	-	-	-
	2	-	-	-	-	-	-	-	-
	3	+	+	-	+	-	-	-	-

Numbers indicate the extent of occurrence (-, no remarkable lesion; +, slight; ++, moderate; +++, severe). MS, mucus hypersecretion; GD, goblet cell distension; VC, vascular congestion; SE, subepithelial edema; DE, discontinuation of epithelium; PN, pyknotic nuclei; H, hemorrhage; SL, sloughing of epithelium. Dose of insulin was 4 IU/kg.

Table 22. Summary of the effects of insulin NC on morphological changes of the rat nasal epithelium in region (iii) after 4 h single intranasal administration (n = 3)

Treatments	Rat	Mild		Moderate			Severe		
	No.	MS	GD	VC	SE	DE	PN	SL	H
Buffer	1	-	-	-	-	-	-	-	-
	2	-	-	-	-	-	-	-	-
	3	-	-	-	-	-	-	-	-
Ins sol	1	-	-	-	-	-	-	-	-
	2	-	-	-	-	-	-	-	-
	3	-	-	-	-	-	-	-	-
Ins/TMC400-40 NC (1:0.3)	1	++	-	+	++	-	-	-	-
	2	+	-	-	++	-	-	-	-
	3	-	-	+	-	-	-	-	-
Ins/TMC400-40 NC (1:1)	1	++	-	+	++	-	+	+	-
	2	-	-	-	+	-	+	+	-
	3	+	-	-	++	-	-	-	-
Ins/TMC400-40 NC (1:5)	1	++	-	+	+++	+++	+++	+++	+++
	2	+	-	-	+++	+++	+++	+++	+++
	3	+	-	+	+++	+++	+++	+++	+++
Ins/PEG(5k)$_{298}$-g-TMC400-40 NC (1:5)	1	+	-	+	-	-	+	+	-
	2	-	-	-	-	-	-	-	-
	3	+	-	-	-	-	+	+	-
Ins/PEG(5k)$_{680}$-g-TMC400-40 NC (1:5)	1	-	-	+	-	-	-	-	-
	2	-	-	-	-	-	-	-	-
	3	-	-	+	-	-	-	-	-

Numbers indicate the extent of occurrence (-, no remarkable lesion; +, slight; ++, moderate; +++, severe). MS, mucus hypersecretion; GD, goblet cell distension; VC, vascular congestion; SE, subepithelial edema; DE, discontinuation of epithelium; PN, pyknotic nuclei; H, hemorrhage; SL, sloughing of epithelium. Dose of insulin was 4 IU/kg.

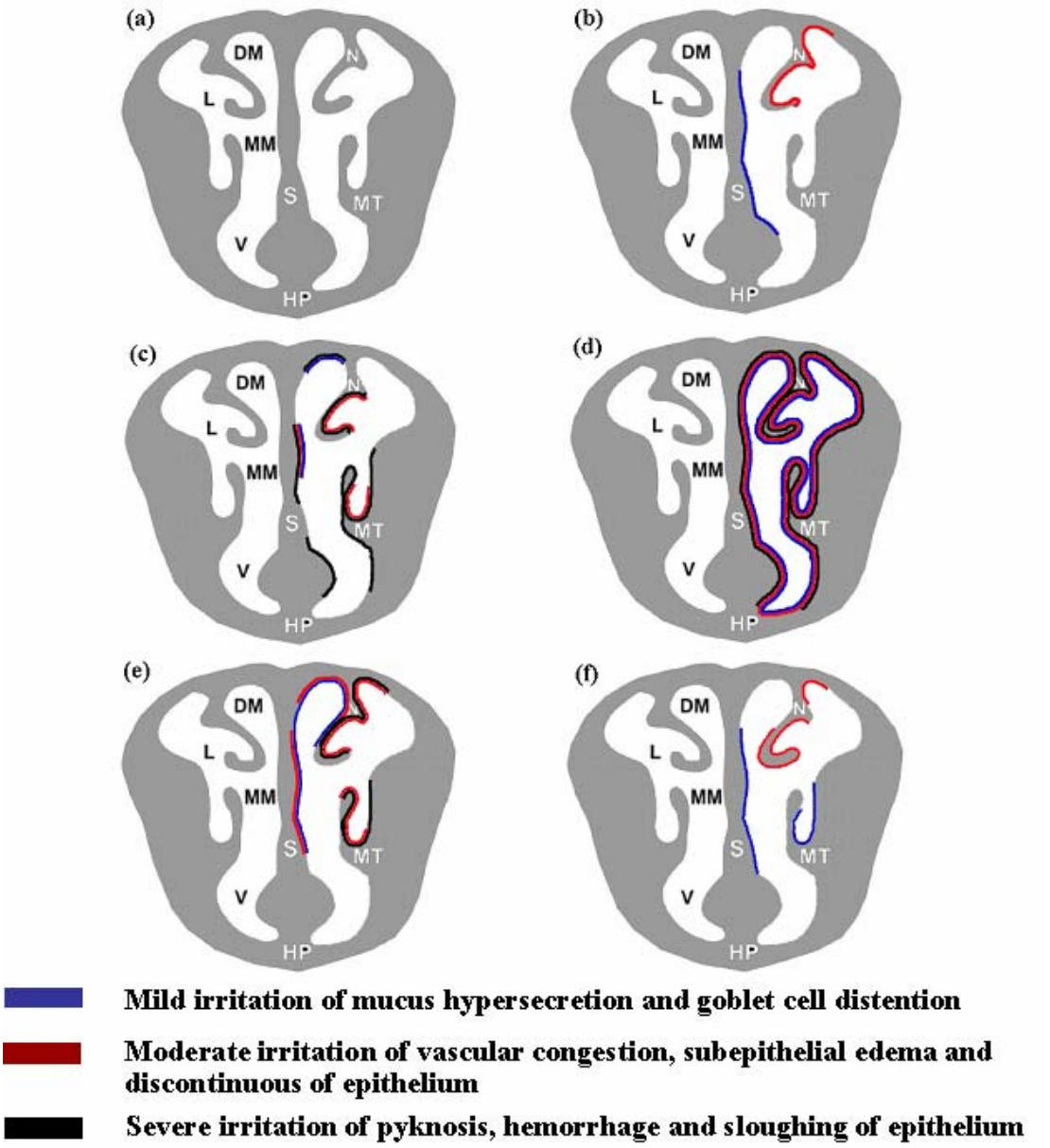

Figure 52. Diagram of location of lesions in region (ii) after 4 h exposed to (a) insulin solution, (b) Ins/TMC400-40 NC (1:0.3), (c) Ins/TMC400-40 NC (1:1), (d) Ins/TMC400-40 NC (1:5), (e) Ins/PEG(5k)$_{298}$-g-TMC400-40 NC (1:5) and (f) Ins/PEG(5k)$_{680}$-g-TMC400-40 NC (1:5). N, nasoturbinate; MT, maxilloturbinate; HP, hard palate; S, septum; V, ventral meatus; MM, middle meatus; L, lateral meatus; DM, dorsomedial meatus. Dose of insulin was 4 IU/kg.

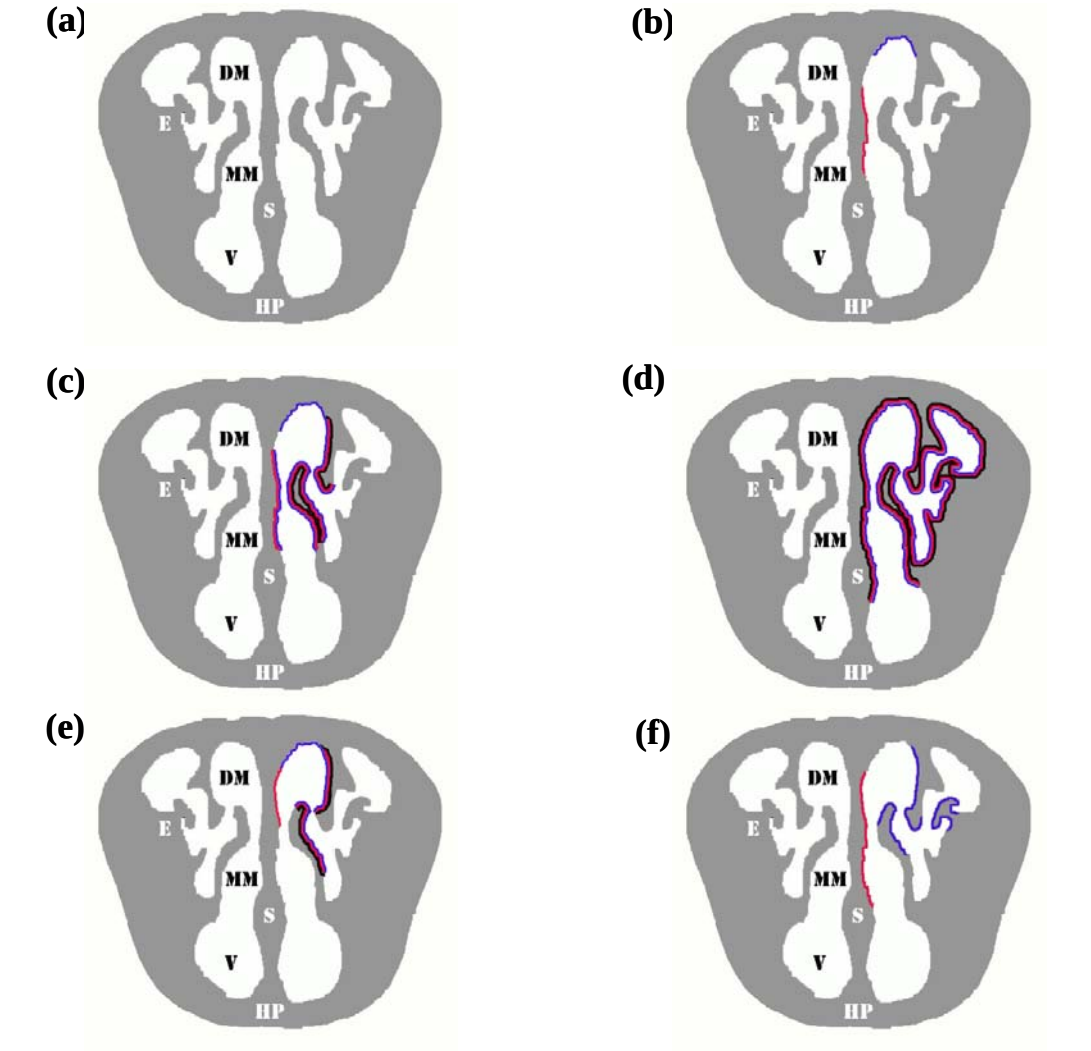

Figure 53. Diagram of location of lesions in region (iii) after 4 h exposed to (a) insulin solution, (b) Ins/TMC400-40 NC (1:0.3), (c) Ins/TMC400-40 NC (1:1), (d) Ins/TMC400-40 NC (1:5), (e) Ins/PEG(5k)$_{298}$-g-TMC400-40 NC (1:5) and (f) Ins/PEG(5k)$_{680}$-g-TMC400-40 NC (1:5). E, ethmoid turbinates; HP, hard palate; S, septum; V, ventral meatus; MM, middle meatus; L, lateral meatus; DM, dorsomedial meatus. Dose of insulin was 4 IU/kg.

13.2.1 Isotonic 10 mM Tris buffer and insulin solution

The epithelium of groups treated with isotonic Tris buffer and insulin solution exhibited no sign of irritation. The epithelial cells remained unaffected in all sections studied. However, some rats demonstrated slight mucus secretion in both sides which was considered to be normal incidence since the rats were not kept in a tightly controlled, dust-free area (Figure 54).

13.2.2 Effect of polymer concentration

13.2.2.1 Insulin/TMC400-40 NC (Ins:Pol = 1:0.3)

In the region (ii), the nasal tissue exposed to 1:0.3 insulin/TMC400-40 NC exhibited moderate increase in goblet cell distention compare to the undosed side, but this was restricted only to the septal region without flow into the dorsal meatus (Figure 55a). However, slight subepithelial edema was found on nasoturbinate in lateral meatus which might be contributed to the dorsal position of the rat during the administration.

The olfactory epithelium throughout region (iii) of the dosed side showed slight vascular congestion and moderate subepithelial edema, which present only on the medial part of septum (Figure 55b).

13.2.2.2 Insulin/TMC400-40 NC (Ins:Pol = 1:1)

The administration of the 1:1 insulin/TMC400 NC demonstrated the discharge of mucus, subepithelial edema and considerable epithelial disruption both in regions (ii) and (iii) (Figures 56a and 56b). An epithelium was still maintained over all surfaces. The epithelial disruptions were observed on the septum, turbinates and lateral wall on the dosed side of the region (ii) and turbinates on the dosed side of the region (iii). Besides, the vascular congestion was also seen on the medial part of septum in the region (iii), as shown in Figure 56c.

13.2.2.3 Insulin/TMC400-40 NC (Ins:Pol = 1:5)

The epithelium exposed to the insulin/TMC400 NC exhibited severe damage, including subepithelial edema, epithelial necrosis (pyknosis), hemorrhage and sloughing of epithelial cells (Figures 57 and 58). Complete loss of

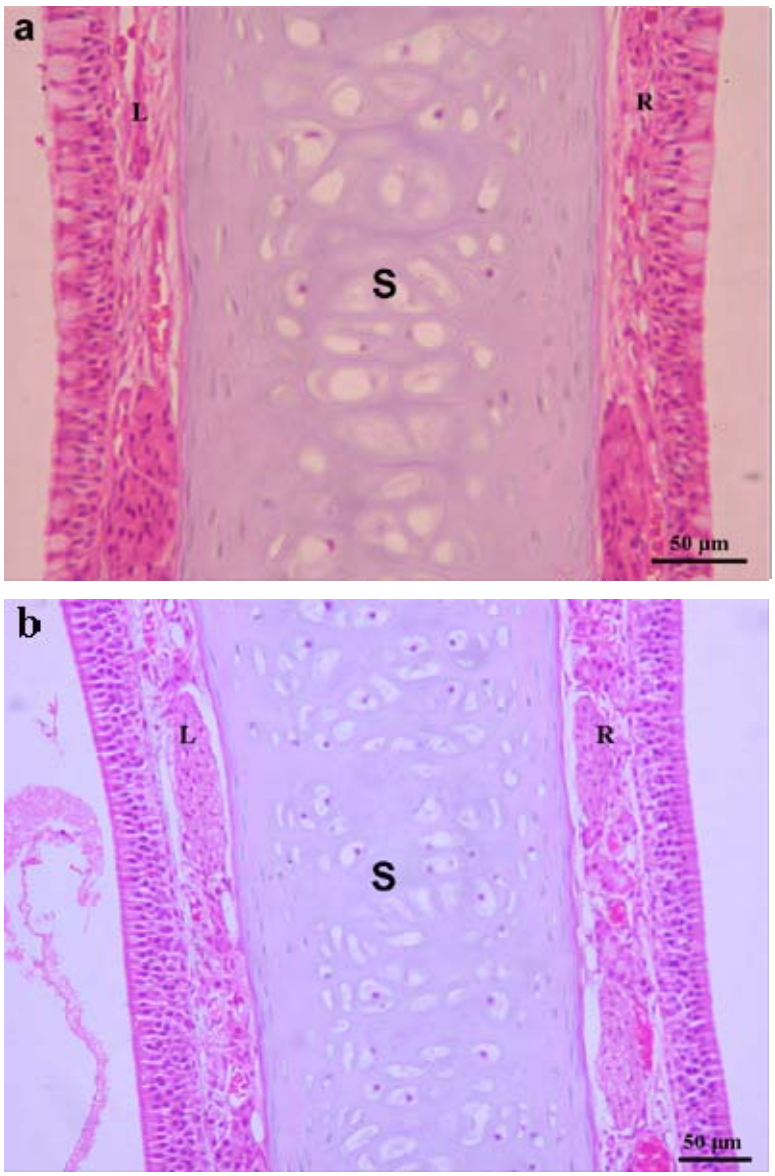

Figure 54. Photomicrographs of a vertical section from (a) region (ii) and (b) region (iii) of the rat nasal cavity 4 h after dosing 20 µl of 4 IU/kg insulin solution. L, undosed side; R, dosed side; S, nasal septum. HE staining.

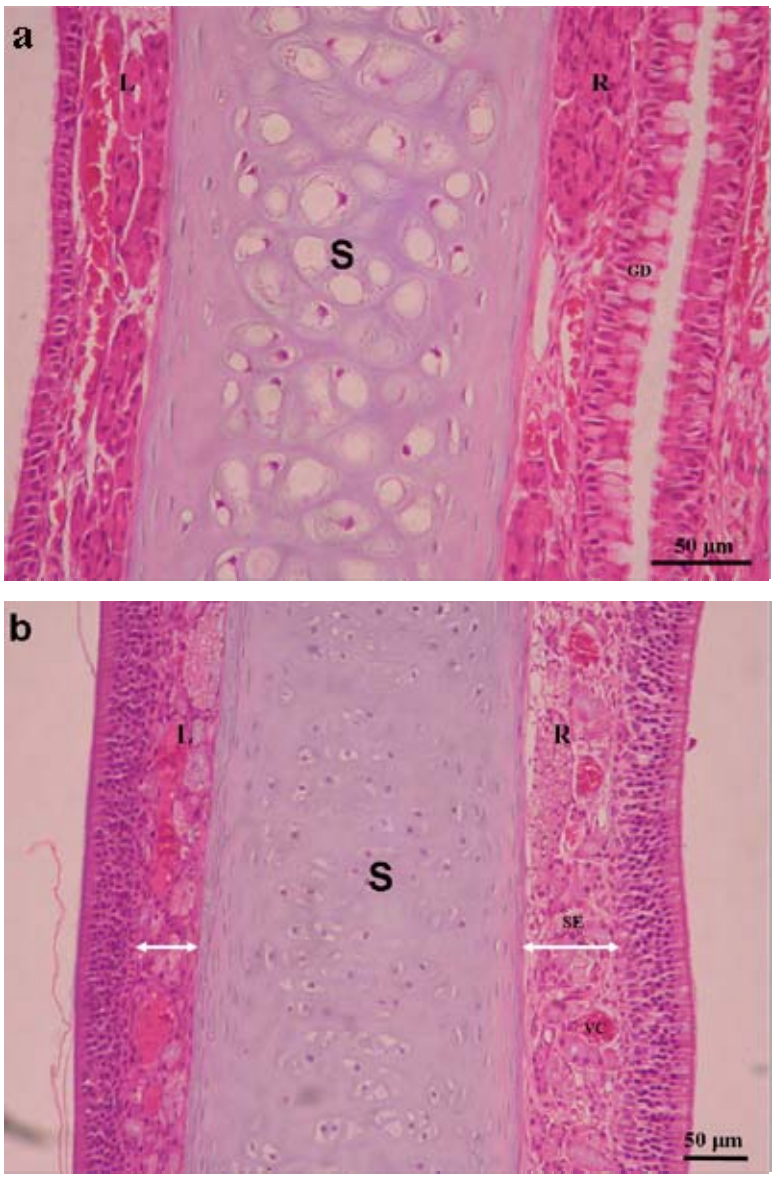

Figure 55. Photomicrographs of a vertical section from (a) region (ii) and (b) region (iii) of the rat nasal cavity after 4 h nasal administration of Ins/TMC400-40 NC (4 IU/kg insulin, Ins:Pol = 1:0.3). The dosed side (R) of region (ii) shows moderate goblet cell distension (GD) and that of region (iii) shows slight vascular congestion (VC) and moderate subepithelial edema (SE). L, undosed side; S, nasal septum. HE staining.

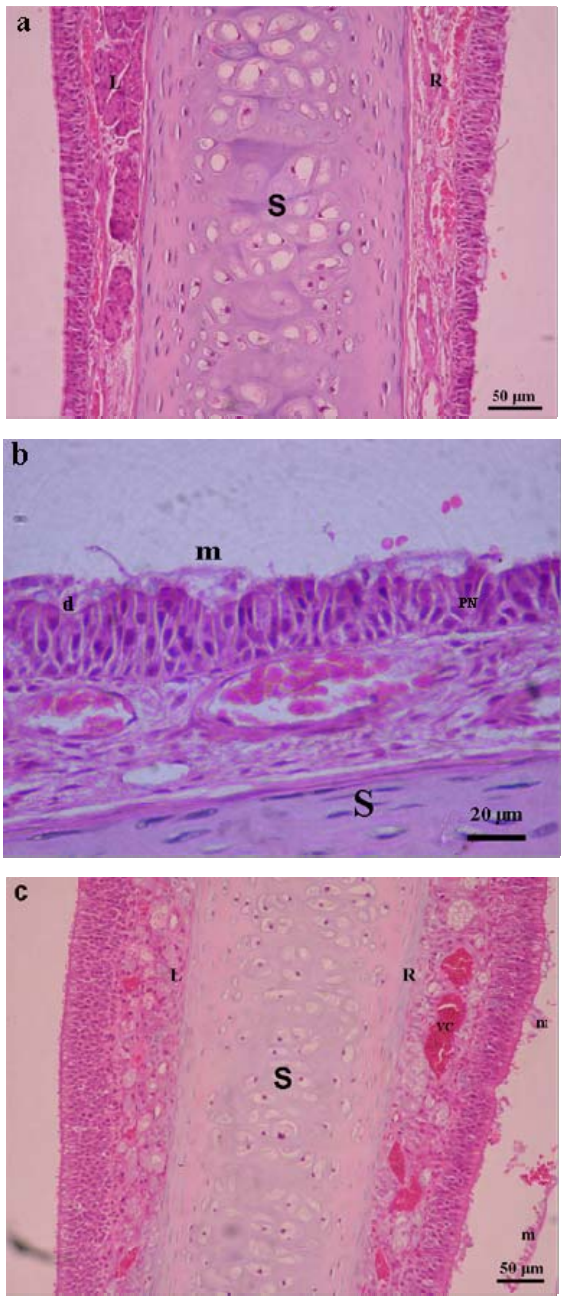

Figure 56. Photomicrographs of a vertical section from (a) region (ii) and (c) region (iii) of the rat nasal cavity after 4 h nasal administration of Ins/TMC400-40 NC (4 IU/kg insulin, Ins:Pol = 1:1). Figure 56b is higher magnification for dosed side (R) of Figure 56a showing discharged mucus (m), pyknotic nuclei (PN) and epithelial disruption (d). The dosed side (R) of region (iii) shows mucus hypersecretion (m) and vascular congestion. L, undosed side; S, nasal septum. HE staining.

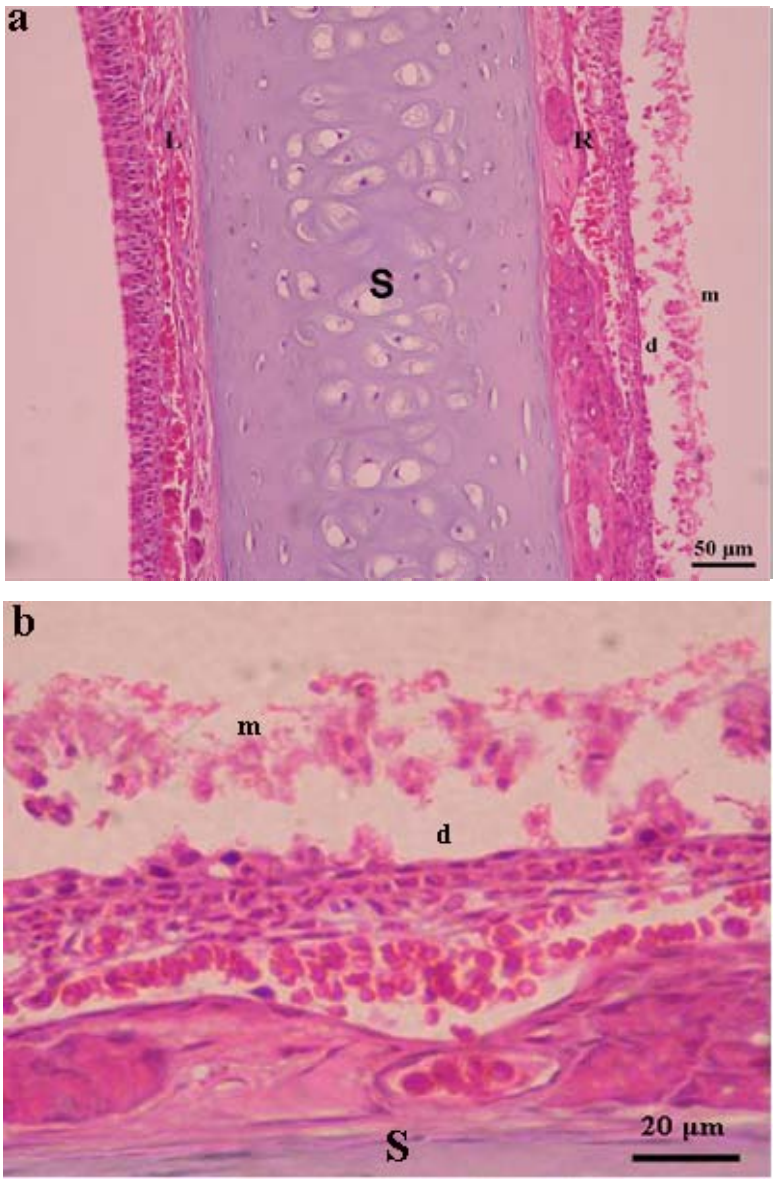

Figure 57. Photomicrographs of a vertical section from region (ii) of the rat nasal cavity after 4 h nasal administration of Ins/TMC400-40 NC (4 IU/kg insulin, Ins:Pol = 1:5). Figure 57b is higher magnification for dosed side (R) of Figure 57a showing a denuded basement membrane with discharged mucus (m) containing cells shed from the epithelium in the lumen. L, undosed side; S, nasal septum; d, epithelial disruption. HE staining.

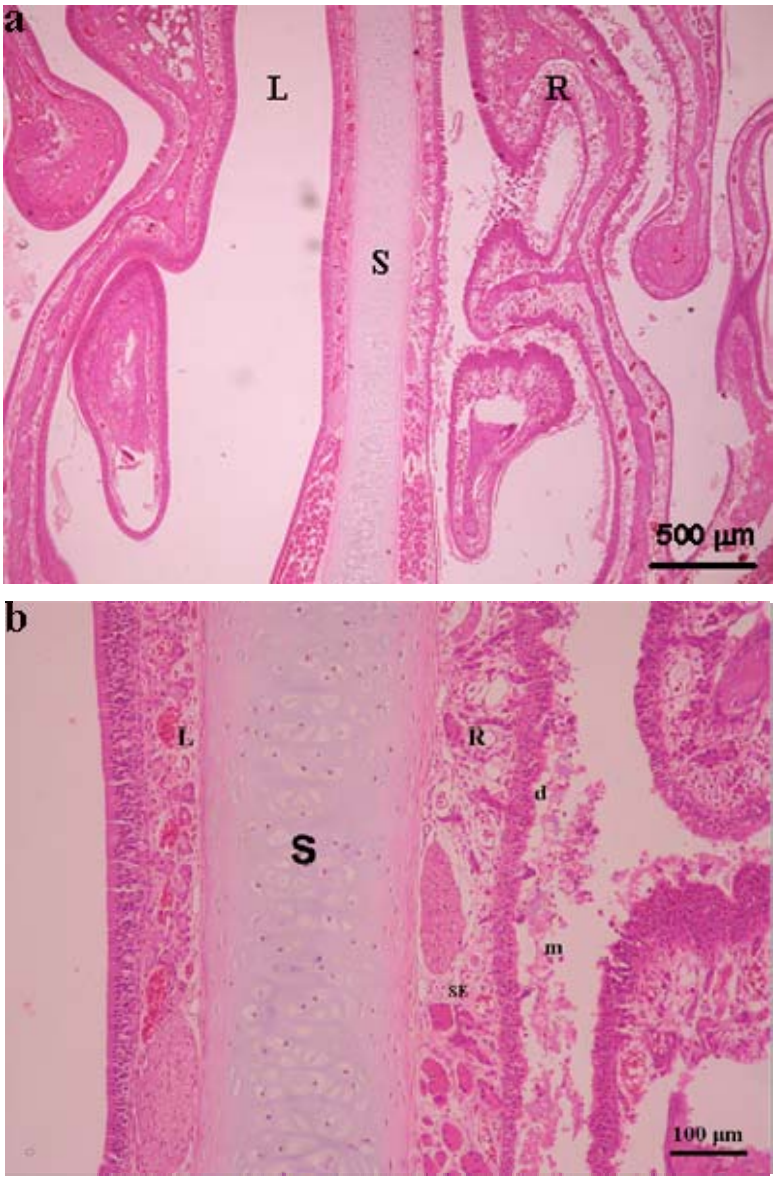

Figure 58. Photomicrographs of a vertical section from region (iii) of the rat nasal cavity after 4 h nasal administration of Ins/TMC400-40 NC (4 IU/kg insulin, Ins:Pol = 1:5). Figure 58b is higher magnification for dosed side (R) of Figure 58a showing a discharged mucus (m) containing cells shed from the epithelium in the lumen., subepithelial edema (SE) and epithelial disruption (d). L, undosed side; S, nasal septum. HE staining.

epithelium occurred in some places and large quantities of mucus were observed in the nasal cavity. The incidences extended to all regions of the nasal cavity both in region (ii) and (iii) cross-sections. Although the irritating effects of insulin/TMC400 NC affected both the respiratory and olfactory epithelia, the effects were more pronounced in the olfactory area, especially in region (iii).

The acute histological effect of these insulin/TMC400-40 NC on the nasal epithelium was therefore ranked as 1:5 insulin/TMC400-40 NC > 1:1 insulin/TMC400-40 NC > 1:0.3 insulin/TMC400-40 NC > insulin solution. Moreover, it was observed that the irritating effects of insulin/TMC400-40 NC to olfactory epithelium were pronounced than those to respiratory epithelium, especially 1:5 insulin/TMC400-40 NC. This could be due to the high positive charge and mucoadhesive properties of the NC and free TMC400-40 as well as turnover time of mucus covered epithelium. Prolonged residence time of NC and/or free TMC400-40 on the epithelium might cause the increase in irritating effects. In fact, mucus covering the olfactory epithelium moves very slowly with a turnover time of probably several days. In contrast, the mucus covering the respiratory epithelium is driven along at rate of 1 to 30 mm/min by synchronized beating of the surface cilia with an estimated turnover time of about 10 min (135). Recently, Amidi et al. (17) studied the influence on cilia beat frequency (CBF) of TMC solution/nanoparticles on excised chicken embryo trachea and found that TMC exhibited a cilio-inhibiting effect. Therefore, it is reasonable to assume that the damaging effect of insulin/TMC400-40 NC resulted from retention of NC and/or free TMC400-40 on the nasal mucosa.

Coupled with the pharmacodynamic data, these acute morphological findings consistently correlate with the F_{dyn} of nasal administration of insulin/TMC400-40 NC, suggesting that the enhancement of insulin absorption by TMC400-40 NC when increasing TMC400-40 mass ratio was probably due to nasal membrane damaging effects. Therefore, using TMC400-40 NC as the nasal insulin absorption enhancer, the ratio of insulin and TMC400-40 in the formulation should be optimized to obtain the balance between activity and safety.

13.2.3 Effect of PEG substitution of TMC

13.2.3.1 Insulin/PEG(5k)$_{298}$-g-TMC400-40 NC (Ins:Pol=1:5)

Compared to 1:5 insulin/TMC400-40 NC, the 1:5 insulin /PEG(5k)$_{298}$-g-TMC400-40 NC appeared to exhibit the subepithelial edema, epithelial disruption, hemorrhage and pyknosis in all sections from region (ii) and (iii). The incidence and severity were less than the insulin/TMC400-40 NC and limited to the lateral meatus (Figure 59). There was a slight increase in mucus discharge on the dorsal meatus of region (ii). The goblet cell distention was also observed on the medial part of nasal septum in region (ii). Overall, the insulin/PEG(5k)$_{298}$-g-TMC400-40 NC affected both the respiratory and olfactory epithelia, although the effects were most prominent in the respiratory area.

13.2.3.1 Insulin/PEG(5k)$_{680}$-g-TMC400-40 NC (Ins:Pol=1:5)

In the region (ii), The nasal respiratory epithelium along septum exposed to the insulin/PEG(5k)$_{680}$-g-TMC400-40 NC demonstrated a mild level of irritation with slight mucus secretion and goblet cell distension (Figure 60a). Small lesions of vascular congestion and subepithelial edema were observed on the nasoturbinate. There were no detached cells in the lumen of the cavity. The olfactory epithelium throughout region (iii) of the dosed side was unaffected except for slight vascular congestion which was present only on the medial part of septum (Figure 60b).

From the results obtained, the incidences and severities of irritation were in the rank order: insulin/TMC400-40 NC > insulin/PEG(5k)$_{298}$-g-TMC400-40 NC > insulin/PEG(5k)$_{680}$-g-TMC400-40 NC > insulin solution. These results were found to correlate with the improved insulin absorption effects of these NC. The irritating effects of insulin NC correlated to the properties of polymer used. Previously, Mao et al. studied the in vitro cytotoxicity of TMC and PEGylated TMC copolymers with L929 mouse fibroblast cells and reported that PEGylation decreased cytotoxicity of TMC which decreased with the increase in the number of PEG substitution (45). Besides the shielding effect of PEG chain on a proportion of the positive charges present on TMC, the less irritating effect of the insulin NC prepared from PEGylated TMC copolymers could be from the properties of PEG. Due to a biocompatible, non-toxic, non-immunogenic and water soluble polymer, PEG is often

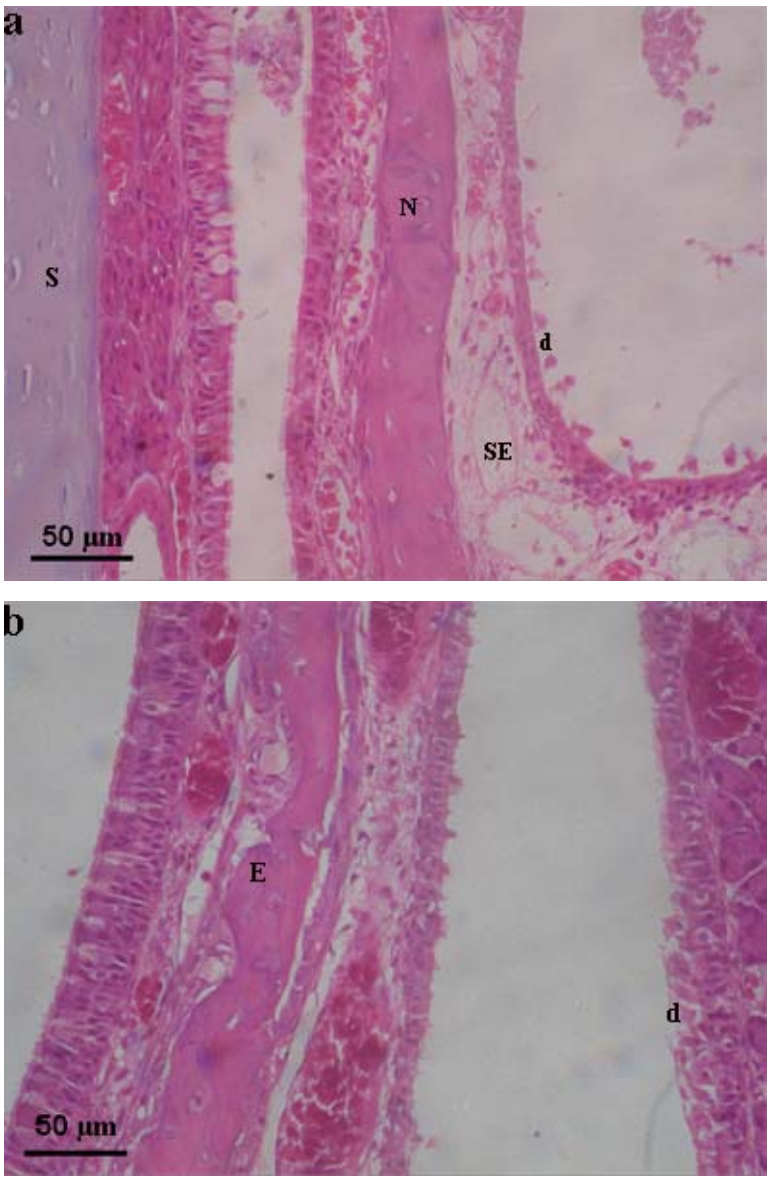

Figure 59. Photomicrographs of a vertical section of dosed side from (a) region (ii) and (b) region (iii) of the rat nasal cavity after 4 h nasal administration of Ins /PEG(5k)$_{298}$-g-TMC400-40 NC (4 IU/kg insulin, Ins:Pol = 1:5). E, ethmoid turbinate; d, epithelial disruption; N, nasoturbinate; S, nasal septum; SE, subepithelial edema. HE staining.

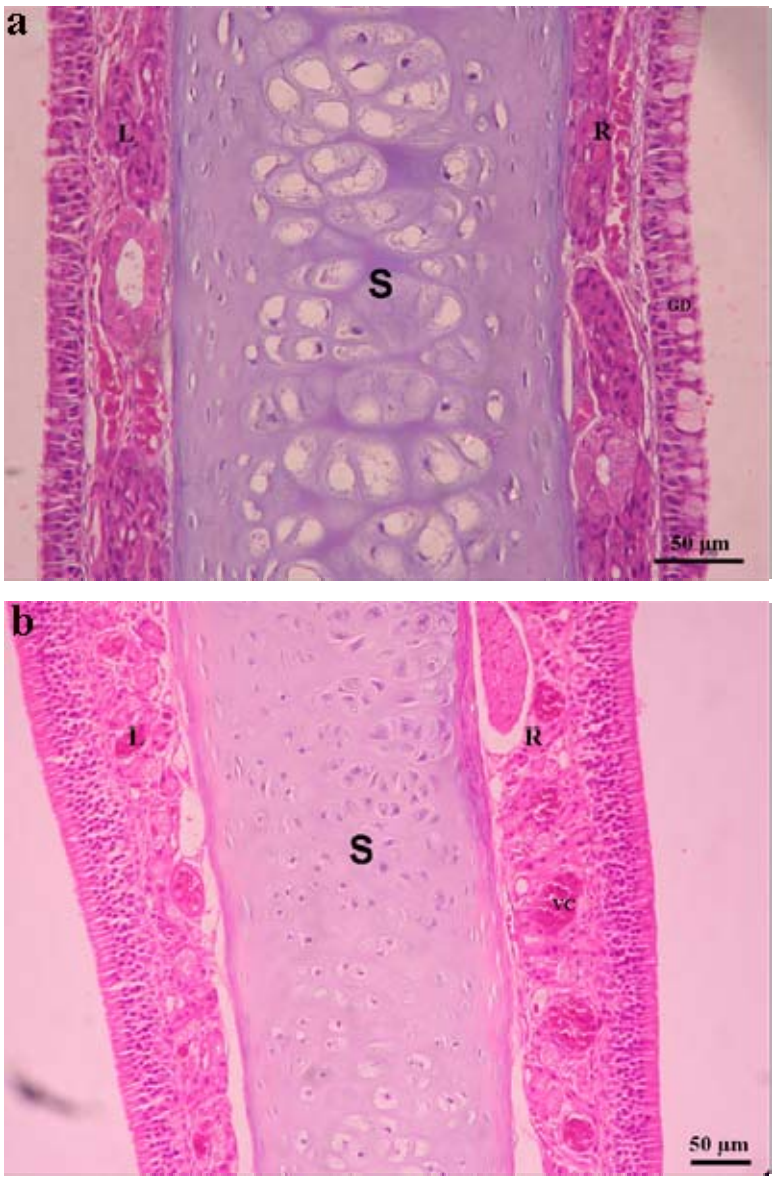

Figure 60. Photomicrographs of a vertical section from (a) region (ii) and (b) region (iii) of the rat nasal cavity after 4 h nasal administration of Ins /PEG(5k)$_{680}$-g-TMC400-40 NC (4 IU/kg insulin, Ins:Pol = 1:5). The dosed side (R) of region (ii) goblet cell distension (GD) and that of region (iii) shows vascular congestion (VC). L, undosed side; S, nasal septum. HE staining.

used in nasal drug delivery to improve biocompatibility and transmucosal transport (106, 132, 255, 256). For instance, nasal administration of 1% w/v bile salt enhancer, sodium glucocholate (SGC) exhibited a strong damaging effect to nasal epithelium (75). However, when nasally administering 1% w/v SGC with PEG-600, slight histological changes of the nasal epithelium were observed (255).

13.3 Reversibility of nasal epithelium

Based on the morphological changes of nasal epithelium after 4 h intranasally administration of insulin NC, the insulin NC composed of TMC400-40 was practically toxic to both respiratory and olfactory epithelia. In order to elucidate a reversibility of damaged nasal epithelium, nasal epithelium after 24 h exposure to 1:5 insulin/TMC400-40 NC was examined.

13.3.1 Respiratory epithelium

Light microscopic examination of the respiratory epithelium of the undosed side revealed ciliated pseudostratified columnar epithelium densely populated with mucus filled goblet cells (Figure 61a). In the dosed side, reparations of epithelium were observed (Figure 61b). The dosed septum was lined by non-ciliated cuboidal epithelium or often termed transitional epithelium with randomly arranged cells. The extrusion of mucus occurred in some area. However, on particular part of the dosed septum, only the basement membrane and a necrosis of epithelial cells occurred. In addition, it was observed that blood vessels in the lamina propria of the dosed side were much larger than those of the undosed side.

13.3.2 Olfactory epithelium

The normal morphologic characteristics of the olfactory epithelium on the undosed side of the nasal cavity are shown in Figure 62a. The olfactory epithelium after 24 h post exposure to the insulin/TMC400-40 NC is presented in Figure 62b. There was regeneration of the epithelium and some areas of olfactory epithelium underwent metaplasia into respiratory epithelium. When comparing between the undosed and dosed sides of the nasal septum, it was found that on the

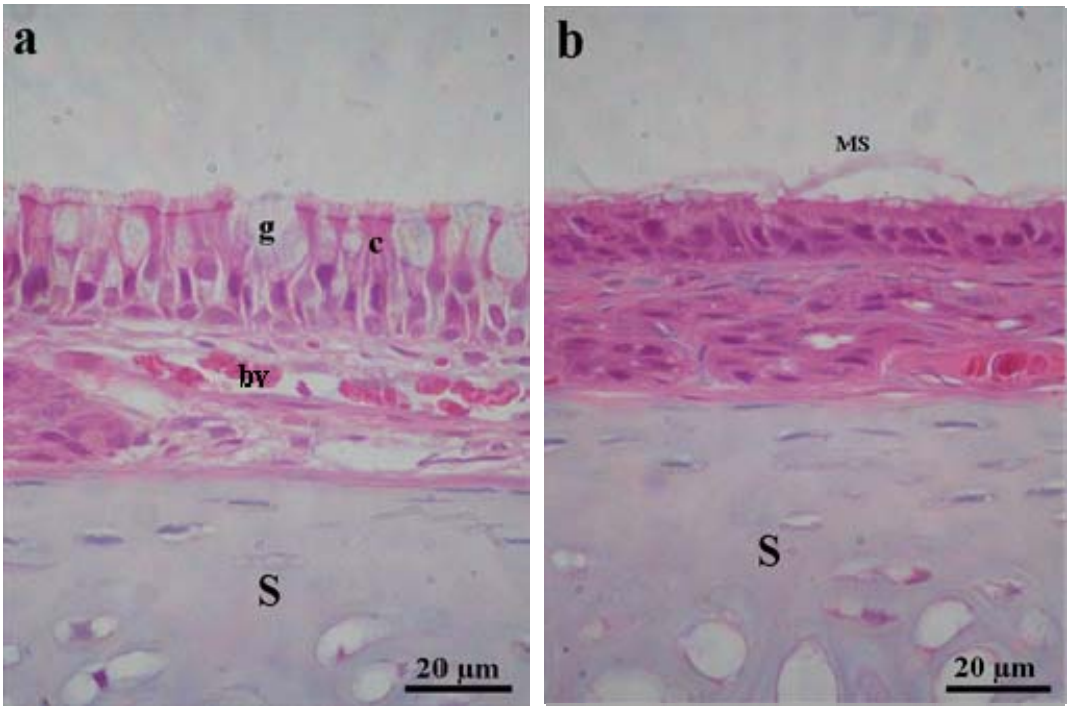

Figure 61. Photomicrographs of respiratory epithelium from region (ii) after 24 h nasal administration of insulin/TMC400-40 NC (4 IU/kg insulin, Ins:Pol = 1:5). (a) undosed side showing normal respiratory epithelium; (b) dosed side showing epithelial regeneration with mucus secretion; bv, blood vessel; c, ciliated cell; g, goblet cell; MS, mucus secretion; S, nasal septum. HE staining.

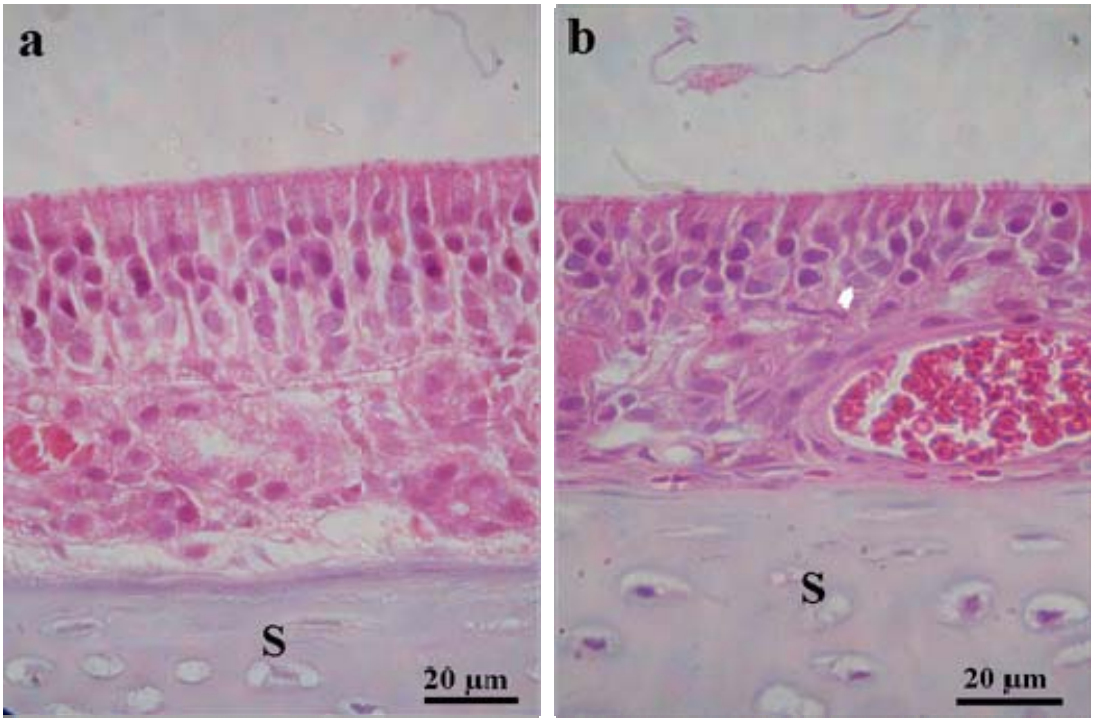

Figure 62. Photomicrographs of olfactory epithelium from region (iii) after 24 h nasal administration of insulin/TMC400-40 NC (4 IU/kg insulin, Ins:Pol = 1:5). (a) undosed side showing normal olfactory epithelium; (b) dosed side showing olfactory epithelium regeneration with respiratory metaplasia (white arrow head); S, nasal septum. HE staining.

dosed epithelial septum, a boundary between epithelium and laminar propria was not clearly identified.

From the results obtained, it implies that polymers did not show a permanent effect on the rat nasal mucosa. After polymers were cleared from the nasal cavity, the nasal mucosa appeared to be reversible and able to return to its normal original state (257). However, it should be born in mind that the 1:5 insulin/TMC400-40 NC was graded as causing severe effect of epithelial disruption, so that the reversibility of the nasal mucosa should not have occurred within such a short time as observed here. Indeed, the capacity of ciliated epithelium to repair itself is remarkably effective. For example, restoration of the denuded basement membrane by hydrogen sulfide can be completed in 10 days (258). On the other hand, the olfactory epithelium has limited capacity for regeneration. After a period of weeks to months, the olfactory epithelium may recover to near normal morphology. When damage is extensive, ulcerated areas are replaced by ciliated and goblet cells, eventually causing reduction or loss of olfactory function. This may be due to the fact the neuron cells are destroyed and the remaining sustentacular cells proliferate and assume columnar respiratory characteristics (135, 258, 259).

13.4 Subacute histopathological effect of nasal insulin formulations

The extent of the morphological changes of the rat nasal epithelium in region (ii) and (iii) after one-week daily exposure to the nasal insulin formulations are summarized in Tables 23 and 24, respectively. The distribution of epithelial lesions of regions (ii) and (iii) after one-week daily exposed to each nasal formulation are summarized in Figures 63 and 64, respectively.

13.4.1 Isotonic 10 mM Tris buffer and insulin solution

In the groups treated with isotonic Tris buffer, all regions of the dosed side of the nasal cavity were covered by an intact, undamaged epithelium layer, comparable to that observed in the undosed side.

Exposure to repeated administration of insulin solution resulted in mild level of irritation to the respiratory epithelium. There was moderate goblet cell distention with a slight increase in mucus discharge on the dosed size compared to the

Table 23. Summary of the effects of insulin NC on morphological changes of the rat nasal epithelium in region (ii) after one-week daily intranasal administration (n = 3)

Treatments	Rat	Mild		Moderate			Severe		
	No.	MS	GD	VC	SE	DE	HP	MP	A
Buffer	1	-	-	-	-	-	-	-	-
	2	-	-	-	-	-	-	-	-
	3	-	-	-	-	-	-	-	-
Ins sol	1	+	++	-	-	-	-	-	-
	2	-	-	-	-	-	-	-	-
	3	+	+++	-	-	-	-	-	-
Ins/TMC400-40 NC (1:0.3)	1	++	+++	+	-	-	+	-	-
	2	+	+++	-	-	-	+	-	-
	3	+	+++	-	-	-	-	-	-
Ins/TMC400-40 NC (1:1)	1	+	+++	-	-	+	++	++	-
	2	-	+++	-	-	-	-	++	-
	3	-	+++	-	-	-	-	+	
Ins/TMC400-40 NC (1:5)	1	++	+++	++	++	++	+++	+++	+++
	2	-	++	++	+++	++	+++	+++	+++
	3	+++	+++	+	++	+	+++	+++	+++
Ins/PEG(5k)$_{298}$-g-TMC400-40 NC (1:5)	1	+	+++	-	-	-	++	+	-
	2	-	++	-	-	+	+++	+	-
	3	-	++	-	-	-	++	+	-
Ins/PEG(5k)$_{680}$-g-TMC400-40 NC (1:5)	1	++	+++	-	-	-	-	-	-
	2	-	+	-	-	-	-	-	-
	3	-	+++	-	-	-	-	-	-

Numbers indicate the extent of occurrence (-, no remarkable lesion; +, slight; ++, moderate; +++, severe). MS, mucus hypersecretion; GD, goblet cell distension; VC, vascular congestion; SE, subepithelial edema; DE, discontinuation of epithelium; HP, hyperplasia; MP, metaplasia; A, atrophy. Dose of insulin was 4 IU/kg.

Table 24. Summary of the effects of insulin NC on morphological changes of the rat nasal epithelium in region (iii) after one-week daily intranasal administration (n = 3)

Treatments	Rat	Mild		Moderate			Severe		
	No.	MS	GD	VC	SE	DE	HP	MP	A
Buffer	1	-	-	-	-	-	-	-	-
	2	-	-	-	-	-	-	-	-
	3	-	-	-	-	-	-	-	-
Ins sol	1	-	-	-	-	-	-	-	-
	2	-	-	-	-	-	-	-	-
	3	-	-	-	-	-	-	-	-
Ins/TMC400-40 NC (1:0.3)	1	+	-	-	+	-	-	-	-
	2	+	-	-	-	-	-	-	-
	3	-	-	-	-	-	-	-	-
Ins/TMC400-40 NC (1:1)	1	+	-	+	+	+	++	++	++
	2	-	-	-	+	-	++	++	+
	3	+	-	-	+	+	+++	++	++
Ins/TMC400-40 NC (1:5)	1	-	-	+	++	+++	+++	+++	+++
	2	-	-	-	+	++	+++	+++	+++
	3	-	-	-	++	++	+++	+++	+++
Ins/PEG(5k)$_{298}$-g-TMC400-40 NC (1:5)	1	+	-	-	++	+	++	++	++
	2	+	-	-	-	+	+	+++	++
	3	-	-	-	-	+	+	++	+
Ins/PEG(5k)$_{680}$-g-TMC400-40 NC (1:5)	1	-	-	+	-	-	-	-	-
	2	-	-	-	-	-	-	-	-
	3	-	-	+	-	-	-	-	-

Numbers indicate the extent of occurrence (-, no remarkable lesion; +, slight; ++, moderate; +++, severe). MS, mucus hypersecretion; GD, goblet cell distension; VC, vascular congestion; SE, subepithelial edema; DE, discontinuation of epithelium; HP, hyperplasia; MP, metaplasia; A, atrophy. Dose of insulin was 4 IU/kg.

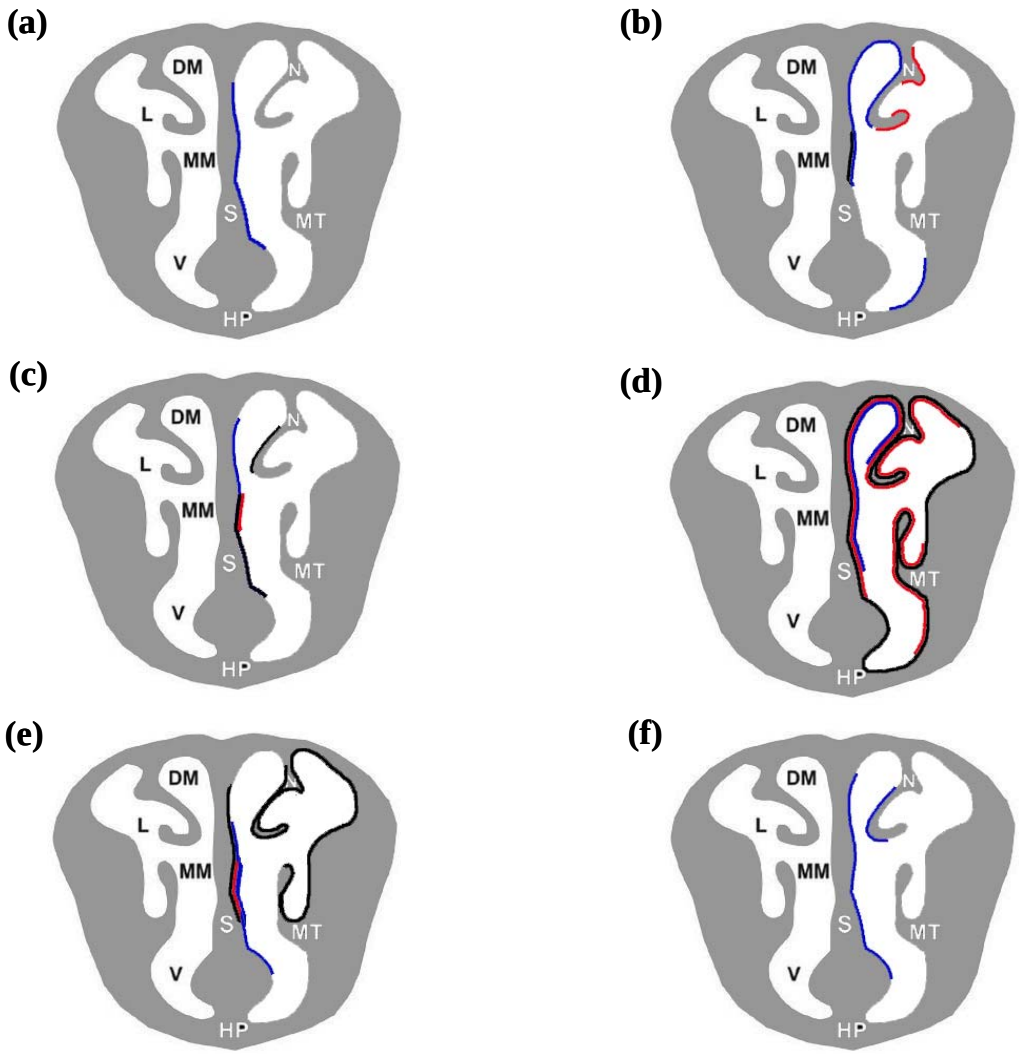

Figure 63. Diagram of location of lesions in region (ii) after one-week daily exposed to (a) insulin solution, (b) Ins/TMC400-40 NC (1:0.3), (c) Ins/TMC400-40 NC (1:1), (d) Ins/TMC400-40 NC (1:5), (e) Ins/PEG(5k)$_{298}$-g-TMC400-40 NC (1:5) and (f) Ins/PEG(5k)$_{680}$-g-TMC400-40 NC (1:5). N, nasoturbinate; MT, maxilloturbinate; HP, hard palate; S, septum; V, ventral meatus; MM, middle meatus; L, lateral meatus; DM, dorsomedial meatus. Dose of insulin was 4 IU/kg.

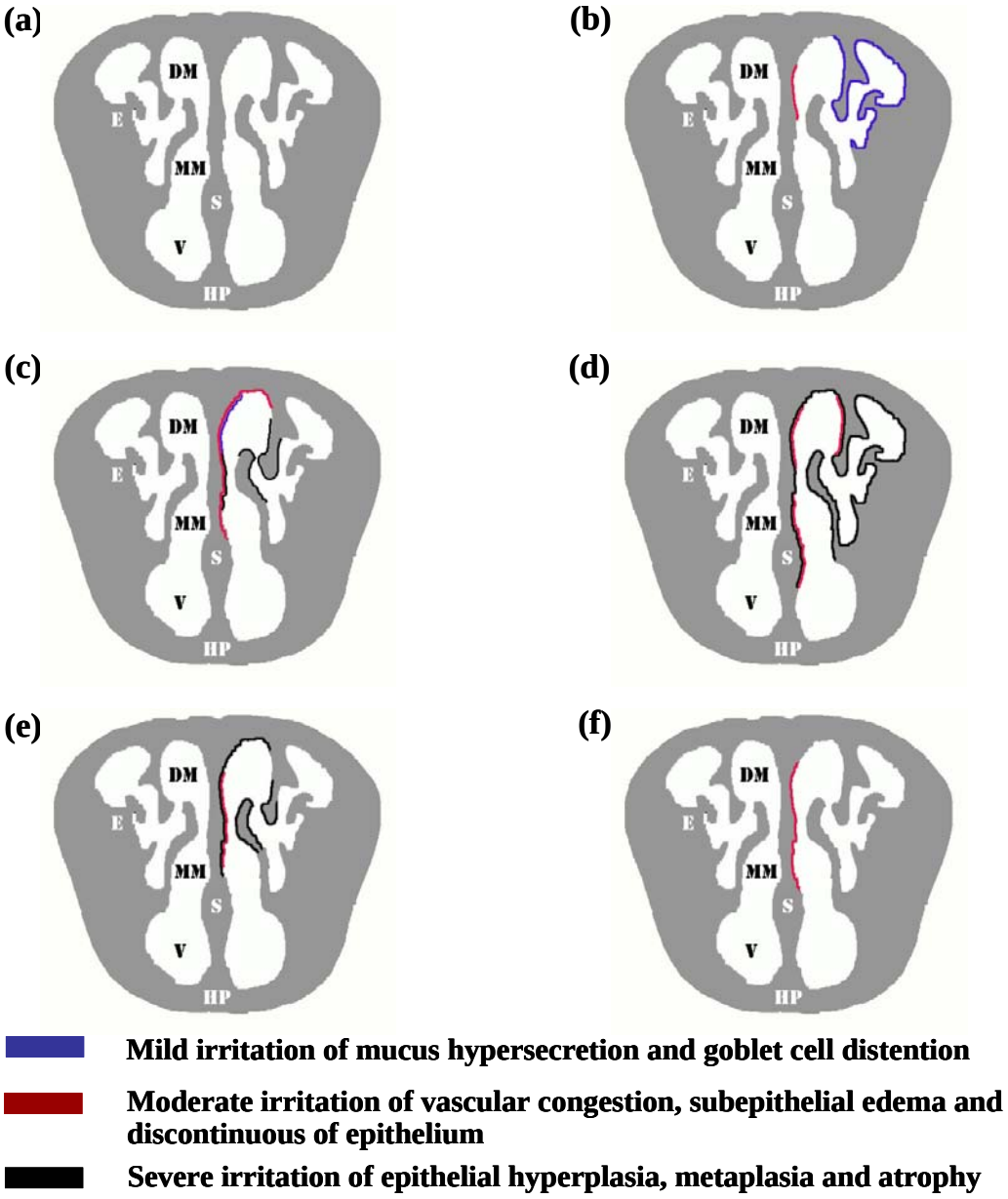

Figure 64. Diagram of location of lesions in region (iii) after one-week daily exposed to (a) insulin solution, (b) Ins/TMC400-40 NC (1:0.3), (c) Ins/TMC400-40 NC (1:1), (d) Ins/TMC400-40 NC (1:5), (e) Ins/PEG(5k)$_{298}$-g-TMC400-40 NC (1:5) and (f) Ins/PEG(5k)$_{680}$-g-TMC400-40 NC (1:5). E, ethmoid turbinates; HP, hard palate; S, septum; V, ventral meatus; MM, middle meatus; L, lateral meatus; DM, dorsomedial meatus. Dose of insulin was 4 IU/kg.

control side, but this was generally restricted to the septal regions only, without flow into the dorsal meatus (Figure 65a). Additional, the irritating effects of insulin solution was not widespread to olfactory epithelium in region (iii).

13.4.2 Insulin/TMC400-40 NC (Ins:Pol = 1:0.3)

In the region (ii), the moderate mucus hypersecretion and extensive goblet cell distension and subsequent extension in epithelial height were observed on the respiratory epithelium lining the medial septum and nasoterbinate. The affected area extended to the olfactory epithelium lining the dorsal meatus. On the particular part of medial septum, globlet cell hyperplasia, characterizing by increased numbers of goblet cell in respiratory epithelium was slightly observed (Figure 65b). The slight lesion of vascular congestion was observed on the nasoturbinate of lateral meatus. In the region (iii), there was slight mucus hypersecretion on the dorsal and lateral meatus. The slight subepithelial edema was seen on the dorsal part of septum.

13.4.3 Insulin/TMC400-40 NC (Ins:Pol = 1:1)

Restricting the nasal septum in region (ii) cross-section, the exposure to repeated administration of 1:1 insulin/TMC400-40 NC resulted in extensive goblet cell distension on the dorsal septum, slight epithelial discontinuation on the medial septum and epithelial hyperplasia on the medial and ventral septa. The epithelial hyperplasia was characterized by a thickening of the epithelium due to an increase in the number of the epithelial cells (Figure 65c). Additional, the olfactory epithelium covering the nasoterbinate in the dorsal meatus was replaced by ciliated (respiratory-like) epithelium indicating respiratory metaplasia. The respiratory metaplasia was also observed on the olfactory epithelium lining the medial part of septum and turbinates in region (iii) as shown in Figure 65d.

13.4.4 Insulin/TMC400-40 NC (Ins:Pol = 1:5)

In the histopathological examination of nasal tissues after one-week exposure to the 1:5 insulin/TMC400-40 NC, the severe lesions including hyperplasia, metaplasia and atrophy, occurred over the nasal cavity both in region (ii) and (iii) cross-sections. The type of lesions depended on the type of epithelium and area in the

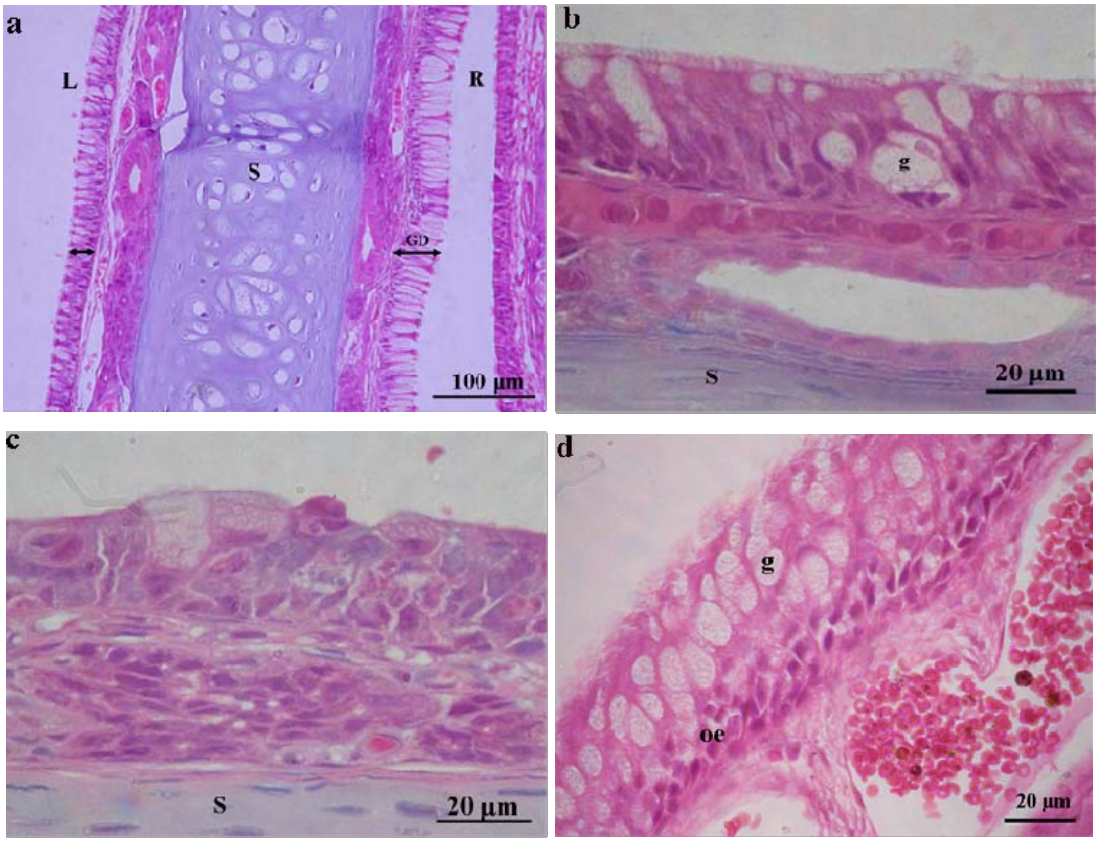

Figure 65. Photomicrographs of rat nasal epithelium after one-week daily nasal administration. (a) respiratory epithelium from region (ii) treated with insulin solution (4 IU/kg) showing moderate goblet cell distension and subsequent extension in epithelium height; (b) respiratory epithelium from region (ii) treated with Ins/TMC400-40 NC (4 IU/kg insulin, Ins:Pol = 1:0.3) showing slight goblet cell hyperplasia; (c) respiratory epithelium from region (ii) treated with Ins/TMC400-40 NC (4 IU/kg insulin, Ins:Pol = 1:1) showing epithelial hyperplasia; (d) olfactory epithelium lining ethmoid turbinate from region (iii) treated with Ins/TMC400-40 NC (4 IU/kg insulin, Ins:Pol = 1:1) showing respiratory metaplasia with goblet cell hyperplasia; g, goblet cell; GD, goblet cell distension; L, undosed side; R, dosed side; oe, olfactory epithelium; S, nasal septum. HE staining.

nasal cavity. The morphological changes of the respiratory and olfactory epithelia are presented in Figures 66 and 67, respectively.

Restricting the nasal septum in region (ii) cross-section, the incidences of cilia loss, goblet cell distension with slight mucus extrusion (Figure 66a), goblet cell hyperplasia (Figure 66b) and subsequent extension in epithelium height were observed on the medial part of the septum. There were epithelial hyperplasia with epithelial disarrangement and cysts on the ventral part of the septum (Figures 66c and 65d). The epithelial hyperplasia was also found in the lateral and ventral meatus as well as on lateral wall in the medial meatus. The cystic formation was identified by a clear space on the epithelium (Figure 66c). The olfactory epithelium covering the dorsal part of the septum was replaced by ciliated (respiratory-like) epithelium and subepithelial glands resulting in unclear boundary between epithelium and laminar propria. On the dorsal meatus of the cavity, the mucus extrusion and atrophy of olfactory epithelium occurred. Atrophy of olfactory epithelium was characterized by decreased epithelial thickness and decreased in numbers of olfactory sensory cells. The vascular congestion and subepithelial edema were seen on the nasoturbinate and maxilloturbinate. Moreover, the incidence of Pyknotic nuclei was found throughout the entire area of nasal cavity.

In the region (iii) of the nasal cavity, the microscopic changes of olfactory epithelium after repeated exposure to the 1:5 insulin/TMC400-40 NC were composed of cysts, respiratory metaplasia, hyperplasia and atrophy of epithelium (Figures. 67a – 67d) . The incidence of epithelial hyperplasia resulted in an undulating rugose surface (Figure 67c). Furthermore, it was found that lesions in olfactory epithelium were extended to the underlying lamina propria which the atrophy of nerve bundles and/or Bowman's glands and subepithelial gland hyperplasia can be observed. The increased subepithelial glands were extended to the epithelial area so that the epithelial boundaries could not be clearly identified (Figure 67d).

13.4.5 Insulin/PEG(5k)$_{298}$-g-TMC400-40 NC (Ins:Pol = 1:5)

The effects of the repeated administered insulin/PEG(5k)$_{298}$-g-TMC400-40 NC to both respiratory and olfactory epithelia are presented in Figure 68 which were similar to those of the repeated administered insulin/TMC400-40 NC.

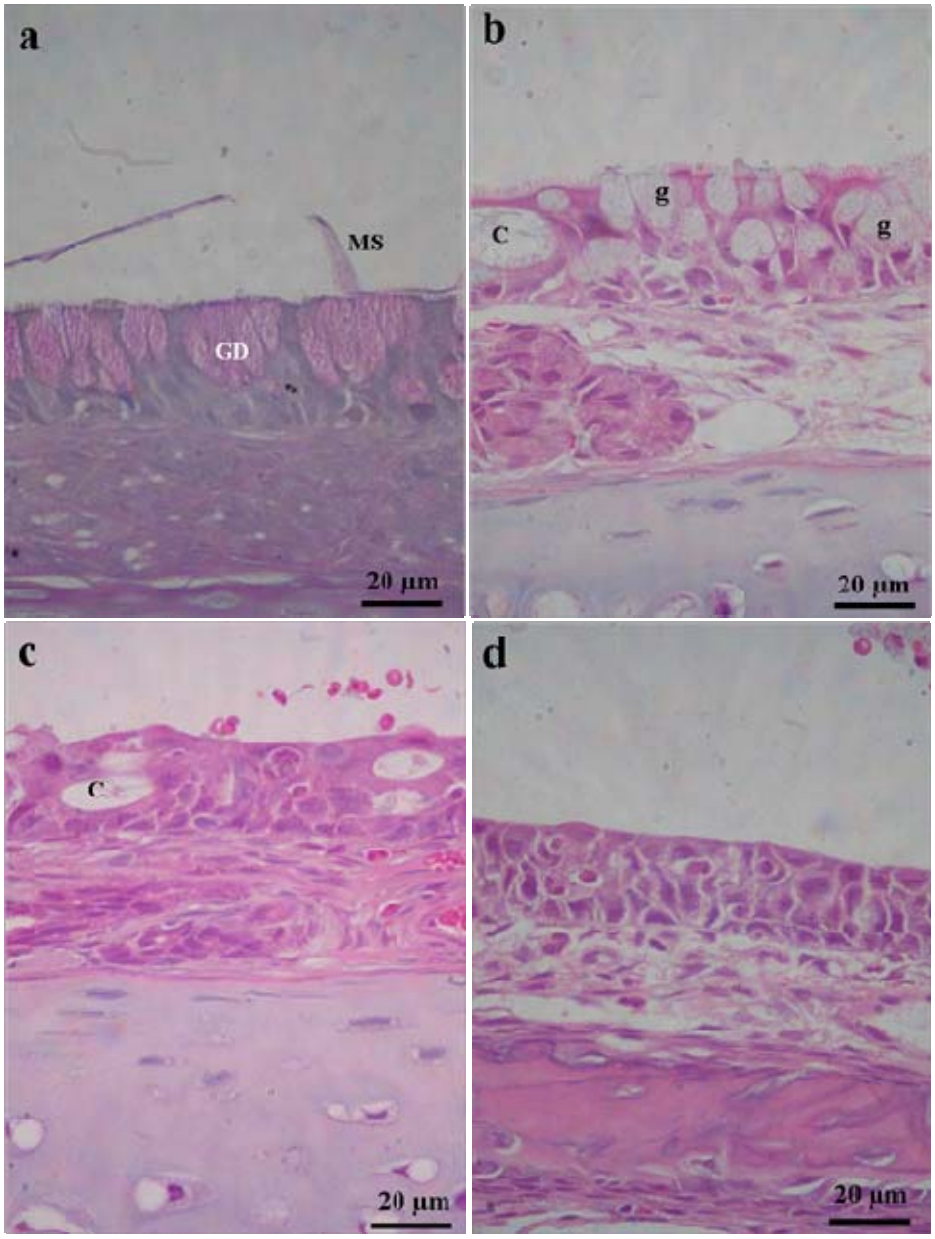

Figure 66. Photomicrographs of respiratory epithelium from region (ii) after one-week daily nasal administration of insulin/TMC400-40 NC (4 IU/kg insulin, Ins:Pol = 1:1) showing (a) goblet cell distension and mucus secretion (PAS staining), (b) goblet cell hyperplasia (HE staining) (c) cystic formation (HE staining) and (d) regeneration with thickening of epithelial layer (HE staining). C, cyst; g, goblet cell; GD, goblet cell distension; MS, mucus hypersecretion.

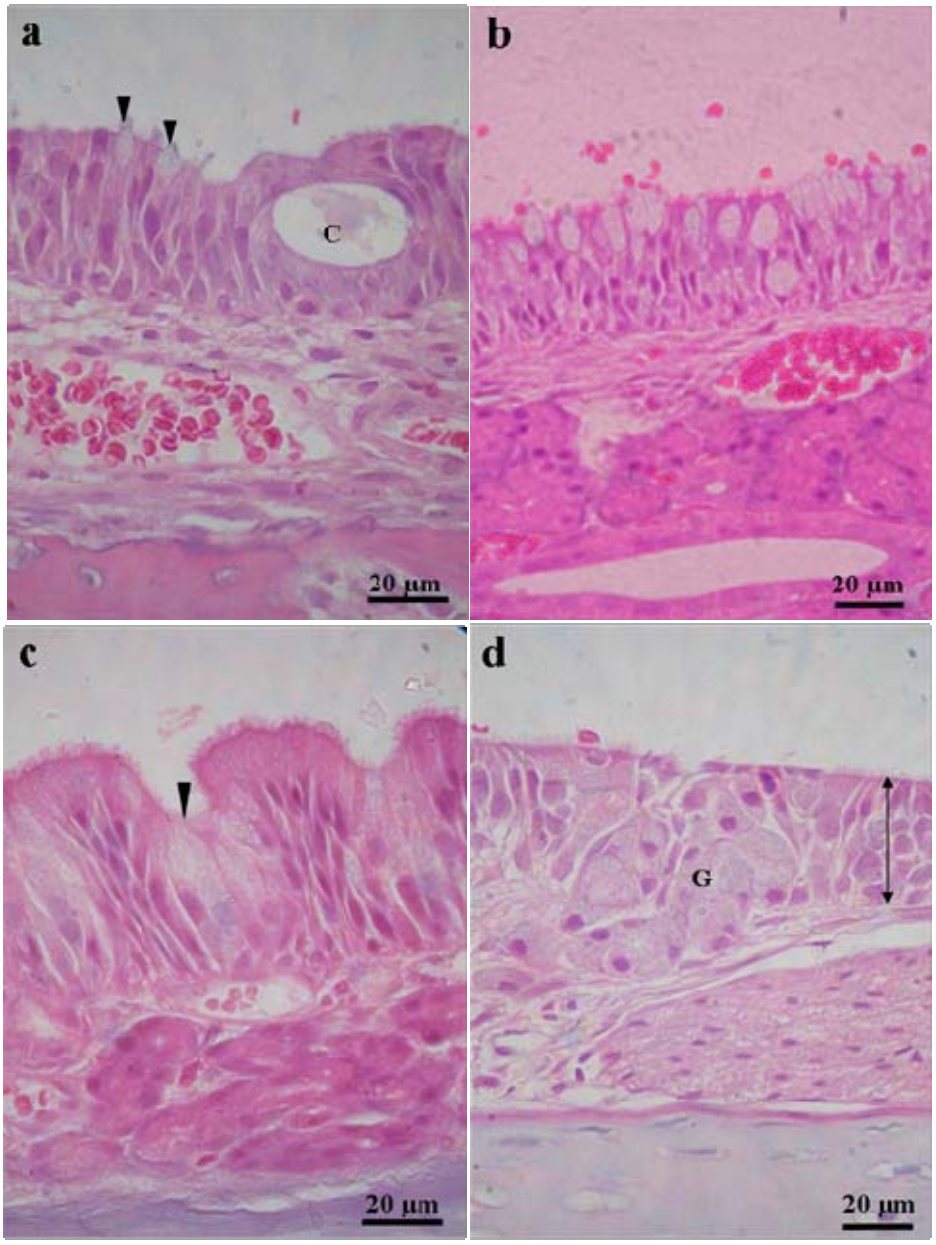

Figure 67. Photomicrographs of olfactory epithelium from region (iii) after one-week daily nasal administration of insulin/TMC400-40 NC (4 IU/kg insulin, Ins:Pol = 1:1) showing (a) cystic formation and respiratory metaplasia (arrow head), (b) respiratory metaplasia, (c) epithelial hyperplasia with respiratory metaplasia (arrow head) and (d) pressure atrophy of olfactory epithelium (double-headed arrows) with subepithelial gland hyperplasia. C, cyst; G, subepithelial gland. HE staining.

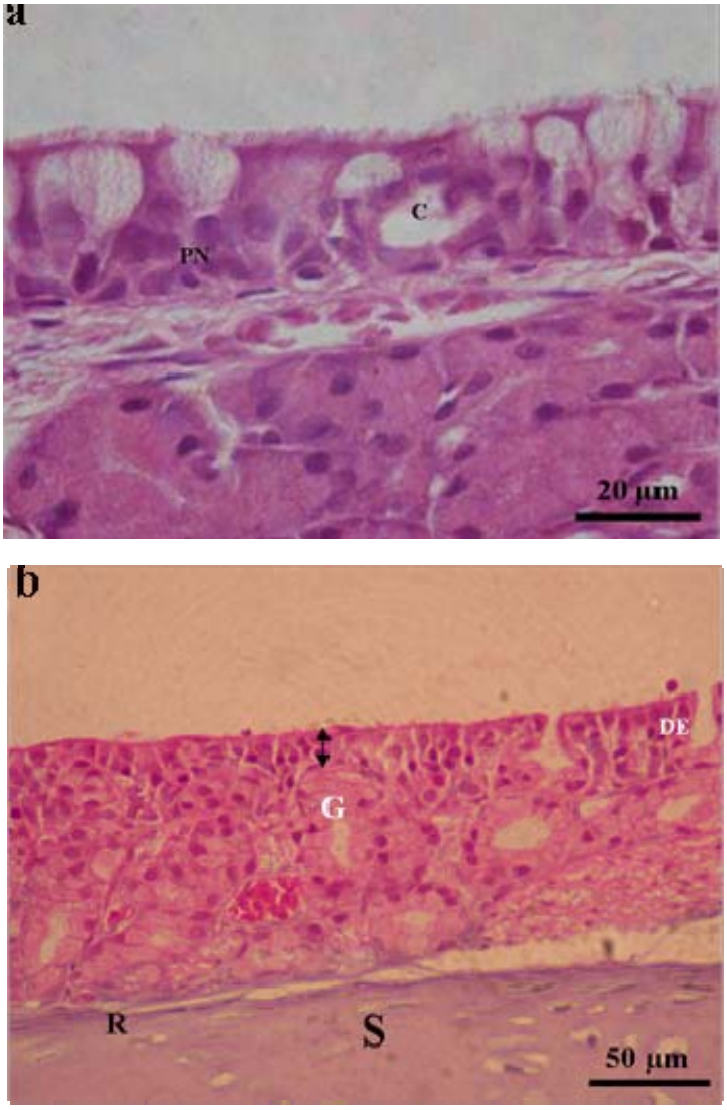

Figure 68. Photomicrographs of a vertical section of dosed side from (a) region (ii) and (b) region (iii) of the rat nasal cavity after one-week daily nasal administration of Ins/PEG(5k)$_{298}$-g-TMC400-40 NC (4 IU/kg insulin, Ins:Pol = 1:5). Figure 68a shows respiratory epithelium with goblet cell hyperplasia and cystic formation. Figure 68b shows olfactory epithelium with pressure atrophy of the olfactory epithelium (double-headed arrows), epithelial discontinuation and subepithelial gland hyperplasia. C, cyst; DE, discontinuation of epithelium; G, subepithelial gland; PN, pyknotic nuclei; R, dosed side; S, nasal septum. HE staining.

However, the severity and distribution of lesions occurred from the insulin/PEG(5k)$_{298}$-g-TMC400-40 NC were less than those occurred from the insulin/TMC400-40 NC. The affected areas by the insulin/PEG(5k)$_{298}$-g-TMC400-40 NC in region (ii) were distributed over the nasal septum, nasoturbinate and lateral meatus while the central lesions in the region (iii) cross-section occurred in the olfactory epithelium lining the nasal septum, turbinates and dorsal meatus.

13.4.6 Insulin/PEG(5k)$_{680}$-g-TMC400-40 NC (Ins:Pol = 1:5)

In region (ii), the intermediate extent of mucus secretion and extensive goblet cell distension were observed on the respiratory epithelium lining the medial septum and nasoterbinate. A few sign of moderate irritation, vascular congestion was found in the dorsal meatus of the region (iii) cross-section.

From the results obtained, the severity of nasal lesions in rats exposed to insulin NC was dependent upon NC structure which exhibited its own characteristic pattern of lesion distribution. It was noted that the responses of nasal epithelium after one-week daily exposure of the insulin/TMC400-40 and insulin/PEG(5k)$_{298}$-g-TMC400-40 NC were similar to those after long-term exposure of inhaled toxicants (79, 135, 203, 260). This could be explained by the usual mechanisms of nasal epithelium to respond toxic insult.

Response to repeated injury of respiratory epithelium typically starts as degeneration, vacuolation, necrosis and/or sloughing of surface epithelium, followed by regeneration. Hyperplastic changes are usually observed as adaptive response to irritants, characterizing by thickening of the epithelium due to an increase in the number of the cell. In goblet cell hyperplasia, mucosal invagination with formation of intraepithelial ‘pseudoglands’ may occur. Another adaptation of the respiratory epithelium is a development of a modified and possibly more resistant epithelial barrier to the irritants in a process known as metaplasia. Adaptive squamous cell metaplasia is a common response to injury in respiratory epithelium. It can occur within areas of epithelial regeneration or hyperplasia and characterizes the replacement of the more susceptible respiratory epithelium by the more resistant squamous epithelium (135, 202, 203, 261).

The olfactory epithelium responds to repeated injury in a similar manner to that of the respiratory epithelium. Squamous metaplasia occurs rarely while respiratory metaplasia occurs largely in the olfactory region and leading to the development of an epithelial type that resembles respiratory epithelium. In addition, destruction of the olfactory receptor cells will result in atrophy of the overlying neural/sustentacular layer and eventual loss of axon bundles in the adjacent lamina propria. Changes in Bowman's glands may include hyperplasia, atrophy (135, 202, 203, 261).

Taking the pharmacodynamic data and histopathological results in the consideration, we conclude that the enhancement of insulin absorption by $PEG(5k)_{680}$-g-TMC400-40 NC was slightly lower than that of unmodified TMC400-40 NC; however, the NC of $PEG(5k)_{680}$-g-TMC400-40 demonstrated only mild irritation of the nasal epithelium which could possibly be advantageous for nasal delivery systems of peptide and protein drugs.

CHAPTER V
CONCLUSION

In this study, the work can be mainly divided into four parts: (i) TMC synthesis and characterization, (ii) development and comparative study of self-assembly insulin NC and insulin NP, (iii) the role of mucoadhesion of insulin NC in insulin uptake and transport and (iv) *in vivo* nasal absorption of insulin NC in rat and morphological integrity of nasal epithelium. The result from this study led to provide the following conclusion.

1. TMC synthesis and characterization

TMC with different DQ and DD were synthesized by reductive methylation of chitosan in a presence of a strong base at elevated temperature. The influence of DQ and DD on physicochemical properties and cytotoxicity of TMC was investigated. It was found that the number of methylation process and duration of reaction were demonstrated to affect the DQ and DD. An increased number of reaction steps increased DQ and decreased DD, while an extended duration of reaction increased both DQ and DD. The results also showed that M_w of TMC was in the range of 266 – 542 kDa and TMC in 2% HAc/0.2 M NaAc behaved as a spherical structure, approximating a random coil. The highest solubility was found in TMC of an intermediate DQ (40%) regardless of DD. The effect of DD on the physicochemical properties and cytotoxicity was obviously observed when proportion of DD to DQ was higher than 1. TMC with relatively high DD showed reduction in both solubility and mucoadhesion and hence decreased cytotoxicity. Nontoxic TMC was observed at DD was ca 3-fold higher than DQ. However, the influence of DD was insignificant when DQ of TMC was higher than 40% at which physicochemical properties and cytotoxicity were mainly dependent upon DQ.

The results from this study represent helpful information on the synthesis of suitable properties of TMC.

2. Development and comparative study of self-assembly insulin NC and insulin NP

In this study, self-assembly insulin NC and insulin NP based on TMC and PEGylated TMC were developed using two techniques; polyelectrolyte complexation and ionotropic gelation with TPP counter ion as carriers for the intranasal administration of insulin. The influence of TPP in formulation on colloidal and insulin stability was also elucidated. The results showed that polymer/insulin (+/–) charge ratio played an important role in NC and NP formation. Stable, uniform, and spherical NC with high insulin association efficiency were formed at or close to optimized polymer/insulin (+/–) charge ratio, depending on polymer structure. The highest AE of NP with narrow size distribution was achieved at specific TPP amount depending on the polymer structure and the polymer/insulin (+/–) charge ratio. Moreover, NP exhibited a bigger particle size and lower zeta potential than NC at the same polymer/insulin mass ratio. All NC were more stable in pH 6.8 physiological fluid than NP. The NC and NP appeared to play some role in protecting insulin from degradation at higher temperature even at 50°C and the protecting effect of the NC was higher than the NP. Although insulin did not degrade by ApM, the NC protected associated insulin from degradation in the presence of trypsin more efficiently than NP. In addition, it was found that all polymers did not affect the activity of ApM and trypsin. The presence of TPP accelerated the degradation of free insulin and insulin loaded NP by trypsin which increased with increasing TPP concentration.

On the basis of these results, polyelectrolyte complexation can be suggested as a potentially useful technique for generating insulin delivery systems for intranasal administration.

3. The role of mucoadhesion of insulin NC in insulin uptake and transport

The mucoadhesive mechanism of TMC and PEGylated TMC as well as behaviors of corresponding insulin NC after adhering to mucus layer were investigated using mucin particle method and mucus-secreting E12 monolayer. All PEGylated TMC400-40 showed significantly higher levels of adhesion to mucus than unmodified TMC. The copolymer composed of 298 PEG chains per TMC

macromolecules (PEG(5k)$_{298}$-g-TMC400-40) exhibited the highest level of mucoadhesion, being 3.4 times higher than TMC400-40. The higher mucoadhesive properties of PEGylated TMC were resulted from the synergistic effects of interpenetration of PEG chains into the mucus and electrostatic interaction between positive charged TMC and anionic glycoproteins present in the mucus layer. On the contrary, the mucoadhesion of TMC was predominantly electrostatic which was dependent upon the DQ and DD of TMC. Compared to unmodified TMC400-40, insulin NC based on copolymers demonstrated no evidence of insulin uptake improvement due to complete release of insulin from NC after adhering to mucus. CLSM revealed the localization of TMC and its corresponding insulin NC at cell surface membranes of E12.

4. *in vivo* nasal absorption of insulin NC in rat and morphological integrity of nasal epithelium

The potential and safety of TMC and PEGylated TMC NC as carriers for improving the systemic absorption of insulin following nasal administration were performed in Wistar male rats. Different insulin NC were administered intranasally to the anesthetized rats. Changes in blood glucose level were monitored over 4 h and pharmacological bioavailability was calculated. Histology of the nasal cavity after 4 h once and one-week daily intranasal administration was examined after HE staining by light microscopy. The results showed that All NC decreased blood glucose level up to in range of 34 – 47% of the basal glucose concentration, at about 98 – 120 min after nasal instillation. The relative bioavailabilities, F_{dyn}, for all insulin NC were in the range of 9.1 – 12.3%, in contrast to 3.9% for insulin solution. It was observed that the hypoglycemic response of the insulin NC consistently correlated with the acute alteration in nasal morphology which increased with increasing polymer ratio and decreased with increasing PEG substitution degree. After 4 h once administration, morphological changes induced by insulin/PEG(5k)$_{680}$-g-TMC400-40 NC were graded as mild irritation and mainly located at the respiratory epithelium. The insulin NC of PEG(5k)$_{298}$-g-TMC400-40 and TMC400-40 induced the severe irritations including necrosis, hemorrhage and/or epithelial disruption both in respiratory and olfactory epithelia. However, the effects of the insulin/TMC400-40 NC were much

more severe and widespread. After daily administration for one week, insulin/PEG(5k)$_{680}$-g-TMC400-40 NC showed only mild irritation of goblet cell distension and mucus hypersecretion. Similar to insulin/PEG(5k)$_{298}$-g-TMC400-40 NC, insulin/TMC400-40 NC induced lesions of epithelial hyperplasia, metaplasia and atrophy in both the respiratory and olfactory epithelia, but the effects were more extensive over the nasal cavity.

From the results obtained, it can be concluded that PEG(5k)$_{680}$-g-TMC400-40 NC is promising potential carrier for nasal delivery of insulin as safe absorption enhancers. In contrast, TMC NC appears to be the most damaging absorption enhancer.

REFERENCES

1. Bliss M. The history of insulin. Diabetes Care 1993;16 Suppl 3:4-7.
2. Lalej-Bennis D, Boillot J, Bardin C, Zirinis P, Coste A, Escudier E, et al. Efficacy and tolerance of intranasal insulin administered during 4 months in severely hyperglycaemic Type 2 diabetic patients with oral drug failure: a cross-over study. Diabet Med 2001;18(8):614-618.
3. UKPDS33. Intensive blood-glucose control with sulfonylureas or insulin compared with conventional treatment and risk of complications in patients with type 2 diabetes. lancet 1998;352:837-853.
4. Pickup JC. An introduction to the problems of insulin delivery. In: Pickup JC, editor. Biotechnology of insulin therapy. Oxford: Blackwell Scientific; 1991. p. 1-23.
5. Schilling RJ, Mitra AK. Degradation of insulin by trypsin and alpha-chymotrypsin. Pharm Res 1991;8(6):721-727.
6. Owens DR, Bolli GB, Zinman B. Future options for insulin therapy. Current Science 2002;83(12):1548-1555.
7. Owens DR, Zinman B, Bolli G. Alternative routes of insulin delivery. Diabet Med 2003;20(11):886-898.
8. Cefalu WT. Concept, strategies, and feasibility of noninvasive insulin delivery. Diabetes Care 2004;27(1):239-246.
9. Romeo VD, deMeireles J, Sileno AP, Pimplaskar HK, Behl CR. Effects of physicochemical properties and other factors on systemic nasal drug delivery. Adv Drug Deliv Rev 1998;29(1-2):89-116.
10. Hinchcliffe M, Illum L. Intranasal insulin delivery and therapy. Adv Drug Deliv Rev 1999;35(2-3):199-234.
11. McMartin C, Hutchinson LE, Hyde R, Peters GE. Analysis of structural requirements for the absorption of drugs and macromolecules from the nasal cavity. J Pharm Sci 1987;76(7):535-540.

12. Romeo VD, deMeireles JC, Gries WJ, Xia WJ, Sileno AP, Pimplaskar HK, et al. Optimization of systemic nasal drug delivery with pharmaceutical excipients. Adv Drug Deliv Rev 1998;29(1-2):117-133.
13. Vila A, Sanchez A, Janes K, Behrens I, Kissel T, Vila Jato JL, et al. Low molecular weight chitosan nanoparticles as new carriers for nasal vaccine delivery in mice. Eur J Pharm Biopharm 2004;57(1):123-131.
14. Prego C, Garcia M, Torres D, Alonso MJ. Transmucosal macromolecular drug delivery. J Control Release 2005;101(1-3):151-162.
15. Fernandez-Urrusuno R, Calvo P, Remunan-Lopez C, Vila-Jato JL, Alonso MJ. Enhancement of nasal absorption of insulin using chitosan nanoparticles. Pharm Res 1999;16(10):1576-1581.
16. Dyer AM, Hinchcliffe M, Watts P, Castile J, Jabbal-Gill I, Nankervis R, et al. Nasal delivery of insulin using novel chitosan based formulations: a comparative study in two animal models between simple chitosan formulations and chitosan nanoparticles. Pharm Res 2002;19(7):998-1008.
17. Amidi M, Romeijn SG, Borchard G, Junginger HE, Hennink WE, Jiskoot W. Preparation and characterization of protein-loaded N-trimethyl chitosan nanoparticles as nasal delivery system. J Control Release 2006;111(1-2):107-116.
18. Cui F, Qian F, Yin C. Preparation and characterization of mucoadhesive polymer-coated nanoparticles. Int J Pharm 2006;316(1-2):154-161.
19. Sieval AB, Thanou M, Kotze AF, Verhoef JC, Brussee J, Junginger HE. Preparation and NMR characterization of highly substituted N-trimethyl chitosan chloride. Carbohydr Polym 1998;36:157-165.
20. Baumann H, Faust V. Concepts for improved regiodelective placement of O-sulfo, N-sulfo, N-acetyl, and N-carboxymethyl groups in chitosan derivatives. Carbohydr Res 2001;331:43-57.
21. Bernkop-Schnurch A, Hornof M, Guggi D. Thiolated chitosans. Eur J Pharm Biopharm 2004;57(1):9-17.

22. Bernkop-Schnurch A, Guggi D, Pinter Y. Thiolated chitosans: development and in vitro evaluation of a mucoadhesive, permeation enhancing oral drug delivery system. J Control Release 2004;94(1):177-186.
23. saito H, Wu X, Harris J, Hoffman A. Graft copolymers of poly(ethylene glycol)(PEG) and chitosan. Macromol Raoid Commun 1997;18:547-550.
24. Muzzarelli RAA, Tanfani F. The N-permethylation of chitosan and the preparation of N-trimethyl chitosan iodide. Carbohydr Polym 1985;5(4):297-307.
25. Domard A, Rinaudo M, Terrassin C. New method for the quaternization of chitosan. Int J Bio Macromol 1986;8(2):105-107.
26. Kotze AF, Luessen HL, de Leeuw BJ, de Boer BG, Verhoef JC, Junginger HE. N-trimethyl chitosan chloride as a potential absorption enhancer across mucosal surfaces: in vitro evaluation in intestinal epithelial cells (Caco-2). Pharm Res 1997;14(9):1197-1202.
27. Kotze AF, Thanou MM, Luebetaen HL, de Boer AG, Verhoef JC, Junginger HE. Enhancement of paracellular drug transport with highly quaternized N-trimethyl chitosan chloride in neutral environments: in vitro evaluation in intestinal epithelial cells (Caco-2). J Pharm Sci 1999;88(2):253-257.
28. Thanou MM, Kotze AF, Scharringhausen T, Luessen HL, de Boer AG, Verhoef JC, et al. Effect of degree of quaternization of N-trimethyl chitosan chloride for enhanced transport of hydrophilic compounds across intestinal caco-2 cell monolayers. J Control Release 2000;64(1-3):15-25.
29. Hamman JH, Schultz CM, Kotze AF. N-trimethyl chitosan chloride: optimum degree of quaternization for drug absorption enhancement across epithelial cells. Drug Dev Ind Pharm 2003;29(2):161-172.
30. Thanou M, Verhoef JC, Marbach P, Junginger HE. Intestinal absorption of octreotide: N-trimethyl chitosan chloride (TMC) ameliorates the permeability and absorption properties of the somatostatin analogue in vitro and in vivo. J Pharm Sci 2000;89(7):951-957.
31. Thanou M, Florea BI, Langemeyer MW, Verhoef JC, Junginger HE. N-trimethylated chitosan chloride (TMC) improves the intestinal

permeation of the peptide drug buserelin in vitro (Caco-2 cells) and in vivo (rats). Pharm Res 2000;17(1):27-31.

32. Thanou M, Verhoef JC, Verheijden JH, Junginger HE. Intestinal absorption of octreotide using trimethyl chitosan chloride: studies in pigs. Pharm Res 2001;18(6):823-828.
33. van der Merwe SM, Verhoef JC, Verheijden JH, Kotze AF, Junginger HE. Trimethylated chitosan as polymeric absorption enhancer for improved peroral delivery of peptide drugs. Eur J Pharm Biopharm 2004;58(2):225-235.
34. Di Colo G, Burgalassi S, Zambito Y, Monti D, Chetoni P. Effects of different N-trimethyl chitosans on in vitro/in vivo ofloxacin transcorneal permeation. J Pharm Sci 2004;93(11):2851-2862.
35. Baudner BC, Verhoef JC, Giuliani MM, Peppoloni S, Rappuoli R, Del Giudice G, et al. Protective immune responses to meningococcal C conjugate vaccine after intranasal immunization of mice with the LTK63 mutant plus chitosan or trimethyl chitosan chloride as novel delivery platform. J Drug Target 2005;13(8-9):489-498.
36. Amidi M, Romeijn SG, Verhoef JC, Junginger HE, Bungener L, Huckriede A, et al. N-Trimethyl chitosan (TMC) nanoparticles loaded with influenza subunit antigen for intranasal vaccination: Biological properties and immunogenicity in a mouse model. Vaccine 2007;25(1):144-153.
37. Sandri G, Rossi S, Bonferoni MC, Ferrari F, Zambito Y, Di Colo G, et al. Buccal penetration enhancement properties of N-trimethyl chitosan: Influence of quaternization degree on absorption of a high molecular weight molecule. Int J Pharm 2005;297(1-2):146-155.
38. Sandri G, Poggi P, Bonferoni MC, Rossi S, Ferrari F, Caramella C. Histological evaluation of buccal penetration enhancement properties of chitosan and trimethyl chitosan. J Pharm Pharmacol 2006;58(10):1327-1336.
39. Florea BI, Thanou M, Junginger HE, Borchard G. Enhancement of bronchial octreotide absorption by chitosan and N-trimethyl chitosan shows linear in vitro/in vivo correlation. J Control Release 2006;110(2):353-361.

40. Li HY, Birchall J. Chitosan-modified dry powder formulations for pulmonary gene delivery. Pharm Res 2006;23(5):941-950.
41. He W, Du Y, Dai W, Wu Y, Zhang M. Effect of N-trimethyl chitosan chloride as an absorption enhancer on properties of insulin liquid suppository in vitro and in vivo. J Appl Polym Sci 2006;99(3):1140-1146.
42. Snyman D, Hamman JH, Kotze AF. Evaluation of the mucoadhesive properties of N-trimethyl chitosan chloride. Drug Dev Ind Pharm 2003;29(1):61-69.
43. Snyman D, Kotze AF, Walls TH, Govender T, Lachmann G. Conformational characterization of quaternized chitosan polymers. In: Proc Intern Symp Control Rel Bioact Mater; 2004; 2004. p. 211.
44. Thanou MM, Verhoef JC, Romeijn SG, Nagelkerke JF, Merkus FW, Junginger HE. Effects of N-trimethyl chitosan chloride, a novel absorption enhancer, on caco-2 intestinal epithelia and the ciliary beat frequency of chicken embryo trachea. Int J Pharm 1999;185(1):73-82.
45. Mao S, Shuai X, Unger F, Wittmar M, Xie X, Kissel T. Synthesis, characterization and cytotoxicity of poly(ethylene glycol)-graft-trimethyl chitosan block copolymers. Biomaterials 2005;26(32):6343-6356.
46. Kean T, Roth S, Thanou M. Trimethylated chitosans as non-viral gene delivery vectors: cytotoxicity and transfection efficiency. J Control Release 2005;103(3):643-653.
47. Mao S, Bakowsky U, Jintapattanakit A, Kissel T. Self-assembled polyelectrolyte nanocomplexes between chitosan derivatives and insulin. J Pharm Sci 2006;95(5):1035-1048.
48. Germershaus O, Mao S, Sitterberg J, Bakowsky U, Kissel T. Gene delivery using chitosan, trimethyl chitosan or polyethylenglycol-graft-trimethyl chitosan block copolymers: establishment of structure-activity relationships in vitro. J Control Release 2008;125(2):145-154.
49. Kim BY, Jeong JH, Park K, Kim JD. Bioadhesive interaction and hypoglycemic effect of insulin-loaded lectin-microparticle conjugates in oral insulin delivery system. J Control Release 2005;102(3):525-538.

50. Venter JP, Kotze AF, Auzely-Velty R, Rinaudo M. Synthesis and evaluation of the mucoadhesivity of a CD-chitosan derivative. Int J Pharm 2006;313(1-2):36-42.
51. He P, Davis SS, Illum L. In vitro evaluation of the mucoadhesive properties of chitosan microspheres. Int J Pharm 1998;166:75-68.
52. Hagerstrom H, Edsman K. Limitations of the rheological mucoadhesion method: the effect of the choice of conditions and the rheological synergism parameter. Eur J Pharm Sci 2003;18(5):349-357.
53. Takeuchi H, Thongborisute J, Matsui Y, Sugihara H, Yamamoto H, Kawashima Y. Novel mucoadhesion tests for polymers and polymer-coated particles to design optimal mucoadhesive drug delivery systems. Adv Drug Deliv Rev 2005;57(11):1583-1594.
54. Keely S, Rullay A, Wilson C, Carmichael A, Carrington S, Corfield A, et al. In vitro and ex vivo intestinal tissue models to measure mucoadhesion of poly (methacrylate) and N-trimethylated chitosan polymers. Pharm Res 2005;22(1):38-49.
55. Chae SY, Jang MK, Nah JW. Influence of molecular weight on oral absorption of water soluble chitosans. J Control Release 2005;102(2):383-394.
56. Damage C, Vonderscher J, Marbach P, Pinget M. Poly(alkylcyanoacrylate) nanocapsules as a delivery system in the rat for octreotide, a long-acting somatostatin analogue. J Pharm Pharmaco 1997;49:949-954.
57. Sakuma S, Ishida Y, Sudo R, Suzuki N, Kikuchi H, Hiwatari K-i, et al. Stabilization of salmon calcitonin by polystyrene nanoparticles having surface hydrophilic polymeric chains, against enzymatic degradation. Int J Pharm 1997;159:181-189.
58. Pan Y, Zheng JM, Zhao HY, Li YJ, Xu H, Wei G. Relationship between drug effects and particle size of insulin-loaded bioadhesive microspheres. Acta Pharmacol Sin 2002;23(11):1051-1056.
59. Pan Y, Li YJ, Zhao HY, Zheng JM, Xu H, Wei G, et al. Bioadhesive polysaccharide in protein delivery system: chitosan nanoparticles improve the intestinal absorption of insulin in vivo. Int J Pharm 2002;249(1-2):139-147.

60. Grenha A, Seijo B, Remunan-Lopez C. Microencapsulated chitosan nanoparticles for lung protein delivery. Eur J Pharm Sci 2005;25(4-5):427-437.
61. Boonsongrit Y, Mitrevej A, Mueller BW. Chitosan drug binding by ionic interaction. Eur J Pharm Biopharm 2006;62(3):267-274.
62. Xia J, Dubin PL. Protein-polyelectrolyte complexes. In: Dubin P, Bock J, Davies RM, Schulz DN, Thies C, editors. Macromolecular complexes in chemistry and biology: Springer-Verlag Berlin Heildelberg; 1994. p. 227-247.
63. MacLaughlin FC, Mumper RJ, Wang J, Tagliaferri JM, Gill I, Hinchcliffe M, et al. Chitosan and depolymerized chitosan oligomers as condensing carriers for in vivo plasmid delivery. J Control Release 1998;56:259-272.
64. Ekelund K, Osth K, Pahlstorp C, Bjork E, Ulvenlund S, Johansson F. Correlation between epithelial toxicity and surfactant structure as derived from the effects of polyethyleneoxide surfactants on caco-2 cell monolayers and pig nasal mucosa. J Pharm Sci 2005;94(4):730-744.
65. Mao S, Germershaus O, Fischer D, Linn T, Schnepf R, Kissel T. Uptake and transport of PEG-graft-trimethyl-chitosan copolymer-insulin nanocomplexes by epithelial cells. Pharm Res 2005;22(12):2058-2068.
66. Grainger CI, Greenwell LL, Lockley DJ, Martin GP, Forbes B. Culture of Calu-3 cells at the air interface provides a representative model of the airway epithelial barrier. Pharm Res 2006;23(7):1482-1490.
67. Grenha A, Grainger CI, Dailey LA, Seijo B, Martin GP, Remunan-Lopez C, et al. Chitosan nanoparticles are compatible with respiratory epithelial cells in vitro. Eur J Pharm Sci 2007;31(2):73-84.
68. Marttin E, Schipper NG, Verhoef JC, Merkus FW. Nasal mucociliary clearance as a factor in nasal drug delivery. Adv Drug Deliv Rev 1998;29(1-2):13-38.
69. Tengamnuay P, Sahamethapat A, Sailasuta A, Mitra AK. Chitosans as nasal absorption enhancers of peptides: comparison between free amine chitosans and soluble salts. Int J Pharm 2000;197(1-2):53-67.

70. Persyn JT, McDonough JA, Nino JA, Dixon H, Boland EJ. Mucosal delivery of cytotoxic therapeutic agents: response of rat nasal mucosa to microencapsulated ethopropazine HCl enantiomer. J Microencapsul 2005;22(7):737-744.
71. Simon M, Wittmar M, Kissel T, Linn T. Insulin containing nanocomplexes formed by self-assembly from biodegradable amine-modified poly(vinyl alcohol)-graft-poly(L-lactide): bioavailability and nasal tolerability in rats. Pharm Res 2005;22(11):1879-1886.
72. Chandler SG, Illum L, Thomas NW. Nasal absorption in the rat. I: A method to demonstrate the histological effects of nasal formulations. Int J Pharm 1991;70:19-27.
73. Gill IJ, Fisher AN, Hinchcliffe M, Whetstone J, Farraj N, De Ponti R, et al. Cyclodextrins as protection agents against enhancer deamage in nasal delivery systems II. Effect on in vivo absorption of insulin and histopathology of nasal membrane. Eur J Pharm Sci 1994;1:237-248.
74. Chandler SG, Thomas NW, Illum L. Nasal absorption in the rat. III. Effect of lysophospholipids on insulin absorption and nasal histology. Pharm Res 1994;11(11):1623-1630.
75. Marttin E, Verhoef JC, Romeijn SG, Zwart P, Merkus FWHM. Acute histopathological effects of benzalkonium chloride and absorption enhancers on rat nasal epithelium in vivo. Int J Pharm 1996;141:151-160.
76. Lomax LG, Krivanek ND, Frame SR. Chronic inhalation toxicity and oncogenicity of methyl methacrylate in rats and hamsters. Food Chem Toxicol 1997;35:393-407.
77. Dhawan S, Singla AK, Sinha VR. Evaluation of mucoadhesive properties of chitosan microspheres prepared by different methods. AAPS PharmSciTech 2004;5(4):e67.
78. Jeong GN, Jo GJ, Jo UB, Yu IJ. Effects of repeated welding fumes exposure on the histological structure and mucins of nasal respiratory mucosa in rats. Toxicol Lett 2006;167(1):19-26.
79. Okuda H, Takeuchi T, Senoh H, Arito H, Nagano K, Yamamoto S, et al. Effects of inhalation exposure to propylene oxide on respiratory tract,

reproduction and development in rats. J Occup Health 2006;48(6):462-473.

80. Williams G, Pickup JC. Handbook of diabetes. 3 ed. London: Blackwell Publishing; 2004.
81. Sadrzadeh N, Glembourtt MJ, Stevenson CL. Peptide drug delivery strategies for the treatment of diabetes. J Pharm Sci 2007;96(8):1925-1954.
82. Cefalu WT. Evaluation of alternative strategies for optimizing glycemia: progress to date. Am J Med 2002;113 Suppl 6A:23S-35S.
83. Hirsch IB. Insulin analogues. N Engl J Med 2005;352(2):174-183.
84. Gomez-Perez FJ, Rull JA. Insulin therapy: current alternatives. Arch Med Res 2005;36(3):258-272.
85. Davis SS. Overcoming barriers to the oral adminstration of peptide drugs. Trends Pharmacol Sci 1990;11:353-355.
86. Kohler D. Aerosols for systemic treatment. Lung 1990;168:677-684 (Suppl.).
87. Hussain AA. Intranasal drug delivery. Adv Drug Deliv Rev 1998;29(1-2):39-49.
88. McMahon GT, Arky RA. Inhaled insulin for diabetes mellitus. N Engl J Med 2007;356(5):497-502.
89. Marschutz MK, Caliceti P, Bernkop-Schnurch A. Design and in vivo evaluation of an oral delivery system for insulin. Pharm Res 2000;17(12):1468-1474.
90. Malkov D, Angelo R, Wang HZ, Flanders E, Tang H, Gomez-Orellana I. Oral delivery of insulin with the eligen technology: mechanistic studies. Curr Drug Deliv 2005;2(2):191-197.
91. Krauland AH, Guggi D, Bernkop-Schnurch A. Oral insulin delivery: the potential of thiolated chitosan-insulin tablets on non-diabetic rats. J Control Release 2004;95(3):547-555.
92. Iwanaga K, Ono S, Narioka K, Morimoto K, Kakemi M, Yamashita S, et al. Oral delivery of insulin by using surface coating liposomes: Improvement of stability of insulin in GI tract. Int J Pharm 1997;157(1):73-80.

93. Qi R, Ping QN. Gastrointestinal absorption enhancement of insulin by administration of enteric microspheres and SNAC to rats. J Microencapsul 2004;21(1):37-45.
94. Ma Z, Lim TM, Lim LY. Pharmacological activity of peroral chitosan-insulin nanoparticles in diabetic rats. Int J Pharm 2005;293(1-2):271-280.
95. Radwan MA, Aboul-Enein HY. The effect of oral absorption enhancers on the in vivo performance of insulin-loaded poly(ethylcyanoacrylate) nanospheres in diabetic rats. J Microencapsul 2002;19(2):225-235.
96. Luo Y, Xu H, Huang K, Gao Z, Peng H, Sheng X. Study on a nanoparticle system for buccal delivery of insulin. Conf Proc IEEE Eng Med Biol Soc 2005;5:4842-4845.
97. Xu HB, Huang KX, Zhu YS, Gao QH, Wu QZ, Tian WQ, et al. Hypoglycaemic effect of a novel insulin buccal formulation on rabbits. Pharmacol Res 2002;46(5):459-467.
98. Hosny EA, Elkheshen SA, Saleh SI. Buccoadhesive tablets for insulin delivery: in-vitro and in-vivo studies. Boll Chim Farm 2002;141(3):210-217.
99. Yang TZ, Wang XT, Yan XY, Zhang Q. Phospholipid deformable vesicles for buccal delivery of insulin. Chem Pharm Bull (Tokyo) 2002;50(6):749-753.
100. Cui CY, Lu WL, Xiao L, Zhang SQ, Huang YB, Li SL, et al. Sublingual delivery of insulin: effects of enhancers on the mucosal lipid fluidity and protein conformation, transport, and in vivo hypoglycemic activity. Biol Pharm Bull 2005;28(12):2279-2288.
101. al-Waili NS. Sublingual human insulin for hyperglycaemia in type I diabetes. J Pak Med Assoc 1999;49(7):167-169.
102. Yu S, Zhao Y, Wu F, Zhang X, Lu W, Zhang H, et al. Nasal insulin delivery in the chitosan solution: in vitro and in vivo studies. Int J Pharm 2004;281(1-2):11-23.
103. Dondeti P, Zia H, Needhan TE. In vivo evaluation of spray formulations of human insulin for nasal delivery. Int J Pharm 1995;122:91-105.

104. D'Souza R, Mutalik S, Venkatesh M, Vidyasagar S, Udupa N. Nasal insulin gel as an alternate to parenteral insulin: Formulation, preclinical and clinical studies. AAPS PharmSciTech 2005;6(2):E184-E189.
105. Varshosaz J, Sadrai H, Heidari A. Nasal delivery of insulin using bioadhesive chitosan gels. Drug Deliv 2006;13(1):31-38.
106. Zhang X, Zhang H, Wu Z, Wang Z, Niu H, Li C. Nasal absorption enhancement of insulin using PEG-grafted chitosan nanoparticles. Eur J Pharm Biopharm 2008;68(3):526-534.
107. Krauland AH, Leitner VM, Grabovac V, Bernkop-Schnurch A. In vivo evaluation of a nasal insulin delivery system based on thiolated chitosan. J Pharm Sci 2006;95(11):2463-2472.
108. Reger MA, Craft S. Intranasal insulin administration: a method for dissociating central and peripheral effects of insulin. Drugs Today (Barc) 2006;42(11):729-739.
109. Kupila A, Sipila J, Keskinen P, Simell T, Knip M, Pulkki K, et al. Intranasally administered insulin intended for prevention of type 1 diabetes--a safety study in healthy adults. Diabetes Metab Res Rev 2003;19(5):415-420.
110. Matsuyama T, Morita T, Horikiri Y, Yamahara H, Yoshino H. Influence of fillers in powder formulations containing N-acetyl-L-cysteine on nasal peptide absorption. J Control Release 2007;120(1-2):88-94.
111. Hilsted J, Madsbad S, Hvidberg A, Rasmussen MH, Krarup T, Ipsen H, et al. Intranasal insulin therapy: the clinical realities. Diabetologia 1995;38(6):680-684.
112. Laube BL. Treating diabetes with aerosolized insulin. Chest 2001;120(3 Suppl):99S-106S.
113. Amidi M, Krudys KM, Snel CJ, Crommelin DJ, Della Pasqua OE, Hennink WE, et al. Efficacy of pulmonary insulin delivery in diabetic rats: use of a model-based approach in the evaluation of insulin powder formulations. J Control Release 2008;127(3):257-266.
114. Amidi M, Pellikaan HC, de Boer AH, Crommelin DJ, Hennink WE, Jiskoot W. Preparation and physicochemical characterization of supercritically dried

insulin-loaded microparticles for pulmonary delivery. Eur J Pharm Biopharm 2008;68(2):191-200.

115. Kawashima Y, Yamamoto H, Takeuchi H, Fujioka S, Hino T. Pulmonary delivery of insulin with nebulized DL-lactide/glycolide copolymer (PLGA) nanospheres to prolong hypoglycemic effect. J Control Release 1999;62(1-2):279-287.
116. Park EJ, Werner J, Smith NB. Ultrasound mediated transdermal insulin delivery in pigs using a lightweight transducer. Pharm Res 2007;24(7):1396-1401.
117. Martanto W, Davis SP, Holiday NR, Wang J, Gill HS, Prausnitz MR. Transdermal delivery of insulin using microneedles in vivo. Pharm Res 2004;21(6):947-952.
118. Cevc G. Transdermal drug delivery of insulin with ultradeformable carriers. Clin Pharmacokinet 2003;42(5):461-474.
119. Lee YC, Simamora P, Pinsuwan S, Yalkowsky SH. Review on the systemic delivery of insulin via the ocular route. Int J Pharm 2002;233(1-2):1-18.
120. Xuan B, McClellan DA, Moore R, Chiou GCY. Alternative delivery of insulin via eye drops. Diabetes Technology & Therapeutics 2007;7(5):695-698.
121. Kosior A. Investigation of physical and hypoglycaemic properties of rectal suppositories with chosen insulin. Acta Pol Pharm 2002;59(5):353-358.
122. Onuki Y, Morishita M, Takayama K, Tokiwa S, Chiba Y, Isowa K, et al. In vivo effects of highly purified docosahexaenoic acid on rectal insulin absorption. Int J Pharm 2000;198(2):147-156.
123. Degim Z, Degim T, Acarturk F, Erdogan D, Ozogul C, Koksal M. Rectal and vaginal administration of insulin-chitosan formulations: an experimental study in rabbits. J Drug Target 2005;13(10):563-572.
124. Golomb G, Avramoff A, Hoffman A. A new route of drug administration: Intrauterine delivery of insulin and calcitonin. Pharm Res 1993;10(6):828-833.
125. Gizurarson S, Bechgaard E. Study of nasal enzyme activity towards insulin. In vitro. Chem Pharm Bull 1991;39(8):2155-2157.
126. Mayor SH, Illum L. Investigation of the effect of anaesthesia on nasal absorption of insulin in rats. Int J Pharm 1997;149:123-129.

127. Carstens S, Danielsen G, Guldhammer B, Frederiksen O. Transport of insulin across rabbit nasal mucosa in vitro induced by didecanoyl-L-alpha-phosphatidylcholine. Diabetes 1993;42(7):1032-1040.
128. Drejer K, Vaag A, Bech K, Hansen P, Sorensen AR, Mygind N. Intranasal administration of insulin with phopholipid as absorption enhancer: Pharmacokinetics in normal subjects. Diabetic Med 1992;9:335-340.
129. Arnold JJ, Ahsan F, Meezan E, Pillion DJ. Correlation of tetradecylmaltoside induced increases in nasal peptide drug delivery with morphological changes in nasal epithelial cells. J Pharm Sci 2004;93(9):2205-2213.
130. Tengamnuay P, Mitra AK. Bile salt-fatty acid mixed micelles as nasal absorption promoters of peptides. II. In vivo nasal absorption of insulin in rats and effects of mixed micelles on the morphological integrity of the nasal mucosa. Pharm Res 1990;7(4):370-375.
131. Ahsan F, Arnold JJ, Meezan E, Pillion DJ. Mutual inhibition of the insulin absorption-enhancing properties of dodecylmaltoside and dimethyl-beta-cyclodextrin following nasal administration. Pharm Res 2001;18(5):608-614.
132. Wu J, Wei W, Wang LY, Su ZG, Ma GH. A thermosensitive hydrogel based on quaternized chitosan and poly(ethylene glycol) for nasal drug delivery system. Biomaterials 2007;28(13):2220-2232.
133. Krauland AH, Guggi D, Bernkop-Schnurch A. Thiolated chitosan microparticles: A vehicle for nasal peptide drug delivery. Int J Pharm 2006;307:270-277.
134. Varshosaz J, Sadrai H, Alinagari R. Nasal delivery of insulin using chitosan microspheres. J Microencapsul 2004;21(7):761-774.
135. Harkema JR, Carey SA, Wagner JG. The nose revisited: a brief review of the comparative structure, function, and toxicologic pathology of the nasal epithelium. Toxicol Pathol 2006;34(3):252-269.
136. Mygind N, Dahl R. Anatomy, physiology and function of the nasal cavities in health and disease. Adv Drug Deliv Rev 1998;29:3-12.

137. Ugwoke MI, Agu RU, Verbeke N, Kinget R. Nasal mucoadhesive drug delivery: background, applications, trends and future perspectives. Adv Drug Deliv Rev 2005;57(11):1640-1665.
138. www.tau.ac.il/Research-Authority/trends/nose.html (accessed Jul 2008).
139. Illum L. Nanoparticulate systems for nasal delivery of drugs: a real improvement over simple systems? J Pharm Sci 2007;96(3):473-483.
140. http://sxxz.blogspot.com/2005/03/nose-knows-stem-cells.html (accessed Jul 2008).
141. Khanvilkar K, Donovan MD, Flanagan DR. Drug transfer through mucus. Adv Drug Deliv Rev 2001;48(2-3):173-193.
142. Matsuyama T, Morita T, Horikiri Y, Yamahara H, Yoshino H. Enhancement of nasal absorption of large molecular weight compounds by combination of mucolytic agent and nonionic surfactant. J Control Release 2006;110(2):347-352.
143. Matsuyama T, Morita T, Horikiri Y, Yamahara H, Yoshino H. Improved nasal absorption of salmon calcitonin by powdery formulation with N-acetyl-L-cysteine as a mucolytic agent. J Control Release 2006;115(2):183-188.
144. Charlton S, Jones NS, Davis SS, Illum L. Distribution and clearance of bioadhesive formulations from the olfactory region in man: effect of polymer type and nasal delivery device. Eur J Pharm Sci 2007;30(3-4):295-302.
145. Sarkar MA. Drug metabolism in the nasal mucosa. Pharm Res 1992;9(1):1-9.
146. Ohkubo K, Baraniuk JN, Hohman R, Merida M, Hersh LB, Kaliner MA. Aminopeptidase activity in human nasal mucosa. J Allergy Clin Immun 1998;102(5):741-750.
147. Kubisova I, Pospisilova B. Histochemical study of aminopeptidase M, aminopeptidase A, and gamma-glutamyltransferase in the nasal cavity of laboratory rodents andman. Sb Ved Pr Lek Fak Karlovy Univerzity Hradci Kralove 1994;37(1):13-17.
148. Lang SR, Staudenmann W, James P, Manz HJ, Kessler R, Galli B, et al. Proteolysis of human calcitonin in excised bovine nasal mucosa: elucidation of the metabolic pathway by liquid secondary ionization

mass spectrometry (LSIMS) and matrix assisted laser desorption ionization mass spectrometry (MALDI). Pharm Res 1996;13(11):1679-1685.

149. Simon M, Wittmar M, Bakowsky U, Kissel T. Self-assembling nanocomplexes from insulin and water-soluble branched polyesters, poly[(vinyl-3-(diethylamino)- propylcarbamate-co-(vinyl acetate)-co-(vinyl alcohol)]-graft- poly(L-lactic acid): a novel carrier for transmucosal delivery of peptides. Bioconjug Chem 2004;15(4):841-849.
150. Sun W, Mao S, Mei D, Kissel T. Self-assembled polyelectrolyte nanocomplexes between chitosan derivatives and enoxaparin. Eur J Pharm Biopharm 2008;69(2):417-425.
151. Sato T, Mattison KW, Dubin PL, Kamachi M, Morishima Y. Effect of protein aggregation on the binding if lysozyme to pyrene-labeled polyanions. Langmuir 1998;14:5430-5437.
152. Lee KY, Kwon IC, Kim YH, Jo WH, Jeong SY. Preparation of chitosan self-aggregates as a gene delivery system. J Control Release 1998;51(2-3):213-220.
153. Liu W, Sun S, Cao Z, Zhang X, Yao K, Lu WW, et al. An investigation on the physicochemical properties of chitosan/DNA polyelectrolyte complexes. Biomaterials 2005;26(15):2705-2711.
154. Tsuboi A, Izumi T, Hirata M, Xia J, Dubin PL, Kokufuta E. Complexation of proteins with a strong polyanion in an aqueous salt-free system. Langmuir 1996;12:6295-6303.
155. Moustafine RI, Kabanova TV, Kemenova VA, Van den Mooter G. Characteristics of interpolyelectrolyte complexes of Eudragit E100 with Eudragit L100. J Control Release 2005;103(1):191-198.
156. van der Merwe SM, Verhoef JC, Kotze AF, Junginger HE. N-trimethyl chitosan chloride as absorption enhancer in oral peptide drug delivery. Development and characterization of minitablet and granule formulations. Eur J Pharm Biopharm 2004;57(1):85-91.

157. Hamman JH, Kotze AF. Effect of the type of base and number of reaction steps on the degree of quaternization and molecular weight of N-trimethyl chitosan chloride. Drug Dev Ind Pharm 2001;27(5):373-380.
158. Polnok A, Borchard G, Verhoef JC, Sarisuta N, Junginger HE. Influence of methylation process on the degree of quaternization of N-trimethyl chitosan chloride. Eur J Pharm Biopharm 2004;57(1):77-83.
159. Kotze AF, Thanou MM, Luessen HL, de Boer BG, Verhoef JC, Junginger HE. Effect of the degree of quaternization of N-trimethyl chitosan chloride on the permeability of intestinal epithelial cells (Caco-2). Eur J Pharm Biopharm 1999;47(3):269-274.
160. Haas J, Ravi Kumar MN, Borchard G, Bakowsky U, Lehr CM. Preparation and characterization of chitosan and trimethyl-chitosan-modified poly-(epsilon-caprolactone) nanoparticles as DNA carriers. AAPS PharmSciTech 2005;6(1):E22-30.
161. Hamman JH, Stander M, Kotze AF. Effect of the degree of quaternisation of N-trimethyl chitosan chloride on absorption enhancement: in vivo evaluation in rat nasal epithelia. Int J Pharm 2002;232(1-2):235-242.
162. He W, Guo X, Zhang M. Transdermal permeation enhancement of N-trimethyl chitosan for testosterone. Int J Pharm 2008;356(1-2):82-87.
163. Sahlin JJ, Peppas NA. Enhanced hydrogel adhesion by polymer interdiffusion: use of linear poly(ethylene glycol) as an adhesion promoter. J Biomater Sci Polym Ed 1997;8(6):421-436.
164. Serra L, Domenech J, Peppas NA. Design of poly(ethylene glycol)-tethered copolymers as novel mucoadhesive drug delivery systems. Eur J Pharm Biopharm 2006;63(1):11-18.
165. Bernkop-Schnurch A. Mucoadhesive polymers. In: Dumitriu S, editor. Polymeric biomaterial. 2 ed. New York: Marcel Dekker; 2002.
166. Woolfson AD, Malcolm RK, McCarron PA, Jones DS. Bioadhesive drug delivery systems. In: Dumitriu S, editor. Polymeric biomaterials. New York: Marcel Dkker, Inc.; 2002.
167. Smart JD. The basics and underlying mechanisms of mucoadhesion. Adv Drug Deliv Rev 2005;57(11):1556-1568.

168. Rossi S, Ferrari F, Bonferoni MC, Caramella C. Characterization of chitosan hydrochloride--mucin rheological interaction: influence of polymer concentration and polymer:mucin weight ratio. Eur J Pharm Sci 2001;12(4):479-485.
169. Grabovac V, Guggi D, Bernkop-Schnurch A. Comparison of the mucoadhesive properties of various polymers. Adv Drug Deliv Rev 2005;57(11):1713-1723.
170. Kafedjiiski K, Krauland AH, Hoffer MH, Bernkop-Schnurch A. Synthesis and in vitro evaluation of a novel thiolated chitosan. Biomaterials 2005;26(7):819-826.
171. Kockisch S, Rees GD, Young SA, Tsibouklis J, Smart JD. Polymeric microspheres for drug delivery to the oral cavity: an in vitro evaluation of mucoadhesive potential. J Pharm Sci 2003;92(8):1614-1623.
172. Quintanar-Guerrero D, Villalobos-Garcia R, Alvarez-Colin E, Cornejo-Bravo JM. In vitro evaluation of the bioadhesive properties of hydrophobic polybasic gels containing N,N-dimethylaminoethyl methacrylate-co-methyl methacrylate. Biomaterials 2001;22(9):957-961.
173. Buckton G, Cappuccinello MM. Modeling mucoadhesion by use of surface energy terms obtained by the Lewis acid-Lewis base approach: III. An interaction between Teflon and carbopol. Pharm Res 1998;15(3):502-503.
174. Rillosi M, Buckton G. Modelling mucoadhesion by use of surface energy terms obtained from the Lewis acid-Lewis base approach. II. Studies on anionic, cationic, and unionisable polymers. Pharm Res 1995;12(5):669-675.
175. Hassan EE, Gallo JM. A simple rheological method for the in vitro assessment of mucin-polymer bioadhesive bond strength. Pharm Res 1990;7(5):491-495.
176. Rossi S, Bonferoni MC, Lippoli G, Bertoni M, Ferrari F, Caramella C, et al. Influence of mucin type on polymer-mucin rheological interactions. Biomaterials 1995;16(14):1073-1079.

177. Fuongfuchat A, Jamieson AM, Blackwell J, Gerken TA. Rheological studies of the interaction of mucins with alginate and polyacrylate. Carbohydr Res 1996;284(1):85-99.

178. Bernkop-Schnurch A, Krajicek ME. Mucoadhesive polymers as platforms for peroral peptide delivery and absorption: synthesis and evaluation of different chitosan-EDTA conjugates. J Control Release 1998;50(1-3):215-223.

179. Mortazavi SA. An in vitro assessment of mucus / mucoadhesive interactions. Int J Pharm 1995;124:173-182.

180. Madsen F, Eberth K, Smart JD. A rheological examination of the mucoadhesive/mucus interaction: the effect of mucoadhesive type and concentration. J Control Release 1998;50(1-3):167-178.

181. Rossi S, Bonferoni MC, Caramella C, Ironi L, Tentoni S. Model-based interpretation of creep profiles for the assessment of polymer-mucin interaction. Pharm Res 1999;16(9):1456-1463.

182. Leitner VM, Marschutz MK, Bernkop-Schnurch A. Mucoadhesive and cohesive properties of poly(acrylic acid)-cysteine conjugates with regard to their molecular mass. Eur J Pharm Sci 2003;18(1):89-96.

183. Wang J, Tabata Y, Bi D, Morimoto K. Evaluation of gastric mucoadhesive properties of aminated gelatin microspheres. J Control Release 2001;73(2-3):223-231.

184. Rossi S, Ferrari F, Bonferoni MC, Caramella C. Characterization of chitosan hydrochloride-mucin interaction by means of viscosimetric and turbidimetric measurements. Eur J Pharm Sci 2000;10(4):251-257.

185. Harding SE. Mucoadhesive interactions. Biochem Soc Trans 2003;31(Pt 5):1036-1041.

186. Deacon MP, Davis SS, R.J. W, Nordman H, Carlstedt I, Errington N, et al. Are chitosan-mucin interactions specific to different regions of the stomach? Velocity ultracentrifugation offers a clue. Carbohydr Polym 1999;38:235-238.

187. Qaqish RB, Amiji MM. Synthesis of a fluorescent chitosan derivative and its application for the study of chitosan-mucin interactions. Carbohydr Polym 1999;38:99-107.

188. Patel MM, Smart JD, Nevell TG, Ewen RJ, Eaton PJ, Tsibouklis J. Mucin/poly(acrylic acid) interactions: a spectroscopic investigation of mucoadhesion. Biomacromolecules 2003;4(5):1184-1190.

189. Shimoda J, Onishi H, Machida Y. Bioadhesive characteristics of chitosan microspheres to the mucosa of rat small intestine. Drug Dev Ind Pharm 2001;27(6):567-576.

190. Ponchel G, Montisci M-J, Dembri A, Durrer C, Duchene D. Mucoadhesion of colloidal particulate systems in the gastro-intestinal tract. Eur J Pharm Biopharm 1997;44:25-31.

191. Akiyama Y, Nagahara N, Kashihara T, Hirai S, Toguchi H. In vitro and in vivo evaluation of mucoadhesive microspheres prepared for the gastrointestinal tract using polyglycerol esters of fatty acids and a poly(acrylic acid) derivative. Pharm Res 1995;12(3):397-405.

192. Kawashima Y, Yamamoto H, Takeuchi H, Kuno Y. Mucoadhesive DL-lactide/glycolide copolymer nanospheres coated with chitosan to improve oral delivery of elcatonin. Pharm Dev Technol 2000;5(1):77-85.

193. Wang J, Tauchi Y, Deguchi Y, Morimoto K, Tabata Y, Ikada Y. Positively charged gelatin microspheres as gastric mucoadhesive drug delivery system for eradication of H. pylori. Drug Deliv 2000;7(4):237-243.

194. Zhu X, Degraaf J, Winnik FM, Leckband D. pH-dependent mucoadhesion of a poly(N-isopropylacrylamide) copolymer reveals design rules for drug delivery. Langmuir 2004;20(24):10648-10656.

195. Cleary J, Bromberg L, Magner E. Adhesion of polyether-modified poly(acrylic acid) to mucin. Langmuir 2004;20(22):9755-9762.

196. Patel D, Smith JR, Smith AW, Grist N, Barnett P, Smart JD. An atomic force microscopy investigation of bioadhesive polymer adsorption onto human buccal cells. Int J Pharm 2000;200(2):271-277.

197. Behrens I, Pena AI, Alonso MJ, Kissel T. Comparative uptake studies of bioadhesive and non-bioadhesive nanoparticles in human intestinal cell

lines and rats: the effect of mucus on particle adsorption and transport. Pharm Res 2002;19(8):1185-1193.

198. Gabor F, Stangl M, Wirth M. Lectin-mediated bioadhesion: binding characteristics of plant lectins on the enterocyte-like cell lines Caco-2, HT-29 and HCT-8. J Control Release 1998;55(2-3):131-142.
199. Behrens I, Stenberg P, Artursson P, Kissel T. Transport of lipophilic drug molecules in a new mucus-secreting cell culture model based on HT29-MTX cells. Pharm Res 2001;18(8):1138-1145.
200. Weissenboeck A, Bogner E, Wirth M, Gabor F. Binding and uptake of wheat germ agglutinin-grafted PLGA-nanospheres by caco-2 monolayers. Pharm Res 2004;21(10):1917-1923.
201. Dorato MA. Toxicological evaluation of intranasal peptide and protein drugs. In: Hsieh DS, editor. Drug permeation enhancement: theory and applications. New York: Marcel Dekker; 1994. p. 345-380.
202. McInnes E, Miller R. A review of upper respiratory tract inhalation pathology. Comparative Clinical Pathology 2007;16(4):215-222.
203. Renne RA, Gideon KM, Harbo SJ, Staska LM, Grumbein SL. Upper respiratory tract lesions in inhalation toxicology. Toxicol Pathol 2007;35(1):163-169.
204. Anthonsen MW, Varum KM, Smidsrod O. Solution properties of chitosans: conformation and chain stiffness of chitosans with different degrees of N-acetylation. Carbohydr Polym 1993;22:193-201.
205. Qin C, Xiao Q, Li H, Fang M, Liu Y, Chen X, et al. Calorimetric studies of the action of chitosan-N-2-hydroxypropyl trimethyl ammonium chloride on the growth of microorganisms. Int J Biol Macromol 2004;34(1-2):121-126.
206. Fischer D, Li Y, Ahlemeyer B, Krieglstein J, Kissel T. In vitro cytotoxicity testing of polycations: influence of polymer structure on cell viability and hemolysis. Biomaterials 2003;24(7):1121-1131.
207. Calvo P, Remunan-Lopez C, Vila Jato JL, Alonso MJ. Novel hydrophilic chitosan-polyethylene oxide nanoparticles as protein carriers. J Appl Polym Sci 1997;63:125-132.

208. Bernkop-Schnurch A, Pasta M. Intestinal peptide and protein delivery: novel bioadhesive drug-carrier matrix shielding from enzymatic attack. J Pharm Sci 1998;87(4):430-434.

209. Merdan T, Kunath K, Fischer D, Kopecek J, Kissel T. Intracellular processing of poly(ethylene imine)/ribozyme complexes can be observed in living cells by using confocal laser scanning microscopy and inhibitor experiments. Pharm Res 2002;19(2):140-146.

210. Walter E, Kissel T. Heterogeneity in the human intestinal cell line Caco-2 leads to differences in transepithelial transport. Eur J Pharm Sci 1995;3:215-230.

211. Trakranrungsie N, Sutanonpaiboon J, Chouapranom V, Huttayananont S, Jitasombuti P. Thecomparative anesthetic effects of Zoletil and Zoletil plus xylazine and the effect of repeated dosing in golden hamster. In: Proceedings of the 26th Veterinary Annual Conference; 2000 Nov, 15-17; Bangkok, Thailand; 2000. p. 231-244.

212. Crawford K. Rat anaesthesia and dissection. In: http://bioweb.wku.edu/faculty/Crawford/ratlab.htm (accessed Nov 2006).

213. Curti E, de Britto D, Campana-Filho SP. Methylation of chitosan with iodomethane: Effect of reaction conditions on chemoselectivity and degree of substitution. Macromolecular Bioscience 2003;3(10):571-576.

214. Mao S, Augsten C, Mäder K, Kissel T. Characterization of chitosan and its derivatives using asymmetrical flow field-flow-fractionation: A comparison with traditional methods. Journal of Pharmaceutical and Biomedical Analysis 2007;45(5):736-741.

215. Snyman D, Hamman JH, Kotze JS, Rollings JE, Kotze AF. The relationship between the absolute molecular weight and the degree of quaternization of N-trimethyl chitosan chloride. Carbohydr Polym 2002;50:145-150.

216. Errington N, Harding SE, Varum KM, Illum L. Hydrodynamic characterization of chitosans varying in degree of acetylation. Int J Biol Macromol 1993;15(2):113-117.

217. Tsaih ML, Chen RH. Effect of molecular weight and urea on the conformation of chitosan molecules in dilute solutions. Int J Biol Macromol 1997;20(3):233-240.
218. Chen RH, Tsaih ML. Effect of temperature on the intrinsic viscosity and conformation of chitosans in dilute HCl solution. Int J Biol Macromol 1998;23(2):135-141.
219. Tsaih ML, Chen RH. Effects of ionic strength and pH on the diffusion coefficients and conformation of chitosans molecule in solution. J Appl Polym Sci 1999;73(10):2041-2050.
220. Gamzazade AI, Slimak VM, Skljar AM, Stykova EV, Pavlova SSA, Rogozin SV. Investigation of the hydrodynamic properties of chitosan solutions. Acta Polym 1985;36(8):420-424.
221. Jiang X, Chen L, Zhong W. A new linear potentiometric titration method for the determination of deacetylation degree of chitosan. Carbohydr Polym 2003;54(4):457-463.
222. Zhang Y, Xue C, Xue Y, Gao R, Zhang X. Determination of the degree of deacetylation of chitin and chitosan by X-ray powder diffraction. Carbohydr Res 2005;340(11):1914-1917.
223. Balazs N, Sipos P. Limitations of pH-potentiometric titration for the determination of the degree of deacetylation of chitosan. Carbohydr Res 2007;342(1):124-130.
224. Yang T-C, Chou C-C, Li C-F. Preparation, water solubility and rheological property of the N-alkylated mono or disaccharide chitosan derivatives. Food Res Int 2002;35(8):707-713.
225. Holme KR, Perlin AS. Chitosan N-sulfate. A water-soluble polyelectrolyte. Carbohydr Res 1997;302(1-2):7-12.
226. Hejazi R, Amiji M. Chitosan-based gastrointestinal delivery systems. J Control Release 2003;89(2):151-165.
227. Sinko PJ. Martin's physical pharmacy and pharmaceutical sciences 5th ed. New York: Lippincott Williams & Wilkins; 2006.

228. Huang M, Khor E, Lim LY. Uptake and cytotoxicity of chitosan molecules and nanoparticles: effects of molecular weight and degree of deacetylation. Pharm Res 2004;21(2):344-353.
229. Petersen H, Fechner PM, Fischer D, Kissel T. Synthesis, characterization, and biocompatibility of polyethylenimine-graft-poly(ethylene glycol) block copolymers. Macromolecules 2002;35:6867-6874.
230. Glodde M, Sirsi SR, Lutz GJ. Physiochemical properties of low and high molecular weight poly(ethylene glycol)-grafted poly(ethylene imine) copolymers and their complexes with oligonucleotides. Biomacromolecules 2006;7(1):347-356.
231. Fiebrig I, Harding SE, Rowe AJ, Hyman SC, Davis SS. Transmission electron microscopy studies on pig gastric mucin and its interactions with chitosan. Carbohydr Polym 1995;28:239-244.
232. Brange J. Galenics of insulin: The physio-chemical and pharmaceutical aspects of insulin and insulin preparation. Berlin: Springer-Verlag; 1987.
233. Fredheim GE, Christensen BE. Polyelectrolyte Complexes: Interactions between Lignosulfonate and Chitosan. Biomacromolecules 2003;4(2):232-239.
234. Shi HG, Farber L, Michaels JN, Dickey A, Thompson KC, Shelukar SD, et al. Characterization of crystalline drug nanoparticles using atomic force microscopy and complementary techniques. Pharm Res 2003;20(3):479-484.
235. Janes KA, Alonso MJ. Depolymerized chitosan nanoparticles for protein delivery: Preparation and characterization. J Appl Polym Sci 2003;88(12):2769-2776.
236. Ma Z, Yeoh HH, Lim LY. Formulation pH modulates the interaction of insulin with chitosan nanoparticles. J Pharm Sci 2002;91(6):1396-1404.
237. Berger J, Reist M, Mayer JM, Felt O, Gurny R. Structure and interactions in chitosan hydrogels formed by complexation or aggregation for biomedical applications. Eur J Pharm Biopharm 2004;57(1):35-52.
238. Mao HQ, Roy K, Troung-Le VL, Janes KA, Lin KY, Wang Y, et al. Chitosan-DNA nanoparticles as gene carriers: synthesis, characterization and transfection efficiency. J Control Release 2001;70(3):399-421.

239. Brange J, Langkjaer L. Chemical stability of insulin 3. Influences of excipients, formulation, and pH. Acta Pharm Nord 1992;4:149-158.

240. van de Weert M, Hennink WE, Jiskoot W. Protein instability in poly(lactic-co-glycolic acid) microparticles. Pharm Res 2000;17(10):1159-1167.

241. Frokjaer S, Otzen DE. Protein drug stability: a formulation challenge. Nat Rev Drug Discov 2005;4(4):298-306.

242. Akiyoshi K, Kobayashi S, Shichibe S, Mix D, Baudys M, Kim SW, et al. Self-assembled hydrogel nanoparticle of cholesterol-bearing pullulan as a carrier of protein drugs: complexation and stabilization of insulin. J Control Release 1998;54(3):313-320.

243. Tsuchida E, Takeoka S. Interpolymer complexes and their ion-conduction, Macromolecule complexes in chemistry and biology: Springer-Verlag Berlin Heidelberg; 1994.

244. Kotze AF, de Leeuw BJ, Luessen HL, de Boer AG, Verhoef JC, Junginger HE. Chitosans for enhanced delivery of therapeutic peptides across intestinal epithelial: in vitro evaluation in Caco-2 cell monolayers. Int J Pharm 1997;159:243-253.

245. Luessen HL, Rentel C-O, Kotze AF, Lehr CM, de Boer AG, Verhoef JC, et al. Mucoadhesive polymers in peroral peptide drug delivery. IV. Polycarbophil and chitosan are potent enhancers of peptide transport across intestinal mucosae in vitro. J Control Release 1997;45:15-23.

246. Bernkop-Schnurch A, Dundalek K. Novel bioadhesive drug delivery system protecting (poly)peptides from gastric enzymatic degradation. Int J Pharm 1996;138(1):75-83.

247. Yeh MK. The stability of insulin in biodegradable microparticles based on blends of lactide polymers and polyethylene glycol. J Microencapsul 2000;17(6):743-756.

248. Young JD, Carpenter FH. Isolation and Characterization of Products Formed by the Action of Trypsin on Insulin. J. Biol. Chem. 1961;236(3):743-748.

249. Meaney C, O'Driscoll C. Mucus as a barrier to the permeability of hydrophilic and lipophilic compounds in the absence and presence of sodium

taurocholate micellar systems using cell culture models. Eur J Pharm Sci 1999;8(3):167-175.

250. Luo Y, Kirker KR, Prestwich GD. Cross-linked hyaluronic acid hydrogel films: new biomaterials for drug delivery. J Control Release 2000;69(1):169-184.
251. Illum L, Farraj NF, Davis SS. Chitosan as novel nasal delivery system for peptide drugs. Pharm Res 1994;11:1186-1189.
252. Anwana AB, Garland HO. Intracellular dehydration on the rat made diabetic with streptozotocin: effect of infusion. J Endocrinol 1991;128(3):333-337.
253. Bellush LL, Henley WN. Altered responses to enviromental stress in streptozotocin-diabetic rats. Physiology and Behavior 1990;47(2):231-238.
254. Otto K. Anesthesia, analgesia and euthanasia. In: Hedrich HJ, Bullock G, editors. The laboratory mouse. London, UK: Elsevier Academic Press; 2004. p. 555.
255. Donovan MD, Flynn GL, Amidon GL. The molecular weight dependence of nasal absorption: The effect of absorption enhancers. Pharm Res 1990;7:808-815.
256. Vila A, Gill H, McCallion O, Alonso MJ. Transport of PLA-PEG particles across the nasal mucosa: effect of particle size and PEG coating density. J Control Release 2004;98(2):231-244.
257. Tengamnuay P, Sailasuta A, Ritthidej GC. Efficacy and mechanistic studies of chitosan as nasal absorption enhancer of peptide drugs. Bangkok: Chulalongkorn University; 1998.
258. Lopez A. Respiratory system. In: McGavin MD, Zachary JF, editors. Pathologic basic veterinary disease. 4 ed. St. Louis, Missouri: Mosby Elsevier; 2007. p. 463.
259. McInnes FJ, O'Mahony B, Lindsay B, Band J, Wilson CG, Hodges LA, et al. Nasal residence of insulin containing lyophilised nasal insert formulations, using gamma scintigraphy. Eur J Pharm Sci 2007;31(1):25-31.

260. Dorman DC, Miller KL, D'Antonio A, James RA, Morgan KT. Chloroform-induced olfactory mucosal degeneration and osseous ethmoid hyperplasia are not associated with olfactory deficits in Fischer 344 rats. Toxicology 1997;122(1-2):39-50.

261. Braun A, Ernst H, Hoymann HG, Rittinghausen S. Respiratory tract. In: Hedrich HJ, Bullock G, editors. The laboratory mouse. London, UK: Elsevier Academic Press; 2004. p. 225.

262. www.uni-oldenburg.de/tchemie/Ubbelohde.htm (accessed Aug 2008).

263. Mao S, Shuai X, Unger F, Simon M, Bi D, Kissel T. The depolymerization of chitosan: effects on physicochemical and biological properties. Int J Pharm 2004;281(1-2):45-54.

264. Kasaai MR, Arul J, Charlet G. Intrinsic viscosity - molecular weight relationship for chitosan. J Polym Sci Pol Phys 2000;38:2591-2598.

APPENDIX

APPENDIX A
HPLC ASSAY FOR INSULIN

The example of HPLC chromatogram of insulin was shown in Figures 69. It can be noticed that the analysis method could separate the peaks of the drug and the components of the vehicle. The retention times of the insulin were approximate 5.6 min.

Figure 70 present example of standard curve of insulin. It was found that the standard curve gave high linear relationship between drug concentration and peak area ($R^2 > 0.99$). The detector limit of insulin was 1 μg/ml. It was found that the analytical method could detect low amounts of insulin. Therefore, the analytical methods were robust and sensitive enough for use in quantitative assays of insulin in this study.

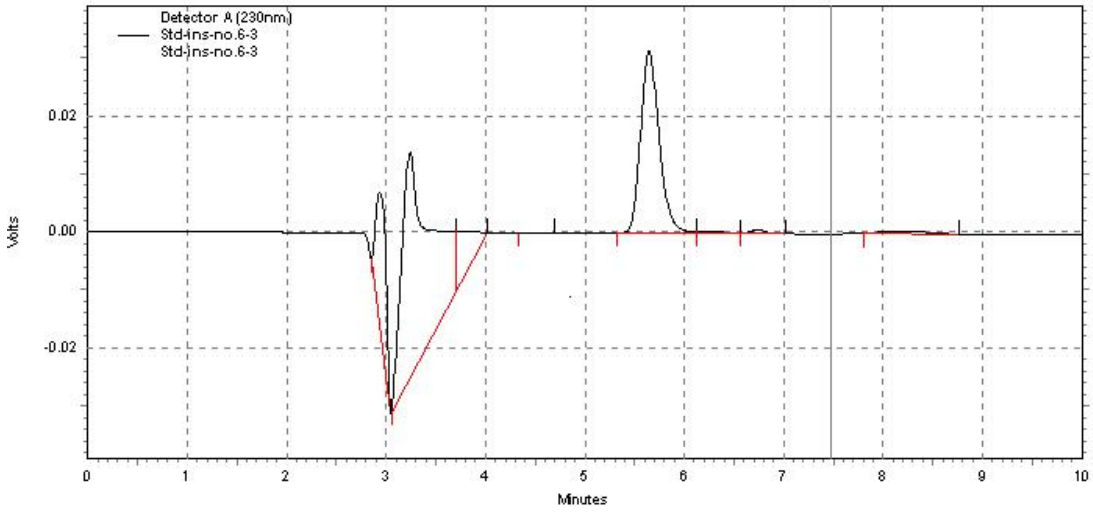

Figure 69. HPLC chromatogram of insulin.

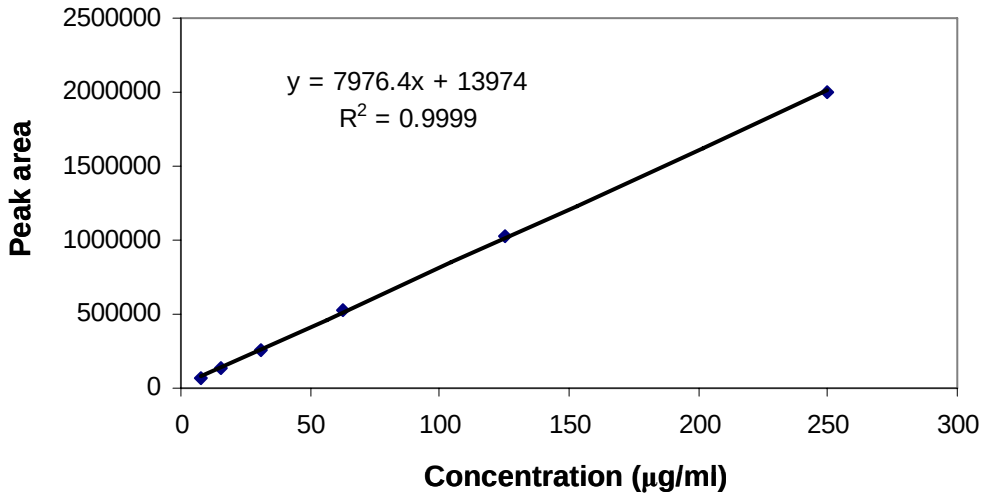

Figure 70. Standard curve of insulin.

APPENDIX B
INTRINSIC VISCOSITY

Intrinsic viscosity [η] is the simplest and cheapest measurement of the most precise measurements in polymer science. It is a measure of the solute's contribution to the viscosity, η of a solution which is measured from the flow time of a solution through a simple glass capillary. It is defined as

$$[\eta] = \lim_{\varphi \to 0} \frac{\eta - \eta_0}{\eta_0 \varphi} \qquad \text{(Eq. 16)}$$

where η_0 is the viscosity in the absence of the solute and φ is the volume fraction of the solute in the solution.

1. Intrinsic viscosity measurement

The most useful kind of viscometer for determining intrinsic viscosity is the "suspended level" or Ubbelohde viscometer as shown in Figure 71. The running times of the solution and solvent were used to calculate the kinematic viscosity. The relationship between kinetic viscosity and dynamic viscosity is

$$\nu = \frac{\eta}{\rho} \qquad \text{(Eq. 17)}$$

where ν is the kinematic viscosity in stokes; η is the dynamic viscosity in poise; and ρ is the density in g/cm^3. Since the concentrations are small and the density of the solution and solvent are close to 1 g/cm^3, therefore, the stoke (centistokes) is equal to poise (centipoise). The solution and solvent viscosity are used to calculate the relative viscosity (η_{rel}), specific viscosity (η_{sp}), reduced viscosity (η_{red}) and inherent viscosity (η_{inh}) as follows.

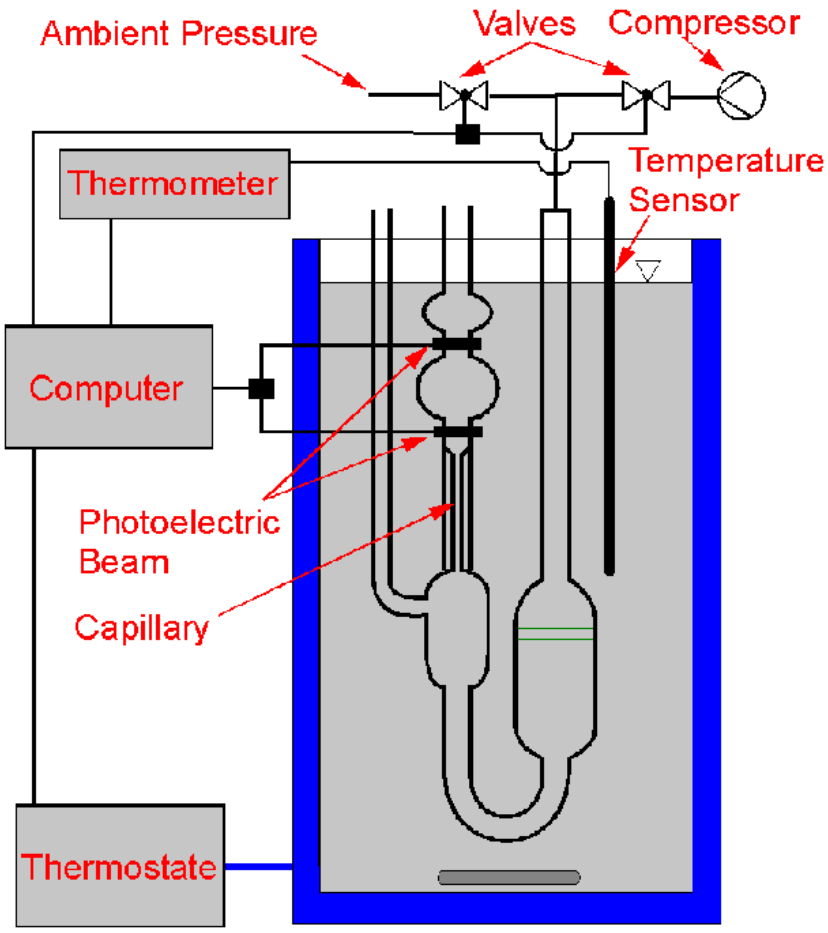

Figure 71. The ubbelohde capillary viscometer (262).

$$\eta_{rel} = \frac{t}{t_0} \quad \text{(Eq. 18)}$$

$$\eta_{sp} = \frac{t}{t_0} - 1 \quad \text{(Eq. 19)}$$

$$\eta_{red} = \frac{\eta_{sp}}{c} \quad \text{(Eq. 20)}$$

$$\eta_{inh} = \frac{\ln \eta_{rel}}{c} \quad \text{(Eq. 21)}$$

where t is the running time of solutions, t_0 is that of the solvent, and c is the solute concentrations in g/L (218). The intrinsic viscosity is determined by the common intercept of both Huggins (η_{red} vs. c) and Kraemer (η_{inh} vs. c) plots on the ordinary at c = 0 (218, 263) as follows:

$$[\eta] = \lim_{c \to 0} \eta_{red} \equiv \lim_{c \to 0} \eta_{inh} \quad \text{(Eq. 22)}$$

A representative plot for intrinsic viscosity calculation of TMC400-40 was showed in Figure 72.

2. Molecular weight determination of chitosan

The relationships between intrinsic viscosity and average molecular weight are commonly used to evaluate the degree of polymerization of macromolecules, as polymers and polysaccharides. If a whole set of data are properly determined, the resulting K and *a* parameters of the correspondent Mark-Houwink equation can be used to calculate viscosity-average molecular weights, as follows:

$$[\eta] = KM_v^{a} \quad \text{(Eq. 23)}$$

or $$\log[\eta] = \log K + a \log M_v \quad \text{(Eq. 24)}$$

where $[\eta]$ is the intrinsic viscosity of the polymer fragment, M_v is the viscosity-average molecular weight, K and *a* are empirical parameters.

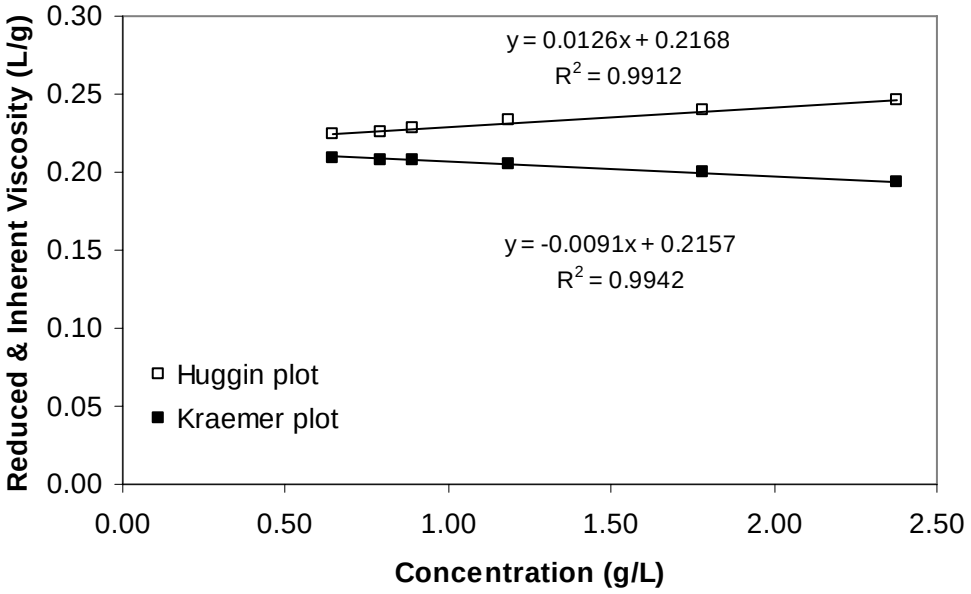

Figure 72. A representative plot for intrinsic viscosity calculation (TMC400-40). Both η_{red} and η_{inh} are plotted on the same graph and the common intercept of the plots on the ordinate at c = 0 is the intrinsic viscosity.

In case of chitosan, the parameters K and *a* are influenced by degree of deacetylation of chitosans, temperature, pH and ionic strength of the solvent which can be determined experimentally by evaluating the intrinsic viscosities of solutions of polymers for which the molecular weight has been determined by an independent method.

Several authors have reported the K and *a* values for chitosan of varying degree of deacetylation, in various solvent systems, as summarized in table 25. As to the chitosans with a degree of deacetylation value of 85 ± 3% (degree of acetylation, DA of 15 ± 3%) in 2% HAc/0.2 M NaAc at 25°C, the constants $K = 1.38 \times 10^{-5}$ and $a = 0.85$ were reported (220). The viscosity-average molecular weight of the chitosan was therefore calculated as follows:

$$M_v = \left(\frac{[\eta]}{1.38 \times 10^{-5}} \right)^{1/0.85} \qquad \text{(Eq. 25)}$$

As a representative example, the calculation of viscosity-average molecular weight of the chitosan used in this study was showed in Figure 73.

Table 25. Published Mark-Houwink constants for chitosans with varying of DA and solvents of different pH and ionic strength, μ (264)

Solvent	T (°C)	DA (%)	pH	μ (M)	$K \times 10^5$ (dL · g^{-1})	a	Molecular Weight Range (kDa)	Reference[a]
0.02*M* HAc/NaAc/0.1*M* NaCl	20	0	4.5	0.1	559.0	0.58	15–310	Anthonsen et al., 1993[1]
0.5*M* HAc/0.5*M* NaAc	25	29.5	4.7	0.5	199.0	0.59	115–1590	Yomota et al., 1993[2]
0.3*M* HAc/0.2*M* NaAc	25	2	4.6	0.2	82.0	0.76	100–600	Rinaudo et al., 1993[3]
0.3*M* HAc 0.2*M* NaAc	25	10.5	4.6	0.2	76.0	0.76	100–600	Rinaudo et al., 1993[4]
0.3*M* HAc/0.2*M* NaAc	25	21	4.6	0.2	74.0	0.76	100–600	Rinaudo et al., 1993[5]
0.02*M* HAc/NaAc/0.1*M* NaCl	20	15	4.5	0.1	58.5	0.78	35–245	Anthonesn, et al., 1993[6]
0.25*M* HAc/0.25*M* NaAc	25	21–26	4.7	0.25	15.7	0.79	35–2220	This work[7]
0.2*M* HAc/0.1*M* NaAc	30	0	4.4	0.1	16.8	0.81	194–937	Wange et al., 1991[8]
2% HAc/0.2*M* NaAc	25	15 ± 3	4.5	0.2	13.8	0.85	61–150	Gamzazade et al., 1985[9]
0.2*M* HAc/0.1*M* NaAc	30	9	4.4	0.1	6.59	0.88	211–1260	Wange et al., 1991[10]
0.1*M* HAc/0.2*M* NaCl	25	≈ 20	2.8	0.2	1.81	0.93	48–630	Roberts et al., 1982[11]
0.2*M* HAc 0.1*M* NaAc	30	16	4.4	0.1	1.42	0.96	536–1850	Wange et al., 1991[12]
0.33*M* HAc/0.3*M* NaCl	21	20–22	4.7	0.3	3.41	1.02	13–193	Podogina et al., 1986[13]
0.02*M* HAc/NaAc/0.1*M* NaCl	20	60	4.5	0.1	2.18	1.06	15–164	Podogina et al., 1986[13]
0.2*M* HAc/0.1*M* NaAc	30	31	4.4	0.1	0.104	1.12	477–2510	Wange et al., 1991[15]
0.1*M* HAc/0.02 NaCl	25	≈ 20	2.9	0.02	0.0304	1.26	48–630	Roberts et al., 1982[16]
0.2*M* HAc/0.1*M* NaCl/4*M* urea	20	9	2.6	0.1	89.3	0.71	163–492	Lee, 1974
1% HAc	30		2.8	0.01	4.74	0.72	205–657	Rao, 1993
HAc/0.2*M* NaAc	25	58	4.3	0.2		1.14	4.3–64.1	Errington et al., 1993

Sample : Chitosan (Fluka 28191/414556)

Solvent : 2% Hac / 0.2 M NaAc

Control (t_0) 99.51 s

initial conc 0.1012 g/L

Conc (g/L)	Av. time n = 5 (s)	Relative Viscosity t / t_0	Specific Viscosity $(t / t_0) - 1$	Reduced Viscosity (n_{sp} / c)	Inherent Viscosity $(\ln(t / t_0) / c)$
0.1012	110.89	1.1144	0.1144	1.1300	1.0700
0.1380	115.10	1.1567	0.1567	1.1353	1.0547
0.1898	121.29	1.2189	0.2189	1.1532	1.0428
0.2530	129.55	1.3019	0.3019	1.1932	1.0427
0.3795	147.09	1.4781	0.4781	1.2599	1.0297
0.5060	166.05	1.6687	0.6687	1.3215	1.0119

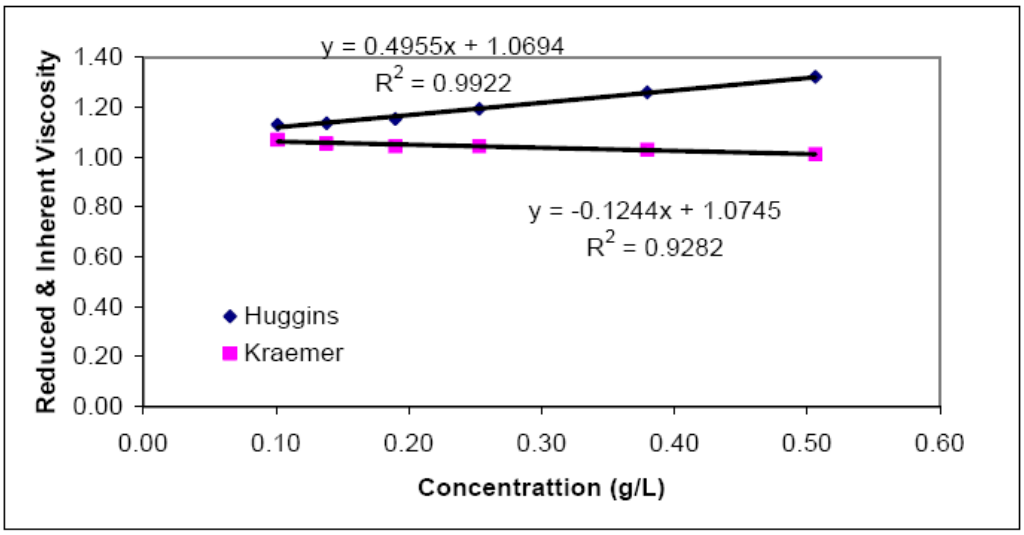

From the curve

Intrinsic Viscosity	1.0694 L/g
Inherent Viscosity	1.0745 L/g
Average Viscosity	1.0720 L/g
Viscosity-average MW	566616 g/mole

Figure 73. The representative calculation of viscosity-average molecular weight of the chitosan.

APPENDIX C
PREPARATION OF BUFFER SOLUTIONS AND REAGENTS

Preparation of insulin solution

Solution A: 11.5 ml of 0.1 N HCl solution is diluted with distilled water to 100 ml.

Solution B: 1.21 g of Tris (hydroxymethyl)-aminomethane is dissolved in 100 ml of distilled water.

- Insulin powder is dissolved in 87 % (v/v) of solution A and 13 % (v/v) of solution is added, resulting in a clear insulin solution in 10 mM Tris buffer at pH 7.4.

Preparation of 10 mM Tris buffer pH 7.4

Tris(hydroxymethyl)-aminomethane	1.21	g
0.1 N HCl	100.0	ml
Distilled water qs.	1000.0	ml

Preparation of isotonic 10 mM Tris buffer pH 7.4 (I = 0.15 M)

Tris(hydroxymethyl)-aminomethane	1.21	g
NaCl	8.58	g
0.1 N HCl	100.0	ml
Distilled water qs.	1000.0	ml

Preparation of uptake and transport medium for cell culture experiment

Tris(hydroxymethyl)-aminomethane	1.21	g
$CaCl_2 \cdot 2H_2O$	0.33	g
$MgCl_2 \cdot 6H_2O$	0.21	g
Glucose$\cdot H_2O$	19.25	g
0.1 N HCl	100.0	ml
Distilled water qs.	1000.0	ml

Preparation of phosphate buffer saline (PBS) pH 7.4

KCl	0.20	g
KH_2PO_4	0.20	g
NaCl	8.00	g
$NaHPO_4$	1.14	g
Distilled water qs.	1000.0	ml

Preparation of 10% neutral-buffered formalin

37-40% formalin	100.0	ml
Distilled water	900.0	ml
$NaH_2PO_4.H_2O$	4.0	g
$Na_2HPO_4.2H_2O$	8.15	g

Preparation of formic acid-sodium citrate decalcifying solution

Solution A:

Sodium citrate	50.0	g
Distilled water	250.0	ml

Solution B:

Formic acid, 90 %	125.0	ml
Distilled water	125.0	ml

- Mix solutions A and B in equal portion for use

APPENDIX D
DOCUMENTARY PROOF OF ETHICAL CLEARANCE

No. 0019

Documentary Proof of Ethical Clearance
Institutional Animal Care and Use Committee
Faculty of Pharmacy, Mahidol University, Bangkok, Thailand

Title of Thesis : Nasal delivery of insulin nanocomplexes

Name of Student : Miss Anchalee Jintapattanakit

Program of Study : Pharmaceutics

Advisor : Assoc.Prof. Varaporn Junyaprasert

Department : Pharmacy

Approved by the Institutional Animal Care and Use Committee

Signature of Chairman : .....
(Assoc.Prof. Supaporn Pongsakorn)

Signature of Dean : .....
(Prof. Ampol Mitrevej)

Date of Approval : 25 October 2006

APPENDIX E

PUBICATIONS

Available online at www.sciencedirect.com
ScienceDirect
International Journal of Pharmaceutics 342 (2007) 240–249
INTERNATIONAL JOURNAL OF PHARMACEUTICS
www.elsevier.com/locate/ijpharm

Pharmaceutical Nanotechnology

Peroral delivery of insulin using chitosan derivatives: A comparative study of polyelectrolyte nanocomplexes and nanoparticles

Anchalee Jintapattanakit [a,b], Varaporn B. Junyaprasert [a], Shirui Mao [b,c], Johannes Sitterberg [b], Udo Bakowsky [b], Thomas Kissel [b,*]

[a] *Department of Pharmacy, Faculty of Pharmacy, Mahidol University, 447 Sri-Ayutthaya, Bangkok 10400, Thailand*
[b] *Department of Pharmaceutics and Biopharmacy, Philipps-Universität Marburg, Ketzerbach 63, D-35032 Marburg, Germany*
[c] *School of Pharmacy, Shenyang Pharmaceutical University, Wenhua Road 103, 110016 Shenyang, China*

Received 17 May 2006; received in revised form 26 April 2007; accepted 8 May 2007
Available online 17 May 2007

Abstract

Polymeric delivery systems based on nanoparticles (NP) have emerged as a promising approach for peroral insulin delivery. Using a trimethyl chitosan (TMC) and a PEG-*graft*-TMC copolymer, polyelectrolyte complexes (PEC) and nanoparticles were prepared and their properties were compared. The amount of insulin was quantified by HPLC and the stability of PEC and NP upon exposure to simulated gastrointestinal (GI) fluid was monitored by dynamic laser light scattering. It was shown that polymer/insulin (+/−) charge ratio played an important role in PEC and NP formation. Stable, uniform, and spherical PEC/NP with high insulin association efficiency (AE) were formed at or close to optimized polymer/insulin (+/−) charge ratio, depending on polymer structure. All PEC were more stable in pH 6.8 simulated intestinal fluid (SIF) than NP. The PEC also appeared to play some role in protecting insulin from degradation at higher temperature and with proteolytic enzyme more efficiently than NP. On the basis of these results, polyelectrolyte complexation can be suggested as a potentially useful technique for generating insulin delivery systems for peroral administration.

Keywords: PEGylated trimethyl chitosan; Polyelectrolyte complexes; Nanoparticles; Insulin; Peroral delivery

1. Introduction

Insulin is a protein composed of two polypeptide chains which are covalently bound by disulfide bonds between cysteine residues. Repeated injections are generally required for the treatment of insulin-dependent diabetes mellitus. Although peroral application is considered as the most convenient route of drug administration, especially in long-term treatment, it is well known that the bioavailability of insulin after oral application is very low due to its instability in the gastrointestinal (GI) tract and its low permeability through the intestinal mucosa, requiring non-oral routes of delivery (Owens et al., 2003). New delivery approaches depend on protecting insulin against enzymatic degradation and enhancing their transport across the intestinal mucosa into the systemic circulation. Various approaches have been proposed to overcome barriers and to attain better oral bioavailability, including the use of surfactants, permeation enhancers, protease inhibitors, enteric coatings, carrier systems and chemical modifications of insulin (Morishita et al., 1992, 1993; Yamamoto, 1994; Carino et al., 2000; Nakashima et al., 2004). Amongst these, the use of colloidal polymeric particulate delivery systems, particularly mucoadhesive nanoparticles (NP) represents a promising concept (Ponchel and Irache, 1998; Takeuchi et al., 2001). NP have been shown to protect peptide drugs from degradation in the GI tract and hence improve their bioavailability (Lenaerts et al., 1990; Damagé et al., 1997). Moreover, mucoadhesive properties also play an important role in oral drug delivery system by prolonging the residence time of drug carriers and also increasing the intimacy of contact between drug and mucus membrane at the absorption sites, thus enhancing the permeability as well as reducing degradation of drugs.

Trimethyl chitosan (TMC) is a partially quarternised derivative of chitosan which is well soluble in a wide pH range (pH 1–9). Moreover TMC shows mucoadhesive properties (Snyman et al., 2003; van de Merwe et al., 2004; Sandri et al., 2005). TMC has been proven to be a potent intestinal absorption enhancer

* Corresponding author. Tel.: +49 6421 282 5881; fax: +49 6421 282 7016.
E-mail address: kissel@staff.uni-marburg.de (T. Kissel).

0378-5173/$ – see front matter © 2007 Elsevier B.V. All rights reserved.
doi:10.1016/j.ijpharm.2007.05.015

of peptide and protein drugs, especially in neutral environments where chitosan is ineffective as an absorption enhancer (Thanou et al., 2000a,b). The best and maximum permeation-enhancing results are achieved with degree of quarternisation ca. 48% (Hamman et al., 2003). However, most of the studies were performed with TMC solution. It is well known that most peptides are unstable in the presence of water leading to the impracticality of solution administration. Thus recent studies have focused on the development of solid oral dosage forms (Polnok et al., 2004a; van de Merwe et al., 2004). With regard to chitosan-based formulations, nearly all insulin-loaded NP have been prepared by ionotropic gelation with tripolyphosphate (TPP) counterions (Dyer et al., 2002; Ma et al., 2002; Pan et al., 2002a,b; Grenha et al., 2005). To the best of our knowledge, no report has been published about insulin-loaded TMC NP. Therefore, TMC-TPP insulin NP were prepared in this study and influence of process parameters on the properties of NP was investigated. Furthermore, recently, polyelectrolyte complexes (PEC) of insulin and TMC/PEG-*graft*-TMC copolymers in the absence of TPP have been developed for intranasal delivery by our research group, with an insulin loading efficiency of up to 95% and the enhancement of insulin uptake in Caco-2 cells (Mao et al., 2005a, 2006). We are interested in the point how the TPP in NP formulation affect the properties of particles compared to PEC. In case of no significant difference, it would be better to fabricate the carriers with only polymer and insulin in order to avoid unforeseen adverse effects from the third component.

Therefore, the aims of the present work were, first, to develop nano-carrier systems based on TMC and PEG-*graft*-TMC copolymer using two techniques; polyelectrolyte complexation and ionotropic gelation with TPP counter ion as carriers for the oral administration of insulin and, second, to elucidate the influence of TPP in formulation on colloidal and insulin stability.

2. Materials and methods

2.1. Materials

Chitosan (400 kDa) was purchased from Fluka (Schnelldorf, Germany) with a degree of deacetylation of 84.7%. Depolymerization was carried out as described previously to obtain chitosan with molecular weight (MW) of ca. 100 kDa (Mao et al., 2004). TMC with quarternisation degree of 40% were prepared by reductive methylation of the parent chitosans based on one reaction step with two subsequent addition steps (Polnok et al., 2004b). PEGylated TMC copolymer, PEG(5k)$_{40}$-*g*-TMC(100) was synthesized by grafting polyethylene glycol (PEG) 5 kDa onto TMC 100 kDa according to the method described previously (Mao et al., 2005b). The following nomenclature was adopted for the copolymer: PEG(X)$_n$-*g*-TMC(100) where X denotes the MW of PEG in kDa and the subscript n represents the average number of PEG chains per TMC macromolecule of 100 kDa. The number of PEG chains grafted per TMC macromolecule (graft ratio) was calculated from integrals of the ^{1}H NMR signals for PEG blocks at ~3.35 ppm (–OCH_3) and TMC blocks at ~3.0 ppm (–$N(CH_3)_2$) and ~3.3 ppm (–$N^+CH_3)_3$). The graft ratio (wt%) was calculated according to the following equation:

$$\text{Graft ratio (wt\%)} = \frac{\text{MW}_{\text{PEG}} \times n}{(\text{MW}_{\text{PEG}} \times n) + \text{MW}_{\text{TMC}}}$$

where MW_{PEG} is the molecular weight of PEG, MW_{TMC} the molecular weight of TMC, and n is the average number of PEG chains per TMC macromolecule calculated by ^{1}H NMR. The properties of the polymers used in the present work are summarized in Table 1.

Human recombinant insulin powder (26.2 IU/mg) was obtained as a gift from Aventis Pharma AG (Frankfurt, Germany). TPP and *N*-Benzoyl-L-arginine ethyl ester (BAEE) were purchased from Fluka. Trypsin (1840 BAEE IU/mg) was obtained from Sigma (Steinheim, Germany). All other chemicals and solvents were of analytical grade.

2.2. Preparation of insulin PEC

Polymer–insulin PEC were prepared by self-assembly, utilizing the electrostatic interactions between the positively charged polymers and negatively charged insulin as a driving force (Mao et al., 2006). Briefly, PEC were prepared by mixing equal volumes of insulin and polymer solutions at the desired ratio (Table 2) under gentle magnetic stirring. The mixture was then incubated for 20 min at room temperature. The pH of polymer and insulin solutions was adjusted to pH 7.4.

2.3. Preparation of insulin NP

Polymer–insulin NP were prepared, based on the ionotropic gelation with TPP (Calvo et al., 1997). Briefly, polymer solutions at appropriate concentration were prepared by dissolving the dry polymer powder in 10 mM Tris buffer, pH 7.4. TPP was dissolved in purified water at various concentrations. The NP were spontaneously formed upon incorporation of equal volume

Table 1
Characteristics of TMC400 and PEG(5k)$_{40}$-*g*-TMC(100)

Polymers (kDa)	Substitution (%)[a]	TMC content (w/w%)	Molecular weight (kDa)[b]	[η] (dL/g)[c]
TMC400	39.0[d]	100	400	2.15
PEG(5k)$_{40}$-*g*-TMC(100)	6.4	32.8 ± 1.0	300	ND

ND, not determined.
[a] Calculation based on the primary amino group content in chitosan.
[b] Calculation based on the composition of the copolymer.
[c] Intrinsic viscosity in 2% acetic acid/0.2 M sodium acetate.
[d] Degree of quaternization.

Table 2
Formulation and characteristics of the polyelectrolyte complexes and nanoparticles with insulin

Formulation	Mass ratio		Charge ratio (Pol/Ins)[a]	Particle size (nm)	Polydispersity index	Zeta potential (mV)	Association efficiency (%)	Process yield (%)
	Pol/Ins	TPP/Pol						
TMC400 PEC-1	0.3:1[b]		1:1	181 ± 7	0.13 ± 0.03	24.7 ± 1.5	83 ± 5	78 ± 1
TMC400 PEC-2	1:1		15:1	142 ± 3*	0.33 ± 0.02[c]	29.2 ± 1.7*	19 ± 1*	34 ± 1*
TMC400 PEC-3	2:1		33:1	104 ± 4*	0.37 ± 0.03*	33.4 ± 2.0*	24 ± 1*	10 ± 1*
TMC400 NP-1	0.3:1[b]	0.6:1	1:1	443 ± 28**	0.27 ± 0.07**	12.3 ± 0.3**	86 ± 2	73 ± 4
TMC400 NP-2	1:1	0.4:1	15:1	227 ± 6**	0.14 ± 0.04**	17.1 ± 0.9**	87 ± 2**	67 ± 1**
TMC400 NP-3	2:1	0.6:1	33:1	228 ± 4**	0.11 ± 0.02**	8.6 ± 0.7**	87 ± 0**	33 ± 0**
PEG(5k)$_{40}$-g-TMC(100) PEC-1	1:1[b]		5:1	232 ± 6	0.28 ± 0.06	24.3 ± 2.2	93 ± 0	45 ± 1
PEG(5k)$_{40}$-g-TMC(100) PEC-2	2:1		9:1	159 ± 5*	0.29 ± 0.03	27.5 ± 1.5*	36 ± 3*	24 ± 2*
PEG(5k)$_{40}$-g-TMC(100) NP-2	2:1	0.1:1	9:1	317 ± 11**	0.18 ± 0.05**	21.0 ± 1.4**	93 ± 0**	50 ± 4**

The initial concentration of insulin was 1 mg/ml in all the formulations. Mean ± S.D.
[a] Calculation based on the polymer/insulin mass ratio.
[b] Optimized polymer/insulin mass ratio for preparation of polyelectrolyte complexes.
* Statistically significant differences ($p < 0.05$) compared with that of PEC at optimal polymer/insulin mass ratio.
** Statistically significant differences ($p < 0.05$) compared with that of PEC at the same polymer/insulin mass ratio.

of TPP solution in the polymer solution under gentle magnetic stirring at room temperature. Insulin solution (1 mg/ml, pH 7.4) was premixed with equal volume of polymer solution before the addition of TPP solution. The final pH values were in the range of 7.4–7.7.

2.4. Characterization of insulin PEC/NP

Measurement of particle size and average count number (ACN) were performed on freshly prepared samples by photon correlation spectroscopy (PCS) using a Autosizer Lo-C (Malvern Instruments, Herrenberg, Germany) equipped with a 10 mW HeNe laser (633 nm) at 90° angle at the temperature of 25 °C. The ACN, measuring in term of kcps (kilo count per second), reflects the signal intensity, which is a measurement of particle concentration in a sample. Average values of particle size were calculated from the data of 10 runs.

The zeta potential of PEC and NP were obtained by laser Doppler velocimetry (LDV) using a Zetasizer Nano ZS (Malvern Instruments, Herrenberg, Germany) at 25 °C in 10 mM Tris buffer pH 7.4. Zeta potential of samples are expressed as mean ± S.D. ($n = 10$).

To determine the association efficiency (AE) and process yield (PY), triplicate batches of PEC and NP were centrifuged at 14,000 rpm for 30 min at room temperature, and the insulin content in the supernatant was determined by RP-HPLC as described elsewhere (Simon et al., 2004). The pellet was then lyophilized and weighed. The AE and PY were calculated as follows:

$$\text{AE}\,(\%) = \frac{\text{total insulin amount} - \text{free insulin amount}}{\text{total insulin amount}} \times 100$$

$$\text{PY}\,(\%) = \frac{\text{particles weight}}{\text{total solids (polymer + insulin + TPP) weight}} \times 100$$

The morphological examination of PEC and NP were conducted by atomic force microscopy (AFM) (NanoWizard™, JPK Instruments, Berlin, Germany). The samples were diluted with ultra pure water and 10 μl of the diluted sample was applied to a freshly cleaved mica surface and allowed to adhere to the surface for a few minutes. The supernatant was removed and the samples were allowed to air-dry (ca. 10 min). Commercially available silicon tips attached to I-type silicon cantilevers with a length of 230 μm, a resonance frequency of about 170 kHz and a scan frequency of 0.8–1.1 Hz were used. All measurements were performed in tapping mode in order to avoid damage of sample surface (Shi et al., 2003).

2.5. Stability of PEC and NP in simulated GI fluids

In order to investigate the stability of PEC and NP in GI fluid, PEC and NP were mixed with pH 1.2 simulated gastric fluid (SGF) or pH 6.8 simulated intestinal fluid (SIF) without enzymes in different ratios. The integrity of the PEC and NP was monitored by dynamic laser light scattering.

2.6. Stability of insulin in PEC and NP

2.6.1. Temperature stability studies

Two milliliters of PEC or NP suspensions, containing 500 μg/ml insulin, were incubated at room temperature, 37 °C, and 50 °C. At predetermined time intervals (0, 15, 60, 145, 360 min), 100 μl aliquot was withdrawn and then 50 μl of 0.25% acetic acid solution was added to dissolve the particles followed by dilution with 10 mM Tris buffer to 1 ml. The insulin content was determined by HPLC. In addition, the stability of pure insulin at different temperatures was assessed under the same conditions. All samples were prepared in triplicate.

2.6.2. Enzymatic stability studies with trypsin

First, trypsin was dissolved in 10 mM Tris buffer pH 7.4, and the concentration was adjusted to 3000 BAEE IU/ml. One hundred microliter of the solution was then added to 900 μl of

insulin solution, PEC and NP suspensions containing 500 μg/ml of insulin. The initial concentrations of insulin and trypsin in the sample solution (1 ml) were 450 μg/ml and 300 BAEE IU/ml, respectively. Three vials of mixture were taken out at predetermined time points and the enzymatic reaction was stopped by the addition of 1 ml of acetonitrile/purified water mixture (3/1, v/v) containing 0.1% trifluoroacetic acid. The insulin concentration was then quantified by HPLC.

In vitro evaluation of trypsin activity in the presence of polymers was also investigated using the method described previously (Sakuma et al., 1997). Briefly, 900 μl of polymer solution corresponding to the polymer concentration in PEC or NP suspension was mixed with 100 μl of trypsin solution (3000 BAEE IU/ml in 10 mM Tris buffer pH 6.8). Subsequently the mixtures were incubated at 37 °C for 30 min. Afterward the samples were centrifuged at 14,000 rpm for 30 min. The enzymatic activity in the supernatant was determined from the change of the absorbance at 253 nm/min, using BAEE as the substrate. Two hundred microliter of supernatant was pipetted into a 1-cm cell. After adding 25.71 μg of BAEE dissolved in 3 ml of 10 mM Tris buffer (pH 6.8), the increase in absorbance (ΔA 253 nm) caused by the hydrolysis of this substrate to *N*-α-benzoylarginine (BA) was recorded at 1 min intervals for 5 min using UV/Vis spectrophotometer (UV-160, Shimadzu). In addition, the enzymatic activity in the absence of polymer was measured under the same condition.

2.7. Calculations and statistics

Results are depicted as mean ± S.D. from at least three measurements. The *t*-test or one-way ANOVA with the Scheffe test applied post hoc for paired comparisons were performed to compare two or multiple groups, respectively. All analyses were determined using the SPSS program (SPPS 9.0 for windows) and differences were considered to be significant at a level of $p < 0.05$.

3. Results and discussion

The aim of the present study was to investigate the influence of TPP in the formulation on the physical stability of particles and that of insulin by using 40%DQ TMC 400 kDa with two techniques, polyelectrolyte complexation and ionotropic gelation with TPP. Previously, it has been shown that PEG(5k)$_{40}$-*g*-TMC(100) could stabilize insulin in PEC more efficiently than chitosan 100 kDa due to hydrophilic PEG chains (Mao et al., 2006). Therefore, it was used here to examine whether it exhibited in the same trend with NP.

3.1. Preparation and characterization of insulin PEC

Self-assembled insulin PEC were prepared by electrostatic interactions between positively charged polymer and negatively charged insulin as a driving force (Scheme 1). Stable, uniform and nano-sized PEC can be formed only at ≥optimal polymer/insulin (+/−) charge ratio with a particle size in the range of 100–320 nm, with a positive surface charge. The optimal (+/−) charge ratio between polymer and insulin was polymer structure dependent: it was 1:1 for TMC400, compared to 5:1 for PEG(5k)$_{40}$-*g*-TMC(100) (Table 2). The PEC were spherical or almost spherical as revealed by their AFM images (Fig. 1a, b and d). However, excessive TMC400 chains are observed in PEC at polymer/insulin (+/−) charge ratio of 15:1 (Fig. 1b).

As shown in Table 2, soluble insulin PEC prepared at optimal polymer/insulin (+/−) charge ratio displayed high insulin AE and PY with low polydispersity index (PDI). On the contrary, the particle size, AE and PY of PEC decreased while the zeta potential and PDI increased with the increased (+/−) charge ratio of polymer to insulin ($p < 0.05$). These results agree well with the results reported by Fredheim and Christensen (2003) who found that the maximum yield of lignosulfonate–chitosan complexes was performed at optimal ligonosulfonate/chitosan (w/w) mixing ratio. The precipitated yield declined when increasing ratio of chitosan. These finding can probably be explained by the conformation of polymer (Snyman et al., 2004). When polymer concentration increased, the charge density and sterical hindrances between the pendant groups (methyl groups and PEG segments) increased, resulting in low flexibility of polymer chains. These hinder insulin to interact with polymer chains, causing low AE and PY. Additionally, a decrease of associated insulin amount in PEC and an increase of positively charged polymer chains towards the external aqueous medium could promote complex condensation, consequently a decreased particle size and high zeta potential PEC were obtained.

3.2. Preparation and characterization of insulin NP

Insulin NP were prepared by ionotropic gelation in a two-step procedure: (a) the complex formation between the two oppositely charged polyelectrolytes, polymer and insulin, and (b) cross-linking with TPP anions as depicted in Scheme 2.

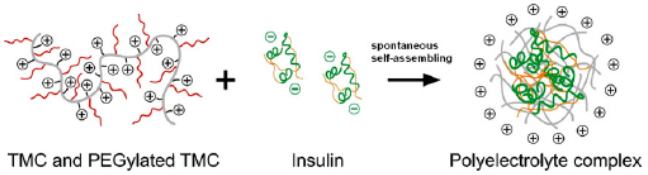

Scheme 1. Schematic representation of insulin polyelectrolyte complex formation.

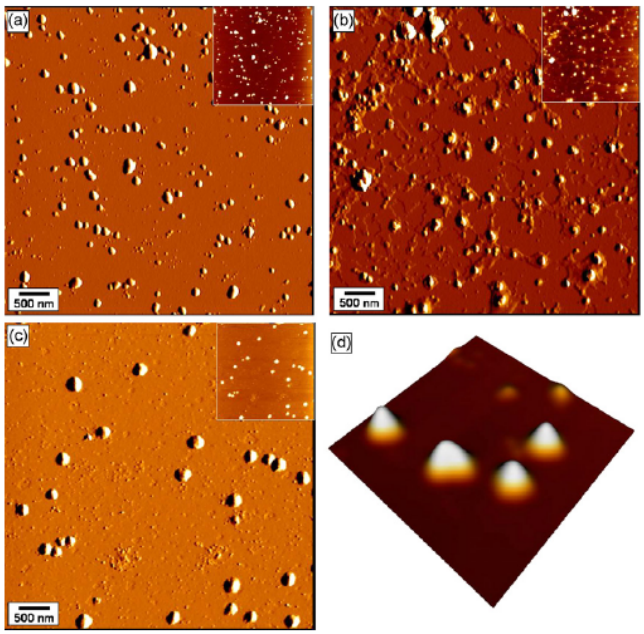

Fig. 1. Atomic force microscopy images (5 μm × 5 μm) of: (a) TMC400-insulin PEC at optimal polymer/insulin mass ratio of 0.3:1, (b) TMC400-insulin PEC at polymer/insulin mass ratio of 1:1, (c) TMC400-insulin NP at polymer/insulin/TPP mass ratio of 1:1:0.4, and (d) three-dimensional image of 0.3:1 TMC400-insulin PEC. The inserts are height mode of each image.

3.2.1. Optimal ratio of TPP and polymer in NP

Many studies have reported that the quantity of TPP in a given formulation has a significant effect on the protein encapsulation and characteristic of NP (Pan et al., 2002a,b; Janes and Alonso, 2003; Grenha et al., 2005). Therefore, the optimal amount of TPP in formulation was investigated in detail.

The optimal condition at which NP were formed was established using dynamic light laser scattering as previously

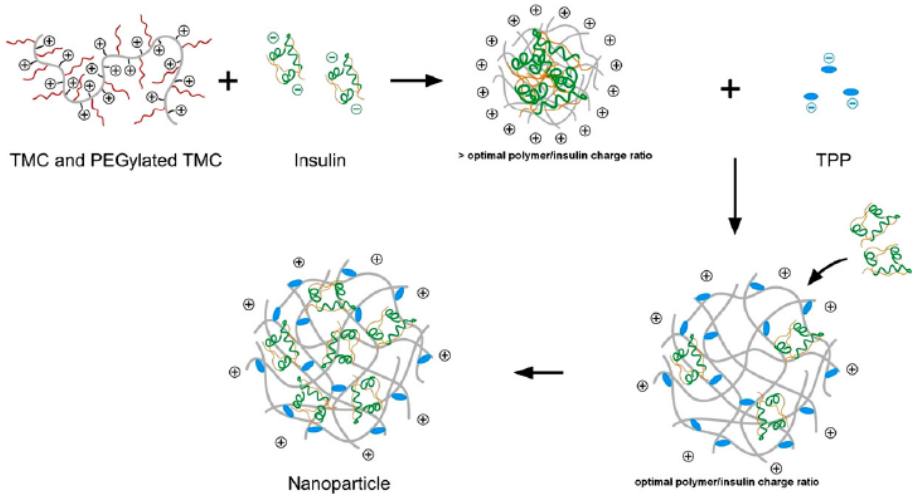

Scheme 2. Schematic representation of insulin nanoparticle formation.

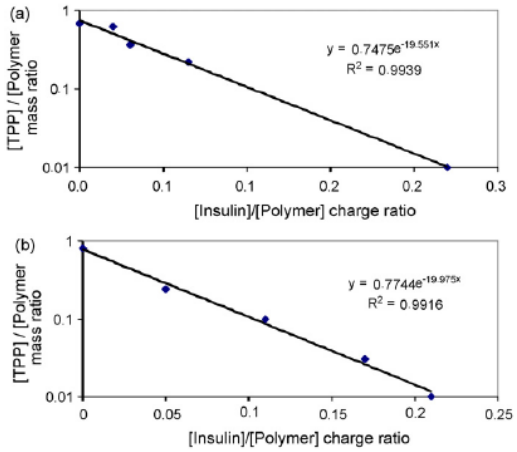

Fig. 2. Correlation between insulin/polymer (+/−) charge ratio and TPP/polymer mass ratio for nanoparticle formation of (a) 40%DQ TMC 400 kDa, (b) PEG(5k)40-*g*-TMC(100).

described (Mao et al., 2006). Mixtures of polymer and insulin with different polymer/insulin (+/−) charge ratio were titrated against TPP solution, and particle size and kcps values were measured. The points at which the kcps values reached a maximum or plateau were denoted as the end point of titration. When adding the TPP solution into polymer–insulin mixtures, kcps values of mixture increased until a plateau, referred to a TPP amount independent region which was reached at a specific TPP volume. After this point, the addition of an excess amount of TPP led to a drop in the kcps values together with considerable increase of particle size. A linear relationship was observed between the logarithm of optimal TPP/polymer mass ratio and insulin/polymer (+/−) charge ratio with correlation coefficient of 0.9939 for TMC400 and 0.9916 for PEG(5k)$_{40}$-*g*-TMC(100) as shown in Fig. 2.

Effect of TPP amount on the properties of NP was also evaluated using TMC400 as an example. In case of NP prepared at optimal TMC400/insulin (+/−) charge ratio of 1:1, no difference in AE and PY between TMC400-insulin NP and PEC prepared at the same polymer/insulin (+/−) charge ratio was observed (Table 2), but particle size of NP was significant larger than that of the PEC and flocculation occurred in a short period of time. However, in case of NP prepared at >polymer/insulin (+/−) charge ratio, compared to PEC at the same 15:1 TMC400/insulin (+/−) charge ratio, incorporation of increasing amounts of TPP with respect to TMC400 led to a significant increase in the particle size, AE and PY ($p < 0.05$) and led to a significant decreased ($p < 0.05$) zeta potential and PDI. Equilibrium was reached at the TPP/TMC400 mass ratio of 0.4:1, as shown in Table 3. Additionally, the results showed linear relationship as a function of the TPP amount with correlation coefficients of 0.9845, 0.9926, 0.9153 and 0.8770 for ACN, zeta potential, PY and AE, respectively.

Compared to insulin, TPP has a much smaller molecular with a higher negative charge density. It can dominate interaction of insulin with positively charged polymers causing a reduction in the positive charge density of polymers, and also in (+/−) charge ratio between polymer and insulin which can be seen from a reduction of zeta potential of particles when increasing TPP amount. The structure of particle is then loose, leading to a larger size and it is very likely that this structure allows them to capture more insulin (Scheme 2). Similar result was found by Grenha et al. (2005) who observed that insulin AE of chitosan NP increased with increasing TPP concentration. Recently, Boonsongrit et al. (2006) reported that adding TPP did not affect the entrapment efficiency of insulin–chitosan microparticles when microparticles were formed at optimal chitosan/insulin mass of 1.25:1. Therefore, it is reasonable to assume that polymer/insulin (+/−) charge ratio plays an important role in PEC and NP formation. The highest insulin AE of NP with a narrow size distribution could be achieved when polymer/insulin (+/−) charge ratio was close to optimal ratio by using specific TPP amount. Fig. 1c displays the AFM image of fresh TMC400-insulin NP prepared at the optimal condition.

3.2.2. *Effect of order of mixing*

In some cases, the mixing order influenced PEC or NP formation (MacLaughlin et al., 1998; Mao et al., 2006). In order to investigate whether the order of mixing affects the physicochem-

Table 3
Influence of TPP/polymer mass ratio on the properties of insulin nanoparticles[a]

Mass ratio (TPP:Pol)	Average count number (kcps)[b]	Particle size (nm)	Polydispersity index	Zeta potential (mV)	Process yield (%)	Association efficiency (%)
0.0:1	283 ± 18	142 ± 3	0.33 ± 0.02	29.2 ± 1.7	34 ± 1	19 ± 1
0.1:1	886 ± 95	217 ± 13	0.38 ± 0.05	26.3 ± 1.8	50 ± 6	46 ± 2
0.2:1 (1)[a]	1257 ± 113	205 ± 10	0.22 ± 0.03	22.5 ± 1.1	57 ± 6	76 ± 2
0.2:1 (2)[c]	1081 ± 86*	184 ± 6*	0.21 ± 0.02	22.6 ± 0.9	58 ± 4	70 ± 1*
0.4:1	2078 ± 147	227 ± 6	0.14 ± 0.04	17.1 ± 0.9	67 ± 1	87 ± 0
0.6:1	2641 ± 152	257 ± 9	0.14 ± 0.04	12.6 ± 1.0	50 ± 6	88 ± 0

The concentration of insulin and TMC are 1 mg/ml in all formulations. $n = 3$. Mean ± S.D.
[a] Nanoparticles were obtained by premixing insulin with polymer solution, prior to nanoparticle formation.
[b] Measured at 90° angle through a 100-μm pin hole.
[c] Nanoparticles were obtained by premixing insulin with TPP solution, prior to nanoparticle formation.
* Statistically significant differences ($p < 0.05$) compared with that of TMC400-insulin premixed NP.

ical properties of NP, taking 0.2:1 TPP/TMC400 mass ratio as an example, insulin was premixed with either the TPP solution or the polymer solution prior to NP formation. As shown in Table 3, no difference of PY was found between TMC400-insulin premixed and TPP-insulin premixed NP ($p > 0.05$), while bigger size with higher ACN and AE were observed with TMC400-insulin premixed NP ($p < 0.05$).

The results are inconsistent with previous reports by Ma et al. (2002) in which no influence of mixing order on the size and ACN of chitosan–insulin NP was observed. However, they did not investigate effect of mixing order on the insulin AE. We found that such effect influenced insulin AE of TMC400 NP. The higher AE were obtained with TMC400-insulin premixed NP. Similar results were also observed with PEG(5k)$_{40}$-*g*-TMC(100) NP (data not shown). This finding can probably be explained by competition between insulin and TPP to interact with polymers.

3.3. Colloidal stability in simulated GI fluids

In order to evaluate the stability of the PEC and NP in the GI fluids, various ratios of PEC and NP were diluted in either SGF or SIF and the integrity of particles was measured. It was found that all PEC and NP were not stable in SGF and dissociation appeared immediately after adding SGF. This is probably due to the electrostatic repulsion between polymer and insulin at the pH of 1.2 where they exhibit positive charges (the pK_a of TMC is approximately 6.0 (Kotźe et al., 1999) and apparent isoelectronic point of insulin is 6.4).

With regard to dilution with SIF, all PEC appeared to be stable when volume ratio of PEC/SIF was <1:2 with no apparent change in kcps values and particle size. 26% TMC400 PEC and 87% PEG(5k)$_{40}$-*g*-TMC(100) PEC dissociated when SIF was increased to the 1:5 PEC/SIF volume ratio. In contrast to NP, 30% dissociation NP immediately occurred at NP/SIF volume ratio of 1:1, irrespective to the NP structures and dissociating clearly increased with increasing volume of SIF. A linear correlation between the percent of kcps remained and the added volume of SIF was observed with regression coefficient of 0.996 for TMC400 and 1.000 for PEG(5k)$_{40}$-*g*-TMC(100).

Since we found no apparent change in particle size, only the evolution of kcps values are presented in Fig. 3 which clearly showed that the percentage kcps of NP was much less than that of PEC at the same dilution ratio. We hypothesized that the stability of PEC and NP depended on the electrostatic interaction intensity between polymer and insulin which decreased by shielding of counter ion with increasing ionic strength (increasing counter-ion concentration) (Knaul et al., 1999; Mao et al., 2006). Additionally, the attraction between polymer and insulin was reduced by TPP leading to a decrease in physical stability of NP compared to PEC prepared at the same pH. These finding were comparable to the results report previously by Boonsongrit et al. (2006) who found that most of insulin was released within 10 min from the chitosan–insulin microspheres in the pH 7.4 phosphate buffer and in the pH 3 HCl solution indicating the dissociation of microspheres. Possible explanation for the PEC and NP dissociation is that the system pH was close to pH 6.8 of SIF when increasing ratio of SIF. As suggested by Mao et al. (2006), the equivalent pH values for TMC and PEGlyated TMC-insulin PEC are approximately 7.3. We also evaluated the influence of pH on the NP formation and found that the equivalent pH value for TMC400-insulin NP was also approximately 7.3. At lower pH, the particle size increased with decreased system pH (data not shown).

3.4. Effect of ionic strength of the medium on the stability of PEC and NP

In order to confirm whether the electrostatic interaction between polymer and insulin influenced the stability of PEC and NP, TMC400 NP were prepared at different pH of 5.0, 6.8 and 7.4 and their stabilities in a series of concentrated sodium chloride solutions were evaluated. In general, the presence of sodium chloride reduces the electrostatic attraction between the oppositely charged of polymer and insulin by contributing to the counter-ion environment (Berger et al., 2004). It is well known that the charge density of insulin was pH dependent. At the pH of 5.0 where insulin exhibits weakly negatively charged, NP with particle size of 860 nm were obtained indicating a weak interaction between polymer and insulin. Thirty percent of NP dissociation was observed when ionic strength of the solution was 5 mM and 60% NP dissociation at ionic strength of the solution of 15 mM with no apparent change in particle size. On the other hand, NP with particles of 511 and 306 nm were obtained when preparing at pH 6.8 and 7.4, respectively. Only 20% dissociation of NP was found at the ionic strength of 25 mM. In the case of PEC, at pH 7.4, no apparent changes in kcps values and size of TMC400 and PEG(5k)40-*g*-TMC(100)-insulin PEC were observed when the ionic strength of medium is <25 mM.

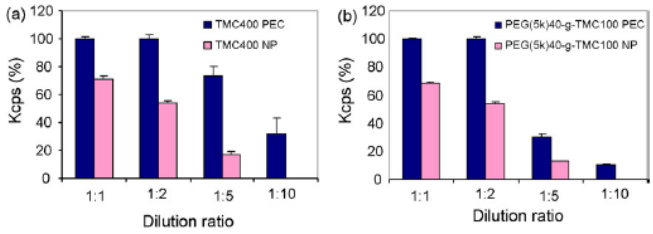

Fig. 3. Colloidal stability of: (a) 40%DQ TMC 400 kDa and (b) PEG(5k)$_{40}$-*g*-TMC(100) after diluting with pH 6.8 simulated intestinal fluid without enzymes. Each value represents the mean ± S.D. of three experiments.

Therefore, polyelectrolyte complexation is an efficient way to prepare nano-carrier systems.

3.5. Effect of temperature on the stability of insulin

Some studies indicated that elevated temperature facilitates PEC and NP formation with the low aggregation tendency (Mao et al., 2001, 2005a). Proteins are very labile molecules sensitive to thermal stress (Brange and Langkjaer, 1992; van de Weert et al., 2000; Frokjaer and Otzen, 2005). Therefore, stability of insulin in the PEC and NP at different temperatures was investigated and compared with that of free insulin solution.

The results of insulin stability at four different temperatures are shown in Fig. 4. It was demonstrated that the PEC and NP could protect insulin from degradation even at higher temperature. At temperature <50 °C, insulin itself was quite stable for at least 2.5 h and degradation was observed at 6 h even at room temperature.

In the case of PEC, they could protect insulin from degradation for at least 6 h even at temperature of 50 °C while approximately 50% of free insulin was degraded. Furthermore, no difference in results was observed between TMC400 and PEG(5k)$_{40}$-*g*-TMC(100) PEC. In the case of NP, they also could protect insulin at least 6 h even at 50 °C and their protecting effect at 50 °C was higher than that at 20 °C ($p < 0.05$). Akiyoshi et al. (1998) also observed this phenomenon. This is probably due to the facilitation of NP formation and compaction at elevated temperature which can be seen from the increased kcps values (ca. 10–20%) with a slight decrease in particle size (ca. 10%), compared to the value at 20 °C (data not shown). Generally, an increase in temperature increases entropy of system which is associated with the release of small counterions initially bond to the polymers, resulting in compaction of particles (Tsuchida and Takeoka, 1994; Fredheim and Christensen, 2003).

With regard to TMC400, the protecting effect of PEC was higher than that of NP, especially at 6 h ($p < 0.05$). These results could be explained from insulin association mechanism. PEC were formed by only columbic interactions between negatively charged insulin and positively charged polymer, which increased with increasing temperature resulting in more PEC (Mao et al., 2006). On the contrary, the ionic gelation method, cross-linked polymer chains by TPP to form reticular structure in which insulin could be captured and electrostatically interacted with remained positively charged polymers. That means the interaction between polymer and insulin could be impaired by TPP molecules. Therefore, the polyelectrolyte complexation is an efficient way to improve the stability of insulin.

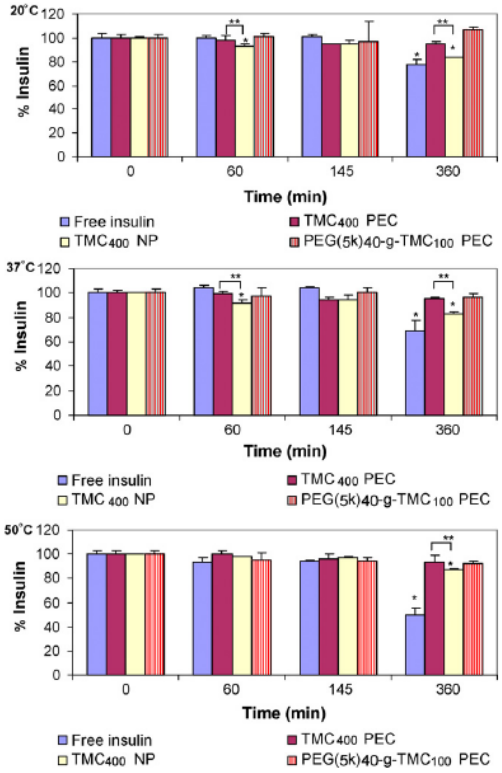

Fig. 4. Stability of insulin in TMC400 PEC, TMC400 NP and PEG(5k)40-*g*-TMC(100) PEC at different temperatures. *Statistically significant differences from the values of at 0 min ($p < 0.05$). **Statistically significant differences from the values of TMC400 PEC ($p < 0.05$).

3.6. Insulin protection from enzymatic degradation

To evaluate the potential role of PEC and NP in protecting insulin from enzyme presence in the digestive tract, the enzymatic stability of insulin was investigated in the presence of serine protease, trypsin. Fig. 5 depicts the residual amount of insulin after incubation of insulin alone and insulin associated PEC and NP with trypsin.

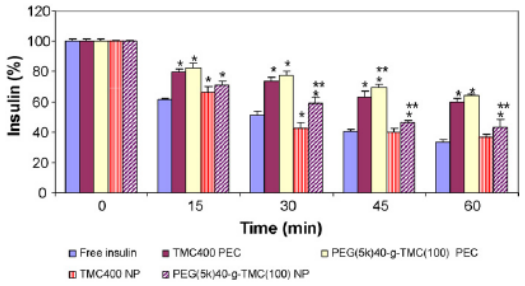

Fig. 5. Enzymatic degradation of insulin by trypsin. Each value represents the mean ± S.D. of three experiments. The initial concentrations of insulin and trypsin were 450 μg/ml and 300 BAEE IU/ml, respectively. TMC400 PEC = [P]/[Ins] of 0.3:1, TMC400 NP = [P]/[Ins]/[TPP] of 1:1:0.2, PEG(5k)$_{40}$-*g*-TMC(100) PEC = [P]/[Ins] of 1:1, PEG(5k)$_{40}$-*g*-TMC(100) NP = [P]/[Ins]/[TPP] of 2:1:0.2. *Statistically significant differences from the values of free insulin ($p < 0.05$). **Statistically significant differences from the values of TMC400 ($p < 0.05$).

Compared to free insulin solution, partial protection of insulin from trypsin digestion was observed with PEC ($p < 0.05$) and the protective effect of PEG(5k)$_{40}$-*g*-TMC(100) PEC was higher than TMC400 PEC ($p < 0.05$). With NP, it seemed that TMC400 NP did not protect insulin from trypsin digestion under similar conditions ($p > 0.05$) and the presence of TPP accelerated the degradation of insulin which can be seen from an increasing in degraded insulin with increased TPP concentration (data not shown). A linear relationship was observed between TPP concentration and degradation rate of insulin with correlation coefficient of 0.9856. Although PEG(5k)$_{40}$-*g*-TMC(100) NP could protect insulin from trypsin digestion ($p < 0.05$), the protective effect was much lower compared to its PEC ($p < 0.05$), probably as a consequence of the loose interaction of polymer and insulin by TPP. Bernkop-Schnürch and Dundalek (1996) observed that trypsin penetrated and digested proteins in NP.

We also examined the possible inhibitory effects of polymers on trypsin. At the polymer concentration corresponding to the concentration in PEC and NP, all polymers did not affect the trypsin activity (data not shown) which agrees well with previously reports (Kotźe et al., 1997; Leuβen et al., 1997). This indicated that the protective effect is unlikely due to inhibition of trypsin's activity but probably due to a shielding effect of polymer on insulin. This shielding effect is achieved through polymer/insulin interaction. Similarly, Malkov et al. (2005) reported insulin could be protected from trypsin digestion by binding of *N*-[8-(2-hydroxybenzoyl)amino]caprylate (SNAC) to insulin. Akiyoshi et al. (1998) also found the complexed insulin with cholesterol-bearing pullulan (CHP) was significantly protected from enzymatic degradation by α-crymotrypsin. Attack of the enzyme was effectively prevented because insulin was tightly complexed to the CHP self-aggregate.

When considering polymer structures, The protective effect of PEG(5k)$_{40}$-*g*-TMC(100) was higher than that of TMC400 both in PEC and NP ($p < 0.05$), probably due to a consequence of the steric effect of polyethylene glycol segments that hinders the enzyme access to the protein (Iwanaga et al., 1997; Yeh, 2000). These results are in agreement with observation made by Mao et al. (2006), suggesting that PEGylated TMC copolymers could improve the stability of insulin in PEC due to hydrophilic PEG chains. Taking all the above results into consideration, complexation with PEGylated TMC copolymers are a promising strategy for insulin carriers.

4. Conclusions

Self-assembled insulin PEC and NP were formed using TMC and PEGylated TMC copolymer. NP exhibited a bigger particle size and lower zeta potential than PEC at the same polymer/insulin mass ratio. The highest AE of NP with narrow size distribution was achieved at specific TPP amount depending on the polymer structure and the polymer/insulin (+/−) charge ratio. PEC showed higher stability in pH 6.8 simulated intestinal fluid than NP prepared at the same condition. PEC also protected associated insulin from degradation even at 50 °C and in the presence of trypsin more efficiently than NP. In addition, it was found that all polymers did not affect the activity of trypsin. Based on the results obtained, it was reasonable to assume that polymer/insulin (+/−) charge ratio played an important role in forming PEC and NP. Stable, uniform, spherical PEC and NP with high insulin AE could be formed at or close to optimal polymer/insulin (+/−) charge ratio, depending on the polymer structure. Physical stability of particles and associated insulin in PEC and NP depended on the electrostatic interactions between positively charged polymers and negatively charged insulin. These studies have contributed much to the understanding of PEC and NP formation with insulin.

In summary, polyelectrolyte complexation seems to be a potentially useful technique for fabricating insulin delivery systems for peroral administration. The mucoadhesive properties of PEC will be further studied.

Acknowledgements

The authors would like to acknowledge the Thailand Research Fund (TRF) through the Royal Golden Jubilee Ph.D. program (Grant No.PHD/0226/2545) and the German Academic Exchange Service (Deutsche Akademische Austauschdienst, DAAD) for financial support.

References

Akiyoshi, K., Kobayashi, S., Shichibe, S., Mix, D., Baudys, M., Kim, S.W., Sunamoto, J., 1998. Self-assembled hydrogel nanoparticle of cholesterol-bearing pullulan as a carrier of protein drugs: complexation and stabilization of insulin. J. Controlled Release 54, 313–320.

Berger, J., Reist, M., Mayer, J.M., Felt, O., Gurny, R., 2004. Structure and interactions in chitosan hydrogels formed by complexation or aggregation for biomedical applications. Eur. J. Pharm. Biopharm. 57, 35–52.

Bernkop-Schnürch, A., Dundalek, K., 1996. Novel bioadhesive drug delivery system protecting (poly)peptides from gastric enzymatic degradation. Int. J. Pharm. 138, 75–83.

Boonsongrit, Y., Mitrevej, A., Mueller, B.W., 2006. Chitosan drug binding by ionic interaction. Eur. J. Pharm. Biopharm. 62, 267–274.

Brange, J., Langkjaer, L., 1992. Chemical stability of insulin. 3: Influence of excipients, formulation, and pH. Acta Pharm. Nord. 4, 149–158.

Calvo, P., Remunan-Lopez, C., Vila-Jato, J.L., Alonso, M.J., 1997. Novel hydrophilic chitosan-polyethylene oxide nanoparticles as protein carriers. J. Appl. Polym. Sci. 63, 125–132.

Carino, G.P., Jacob, J.S., Mathiauty, E., 2000. Nanosphere based on oral insulin delivery. J. Controlled Release 65, 261–269.

Damagé, C., Vonderscher, J., Marbach, P., Pinget, M., 1997. Poly(alkyl-cyanoacrylate) nanocapsules as a delivery system in the rat for octreotide, a long-acting somatostatin analogue. J. Pharm. Pharmacol. 49, 949–954.

Dyer, A.M., Hinchcliffe, M., Watts, P., Castile, J., Jabbal-Gill, I., Nankervis, R., Smith, A., Illum, L., 2002. Nasal delivery of insulin using novel chitosan based formulations: a comparative study in two animal models between simple chitosan formulations and chitosan nanoparticles. Pharm. Res. 19, 998–1008.

Fredheim, G.E., Christensen, B.E., 2003. Polyelectrolyte complexes: interactions between lignosulfonate and chitosan. Biomacromolecules 4, 232–239.

Frokjaer, S., Otzen, D.E., 2005. Protein drug stability: a formulation challenge. Nat. Rev. Drug Disc. 4, 298–306.

Grenha, A., Seijo, B., Remuñán-López, C., 2005. Microencapsulated chitosan nanoparticles for lung protein delivery. Eur. J. Pharm. Sci. 25, 427–437.

Hamman, J.H., Schultz, C.M., Kotźe, A.F., 2003. *N*-trimethyl chitosan chloride: optimum degree of quaternization for drug absorption enhancement across epithelial cells. Drug Dev. Ind. Pharm. 29, 161–172.

Iwanaga, K., Ono, S., Narioka, K., Morimoto, K., Masawo, K., Yamasita, S., Nange, M., Oku, N., 1997. Oral delivery of insulin by using surface coating

liposomes: improvement of stability of insulin in GI tract. Int. J. Pharm. 157, 73–80.

Janes, K.A., Alonso, M.J., 2003. Depolymerized chitosan nanoparticles for protein delivery: preparation and characterization. J. Appl. Polym. Sci. 88, 2769–2776.

Knaul, J.Z., Hudson, S.M., Creber, K.A.M., 1999. Improved mechanical properties of chitosan fibers. J. Appl. Polym. Sci. 72, 1721–1732.

Kotźe, A.F., de Leeuw, B.J., Leuβen, H.L., de Boer, A.G., Verhoef, J.C., Junginger, H.E., 1997. Chitosans for enhanced delivery of therapeutic peptides across intestinal epithelial: in vitro evaluation in Caco-2 cell monolayers. Int. J. Pharm. 159, 243–253.

Kotźe, A.F., Thanou, M.M., Lueßen, H.L., de Boer, B.G., Verhoef, J.C., Junginger, H.E., 1999. Effect of the degree of quaternization of *N*-trimethyl chitosan chloride on the permeability if intestinal epithelial cells (Caco-2). Eur. J. Pharm. Biopharm. 47, 269–274.

Lenaerts, V., Couvreur, P., Grislain, L., Maincent, P., 1990. Nanoparticles as a gastroadhesive drug delivery system. In: Lenaerts, V., Gurny, R. (Eds.), Bioadhesive Drug Delivery Systems. CRC Press, Florida, pp. 93–104.

Leuβen, H.L., Rentel, C.O., Kotźe, A.F., Lehr, C.M., de Boer, A.G., Verhoef, J.C., Junginger, H.E., 1997. Mucoadhesive polymers in peroral peptide drug delivery. IV: Polycarbophil and chitosan are potent enhancers of peptide transport across intestinal mucosae in vitro. J. Controlled Release 45, 14–23.

Ma, Z., Yeoh, H.K., Lim, L.-Y., 2002. Formulation pH modulated the interaction of insulin with chitosan nanoparticles. J. Pharm. Sci. 91, 1396–1404.

MacLaughlin, F.C., Mumper, R.J., Wang, J., Tagliaferri, J.M., Gill, I., Hinchcliffe, M., Rolland, A.P., 1998. Chitosan and depolymerized chitosan oligomers as condensing carriers for in vivo plasmid delivery. J. Controlled Release 56, 259–272.

Malkov, D., Angelo, R., Wang, H., Flanders, E., Tang, H., Gomez-Orellana, I., 2005. Oral delivery of insulin with the eligen® technology: mechanistic studies. Curr. Drug Deliv. 2, 191–197.

Mao, H., Roy, K., Troung-Le, V.L., Janes, K.A., Lin, K.Y., Wang, Y., August, J.T., Leong, K.W., 2001. Chitosan-DNA naoparticles as gene carriers: synthesis, characterization and transfection efficiency. J. Controlled Release 70, 399–421.

Mao, S., Shuai, X., Unger, F., Simon, M., Bi, D., Kissel, T., 2004. The depolymerization of chitosan: effects on physicochemical and biological properties. Int. J. Pharm. 281, 45–54.

Mao, S., Germershaus, O., Fischer, D., Linn, T., Schnepf, R., Kissel, T., 2005a. Uptake and transport of PEG-*graft*-trimethyl-chitosan copolymer-insulin nanocomplexes by epithelial cells. Pharm. Res. 22, 2058–2068.

Mao, S., Shuai, X., Unger, F., Wittmar, M., Xie, X., Kissel, T., 2005b. Synthesis, characterization and cytotoxicity of poly(ethylene glycol)-*graft*-trimethyl chitosan block copolymer. Biomaterials 26, 6343–6356.

Mao, S., Bakowsky, U., Jintapattanakit, A., Kissel, T., 2006. Self-assembled polyelectrolyte nanocomplexes between chitosan derivatives and insulin. J. Pharm. Sci. 95, 1035–1048.

Morishita, M., Norishita, I., Takayama, K., Machida, Y., Nagai, T., 1992. Novel oral microspheres of insulin with protease inhibitor protecting from enzymatic degradation. Int. J. Pharm. 78, 1–7.

Morishita, M., Morishita, I., Takayama, K., Machida, Y., Nagai, T., 1993. Site-dependent effect of aprotinin, sodium caprate, Na_2EDTA and sodium glycocholate on the intestinal absorption of insulin. Biol. Pharm. Bull. 16, 68–72.

Nakashima, K., Miyagi, M., Goto, K., Matsumolto, Y., Ueoka, R., 2004. Enzymatic and hyperglycemia stability of chemically modified insulins with hydrophobic acyl groups. Bioorg. Med. Chem. Lett. 14, 481–483.

Owens, D.R., Zinman, B., Bolli, G., 2003. Alternative routes of insulin delivery. Diab. Med. 20, 886–898.

Pan, Y., Li, Y., Zhao, H., Zheng, J., Xu, H., Wei, G., Hao, J., Cui, F., 2002a. Bioadhesive polysaccharide in protein delivery system: chitosan nanoparticles improve the intestinal absorption of insulin in vivo. Int. J. Pharm. 249, 139–147.

Pan, Y., Zheng, J., Zhao, H., Li, Y., Xu, H., Wei, G., 2002b. Relationship between drug effects and particle size of insulin-loaded bioadhesive microspheres. Acta. Pharmacol. Sin. 23, 1051–1056.

Polnok, A., Verhoef, J.C., Borchard, G., Sarisuta, N., Junginger, H.E., 2004a. In vitro evaluation of intestinal absorption of desmopressin using drug-delivery systems based on superporous hydrogels. Int. J. Pharm. 269, 303–310.

Polnok, A., Verhoef, J.C., Sarisuta, N., Junginger, H.E., 2004b. Influence of methylation process on the degree of quaternization of *N*-trimethyl chitosan chloride. Eur. J. Pharm. Biopharm. 57, 77–83.

Ponchel, G., Irache, J.-M., 1998. Specific and non-specific bioadhesive particulate systems for oral delivery to the gastrointestinal tract. Adv. Drug Deliv. Rev. 34, 191–219.

Sakuma, S., Ishida, Y., Sudo, R., Suzuki, N., Kikuchi, H., Hiwatari, K., Kishida, A., Akashi, M., Hayashi, M., 1997. Stabilization of salmon calcitonin by polystyrene nanoparticles having surface hydrophilic chains, against enzymatic degradation. Int. J. Pharm. 159, 181–189.

Sandri, G., Rossi, S., Bonferoni, M.C., Ferrari, F., Zambito, Y., Di Colo, G., Caramella, C., 2005. Buccal penetration enhancement properties of *N*-trimethyl chitosan: Influence of quaternization degree on absorption of a high molecular weight molecule. Int. J. Pharm. 297, 146–155.

Shi, H.G., Farber, L., Michaels, J.N., Dickey, A., Thompson, K.C., Shelukar, S.D., Hurter, P.N., Reynolds, S.D., Kaufman, M.J., 2003. Characterization of crystalline drug nanoparticles using atomic force microscopy and complementary techniques. Pharm. Res. 20, 479–484.

Simon, A., Wittmar, M., Bakowsky, U., Kissel, T., 2004. Self-assembling nanocomplexes from insulin and water-soluble branched polyesters, poly[(vinyl-2-(diethylamino)-propylcarbamate-*co*-(vinyl acetate)-*co*-vinyl alcohol)]-*graft*-poly(L-lactic acid): a novel carrier for transmucosal delivery of peptides. Bioconjug. Chem. 15, 841–849.

Snyman, D., Hamman, J.H., Kotzé, A.F., 2003. Evaluation of the mucoadhesive properties of *N*-trimethyl chitosan chloride. Drug Dev. Ind. Pharm. 29, 61–69.

Snyman, D., Kotzé, A.F., Walls, T.H., Govender, T., Lachmann, G., 2004. Conformational characterization of quaternised chitosan polymers. Proc. Int. Symp. Controlled Release Bioact. Mater. 31, 211.

Takeuchi, H., Yamamoto, H., Kawashima, Y., 2001. Mucoadhesive nanoparticulate systems for peptide drug delivery. Adv. Drug Deliv. Rev. 47, 39–54.

Thanou, M., Florea, B.I., Langemeyer, M.W., Verhoef, J.C., Junginger, H.E., 2000a. *N*-trimethylated chitosan chloride (TMC) improves the intestinal permeation of the peptide drug buserelin in vitro (Caco-2 cells) and in vivo (rats). Pharm. Res. 17, 27–31.

Thanou, M., Verhoef, J.C., Marbach, P., Junginger, H.E., 2000b. Intestinal absorption of octreotide: *N*-trimethyl chitosan chloride (TMC) ameliorates the permeability and absorption properties of the somatostatin analogue in vitro and in vivo. J. Pharm. Sci. 89, 951–957.

Tsuchida, E., Takeoka, S., 1994. Interpolymer Complexes and their Ion-conduction, Macromolecule Complexes in Chemistry and Biology. Springer-Verlag, Berlin/Heidelberg.

van de Merwe, S.M., Verhoef, J.C., Kotzé, A.F., Junginger, H.E., 2004. *N*-trimethyl chitosan chloride as absorption enhancer in oral peptide drug delivery. Development and characterization of minitablet and granule formulations. Eur. J. Pharm. Biopharm. 57, 85–91.

van de Weert, M., Hennink, W.E., Jiskoot, W., 2000. Protein instability in Poly(lactic-*co*-glycolic acid) microparticles. Pharm. Res. 17, 1159–1167.

Yamamoto, A., 1994. Effects of various protease inhibitors on the intestinal absorption and degradation of insulin in rats. Pharm. Res. 11, 1496–1500.

Yeh, M., 2000. The stability of insulin in biodegradable microspheres based on blends of lactide polymers and poly (ethylene glycol). J. Microencapsul. 17, 743–756.

European Journal of Pharmaceutics and Biopharmaceutics 70 (2008) 563–571

Contents lists available at ScienceDirect

European Journal of Pharmaceutics and Biopharmaceutics

journal homepage: www.elsevier.com/locate/ejpb

Research paper

Physicochemical properties and biocompatibility of *N*-trimethyl chitosan: Effect of quaternization and dimethylation

Anchalee Jintapattanakit [a,b], Shirui Mao [b,c], Thomas Kissel [b], Varaporn Buraphacheep Junyaprasert [a,*]

[a] Department of Pharmacy, Faculty of Pharmacy, Mahidol University, Bangkok, Thailand
[b] Department of Pharmaceutics and Biopharmacy, Philipps-Universität, Marburg, Germany
[c] School of Pharmacy, Shenyang Pharmaceutical University, Shenyang, China

ARTICLE INFO

Article history:
Received 11 December 2007
Accepted in revised form 8 June 2008
Available online 17 June 2008

Keywords:
N-trimethyl chitosan
Degree of quaternization
Degree of dimethylation
Solubility
Mucoadhesive properties
Cytotoxicity

ABSTRACT

The aim of this research was to investigate the effect of degrees of quaternization (DQ) and dimethylation (DD) on physicochemical properties and cytotoxicity of *N*-trimethyl chitosan (TMC). TMC was synthesized by reductive methylation of chitosan in the presence of a strong base at elevated temperature and polymer characteristics were investigated. The number of methylation process and duration of reaction were demonstrated to affect the DQ and DD. An increased number of reaction steps increased DQ and decreased DD, while an extended duration of reaction increased both DQ and DD. The molecular weight of TMC was in the range of 60–550 kDa. From the Mark–Houwink equation, it was found that TMC in 2% acetic acid/0.2 M sodium acetate behaved as a spherical structure, approximating a random coil. The highest solubility was found with TMC of an intermediate DQ (40%) regardless of DD and molecular weight. The effect of DD on the physicochemical properties and cytotoxicity was obviously observed when proportion of DD to DQ was higher than 1. TMC with relatively high DD showed reduction in both solubility and mucoadhesion and hence decreased cytotoxicity. However, the influence of DD was insignificant when DQ of TMC was higher than 40% at which physicochemical properties and cytotoxicity were mainly dependent upon DQ.

1. Introduction

N,N,N-trimethyl chitosan (TMC) is a partially quaternized derivative of chitosan first synthesized by Muzzarelli and Tanfani [1] in an attempt to increase solubility of chitosan in water at neutral and basic pH values. The increase in solubility is achieved by replacing the primary amino group on the C-2 position of chitosan with quaternary amino groups [2]. It has been shown that TMC can decrease the TEER of Caco-2 cell monolayers and increase the transport of several hydrophilic compounds, peptide and protein drugs both *in vitro* (Caco-2 cells) [3–6] and *in vivo* (rats and pigs) [7–9]. Up to date, TMC has received considerable attention in drug and gene delivery not only in peroral route [10] but also in ocular [11], intranasal [12–14], buccal [15,16], pulmonary [17,18] and rectal [19] routes.

It is well known that polymer structure is a main factor influencing its physicochemical properties. Several research groups have studied the structure–physicochemical property relationship of TMC and reported that the properties of TMC depend on degree of quaternization (DQ) at 2-amino groups and degree of *O*-methylation at 3- and 6-hydroxy groups (DO_3 and DO_6, respectively) [6,20,21]. The best permeation enhancement of peptide and protein drugs is achieved when using TMC with DQ ca. 48% [6]. Moreover, high DO_3 and DO_6 found in TMC with high DQ decrease the solubility of the polymer [20]. Although mucoadhesive properties and cytotoxicity of TMC with different DQ have been explored, the results are controversial. Synman et al. [21,22] found that the mucoadhesive properties of TMC decreased with an increase in DQ, whereas Sandri et al. [15] reported the opposite results. Regarding the cytotoxicity, Thanou et al. [23], Amidi et al. [13] and Florea et al. [17] indicated that TMC was non-toxic even at high DQ. However, Mao et al. [24] found that TMC with DQ of 40% exhibited time- and dose-dependent cytotoxic responses which increased with increasing molecular weight. Similar results had been found by Kean et al. [25] who showed that the cytotoxicity of TMC increased with increasing DQ. These discrepancies may be attributed to different degrees of dimethylation (DD) of TMC. TMC with the same DQ but different in DD may show different properties in the mucoadhesion and cytotoxicity. In general, the mucoadhesion and cytotoxicity of TMC can probably be attributed to the interaction between positively charged groups of TMC and anionic components (sialic acid) of the glycoproteins in mucus layer and on the surface of epithelial cells [24]. We hypothesized

* Corresponding author. Department of Pharmacy, Faculty of Pharmacy, Mahidol University, 447 Sri-Ayutthaya Road, Bangkok 10400, Thailand. Tel.: +66 2644 8677 91; fax: +66 2644 8694.
E-mail address: pyvbp@mahidol.ac.th (V.B. Junyaprasert).

0939-6411/$ - see front matter © 2008 Elsevier B.V. All rights reserved.
doi:10.1016/j.ejpb.2008.06.002

that an increase in DD aside from DQ may affect the interaction of polymer and mucus layer/epithelial cells, resulting in the reduction in mucoadhesion and cytotoxicity. However, to the best of our knowledge, no experimental data are available to support this hypothesis. Therefore, the influence of the DQ together with the DD on the mucoadhesive properties and cytotoxicity was simultaneously elucidated.

In this present study, TMC with different DQ and DD was synthesized and characterized. The influence of synthesis process resulting in different DQ and DD was also investigated. The mucoadhesion of TMC was determined using a mucin particle method. The biocompatibility of TMC was characterized by MTT assay using a L929 fibroblast cell line.

2. Materials and methods

2.1. Materials

Chitosan (400 kDa, degree of deacetylation 84.7%) was purchased from Fluka (Steinheim, Germany). Type III mucin from procine stomach and 3-(4,5-dimethyl-thiazol-2-yl)-2,5-diphenyl tetrazolium bromide (MTT) were obtained from Sigma (Deisenhofen, Germany). Dulbecco's modified Eagle's medium (DMEM) was supplied by Gibco (Eggenstein, Germany). Tissue culture materials and plates were from Costar (Bodenheim, Germany). All other chemicals and solvents were of analytical purity.

2.2. Synthesis of N,N,N-trimethyl chitosan chloride

TMC polymers differing in DQ and DD were prepared by reductive methylation of the parent chitosan with CH_3I in the presence of NaOH using the procedure described by Polnok et al. [26] with some modifications. Briefly, in the reaction step 1, a mixture of chitosan, NaI, 15% NaOH was mixed with *N*-methylpyrrolidinone while maintained in a water bath at 60 °C. Subsequently, CH_3I was added to the mixture and the reaction was carried out in the presence of a reflux condenser. Prior to the precipitation of the product from the solution mixture at the end of first reaction step, additional CH_3I and 15% NaOH were added. The reaction was further continued (addition step). In some instances, the precipitated polymer obtained from the first reaction step was mixed with NaI, NaOH in *N*-methylpyrrolidinone. CH_3I was added to the mixture and the reaction was carried out in the presence of a reflux condenser (second reaction step). The product (*N*-trimethyl chitosan iodide) was precipitated and converted to *N*-trimethyl chitosan chloride according to the previously described processes [20]. The reaction conditions of each polymer are summarized in Table 1. For ease of discussion, the abbreviation TMC*x*–*y* was used to describe the polymers where *x* represents the DQ in percent and *y*, the DD in percent.

Table 1
The reaction conditions in the synthesis of TMC polymers

Polymer	Reaction step 1[a] (h)	Reaction step 2[b] (h)	Addition step 1[c] (h)	Addition step 2[c] (h)
TMC10-40	1	–	–	–
TMC20-20	1	–	0.5	–
TMC20-60	1.5	–	–	–
TMC40-10	1	1	–	–
TMC40-40	1.5	–	1.5	–
TMC80-10	1	–	1	1

[a] Twelve milliliters of 15% NaOH added with 12 ml CH_3I in *N*-methylpyrrolidinone containing 2 g chitosan and 4.8 g NaI.
[b] Twelve milliliters of 15% NaOH and 0.6 g NaOH added with 9 ml CH_3I in *N*-methylpyrrolidinone containing precipitated product from first reaction step and 4.8 g NaI.
[c] Added with 12 ml of 15% NaOH and 6 ml CH_3I.

2.3. Characterization of TMC polymer

2.3.1. Degrees of substitution

^{1}H NMR spectra of TMC polymers were recorded on JEOL GX 400D (Tokyo, Japan) by dissolving samples in D_2O at 80 °C with suppression of the water peak. The degrees of substitution corresponding to %DQ, %DD, $\%DO_3$ and $\%DO_6$ were calculated from the data obtained from ^{1}H NMR spectra using the Eqs. (1)–(4) [20] as described below:

$$\%DQ = \left[\frac{[(CH_3)_3]}{[H]} \times \frac{1}{9}\right] \times 100 \quad (1)$$

$$\%DD = \left[\frac{[(CH_3)_2]}{[H]} \times \frac{1}{3}\right] \times 100 \quad (2)$$

$$\%DO_3 = \left[\frac{[(3\text{-}OCH_3)]}{[H]} \times \frac{1}{3}\right] \times 100 \quad (3)$$

$$\%DO_6 = \left[\frac{[(6\text{-}OCH_3)]}{[H]} \times \frac{1}{3}\right] \times 100 \quad (4)$$

where $[(CH_3)_3]$ is the integral of trimethyl amino group at 3.3 ppm, $[(CH_3)_2]$ is the integral of dimethyl amino group at 3.0 ppm, $[(3\text{-}OCH_3)]$ is the integral of methyl group for 3-hydroxyl group at 3.5 ppm, $[(6\text{-}OCH_3)]$ is the integral of methyl group for 6-hydroxyl group at 3.4 ppm and [H] is the integral of the ^{1}H peaks between 4.7 and 5.7 ppm.

2.3.2. Determination of molecular weight

Weight-average molecular weight (M_w), number-average molecular weight (M_n) and molecular weight distribution (M_w/M_n) of TMC were determined by a gel permeation chromatography (GPC) (Water Corporation, Washington, USA) at 30 °C. The GPC equipment consisted of ultrahydrogel linear column (MW resolving range = 1000–20,000,000), Waters 600E pump and Water 2410 refractive index detector. The eluent was 0.5 M acetate buffer. The standards used to calibrate the column were pullulans (MW 5900–788,000).

2.3.3. Intrinsic viscosity measurement

Intrinsic viscosities [η] of TMC were determined in 2% acetic acid/0.2 M sodium acetate (2% HAc/0.2 M NaAc) using an automated Ubbelohde capillary viscometer (Model Schott AVS-360, Germany) with a 0.63-mm capillary diameter at 25 ± 0.1 °C in triplicate. Solution concentrations were adjusted in order to obtain relative viscosity value in the range of 1.1–1.5 which was suitable for the calculation of [η] [27]. Six different concentrations were tested for each sample and each concentration was measured five times. The running times of solution and solvent were used to calculate the specific viscosity, reduced viscosity and inherent viscosity. In order to obtain the most accurate values, [η] was determined as an average of extrapolating both Huggins ($\eta_{sp}/c \sim c$) and Kraemer ($\eta_{inh} \sim c$) plots on the ordinate at $c = 0$ [28].

2.3.4. Determination of potentiometric titration curve

Potentiometric titration curve of TMC was constructed by dissolving 20 mg of polymer in 2 ml of 0.1 N HCl solution. A titrant was a solution of 0.1 N NaOH. Under continuous stirring, titrant was added stepwise and the volume of added NaOH and pH values of solution were recorded thoroughly [11].

2.4. Estimation of water solubility

The pH dependence of the water solubility of TMC was estimated using turbidity measurements. The test sample was dissolved in 0.1 N HCl solution. With the stepwise addition of 0.1 or 1.0 N NaOH solution, the transmittance of the solution was recorded on a Shimadzu UV-160 Spectrophotometer using a quartz cell with an optical path length of 10 mm at 600 nm. The test

was performed at room temperature [29]. In order to investigate the effect of ionic strength, the solutions of 0.1 N HCl and 1.0 N NaOH solutions were adjusted by sodium chloride (NaCl) to achieve the desired ionic strength of 0.05, 0.15 and 0.5 M.

2.5. Mucoadhesion by mucin particle method

Mucoadhesive properties of TMC were evaluated by using the mucin particle method developed by Takeuchi et al. [30]. Submicron-sized mucin (ss-mucin) suspension (1% w/v) was prepared by suspending and continuously stirring mucin type III powder in 10 mM Tris buffer, pH 6.8, for 10 h. Mucin suspension was then incubated at 37 °C overnight. The size of mucin was reduced by ultrasonication (Branson 1200, Connecticut, USA) until particle size was around 300–400 nm. It was then centrifuged at 4000 rpm for 20 min to extract submicron-sized mucin particles in the supernatant portion. The particle size and zeta potential of the precisely size-controlled ss-mucin were 400 ± 12 nm and −16.1 ± 1.8 mV, respectively.

One milliliter of 1% w/v ss-mucin suspension was mixed with different volumes of 1 mg/ml polymer solutions under mild magnetic stirring. Then the particle size and zeta potential values were measured using a Zetasizer Nano ZS (Malvern Instruments, Herrenberg, Germany) equipped with a 4 mW HeNe laser at a wavelength of 633 nm at 25 °C. Scattered light was detected at a 173 °C backward scattering angle. The viscosity (0.88 mPa S) and refractive index (1.33) of water at 25 °C were used for data analysis. All experiments were performed in triplicate.

2.6. Cytotoxicity testing (MTT assay)

In vitro cytotoxicity of TMC was evaluated using a MTT assay according to the method described by Fischer et al. [31]. A mouse connective tissue fibroblast cell line, L929 (DSMZ, Braunschweig, Germany) was plated into 96-well microtiter plates at a density of 8000 cells/well. After 24 h incubation, culture medium was replaced by 100 μl of serial dilutions of the polymers in serum-supplemented tissue culture medium and the cells were incubated for 3 h. Subsequently, polymer solutions were aspirated and replaced by 200 μl DMEM without serum. Twenty microliters sterile-filtered MTT stock solution in phosphate-buffered saline (PBS), pH 7.4 (5 mg/ml) were added in each well reaching a final concentration of 500 g MTT/ml. After 4 h incubation, unreacted dye was aspirated and the formazin crystals were dissolved in 200 μl/well DMSO. Absorption was measured at 570 nm with a background correction of 690 nm using a Titertek Plus MS 212 ELISA reader (ICN, Eschwege, Germany). The relative cell viability (%) compared to control wells containing cell culture medium without polymer was calculated by $[A]_{test}/[A]_{control} \times 100$ ($n = 4$). The IC_{50} was calculated as a polymer concentration which inhibited growth of 50% of cells relative to non-treated control cells.

2.7. Statistical analysis

Results were recorded as means ± SD from at least three measurements. Significance between the mean values was calculated using ANOVA one-way analysis (SPSS 11.5.0 for windows). Probability values of $P < 0.05$ were considered significant.

3. Results and discussion

3.1. Synthesis and characterization of TMC polymers

3.1.1. The degrees of substitution

In this study, TMC was synthesized based on one methylation reaction step followed by subsequent addition steps because it had been demonstrated that the high DQ of TMC with a low degree of *O*-methylation could be achieved as compared to the use of multiple reaction steps [26]. Moreover, it was time-saving owing to the reduction of certain in-process procedures – precipitation, centrifugation and drying of the intermediate product. The degrees of substitution of various TMC polymers are listed in Table 2.

As seen in Table 2, using a one-step reaction, TMC10-40 was obtained with 13.9% DQ and the high substitution degree of DD at 39.1%. When extending the reaction duration from 1 to 1.5 h, DQ increased to 23.4% and DD significantly increased to 65.2% (TMC20-60). However, when increasing additional step for 0.5 h, DQ increased to 23.0% similar to TMC20-60, whereas DD decreased to 20.8% (TMC20-20). Similarly, it was observed that by extending duration of additional step of TMC20-20 from 0.5 to 1 h, DQ of TMC increased from 23.0% to 32.1% and DD from 20.8% to 33.0% (data not shown), therefore, an increase in reaction duration increased both DQ and DD. Comparing between TMC10-40 and TMC40-10 as well as between TMC20-60 and TMC40-40, it was obviously seen that an increase of the number of reaction step increased DQ but decreased DD.

Fig. 1 shows the ^1H NMR spectra of TMC20-20 and TMC20-60. The ^1H signal intensity of dimethylamino group (–$N(CH_3)_2$) of TMC20-60 was stronger than that of TMC20-20. The ratio between the integral of the *N*-trimethylamino group ($N^+(CH_3)_3$) and that of the *N*-dimethylamino group ($N(CH_3)_2$) was approximately 1:3 for TMC20-60 and 1:1 for TMC20-20. The results obtained may be explained by the less basic environment and reduction of methylating agent, CH_3I in the extended reaction step of TMC20-60 which would slow down conversion of an intermediate $N(CH_3)_2$ to a $N^+(CH_3)_3$. Similarly, Curti et al. [32] reported that the *N*-methylation of chitosan or the average DQ was strongly affected by the reaction conditions, i.e. the alkalinity of the medium and the availability of CH_3I.

From the results obtained, it could be suggested that high DQ of TMC with low DD could be obtained by increasing the number of reaction steps, whereas high DQ of TMC with high DD was resulted by extending the duration of the reaction.

3.1.2. Molecular weight

A summary of the M_w and M_w/M_n determined by GPC of TMC polymers is presented in Table 2. All TMC had a relatively wide molecular weight distribution with a polydispersity index in the range of 2.9–4.9.

Although a decrease in molecular weight of TMC with increasing DQ was not distinctly observed as reported by Snyman et al. [33], it was found that the molecular weight depended on the synthesis procedure. It increased with the extension of reaction duration correlated to an increase in DQ and DD as seen in TMC10-40/TMC20-60 and TMC20-20/TMC40-40. Therefore, an addition of methyl groups to the amino groups of chitosan resulted in TMC with high molecular weight.

On the contrary, the molecular weight decreased with increasing number of reaction steps or additional steps as seen in TMC10-40/TMC20-20 and TMC20-60/TMC40-40. Moreover, the molecular weight of TMC40-10 prepared by two reaction steps was markedly decreased in comparison with TMC40-40 prepared by one reaction step followed by one additional step. This was due to the degradation of the polymer in the strong basic environment. The results obtained are consistent with those previously reported by Hamman and Kotze [34] who observed that intrinsic viscosity, an indication of the molecular weight, of TMC increased with increasing reaction duration and decreased with increasing number of reaction steps. Therefore, it can be concluded that the molecular weight of TMC is affected by the addition of methyl groups to the amino groups of chitosan and the polymer degradation by the strong basic environment.

Table 2
Intrinsic viscosity, molecular weight and substitution degrees of TMC polymers

Polymer	$[\eta]^a$ (dl/g)	$M_w{}^b$ ($\times 10^4$ g/mol)	$M_w/M_n{}^b$	DQ (%)	DD (%)	3O-CH_3 (%)	6O-CH_3 (%)
TMC10-40	2.18	37.8	4.86	13.9	39.1	2.4	7.0
TMC20-20	2.09	28.6	3.91	23.0	20.8	11.3	16.7
TMC20-60	2.48	54.2	4.74	23.4	65.2	3.9	9.0
TMC40-10	1.06	6.1	3.25	42.4	12.4	6.1	8.0
TMC40-40	2.15	36.5	2.89	39.0	39.3	4.9	9.3
TMC80-10	2.01	26.6	3.50	76.6	8.5	58.0	52.0

[a] $[\eta]$ for the starting chitosan was 10.70 dl/g.
[b] M_w and M_w/M_n for the starting chitosan were 87.2 $\times$ 10^4 g/mol and 3.50, respectively.

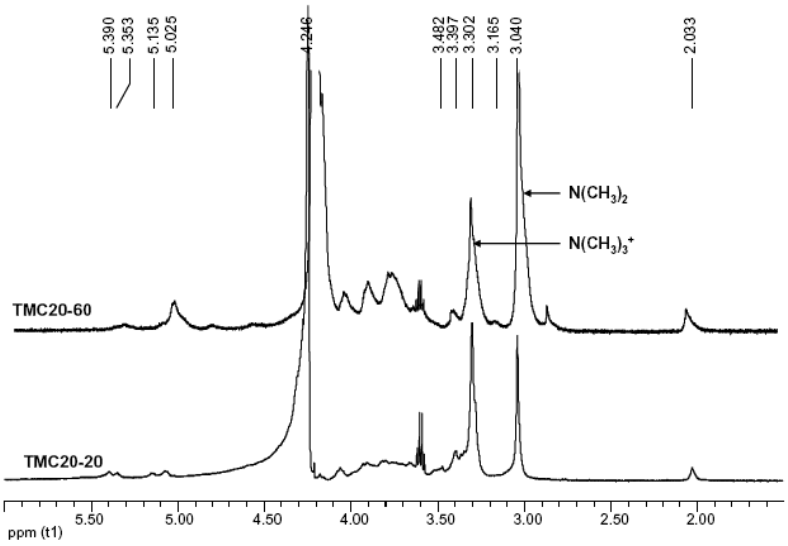

Fig. 1. ^{1}H NMR spectra of TMC20-60 and TMC20-20, prepared in one reaction step and one reaction step with one addition step, respectively.

3.1.3. Intrinsic viscosity

Based on the fact that $[\eta]$ is closely related to polymer-chain conformation, the dependence of $[\eta]$ upon the molecular weight gives information concerning the conformation and the extension of the polymer according to the Mark–Houwink equation

$$[\eta] = KM_v^a$$

where K and a are empirical constants for given solute–solvent system and temperature, $[\eta]$ is the intrinsic viscosity and M_v is the so-called viscosity-average molecular weight which can be substituted with the weight-average molecular weight, M_w. The Mark–Houwink exponent a is used as a parameter to determine the conformation of a polymer. Polymers in the shape of a sphere, random coil or rod have exponent a values of 0, 0.5–0.8 and 1.8, respectively [35,36].

The intrinsic viscosities of TMC in 2% HAc/0.2 M NaAc at 25 °C are given in Table 2. Regardless of the substitution degrees, it was found that the $[\eta]$ of polymer solution increased with an increase in the M_w of the polymer. This is consistent with the previous report by Snyman et al. [33] who observed that the decrease in absolute molecular weight was correlated well with the decreased $[\eta]$ of TMC polymers.

Fig. 2 shows the plot of log $[\eta]$ versus logM_w. The values of 0.39 and 2.14 $\times$ 10^{-4} were obtained for a and K, respectively. The value of Mark–Houwink exponent a suggested that TMC behaved like a spherical structure, approximating a random coil. The result is inconsistent with the observation of Synman et al. [22] who reported that TMC possessed a rod-shaped conformation. This discrepancy could be due to the difference in experimental conditions such as ionic strength, solvent, temperature, and pH value of solution [37,38].

In general, the polymer conformation and the polymer–solvent interactions depend on the number of positive charges (NH_3^+) of chitosan which are related to the degree of deacetylation. Low value of deacetylation degree results in a rigid conformation, leading to a higher degree of expansion of chitosan [28]. In the buffer of 2% HAc/0.2 M NaAc (pH 4.5), chitosan with deacetylation degree of 85% exhibits random coil structure [39]. TMC being a cationic polyelectrolyte with pK_a value of about 6.5 (data shown below), all non-quaternized amino groups are protonated at low pH of the solvent. In this case, electrostatic repulsion forces of the protonated amino groups were hindered due to pendent methyl groups of TMC, leading to the condensed conformation.

3.1.4. Potentiometric titration curves

A potentiometric titration is one of the simplest methods used to determine the degree of deacetylation of chitosan [40,41]. Recently, it has been used with data from elemental analysis to determine DQ of TMC polymers [11].

In this study, a titration curve was generated by dissolving TMC in HCl solution and then titrating potentiometrically with NaOH

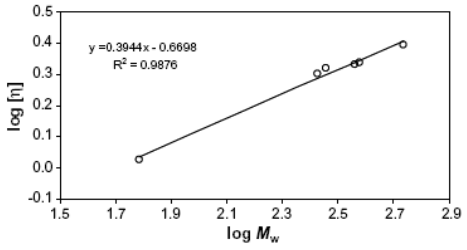

Fig. 2. Intrinsic viscosity of TMC in 2% HAc/0.2 M NaAc at 25 °C as a function of M_w determined by GPC.

solution. The potentiometric titration curve of TMC40-40, a representative example, is depicted in Fig. 3a exhibiting two inflection points. The first of which corresponds to the neutralization of the free acidity, while the second indicates the complete deprotonation of the protonated non-quaternized amine groups. The difference between the two inflection points along the abscissa (shown in Fig. 3b) yields the moles of OH^- required to deprotonate the protonated non-quaternized amino groups of TMC and reflects the amount of $-NH_2$, $-NH(CH_3)$ and $-N(CH_3)_2$ in the titrant solution. Assuming that the rest of the sample is $-N^+(CH_3)_3$ and $-NHCOCH_3$, the DQ value of the specimen could readily be obtained [11].

Since TMC was composed of not only quaternized amines but also mono- and di-methylated amines, it was found that the difference between the two inflection points was affected by DQ and DD. Number of OH^- required to deprotonate the protonated non-quaternized amino groups increased with increasing DD (2.47 mmol OH^-/g polymer for TMC20-20 compared to 2.63 mmol OH^-/g polymer for TMC20-60). When considering DD in the range 30–40%, number of OH^- required decreased linearly with the increase of DQ with regression coefficients of 0.98. Moreover, it was observed that at DD/DQ ratio <1, number of OH^- required decreased with increasing DQ with a linear correlation of 0.99. Therefore, DD would affect the number of OH^-, leading to an error for calculation of DQ. For an accurate result by this method, DQ should be determined and compared within almost the same value of DD or at DQ much higher than DD. In addition to the use of this method to determine DQ, the pK_a of all TMC polymers can be evaluated to be in the range of 6.1–6.4. During titration, the solution of TMC with DQ < 24% became cloudy when the pH >6, which was not found in higher DQ of TMC (discussed in detail in Section 3.2).

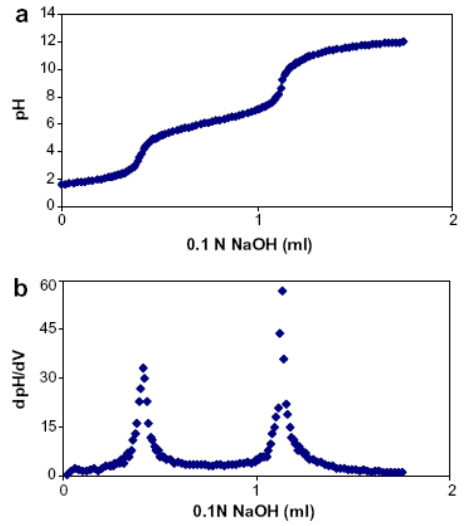

Fig. 3. The results from potentiometric titration of TMC40-40 showing (a) potentiometric titration curve and (b) first derivative curve.

It is well documented in the literature that results obtained from pH-potentiometric titration are influenced by several factors. Balazs and Sipos [42] reported that the moisture content of the air-dry chitosan samples and the ash content caused variations in the values of degree of deacetylation. The precipitation of chitosan during titration also resulted in an error in the determination of deacetylation degree [40]. The precipitated chitosan reduced the concentration and could cover the surface of electrode, and thus the electrode would lose its accuracy. From the limitation of pH-potentiometric titration and the results obtained in this study, it was found that this method would not be suitable for characterization of TMC polymer.

3.2. Solubility of TMC polymers

3.2.1. Effect of degree of quaternization

Fig. 4 shows the pH dependence of the transmittance of the TMC with different DQ. As seen in Fig. 4a, the water solubility of TMC with DQ of 13.9% (TMC10-40) was high at acidic pH but decreased at pH a little over neutrality. The solubility of TMC10-40 in basic pH was abruptly decreased when increasing concentration. In addition, it was observed that the solubility decreased with increasing DD in the basic region, especially when DD/DQ > 1 (data not shown). In contrast, the solubility of TMC with DQ of 42.4% (TMC40-10) was high and retained over a wide pH range (Fig. 4b). The water solubility of TMC was substantially decreased with DQ of 76.6% (TMC80-10), as seen by the low % transmittance (Fig. 4c). However, the solubility of the high DQ of TMC was not pH-dependent (Fig. 4b and c).

The results were comparable to the finding obtained from potentiometric titration mentioned before. The lower solubility of the high DQ of TMC (TMC80-10) was expected due to high degree of *O*-methylation at the 3- and 6-hydroxyl groups [20]. However, the opposite result was found in the low DQ of TMC as reported by Kotze et al. [43] who indicated that TMC with low DQ of 12.6% was highly soluble over a wide pH range even at high concentration of 10% w/v. This discrepancy may be from different DD of TMC. It is possible that the water solubility of TMC polymers with low DQ and relatively high DD decreased in an basic solution because they included about 65–75% of non-quaternized residues, mainly in forms of $-N(CH_3)_2$, $-NH(CH_3)$ and $-NH_2$. The high pendent methyl groups hinder intra- and/or intermolecular interactions resulting in the decreased solubility of the TMC with low DQ.

3.2.2. Effect of ionic strength

The effect of ionic strength on the water solubility of TMC was also investigated. Fig. 5 shows pH dependence of water solubility of TMC10-40 as a function of ionic strength. For TMC with low DQ (<24%), ionic strength did not affect the solubility of polymers at pH lower than their pK_a 6.5, after that the solubility decreased with increasing pH and ionic strength of the medium and the decrease was more pronounced in the higher ionic strength solution. On the other hand, the ionic strength did not affect the solubility of TMC with DQ higher than 40% (data not shown).

It is known that ionic strength affects the hydrodynamic behavior of chitosan and its derivatives. Yang et al. [44] reported that viscosities of *N*-alkylated mono-/disaccharide chitosans with low substitution degree decreased with an increase in ionic strength,

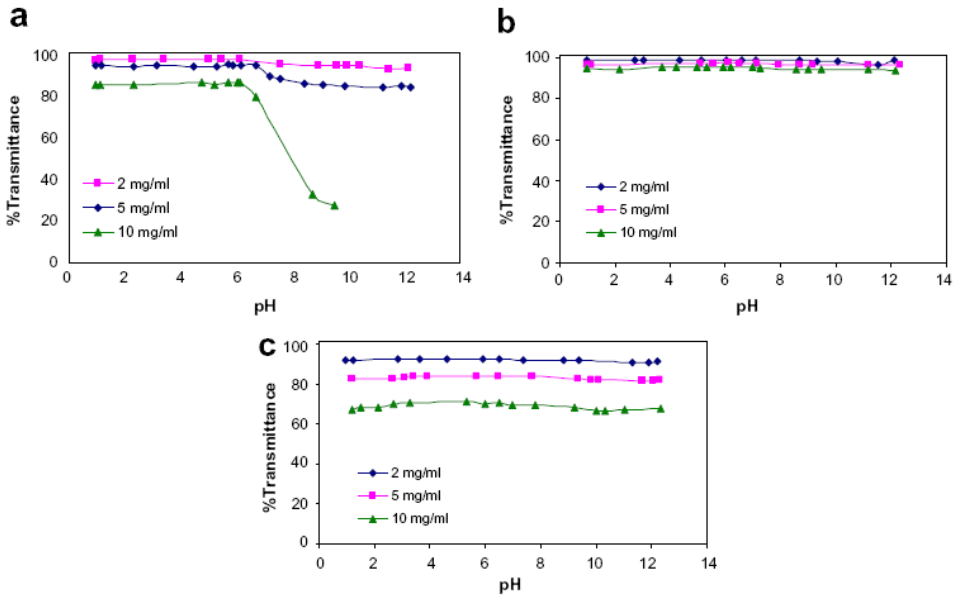

Fig. 4. The pH dependence of water solubility of (a) TMC10-40, (b) TMC40-10 and (c) TMC80-10.

while change in solubility of high substitution degree of chitosan with ionic strength was not marked. Holme and Perlin [45] also observed that ionic strength had an effect on the solubility of *N*-sulfated chitosan. Generally, in high ionic strength solutions, the concentration of the counter-ions is raised which screens the protonated amino group of chitosan and in turn the solubility becomes reduced [46]. This may provide some evidence to support the findings in our experiment.

Taken together, the data from Figs. 4 and 5 imply that the charge density of TMC, represented by DQ, would be an important factor determining its water solubility and the optimum value was an intermediate DQ of 30–40%. In addition, DD obviously affected the solubility properties of TMC when DQ was lower than 24%.

3.3. Polymer–mucin interactions

In this work, mucoadhesive properties of TMC were evaluated by using the mucin particle method based on the change in surface properties of mucin particle, particle size and zeta potential, by the adhesion of the polymer. It was expected that the suspension of ss-mucin particles when mixed with a polymer solution, would induce the ss-mucin particles to aggregate, if the polymer had a strong affinity to them. Procine gastric mucin type III, a commercially available mucin, was chosen in this study. Leitner et al. [47] stated that there is no significant difference in the results obtained with native mucus and hydrated commercial mucin.

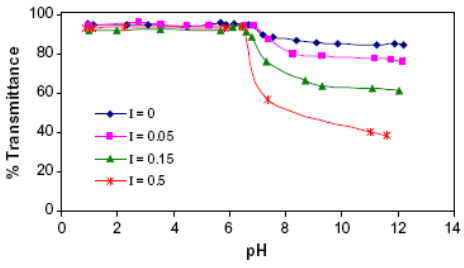

Fig. 5. Effect of ionic strength on the water solubility of 5 mg/ml TMC10-40.

The interaction was determined at pH 6.8 in Tris buffer where chitosan was insoluble and lost mucoadhesive properties. Fig. 6 shows evolution of particle size and zeta potential of ss-mucin particles versus added volume of 1 mg/ml TMC40-40 solution. Two regions could be defined. In region I, polymer did not affect the size and zeta potential of ss-mucin. Increases in size and zeta potential were observed in region II where the aggregation occurred after the zeta potential of ss-mucin exceeded the critical zeta potential of ss-mucin (ca. −7 mV). This finding can be explained by DLVO theory [48]. It was also found that all polymers with different DQ and DD exhibited equal volume of 0.4 ml in region I, indicating that this region was polymer structure independent. This could be explained from the same conformation of TMC polymers. The slope of zeta potential profiles in region II and an extrapolated critical volume (V_c) of polymer used to neutralize negative charge of ss-mucin to zero could be used as indices of mucin–polymer adhesive bond strength of TMC polymers. The stronger the mucoadhesive bond strength, the higher the value of slope as well as the lower the V_c value was observed.

By referring to the results of ss-mucin–polymer interaction studies (Table 3), it can be deduced that TMC exhibited mucoadhesive characteristic and the rank order of mucoadhesive bond strength of TMC was TMC80-10 > TMC20-20 > TMC40-40 > TMC40-10 > TMC10-40 > TMC20-60. Within the same molecular weight of polymer, it was found that the mucoadhesion of TMC depended on the proportion of DD to DQ. The mucoadhesive bond strength of TMC linearly decreased with increased ratio of DD/DQ, as shown in Fig. 7. At the same DD of 40%, the mucoadhesive

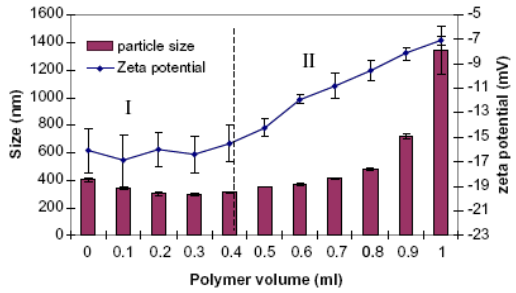

Fig. 6. Change in observed particle size and zeta potential of ss-mucin particles when mixed with the various volumes of 1 mg/ml TMC40-40 solution. Concentration of ss-mucin suspension was 1% w/v at pH 6.8.

bond strength of TMC40-40 was twofold higher than that of TMC10-40. Similarly, at the same DQ of 20%, the mucoadhesive bond strength of TMC20-60 was threefold lower than that of TMC20-20. The results obtained could be explained by the electrostatic interaction between positively charged amino groups of TMC and the negatively charged sialic acid residue of mucus glycoproteins or mucins. When increasing DD, the high number of methyl pendent groups acted to shield the positive charges of TMC which reduced the interaction between polymer and mucin and hence the decreased mucoadhesive properties.

Furthermore, it was observed that the interaction between ss-mucin particles and TMC was molecular weight-dependent. The interaction decreased with decreased molecular weight (TMC40-40 and TMC40-10). No apparent change in surface properties of ss-mucin was detected with 40% DQ TMC derived from chitosan 25 kDa (data not shown). Indeed, the molecular weight of polymer is one of the important factors on mucoadhesive property which has been found in the polymer having the molecular weight above 100,000 g/mol [49]. Taken together, the data obtained suggest that mucoadhesive properties of TMC were influenced by the combination of positive charge density, steric hindrance of pendent groups on polymer and molecular weight.

3.4. Cytotoxicity

The effects of polymer structure on L929 cells were investigated by testing cell viability via MTT assay. The concentration of TMC resulting in 50% inhibition of cell growth, IC_{50} value was evaluated. The results are summarized in Table 4. TMC80-10 was particularly toxic with an IC_{50} of 10 μg/ml. For 40% DQ TMC, a decrease of molecular weight of TMC has caused reduction in toxicity of TMC40-10 compared to TMC40-40. However, TMC10-40 and TMC20-60 were shown to be completely non-toxic with IC_{50} > 1 mg/ml. These appear consistent with the conclusion earlier

Table 3
Characteristics of the interaction between ss-mucin particle and TMC polymers (mean ± SD, $n = 3$)

Polymer	Slope (mV/ml)	V_c[a] (ml)
TMC10-40	5.8 ± 0.4	3.0 ± 0.2
TMC20-20	13.1 ± 1.4	1.4 ± 0.1
TMC20-60	4.6 ± 0.4	3.7 ± 0.5
TMC40-10	7.6 ± 0.9	2.1 ± 0.1
TMC40-40	11.3 ± 0.3	1.7 ± 0.0
TMC80-10	15.3 ± 2.0	1.3 ± 0.1

[a] The extrapolated volume of 1 mg/ml polymer solution used to neutralize negative charge of 1% w/v ss-mucin to zero.

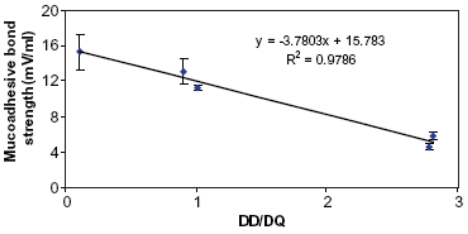

Fig. 7. Correlation between the ratio of DD/DQ of TMC and mucoadhesive bond strength measured by the mucin particle method. Each point represents mean ± SD of three experiments.

Table 4
Cytotoxicity of TMC polymers on L929 fibroblast cells following 3 h incubation as determined by MTT assay ($n = 4$)

Polymer	IC_{50} (μg/ml)
TMC10-40	>1000
TMC20-20	24
TMC20-60	>1000
TMC40-10	14
TMC40-40	12
TMC80-10	10

drawn by Mao et al. [24] and Kean et al. [25] who reported that cytotoxicity of TMC increased with increasing molecular weight and DQ of the TMC. Haas et al. [50] reported that the cytotoxicity on COS-1 cells of TMC with a low DQ (4%) and intermediate DQ (10% and 18%) was less than that of chitosan, meanwhile TMC with high DQ of 66% appeared to be more toxic.

Considering the effect of DQ and DD, it was found that cytotoxicity of TMC was influenced by the proportion ratio of DD to DQ. The cytotoxicity of TMC began to decrease when DD/DQ ratio was higher than 1 and TMC showed non-toxic property when ratio of DD to DQ was about 3:1. Since the cytotoxicity of TMC would probably be a consequence of its relatively positive charge [31,51], this phenomenon could be explained by the steric effect of methyl pendent groups of dimethylamino groups which shielded a proportion of the positive charges present on TMC decreasing the interaction of the positively charged amino groups of TMC with the anionic compartments of glycoproteins on the cell membrane. Due to high positive charge density of TMC40-40, the amount of methyl pendent groups from dimethylamino groups was insufficient to shield its positive charges, leading to low cell viability. Similarly, Mao et al. [24] reported that grafting PEG (polyethylene glycol) on TMC polymer chain can improve the biocompatibility of TMC, and the extent of which is substitution degree and PEG molecular weight-dependent.

Taking data from cytotoxicity and mucoadhesion in consideration, it was observed that cytotoxicity data fairly correlated with mucoadhesive bond strength. These confirmed that the electrostatic interaction between the positively charged amino groups of TMC and the negatively charged residues in mucus layer and on cell membrane was the predominant mechanism for mucoadhesion and cytotoxicity of TMC.

4. Conclusions

This work reports the effects of DQ and DD on the physicochemical properties of TMC in terms of solubility, mucoadhesive properties and cytotoxicity. The synthesis of TMC polymers by using one methylation reaction step with subsequent multiple addition steps resulted in the high DQ and large molecular weight. Furthermore,

it was found that an increase in the number of reaction steps increased DQ and decreased DD, whereas an extended duration of reaction increased both DQ and DD. The results also showed that M_w of TMC was in the range of 60–550 kDa and TMC in 2% HAc/0.2 M NaAc was present in a spherical structure, approximating a random coil. The charge density of TMC, represented by DQ, was an important factor to determine its water solubility and the optimum value was an intermediate DQ of 40% regardless of DD and molecular weight. However, DD obviously affected the solubility properties of TMC when DQ was lower than 24%. Cytotoxicity of TMC correlated with mucoadhesive bond strength showed to be dependent upon the ratio of DD to DQ. The high DD in TMC led to a decrease in both mucoadhesivity and cytotoxicity and the effect of DD was evidently observed when DD/DQ > 1. Non-toxic TMC was observed at DD ca. threefold higher than DQ.

In summary, the effect of DD on the physicochemical properties and cytotoxicity was obviously observed when DD/DQ > 1. TMC with relatively high DD possessed reductions in solubility, mucoadhesive properties and hence decreased cytotoxicity. However, the influence of DD was marginal when DQ of TMC was larger than 40% at which physicochemical properties and cytotoxicity was mainly affected by DQ. The results from this study represent helpful information on the synthesis of suitable properties of TMC.

Acknowledgements

The authors are grateful for financial support from the Thailand Research Fund (TRF) through the Royal Golden Jubilee Ph.D. program (Grant No. PHD/0226/2545) and the German Academic Exchange Service (Deutsche Akademische Austauschdienst, DAAD). We are very pleased to acknowledge the National Metal and Materials Technology Center (MTEC, Pathumthani, Thailand) for GPC experiment.

References

[1] R.A.A. Muzzarelli, F. Tanfani, The N-permethylation of chitosan and the preparation of *N*-trimethyl chitosan iodide, Carbohydr. Polym. 5 (1985) 297–307.
[2] A. Domard, M. Rinaudo, C. Terrassin, New method for the quaternization of chitosan, Int. J. Biol. Macromol. 8 (1986) 105–107.
[3] A.F. Kotze, H.L. Luessen, B.J. de Leeuw, B.G. de Boer, J.C. Verhoef, H.E. Junginger, *N*-trimethyl chitosan chloride as a potential absorption enhancer across mucosal surfaces: in vitro evaluation in intestinal epithelial cells (Caco-2), Pharm. Res. 14 (1997) 1197–1202.
[4] A.F. Kotze, M.M. Thanou, H.L. Luebetaen, A.G. de Boer, J.C. Verhoef, H.E. Junginger, Enhancement of paracellular drug transport with highly quaternized *N*-trimethyl chitosan chloride in neutral environments: in vitro evaluation in intestinal epithelial cells (Caco-2), J. Pharm. Sci. 88 (1999) 253–257.
[5] M.M. Thanou, A.F. Kotze, T. Scharringhausen, H.L. Luessen, A.G. de Boer, J.C. Verhoef, H.E. Junginger, Effect of degree of quaternization of *N*-trimethyl chitosan chloride for enhanced transport of hydrophilic compounds across intestinal caco-2 cell monolayers, J. Control. Release 64 (2000) 15–25.
[6] J.H. Hamman, C.M. Schultz, A.F. Kotze, *N*-trimethyl chitosan chloride: optimum degree of quaternization for drug absorption enhancement across epithelial cells, Drug Dev. Ind. Pharm. 29 (2003) 161–172.
[7] M. Thanou, J.C. Verhoef, P. Marbach, H.E. Junginger, Intestinal absorption of octreotide: *N*-trimethyl chitosan chloride (TMC) ameliorates the permeability and absorption properties of the somatostatin analogue in vitro and in vivo, J. Pharm. Sci. 89 (2000) 951–957.
[8] M. Thanou, B.I. Florea, M.W. Langemeyer, J.C. Verhoef, H.E. Junginger, N-trimethylated chitosan chloride (TMC) improves the intestinal permeation of the peptide drug buserelin in vitro (Caco-2 cells) and in vivo (rats), Pharm. Res. 17 (2000) 27–31.
[9] M. Thanou, J.C. Verhoef, J.H. Verheijden, H.E. Junginger, Intestinal absorption of octreotide using trimethyl chitosan chloride: studies in pigs, Pharm. Res. 18 (2001) 823–828.
[10] A. Jintapattanakit, V.B. Junyaprasert, S. Mao, J. Sitterberg, U. Bakowsky, T. Kissel, Peroral delivery of insulin using chitosan derivatives: a comparative study of polyelectrolyte nanocomplexes and nanoparticles, Int. J. Pharm. 342 (2007) 240–249.
[11] G. Di Colo, S. Burgalassi, Y. Zambito, D. Monti, P. Chetoni, Effects of different *N*-trimethyl chitosans on in vitro/in vivo ofloxacin transcorneal permeation, J. Pharm. Sci. 93 (2004) 2851–2862.
[12] B.C. Baudner, J.C. Verhoef, M.M. Giuliani, S. Peppoloni, R. Rappuoli, G. Del Giudice, H.E. Junginger, Protective immune responses to meningococcal C conjugate vaccine after intranasal immunization of mice with the LTK63 mutant plus chitosan or trimethyl chitosan chloride as novel delivery platform, J. Drug Target. 13 (2005) 489–498.
[13] M. Amidi, S.G. Romeijn, G. Borchard, H.E. Junginger, W.E. Hennink, W. Jiskoot, Preparation and characterization of protein-loaded *N*-trimethyl chitosan nanoparticles as nasal delivery system, J. Control. Release 111 (2006) 107–116.
[14] M. Amidi, S.G. Romeijn, J.C. Verhoef, H.E. Junginger, L. Bungener, A. Huckriede, D.J.A. Crommelin, W. Jiskoot, *N*-trimethyl chitosan (TMC) nanoparticles loaded with influenza subunit antigen for intranasal vaccination: biological properties and immunogenicity in a mouse model, Vaccine 25 (2007) 144–153.
[15] G. Sandri, S. Rossi, M.C. Bonferoni, F. Ferrari, Y. Zambito, G. Di Colo, C. Caramella, Buccal penetration enhancement properties of *N*-trimethyl chitosan: influence of quaternization degree on absorption of a high molecular weight molecule, Int. J. Pharm. 297 (2005) 146–155.
[16] G. Sandri, P. Poggi, M.C. Bonferoni, S. Rossi, F. Ferrari, C. Caramella, Histological evaluation of buccal penetration enhancement properties of chitosan and trimethyl chitosan, J. Pharm. Pharmacol. 58 (2006) 1327–1336.
[17] B.I. Florea, M. Thanou, H.E. Junginger, G. Borchard, Enhancement of bronchial octreotide absorption by chitosan and *N*-trimethyl chitosan shows linear in vitro/in vivo correlation, J. Control. Release 110 (2006) 353–361.
[18] H.Y. Li, J. Birchall, Chitosan-modified dry powder formulations for pulmonary gene delivery, Pharm. Res. 23 (2006) 941–950.
[19] W. He, Y. Du, W. Dai, Y. Wu, M. Zhang, Effect of *N*-trimethyl chitosan chloride as an absorption enhancer on properties of insulin liquid suppository in vitro and in vivo, J. Appl. Polym. Sci. 99 (2006) 1140–1146.
[20] A.B. Sieval, M. Thanou, A.F. Kotze, J.C. Verhoef, J. Brussee, H.E. Junginger, Preparation and NMR characterization of highly substituted *N*-trimethyl chitosan chloride, Carbohydr. Polym. 36 (1998) 157–165.
[21] D. Snyman, J.H. Hamman, A.F. Kotze, Evaluation of the mucoadhesive properties of *N*-trimethyl chitosan chloride, Drug Dev. Ind. Pharm. 29 (2003) 61–69.
[22] D. Snyman, A.F. Kotze, T.H. Walls, T. Govender, G. Lachmann, Conformational characterization of quaternized chitosan polymers, in: Proc. Int. Symp. Control. Release Bioact. Mater., 2004, pp. 211.
[23] M.M. Thanou, J.C. Verhoef, S.G. Romeijn, J.F. Nagelkerke, F.W. Merkus, H.E. Junginger, Effects of *N*-trimethyl chitosan chloride, a novel absorption enhancer, on caco-2 intestinal epithelia and the ciliary beat frequency of chicken embryo trachea, Int. J. Pharm. 185 (1999) 73–82.
[24] S. Mao, X. Shuai, F. Unger, M. Wittmar, X. Xie, T. Kissel, Synthesis, characterization and cytotoxicity of poly(ethylene glycol)-graft-trimethyl chitosan block copolymers, Biomaterials 26 (2005) 6343–6356.
[25] T. Kean, S. Roth, M. Thanou, Trimethylated chitosans as non-viral gene delivery vectors: cytotoxicity and transfection efficiency, J. Control. Release 103 (2005) 643–653.
[26] A. Polnok, G. Borchard, J.C. Verhoef, N. Sarisuta, H.E. Junginger, Influence of methylation process on the degree of quaternization of *N*-trimethyl chitosan chloride, Eur. J. Pharm. Biopharm. 57 (2004) 77–83.
[27] S. Rossi, F. Ferrari, M.C. Bonferoni, C. Caramella, Characterization of chitosan hydrochloride–mucin interaction by means of viscosimetric and turbidimetric measurements, Eur. J. Pharm. Sci. 10 (2000) 251–257.
[28] M.W. Anthonsen, K.M. Varum, O. Smidsrod, Solution properties of chitosans: conformation and chain stiffness of chitosans with different degrees of *N*-acetylation, Carbohydr. Polym. 22 (1993) 193–201.
[29] C. Qin, Q. Xiao, H. Li, M. Fang, Y. Liu, X. Chen, Q. Li, Calorimetric studies of the action of chitosan-*N*-2-hydroxypropyl trimethyl ammonium chloride on the growth of microorganisms, Int. J. Biol. Macromol. 34 (2004) 121–126.
[30] H. Takeuchi, J. Thongborisute, Y. Matsui, H. Sugihara, H. Yamamoto, Y. Kawashima, Novel mucoadhesion tests for polymers and polymer-coated particles to design optimal mucoadhesive drug delivery systems, Adv. Drug Deliv. Rev. 57 (2005) 1583–1594.
[31] D. Fischer, Y. Li, B. Ahlemeyer, J. Krieglstein, T. Kissel, In vitro cytotoxicity testing of polycations: influence of polymer structure on cell viability and hemolysis, Biomaterials 24 (2003) 1121–1131.
[32] E. Curti, D. de Britto, S.P. Campana-Filho, Methylation of chitosan with iodomethane: effect of reaction conditions on chemoselectivity and degree of substitution, Macromol. Biosci. 3 (2003) 571–576.
[33] D. Snyman, J.H. Hamman, J.S. Kotze, J.E. Rollings, A.F. Kotze, The relationship between the absolute molecular weight and the degree of quaternization of *N*-trimethyl chitosan chloride, Carbohydr. Polym. 50 (2002) 145–150.
[34] J.H. Hamman, A.F. Kotze, Effect of the type of base and number of reaction steps on the degree of quaternization and molecular weight of *N*-trimethyl chitosan chloride, Drug Dev. Ind. Pharm. 27 (2001) 373–380.
[35] N. Errington, S.E. Harding, K.M. Varum, L. Illum, Hydrodynamic characterization of chitosans varying in degree of acetylation, Int. J. Biol. Macromol. 15 (1993) 113–117.
[36] M.L. Tsaih, R.H. Chen, Effect of molecular weight and urea on the conformation of chitosan molecules in dilute solutions, Int. J. Biol. Macromol. 20 (1997) 233–240.
[37] R.H. Chen, M.L. Tsaih, Effect of temperature on the intrinsic viscosity and conformation of chitosans in dilute HCl solution, Int. J. Biol. Macromol. 23 (1998) 135–141.
[38] M.L. Tsaih, R.H. Chen, Effects of ionic strength and pH on the diffusion coefficients and conformation of chitosans molecule in solution, J. Appl. Polym. Sci. 73 (1999) 2041–2050.

[39] A.I. Gamzazade, V.M. Slimak, A.M. Skljar, E.V. Stykova, S.S.A. Pavlova, S.V. Rogozin, Investigation of the hydrodynamic properties of chitosan solutions, Acta Polym. 36 (1985) 420–424.
[40] X. Jiang, L. Chen, W. Zhong, A new linear potentiometric titration method for the determination of deacetylation degree of chitosan, Carbohydr. Polym. 54 (2003) 457–463.
[41] Y. Zhang, C. Xue, Y. Xue, R. Gao, X. Zhang, Determination of the degree of deacetylation of chitin and chitosan by X-ray powder diffraction, Carbohydr. Res. 340 (2005) 1914–1917.
[42] N. Balazs, P. Sipos, Limitations of pH-potentiometric titration for the determination of the degree of deacetylation of chitosan, Carbohydr. Res. 342 (2007) 124–130.
[43] A.F. Kotze, M.M. Thanou, H.L. Luessen, B.G. de Boer, J.C. Verhoef, H.E. Junginger, Effect of the degree of quaternization of *N*-trimethyl chitosan chloride on the permeability of intestinal epithelial cells (Caco-2), Eur. J. Pharm. Biopharm. 47 (1999) 269–274.
[44] T.-C. Yang, C.-C. Chou, C.-F. Li, Preparation water solubility and rheological property of the *N*-alkylated mono or disaccharide chitosan derivatives, Food Res. Int. 35 (2002) 707–713.
[45] K.R. Holme, A.S. Perlin, Chitosan N-sulfate. A water-soluble polyelectrolyte, Carbohydr. Res. 302 (1997) 7–12.
[46] R. Hejazi, M. Amiji, Chitosan-based gastrointestinal delivery systems, J. Control. Release 89 (2003) 151–165.
[47] V.M. Leitner, M.K. Marschutz, A. Bernkop-Schnurch, Mucoadhesive and cohesive properties of poly(acrylic acid)-cysteine conjugates with regard to their molecular mass, Eur. J. Pharm. Sci. 18 (2003) 89–96.
[48] P.J. Sinko, Martin's physical pharmacy and pharmaceutical sciences, fifth ed., Lippincott Williams and Wilkins, New York, 2006.
[49] H.E. Junginger, Bioadhesive polymer systems for peptide delivery, Acta Pharm. Technol. 36 (1990) 110–126.
[50] J. Haas, M.N. Ravi Kumar, G. Borchard, U. Bakowsky, C.M. Lehr, Preparation and characterization of chitosan and trimethyl-chitosan-modified poly-(epsilon-caprolactone) nanoparticles as DNA carriers, AAPS Pharm. Sci. Technol. 6 (2005) E22–E30.
[51] M. Huang, E. Khor, L.Y. Lim, Uptake and cytotoxicity of chitosan molecules and nanoparticles: effects of molecular weight and degree of deacetylation, Pharm. Res. 21 (2004) 344–353.

PUBLICATIONS AND PRESENTATIONS

The publications and presentations which have been arisen and are in preparation from this thesis are listed as following.

PUBLICATIONS

Mao S, Bakowsky U, **Jintapattanakit A**, Kissel T. Self-assembled polyelectrolyte nanocomplexes between chitosan derivatives and insulin. J Pharm Sci 2006;95(5):1035-48.

Jintapattanakit A, Junyaprasert VB, Mao S, Sitterberg J, Bakowsky U, Kissel T. Peroral delivery of insulin using chitosan derivatives: A comparative study of polyelectrolyte nanocomplexes and nanoparticles. Int J Pharm 2007;342(1-2):240-249.

Jintapattanakit A, Mao S, Kissel T, Junyaprasert VB. Physicochemical properties and biocompatibility of N-trimethyl chitosan: Effect of quaternization and dimethylation. Eur J Pharm Biopharm 2008;70(2):563-571.

Jintapattanakit A, Junyaprasert VB, Kissel T. The role of mucoadhesion of trimethyl chitosan and PEGylated trimethyl chitosan nanocomplexes in insulin uptake. J Pharm Sci. **(Revision)**

Jintapattanakit A, Kissel T, Junyaprasert VB. Effect of tripolyphosphate on physical and enzymatic stabilities of insulin loaded nanoparticles of *N*-trimethyl chitosan. Mahidol Univ J Pharm Sci (**Accepted**)

Jintapattanakit A, Peungvicha P, Sailasuta A, Kissel T, Junyaprasert VB. Correlation of *in vivo* nasal insulin absorption and morphological change in rat epithelium of insulin-PEGylated trimethyl chitosan nanocomplexes. (In preparation)

Jintapattanakit A, Sailasuta A, Kissel T, Junyaprasert VB. Intranasal delivery of self-assembly insulin nanocomplexes based on trimthyl chitosan and poly(ethylene glycol)-*graft*-trimethyl chitosan: Acute and subacute

histogathological effects on rat nasal epithelium *in vivo*. (In preparation)

Maw EE, Teeranachaideekul V, Jantratid E, **Jintapattanakit A**, Junyaprasert VB. Effects of oil types and surfactants on the physicochemical properties and *in vitro* drug release of hydrophilic and lipophilic drug-loaded nanoemulsions for topical drug delivery. (In preparation)

POSTER PRESENTATIONS

Jintapattanakit A, Mao S, Junyaprasert VB, Kissel T. A comparative study between surface modified chitosan-insulin nanocomplexes and nanoparticles: Proof of oral delivery concept. Controlled Release Society German Chapter Annual Meeting, Jena, Germany, February 23-24, 2006.

Jintapattanakit A, Sitterberg J, Junyaprasert VB, Kissel T. Binding and uptake of mucoadhesive quarternized chitosan- insulin nanocomplexes by mucus secreting HT29-MTX-E12 monolayers. The 33rd Annual Meeting and Exposition of the Controlled Release Society, Vienna, Austria, July 22-26, 2006.

Jintapattanakit A, Kissel T, Junyaprasert VB. Influence of Dimethylation Degree on Mucoadhesive Properties and Cytotoxicity of *N*-Trimethyl Chitosan. RGJ PhD Congress VIII, 2007, Jomtien Palm Beach Resort, Pattaya, Thailand, April 20-22, 2007.

Jintapattanakit A, Kissel T, Junyaprasert VB. Effect of tripolyphosphate on the enzymatic degradation of insulin loaded N-trimethyl chitosan nanoparticles. The 24th Annual Research Conference in Pharmaceutical Sciences, Faculty of Pharmaceutical Sciences, Chulalongkorn University, Bangkok, Thailand, December 12, 2007.

Junyaprasert VB, **Jintapattanakit A**, Peungvicha P, Kissel T. In vivo study of insulin nanocomplexes based on PEGylated Trimethyl chitosan copolymers for intranasal delivery. The 6th World Meeting on Pharmaceutics Biopharmaceutics and Pharmaceutical Technology, Barcelona, Spain, April 7-10, 2008.

Jintapattanakit A, Junyaprasert VB, Kissel T. Mucoadhesive properties of PEG-graft-Trimethyl Chitosan copolymers by means of mucin particle method and

cell culture model. The 6th World Meeting on Pharmaceutics Biopharmaceutics and Pharmaceutical Technology, Barcelona, Spain, April 7-10, 2008.

Jintapattanakit A, Sailasuta A, Kissel T, Junyaprasert VB. Effect of poly(ethylene glycol)-*graft*-trimethyl chitosan copolymer - insulin nanocomplexes on rat nasal epithelium *in vivo*. The AAPS Annual Meeting and Exposition 2008, Atlanta, Georgia, USA. November 16-20, 2008.

ORAL PRESENTATIONS

Jintapattanakit A, Kissel T, Junyaprasert VB. Formulations of insulin loaded Trimethyl chitosan nanoparticles: Influence of polymer/insulin (+/-) charge ratio. The 21st Federation Asian Pharmaceutical Associations Congress, Yogohama, Japan, November 18-21, 2006.

Jintapattanakit A, Kissel T, Junyaprasert VB. A comparative study between surface modified chitosan-insulin nanocomplexes and nanoparticles: Proof of oral delivery concept. The 23rd Annual Research Conference in Pharmaceutical Sciences & JSPS 1st Medicinal Chemistry Seminaar of Asia / Africa Science Platform Program, Faculty of Pharmaceutical Sciences, Chulalongkorn University, Bangkok, Thailand, December 14-15, 2006.

Jintapattanakit A, Kissel T, Junyaprasert VB. Preparation, characterization and stability of insulin-trimethyl chitosan nanocomplexes as novel nasal delivery system. The 5th Indochina Conference on Pharmaceutical Sciences, Bangkok, Thailand, November 21-24, 2007.

Jintapattanakit A, Kissel T, Junyaprasert VB. Effect of quaternization and dimethylation on physicochemical properties and biocompatibility of *N*-trimethyl chitosan. RGJ Seminar Series LIX: Nanotechnology in Drug Delivery, Faculty of Pharmacy, Mahidol University, Bangkok, Thailand, March 20, 2008.

Jintapattanakit A. In vivo study of intranasal insulin nanocomplexes based on poly(ethylene glycol)-graft-trimethyl chitosan. Department of Pharmaceutics and Biopharmacy, Philipps-Universität, Marburg, Germany, April 23, 2008.

BIOGRAPHY

NAME	Miss Anchalee Jintapattanakit
DATE OF BIRTH	7 April 1977
PLACE OF BIRTH	Bangkok, Thailand
INSTITUTIONS ATTENDED	Mahidol University, 1994-1999: Bachelor of Science in Pharmacy (First class honors, silver medal) Tapraya Hospitol, Sagaow, Thailand 1999-2003: Chief of pharmacy department, pharmacist
GRADUATION GRANT	The Thailand Research Fund (TRF) though the Royal Golden Jubilee (RGJ) scholarship (Grant No. PHD/0226/2545) TRF Master Research Grants: TRF-MAG, Thailand Research Fund, Bangkok, Thailand. (Grant No. MRG-OSMEP505S175) Deutscher Akademischer Austauschdienst (DAAD) Scholarship, The German Academic Exchange Service, Bonn, Germany (Code number A/04/20279)
HOME ADDRESS	391 Moo 1, Soi. Samakkee 28, Samakkee Rd., Tasai, Muang, Nonthaburi, Thailand, 11000 Tel. +66 (0) 2952 0868 Fax. +66 (2) 2952 0869 E-mail: jintapatt@yahoo.com,